ORGANOBORON FUNCTIONALIZED CONJUGATED POLYMERS: SYNTHESIS, CHARACTERIZATION AND ANION BINDING STUDY

By Haiyan Li

A dissertation submitted to

the Graduate school – Newark

Rutgers, The State University of New Jersey

in partial fulfillment of requirements for the degree of Doctor of Philosophy

Graduate Program in Chemistry

Written under the direction of Professor Frieder Jäkle and approved by

_____

_____

_____

_____

Newark, New Jersey

October, 2010

ABSTRACT OF THE THESIS

ORGANOBORON FUNCTIONALIZED CONJUGATED POLYMERS: SYNTHESIS, CHARACTERIZATION AND ANION BINDING STUDY

By Haiyan Li

Thesis Director: Professor Frieder Jäkle

Thiophene- and fluorene-based polymers represent two important classes of semiconducting materials and their applications in organic light emitting devices, photovoltaics, organic field-effect transistors and chemical sensors have been extensively investigated. Electron-deficient organoboranes provide interesting characteristics including their ability to act as efficient emitters and charge transport materials in optoelectronic devices and as sensory element for nucleophiles. It is desirable to bring together these two classes of building blocks within one system to form a variety of materials with advantageous properties. We have explored two alternative design principles: (i) the embedding of boron into the conjugated polymer main chain and (ii) the direct attachment of boron as a side group to the conjugated polymer backbone. Three different projects were pursued in this general area:

1. The reactive polymer scaffold poly(fluorenylene(bromo)borane) (PFBBr) with alternating fluorene and borane moieties was prepared via B-Sn exchange reaction. Starting from PFBBr as a universal precursor, we obtained a series of polymers for which we can tune the stability, thermal characteristics, and fluorescence behavior by simple post-polymerization modification reactions. By using the same synthetic strategy, we have also prepared a main chain donor-π-acceptor type polymer based on a combination of fluorene and triphenylamine. As expected for an ambipolar system, this polymer exhibits a remarkable solvatochromic effect in the emission and can be oxidized and reduced electrochemically at moderate potentials.

2. In an alternative approach, a series of polythiophenes with diarylboryl functional groups attached at the lateral positions have been developed in our group by Anand Sundararaman via a post-polymerization borylation route. The electrical and structural properties of the polymer and the chemical stability can be further tuned by variation of the aryl groups on boron, for which the redox active ferrocenyl and sterically bulky Mes or Tip groups were introduced. To further investigate how the main chain chemical structure influences the optoelectronic properties of this type of polymers, we have prepared a class of bis(dimesitylboryl)bithiophene-based alternating copolymers, involving different aromatic π-systems such as fluorene, carbazole and triphenylamine derivatives.

3. Organoboron quinolate chelates are promising as light emitting materials because of their high thermal stability and efficient luminescence. We have prepared two new polymers with both the quinolate ligands and boron centers embedded in the main chain.

The polymers were obtained by a simple one-step procedure that involves metal-free boron-induced ether cleavage reactions.

All the polymers have been characterized by multinuclear NMR spectroscopy, gel permeation chromatography (GPC) and their thermal behavior has been studied by differential scanning calorimetry (DSC) and thermogravimetric analysis (TGA). Their photophysical and electrochemical properties and electronic structures have been investigated by UV-vis absorption and fluorescence spectroscopy, cyclic voltammetry and theoretical calculations for the respective model systems. The tri-coordinate organoboron compounds that were prepared are promising sensory materials and their response towards different anions has been evaluated by UV-vis absorption and fluorescence spectroscopy

Acknowledgments

I am heartily thankful to my supervisor, Prof. Frieder Jäkle, for having given me the opportunity to work in one of his fascinating projects. His encouragement, supervision and support from the preliminary to the concluding level enabled me to develop an understanding of the subject. His truly scientist intuition has made him as a constant oasis of ideas and passions in science, which exceptionally inspire and enrich my growth as a student, a researcher and a scientist.

I gratefully acknowledge my committee members, Prof. Huixin He, Prof. Malika Jeffries-El (Iowa State University) and Prof. Piotr Piotrowiak, for spending their time reading and correcting my thesis, and for their helpful advice and encouragement.

Many thanks go in particular to Prof. Roger Lalancette for helping me with the X-ray crystallographic analysis, Prof. Phil Huskey for helping me with the Gaussian programs and all the professors who taught me throughout my graduate program. I also would like to thank Dr. Lazaros Kakalis for helping me with NMR measurements. I would also like to thank Maria Arujo, Louise Curry, Monica Dabrowski, Lorraine McLendon, Judith Slocum and Paulo Vares for their assistance.

I would also like to thank Prof. Huixin He and her student Rishi R. Parajuli for their collaboration and helpful discussion on the polythiophene/CNT composite project, thank Prof. Suning Wang and Dr. Yi Cui from Queens University in Canada for kindly providing samples of the quinoline ligands and thank Prof. Steven Holdcroft and Dr. Jaclyn Brusso from Simon Fraser University in Canada for helping with the thin film quantum yield measurements.

In addition, my gratitude also belongs to all the former group members and current group members, on whom I could always rely for their ready cooperation and availability, and who have also provided a relaxed working environment. I want to note that, dimesitylboryl and ferrocenylboryl functionalized polythiophene projects in Chapter 2 were started by Anand Sundararaman. The realisation and success of these projects would not have been possible without his great contribution. I also want to thank all the senior students and postdocs Yang Qin, Dr. Krishnan Venkatasubbaiah, Dr. Thilagar Pakkarisamy, Ramez Boshra, Kshitij Parab, Chengzhong Cui and Ami Doshi for sharing their research experience and instrument training at my early research stage.

Finally, I am very grateful to my family and friends for giving me continuous support and encouragement. I would like to dedicate this thesis to my mother Fengqin Ao, my father Shuting Li, my brother Haichen Li and my husband Dezhen Xu, who gave me strength and enthusiasm to pursue my dreams.

Table of Content

List of Schemes

List of Figures

List of Tables

QTBFT

List of Abbreviations

MO   molecular orbital

HOMO   the highest occupied molecular orbital

LUMO   the lowest unoccupied molecular orbital

E_g energy gap

D   donor

A   acceptor

CT   charge transfer

ICT   intramolecular charger transfer

RT   Room temperature

DMF   dimethylformamide

THF   tetrahydrafuran

LDA   lithium diisopropylamide

Cp   cyclopentadienyl

Fl   fluorenyl

Qu   quinoline

Fc	ferrocene
Fc*	decamethylferrocene
Tip	2,4,6-triisopropylphenyl
Mes	2,4,6-trimethylphenyl
Th	thienyl
Ph	phenyl
DSC	differential scanning calorimetry
T_g	glass transition temperature
TGA	thermogravimetric analysis
UV-vis	Ultraviolet-visible
GPC	gel permeation chromatography
MALLS	Multi-angle laser light scattering
M_n	number average molecular weight
M_w	weight average molecular weight
PDI	polydispersity index
MALDI-TOF	matrix-assisted laser desorption ionization time
CV	of flight
NMR	cyclic voltammetry
DFT	nuclear magnetic resonance
GRIM	density functional theory
	Grignard metathesis

General Introduction

1. Conjugated polymers (CPs)

In 2000, three scientists, H. Shirakawa, A. G. MacDiarmid and A. J. Heeger were awarded the Nobel Prize for their pioneering work in conducting polymers,[1,2] which outlines the significance of this type of materials and their expanded market value. Combining the processability, flexibility and weight advantages of the organic polymer with several functional properties such as electronic (conducting and semiconducting) and optical properties (luminescence and non-linear optics), CPs have found their way to different applications in the area of field effect transistors (FETs), light emitting diodes (LEDs), photovoltaics, electrochromic windows, chemical or biosensors,[3-10] in which CPs are being used as charge transport layers, light emitters, sensing elements or photovoltaic active layers.

Polyacetylene, the first and the simplest conducting polymer (**Figure 1**), is difficult to process and unstable in the presence of oxygen and water. Therefore, the CPs that have been extensively studied and widely used are aromatic CPs and their derivatives. Several representative samples are outlined in **Figure 2**.[11-18]

trans-polyacetylene   **cis-polyacetylene**

Figure 1. Chemical structures of polyacetylene
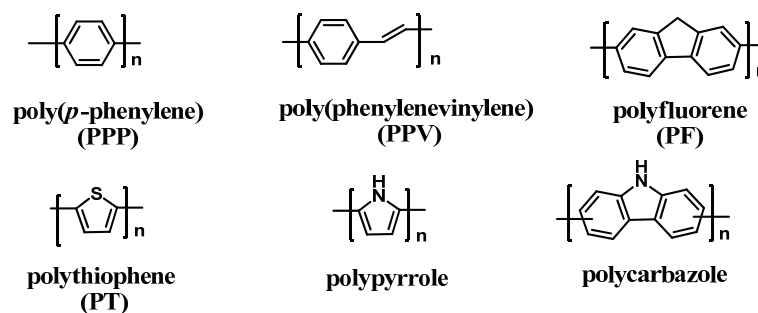
Figure 2. Representative examples of aromatic CPs

Although the chemical structures are different, they all have backbones in which C-C and C=C bonds alternate while each carbon atom carries a π atomic orbital (**Figure 3**). Mixing the unpaired atomic orbitals leads to the formation of two different energy levels: occupied valence molecular orbitals (MOs) constitute the highest occupied MO (HOMO); the anti-bonding combination of the atomic orbitals leads to the lowest unoccupied MO (LUMO) (**Figure 4**).[19] They are equivalent to the valence and conduction bands of solid-state crystalline semiconductors. Neutral CPs are either electrical insulator or semiconductors, but their conductivities can be increased by several orders of magnitude by injecting electrons to the conduction band or by removing electrons from the valence band, which are referred as n-doping and p-doping processes, respectively.
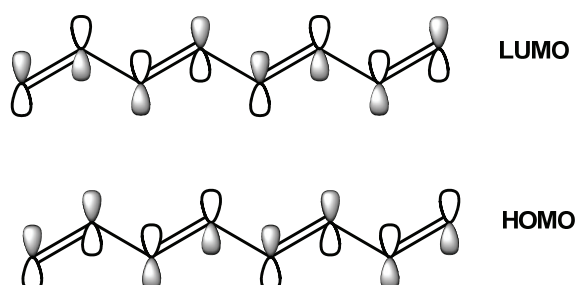
Figure 3. The bond patterns of HOMO and LUMO levels
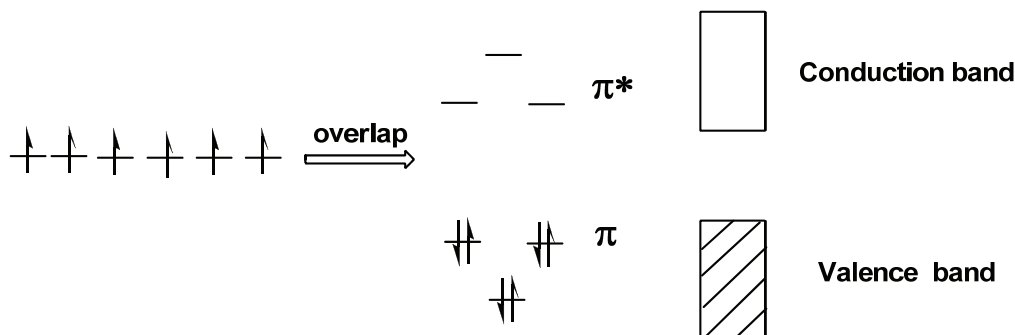
Figure 4. Interactions of the unpaired π-orbitals to form the conduction and valence bands

The application of CPs in organic semiconductors is an interdisciplinary topic including: polymer design, synthesis and processing, device fabrication and measurement. It combines the knowledge and techniques of polymer, supramolecular and nano sciences. We have been focused on the molecular engineering i.e., to synthesize molecules with appropriate electrical and optical properties and processability. The magnitude of the band gap and the energy positions of the HOMO and LUMO energy levels are the most important characteristics to determine the optical and electrical properties of a given CP. In general, the energy gap between the HOMO and LUMO energy levels decreases as the length of conjugation increases.[20] However, when the number of the repeating units exceeds a certain value at which the effective conjugation length is saturated, the band gap starts to level off. Therefore, unlimited extension of the conjugation length results only in a limited reduction of the band gap.[21,22] Several practical strategies have been developed to refine the energy gap of CPs.

The first strategy is on the basis of the two possible resonance structures for the ground state in an aromatic CP, aromatic form and quinoid form. In the aromatic form, each thiophene, benzene or other aromatic unit maintains its aromaticity with confined π-electrons, while delocalization of the flowing π-electrons leads to a resonance structure referred as quinoid form. Changing from the aromatic form to the quinoid form lowers the energy gap by a loss in the stabilization energy since the aromatic form is more stable than the quinoid form. For example, benzene rings with a higher aromaticity cause polyphenylene to have a high energy gap of ca. 3.2 eV. Dilution of the benzene rings by vinyl groups lowers the aromaticity, thus giving a lower energy gap of ca. 2.4 eV. For polythiophene, the energy gap is even lower since the thiophene ring is much less aromatic than the benzene ring. One creative way to increase the quinoid character of polythiophene is represented by polyisothianaphthene (PITN) with an energy band gap of ca. 1 eV, in which each thiophene ring is fused with a more aromatic benzene ring and the quinoid form in the main chain becomes more favorable to maintain the benzene aromaticity (**Figure 5**).[23-25]
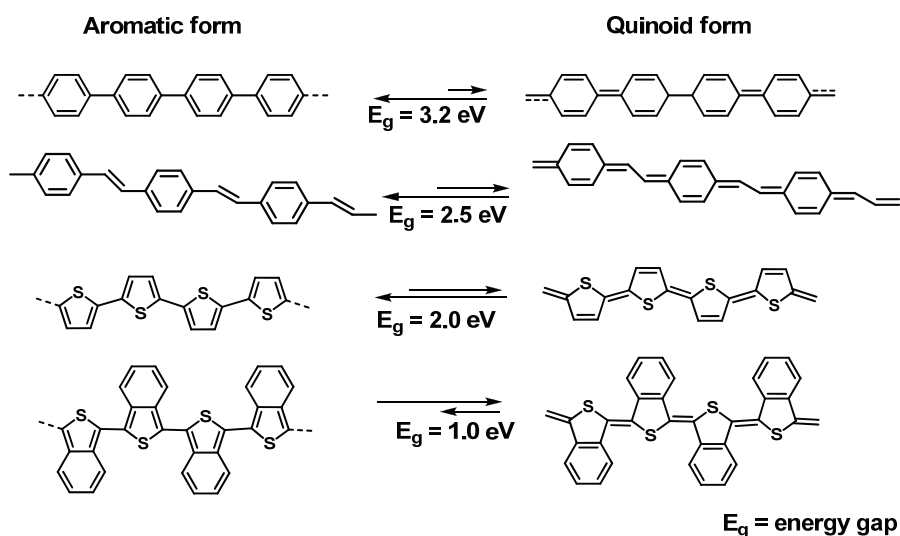
Figure 5. Aromatic and quinoid resonance forms of poly(*p*-phenylene), poly(*p*-phenylenevinylene), polythiophene and polyisothianaphthene

Additionally, molecular modification used to impose steric or electronic effects on conjugated main chains affords various useful strategies for changing the energy gap. Planarization of the conjugated chain by surpassing the structure disorder due to the steric hindrance between the adjacent aromatic rings can effectively reduce the band gap. For example, rigidified by bridging two adjacent thiophene rings with one carbon atom, P1 shows a much lower energy gap of ca. 1.2 eV.[26,27] For P2 the energy gap is further reduced to ca. 1.1 eV (**Figure 6**).[28]

E_g = 1.2 eV E_g = 1.1 eV

P1   **P2**
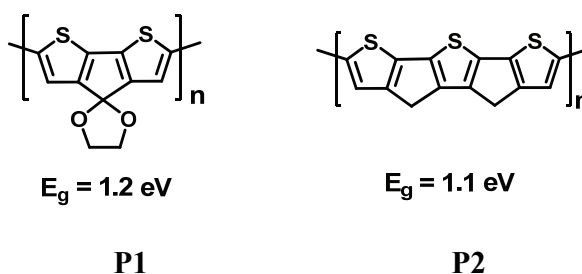
Figure 6. Chemical structures of rigidified P1 and P2

P3
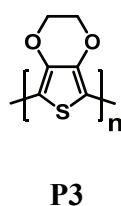
Figure 7. Chemical structure of P3
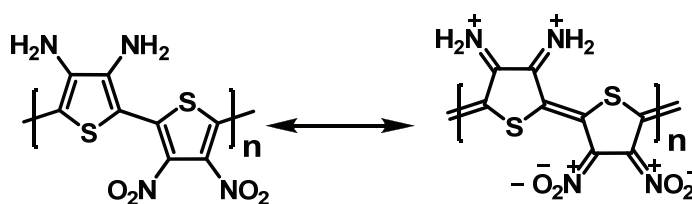
P4

Figure 8. Chemical structure of P4 and its resonance structure

   Incorporation of electron-withdrawing or electron-donating groups is another approach commonly used to perturb the molecular orbitals through either inductive or mesomeric effect. In general, electron-donating groups tend to increase the HOMO energy level, but have less influence on the LUMO energy level, while the electron-withdrawing groups tend to lower the LUMO energy, but show less influence on the HOMO energy level, which both can decrease the energy gap. For example, poly[3,4-(ethylenedioxy)thiophene] (P3) (**Figure 7**) has a energy gap of ca. 1.5 eV, which is about 0.5 eV lower than that of the parent polythiophene.[29] With both electron-donating amino and electron-withdrawing nitro groups attached, P4 has a higher degree of zwitterionic and quinoid character with a significantly reduced energy gap of ca. 1.1 eV (**Figure 8**).[30]
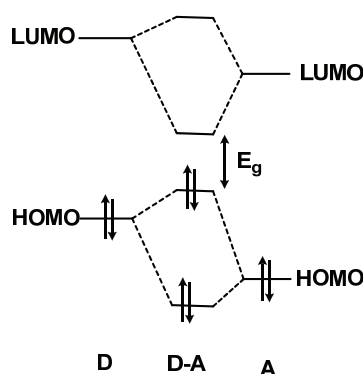
Figure 9. Orbital interactions of donor and acceptor units leading to a smaller band gap in a D-A conjugated polymer
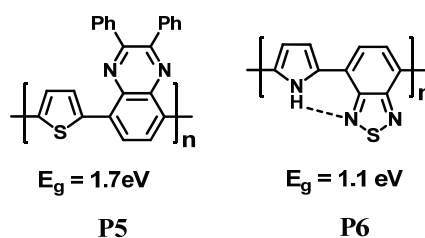
Figure 10. Chemical structures of P5 and P6

Another efficient strategy to manipulate the energy gap is to design polymers with both an electron donor (D) and an electron acceptor (A) attached to the same organic π-segment to form a D-π-A type polymer.[31] Introduction of the push-pull driving forces facilitates electron delocalization and the formation of the quinoid mesomeric structure (D-A→D$^+$=A$^-$) over the conjugated main chain. Photoinduced intramolecular charge transfer (ICT) correlated with the high-lying HOMO of the donor unit and the low-lying LUMO of the acceptor unit can also account for the reduced optical band gap. This can be elucidated in a more explicit and simpler way by introducing the concept of hybridization of the molecular orbital between the donor and acceptor in the D-π-A polymer (**Figure 9**).[23,32] As a matter of fact, the degree of the band gap reduction strongly relies on the strength of the electron donor and acceptor. For instance, P5 with its structure of alternating electron-donating thiophene and electron-withdrawing quinoxaline units has a band gap of 1.7 eV.[33] With pyrrole as a stronger donor and benzothiadiazole as a stronger acceptor, P6 shows a much lower energy gap of 1.1 eV (**Figure 10**).[34] Therefore, a rational design with judicial choice of the D-A pair will allow us to tune the energy band gap over a large range.
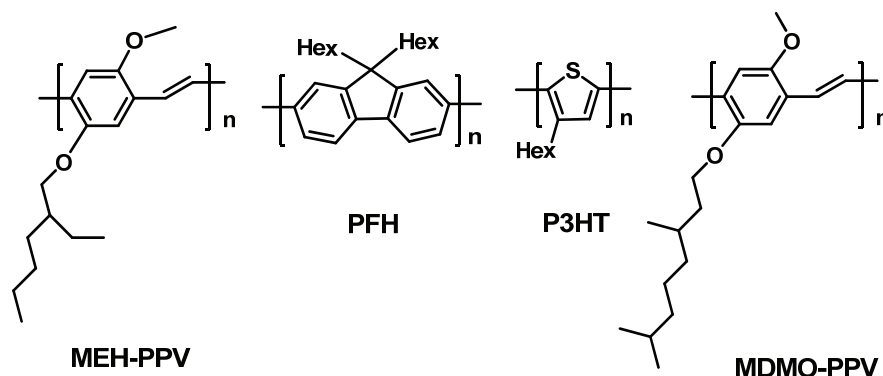
Figure 11. Examples of processable CPs

Another factor associated with the application of CPs is their processability. Unsubstituted CPs are normally insoluble and infusible due to strong inter-chain interactions and chain stiffness, which limits the use of feasible solution processing methods. Therefore solubilising groups are always introduced to render them with reasonable processability. The substituents, to some extent, can impact the main chain conformation, electronic structure and solid state packing, thus varying the overall device characters. It should be noted that branched alkyl chains show stronger influence than the linear ones and increasing the content of the insulating alkyl chains relative to the conjugated portion in the polymer may result in deterioration in the charge mobility. **Figure 11** shows four processable CPs that have been successfully used in organic semiconductors.

CPs that contain metals or metalloids either attached to or directly embedded into π-conjugated backbones are an exciting and promising class of modern materials, endowed with many important properties. Recently, a large number of metal-containing polymers have been prepared and studied, and are of interest because they allow the electronic,

optical, and catalytic properties of metal complexes to be incorporated in a processable form.

2.   Organoboron compounds

Among the metal and metalloid functionalized materials, organoboron-containing polymers have attracted a lot of attention due to their intriguing properties and given arise to exciting applications for linear and non-linear optical materials, emission and electron conduction layers in OLEDs and new probes and sensors for anions. The boron atom in tricoordinate organoboron compounds adopts classical sp^2 hybridization and a trigonal geometry, which allows for facile electron delocalization with the adjacent π systems (**Figure 12**).
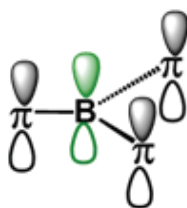
Figure 12. Schematic illustration of tri-coordinate organoboron compounds with π-substituents

The empty p_z orbital results in strong Lewis acidity and make the compounds very sensitive to the nucleophilic attack. Therefore, bulky protecting groups, such as 2,4,6-trimethylphenyl (Mes) or 2,4,6-triisopropylphenyl (Tip) are usually used to prevent the attack of moisture or oxygen and improve the environmental stability of these materials. However, the steric congestion can interrupt the co-planarity between the π-substituents

and the trigonal BC_3 plane, instead leading to a propeller-type conformation. On the other hand, complexation of triarylborane with small anions yields tetracoordinate organoboron species with an sp^3 hybridized boron center, where the original conjugation through boron is destroyed, which is accompanied significant changes in photophysical properties (**Figure 13**). The selective recognition of anions has raised much research attention due to its potential applications in chemical sensors particularly for the detection of fluoride, which is a component in certain phosphonate-based nerve gas agents.

Figure 13. Complexation of tri-coordinate organoboron compounds with nucleophiles (Nu⁻)
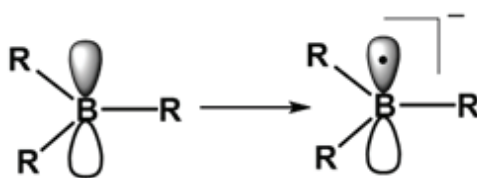
Figure 14. Illustration of the electron-accepting ability of tri-coordinate boron compound
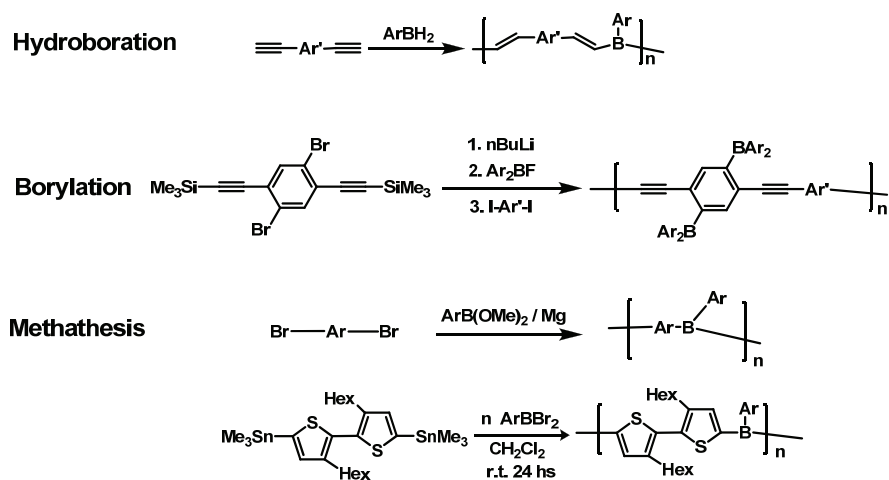
Figure 15. Synthesis of organoboron functionalized CPs

Another characteristic of the empty p_z orbital is its electron-accepting ability. Reduction of the tri-coordinate organoboron compound produces an anion radical. The stability of the anion radical is improved by using bulky substituent groups, such that the anion radical exhibits good stability as evident from a reversible or quasi reversible reduction in an electrochemical study (**Figure 14**).
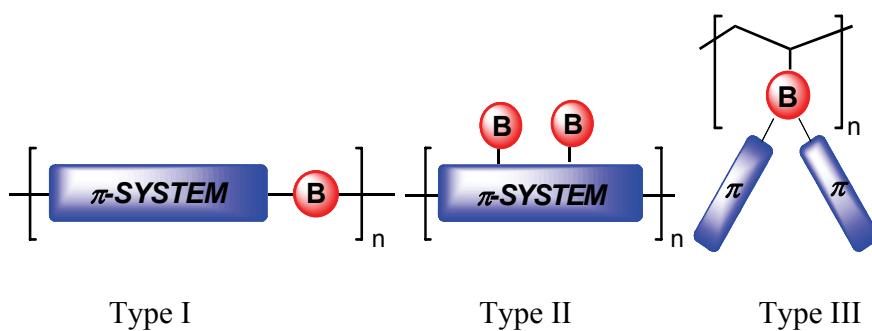
Figure 16. Three architectures of organoboron-containing CPs

Incorporation of organoboron moieties into polymeric systems have been realized by hydroboration,[35-39] metathesis reaction,[40,41] borylation[42-47] (**Figure 15**). In our group,

three type of organoboron-containing polymers have been developed: the boron centers are inserted into the conjugation path (Type I), or, alternatively, attached as lateral substituents to conjugated (Type II) or non-conjugated backbone (Type III). This thesis will only discuss the first two types of CPs.

3.   References

(1)   Shirakawa, H.; Louis, E. J.; MacDiarmid, A. G.; Chiang, C. K.; Heeger, A. J. *J. Chem. Soc., Chem. Commun.* 1977, 578.

(2)   Chiang, C. K.; Fincher, C. R.; Park, Y. W.; Heeger, A. J.; Shirakawa, H.; Louis, E. J.; Gau, S. C.; MacDiarmid, A. G. *Phys. Rev. Lett.* 1977, *39*, 1098.

(3)   Grimsdale, A. C.; Chan, K. L.; Martin, R. E.; Jokisz, P. G.; Holmes, A. B. *Chem. Rev.* 2009, *109*, 897.

(4)   McQuade, D. T.; Pullen, A. E.; Swager, T. M. *Chem. Rev.* 2000, *100*, 2537.

(5)   Thomas III, S. W.; Joly, G. D.; Swager, T. M. *Chem. Rev.* 2007, *107*, 1339.

(6)   Martínez-Máñez, R.; Sancenón, F. *Chem. Rev.* 2003, *103*, 4419.

(7)   Shirota, Y.; Kageyama, H. *Chem. Rev.* 2007, *107* 953.

(8)   Günes, S.; Neugebauer, H.; Sariciftci, N. S. *Chem. Rev.* 2007, *107*, 1324.

(9)   Wen, Y.; Liu, Y. *Adv. Mater.* 2010, *22*, 1.

(10)   Duan, X.; Liu, L.; Feng, F.; Wang, S. *Acc. Chem. Res.* 2010, *43*, 260.

(11)   Beaupre, S.; Boudreault, P.-L. T.; Leclerc, M. *Adv. Mater.* 2010, *22*, ASAP.

(12)   Scherf, U.; List, E. J. W. *Adv. Mater.* 2002, *14*, 477.

(13)   Neher, D. *Macromol. Rapid Commun.* 2001, *22*, 1365.

(14)   Perepichka, F.; Perepichka, D. F.; Meng, H.; Wudl, F. *Adv. Mater.* 2005, *17*, 228.

(15)   Cheng, Y.-J.; Yang, S.-H.; Hsu, C.-S. *Chem. Rev.* 2009, *109*, 5868.

(16)   Barbarella, G.; Melucci, M.; Sotgiu, G. *Adv. Mater.*, *17*, 1581.

(17)   Osaka, I.; McCullough, R. D. *Acc. Chem. Res.* 2008, *41*, 1202.

(18)   MuCullough, R. D. *Adv. Mater.* 1998, *10*, 93.

(19)   Brédas, J.-L.; Cornil, J.; Beljonne, D.; Santos, D. A. D.; Shuai, Z. *Acc. Chem. Res.* 1999, *32*, 26.

(20)   Tour, J. M. *Chem. Rev.* 1996, *96*, 537.

(21)   Wudl, F.; Kobayashi, M.; Heeger, A. J. *J. Org. Chem.* 1984, *49*, 3382.

(22)   Roncali, J. *Chem. Rev.* 1997, *97*, 173.

(23)   Cheng, Y.; Yang, S.; Hsu, C. *Chem. Rev.* 2009, *109*, 5868.

(24)   Brédas, J.-L.; Heeger, A. J.; Wudl, F. *J. Phys. Chem. B* 1986, *85*, 4673.

(25)   Hoogmartens, I.; Adriaensens, P.; Vanderzande, D.; Gelan, J.; Quattrocchi, C.; Lazzaroni, R.; Brédas, J. L. *Macromolecules* 1992, *25*, 7347.

(26)   Brisset, H.; Thobie-Gautier, C.; Gorgues, A.; Jubault, M.; Roncali, J. *J. Chem. Soc., Chem. Commum.* 1994, 1305.

(27)   Orti, E.; Sanchis, M. J.; Viruela, P. M.; Vituela, R. *Synth. Met.* 1999, *101*, 602.

(28)   Roncali, J.; Thobie-Gautier, C. *Adv. Mater.* 1994, *6*, 846.

(29)   Pei, Q.; Zuccarello, G.; Ahlskog, M.; Inganäs, O. *Polymer* 1994, *35*, 1347.

(30)   Zhang, Q. T.; Tour, J. M. *J. Am. Chem. Soc.* 1998, *120*, 5355.

(31)   Kitamura, C.; Tanaka, S.; Yamashita, Y. *Chem. Mater.* 1996, *8*, 570.

(32)   Brocks, G.; Tol, A. *J. Phys. Chem. B* 1996, *100*, 1838.

(33) Yamamoto, T.; Zhou, Z.-H.; Kanbara, T.; Shimura, M.; Kizu, K.; Maruyama, T.; Nakamura, Y.; Fukuda, T.; Lee, B.-L.; Ooba, N.; Tomaru, S.; Kurihara, T.; Kaino, T.; Kubota, K.; Sasaki, S. *J. Am. Chem. Soc.* 1996, *118*, 10389.

(34) van Mullekom, H. A. M.; Vekemans, J. A. J. M.; Meijer, E. W. *Chem. Commun.* 1996, 2163.

(35) Matsumi, N.; Naka, K.; Chujo, Y. *J. Am. Chem. Soc.* 1998, *120*, 5112.

(36) Matsumi, N.; Miyata, M.; Chujo, Y. *Macromolecules* 1999, *32*, 4467.

(37) Matsumi, N.; Chujo, Y.; Lavastre, O.; Dixneuf, P. H. *Organometallics* 2001, *20*, 2425.

(38) Matsumoto, F.; Matsumi, N.; Chujo, Y. *Polym. Bull.* 2001, *46*, 257.

(39) Matsumoto, F.; Chujo, Y. *Pure Appl. Chem.* 2009, *81*, 433.

(40) Matsumi, N.; Umeyama, T.; Chujo, Y. *Polym. Bull.* 2000, *44*, 431.

(41) Matsumi, N.; Naka, K.; Chujo, Y. *J. Am. Chem. Soc.* 1998, *120* 10776.

(42) Qin, Y.; Cheng, G.; Sundararaman, A.; Jäkle, F. *J. Am. Chem. Soc.* 2002, *124*, 12672.

(43) Jäkle, F. *Coord. Chem. Rev.* 2006, *250*, 1107.

(44) Qin, Y.; Cheng, G.; Parab, K.; Sundararaman, A.; Jäkle, F. *Macromol. Symp.* 2003, *196*, 33.

(45) Qin, Y.; Cheng, G.; Parab, K.; Achara, O.; Jäkle, F. *Macromolecules* 2004, *37*, 7123.

(46) Parab, K.; Venkatasubbaiah, K.; Jäkle, F. *J. Am. Chem. Soc.* 2006, *128*, 12879.

(47) Sundararaman, A.; Victor, M.; Varughese, R.; Jäkle, F. *J. Am. Chem. Soc.* 2005, *127*, 13748.

Chapter 1. Main-Chain Organoboron Functionalized Conjugated Polymers

1.1   Introduction

CPs with electron deficient organoboron moieties embedded in the main chain can be viewed as a specific type of copolymers containing organic π-systems alternating with boron centers. Such an arrangement is intended to extend the conjugation through boron via p-π overlap, which often leads to interesting photophysical and electrochemical properties (**Figure 1-1**). On the other hand, tri-coordinate boranes have been recognized for their sensing ability to detect toxic anions. When connected by organic π−segments,

the recognition sites may function in a cooperative fashion and a sensor signal amplification effect can be achieved.
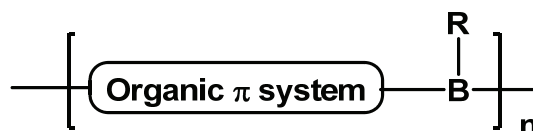
Figure 1-1 Structure of main-chain organoboron CPs

Main chain organoboron CPs are generally achieved by step-wise polymerization techniques including polyaddition and polycondensation reactions. They can be prepared using several well-known organic and organometallic reactions, such as hydroboration reaction, metathesis reaction and metal exchange reaction, etc.

1.1.1 Polyaddition via hydroboration reaction

The preparation of main chain type organoboron CPs using hydroboration reaction was first attempted by Corrieu and coworkers.[1] They reacted 2,5-diethynylthiophene derivatives with BCl_3 / $HSiEt_3$ to afford a series of polymers with different color. However, the presence of extremely sensitive boron chloride groups in the polymer chain prevented further characterization. The molecular weights and UV-vis absorption data are not reported. Since then, main chain boron-containing CPs synthesized via hydroboration were extensively studied by Chujo and coworkers.[2, 3, 4] They improved the chemical stability of the polymers by using bulky arylboranes, such as $MesBH_2$ (Mes = 2,4,6-trimethylphenyl) or $TipBH_2$ (Tip = 2,4,6-triisopropylphenyl), which sterically protect the reactive Lewis acidic boron centers from the attack of oxygen or moisture. As outlined in **Scheme 1-1**, a rich variety of polymers have been produced by reactions with different

aromatic dialkynes. Photophysical studies indicate a certain degree of extended π-conjugation through the vacant p orbital of boron as confirmed by the red shifted absorption for the polymers relative to their respective model compounds in the UV-vis spectra. P1-1a to P1-1d were highly fluorescent and intense blue emissions were observed when excited at 350 nm. Comparably larger Stokes shifts were found for the heteroaromatic polymers, P1-1e and P1-1f containing thiophene and furan subunits in the main chain, which was attributed to the energy transfer from the aromatic donor to the boron acceptor in the excited state. However, the hydroboration reaction of alkynylpyridine is more complicated than expected according to the latest study by Marder et al.[5]
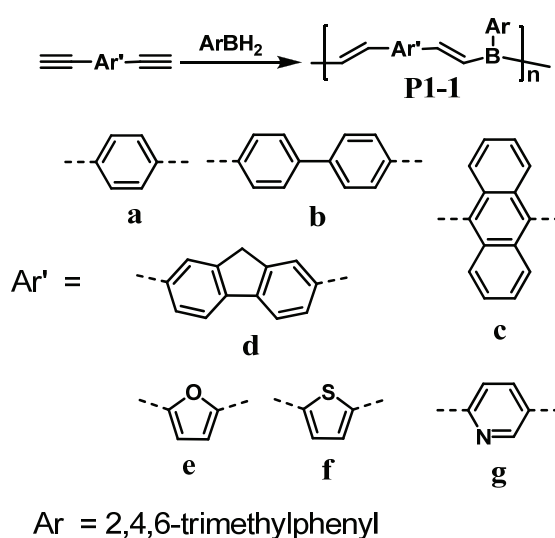
Scheme 1-1. Synthesis of main-chain organoboron CPs via hydroboration reactions

Hydroboration has proven to be a versatile approach applicable to a variety of monomers owing to the mild reaction conditions. For example, by simply replacing the aromatic diethyne with a ruthenium complex containing tetrayne, Chujo and Lavastre

prepared a novel transition metal containing polymer, P1-2, in which the $d_\pi-\pi_\pi^*$ transition was activated by the high electron affinity of the tri-coordinate boron moieties, as evident by an intense charge transfer band centered at 514 nm.[6] Later, another two boron polymers P1-3 containing a Pt or Pd complex were also reported by the same group (**Scheme 1-2**).[7] Unexpectedly, the metal to ligand charge transfer was not observed this time, while the polymers exhibited intense emission at 481 and 498 nm, respectively. This might arise from a mismatch of the energy levels between the transition metal complexes and the boron moieties.
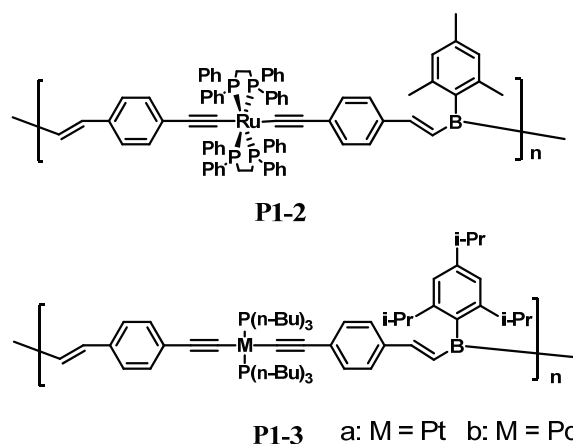
Scheme 1-2. Transition metal containing main chain organoboron polymers

Recently, Wagner and coworkers have reported the polymerization of 9,10-dihydro-9,10-diboraanthracene with aromatic dialkynes via hydroboration (**Scheme 1-3**).[8] The monomer 9,10-dihydro-9,10-diboraanthracene was designed to form two spatially separated but chemically related B-H functionalities, which aimed to minimize the influence of the fist addition on the reactivity of the second B-H bond and at the same

time to maintain molecular orbital overlap between boron and the adjacent aromatic groups.

R = H, OC$_6$H$_{13}$ **P1-4**
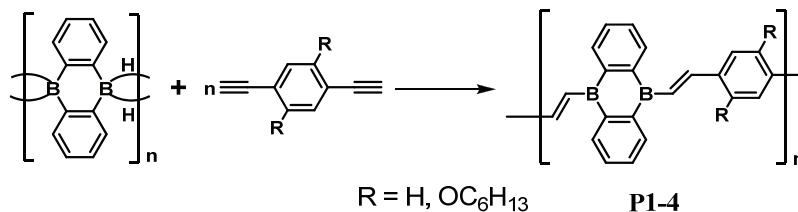
Scheme 1-3. Polymerization of 9,10-dihydro-9,10-diboraanthracene via hydroboration reaction

1.1.2 Polycondensation via metathesis reactions

Polycondensation via metathesis reaction provides an alternative route to organoboron CPs. As shown in **Scheme 1-4**, poly(p-phenylene-borane) (P1-5) and poly(ethynylene-phenylene-ethynylene-borane) (P1-6) type polymers were prepared by reactions of a difunctional Grignard reagent[9] or dilithium reagent[10] with an aryldimethoxylborane. Interestingly, photophysical studies showed that although the absorption for P1-5 emerged in the higher energy region with maxima at 350-370 nm relative to P1-6 at 397 nm, the emission was strongly red-shifted to around λ_{max} = 490 nm relative to λ_{max} = 450 nm for P1-6. Therefore, P1-5 gave a blue green emission while P1-6 gave a visible blue emission under the irradiation of UV light.
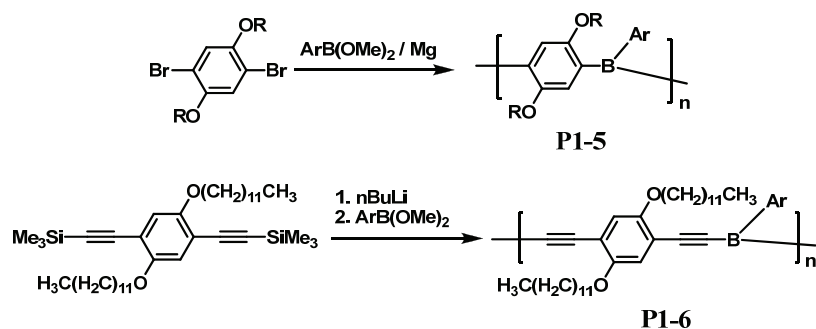
Scheme 1-4. Synthesis of main-chain organoboron CPs via organometallic polycondensation reaction

1.1.3 Other reactions

Some other methods for the preparation of main-chain organoboron CPs are also available. Manners et al. have described the preparation of ferrocenylborane polymers through thermal ring opening polymerization (ROP) (**Scheme 1-5**).[11] The reaction took advantage of the large ring strain existing in the cyclic ferrocenylborane monomers and occurred at 180 °C to afford polymers P1-7. However, P1-7 suffered from low solubility and could not be further characterized.
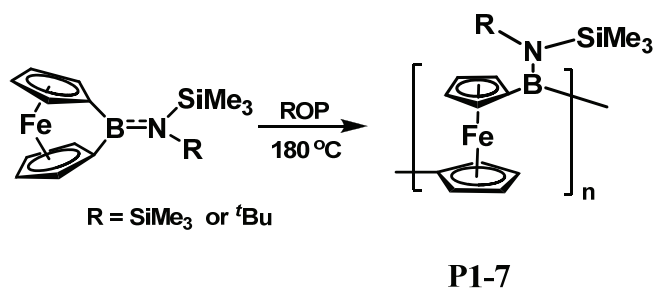
Scheme 1-5. ROP route to the ferrocenylborane polymers

P1-8
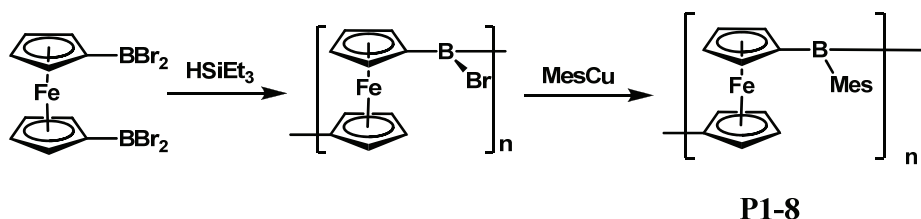
Scheme 1-6. Synthesis of the soluble ferrocenylborane polymer

Wagner's group presented a new synthetic strategy that provides convenient access to a soluble ferrocenylborane polymer (**Scheme 1-6**).[12, 13] Reaction of the difunctional monomer $Fc(BBr_2)_2$ in the presence of 3 eq. of triethylsilane gave a linear polymer [-fc-B(Br)-]$_n$ (fc = ferrocenylene). Simply replacement of the bromo substituents with sterically bulky Mes groups produced a soluble and fairly stable polymer. The linear structure was confirmed from a high resolution MALDI-TOF mass spectrum that showed the expected repeating units. The number average molecular weight M_n was determined to be 5140 by GPC coupled with a multi-angle laser light scattering (MALLS) detector.

P1-9
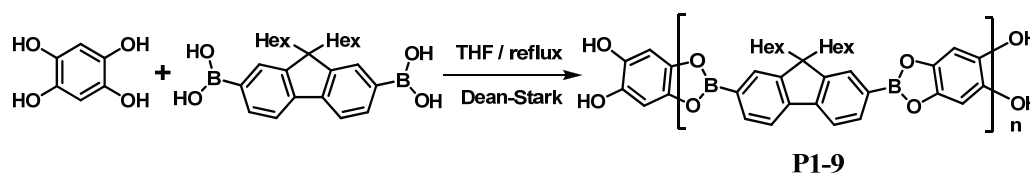
Scheme 1-7. Synthesis of poly(dioxaborole)s via boronate ester formation reaction

In an alternative approach, Lavigne and coworkers have demonstrated the preparation of poly(dioxaborole)s through boronate ester formation reaction, which provides a facile, high yield alternative to the traditional synthesis of CPs (**Scheme 1-7**).[14] Photophysical studies showed that P1-9 exhibits red-shifted absorption and emission compared with those for the dioxaborole oligomers indicative of extended conjugation through the

borole moieties. Furthermore, semiempirical studies indicated that the electron delocalization is approximately 70% as efficient for the oligo(borole)s as that of more traditional CPs such as poly(acetylene) or polythiophene.
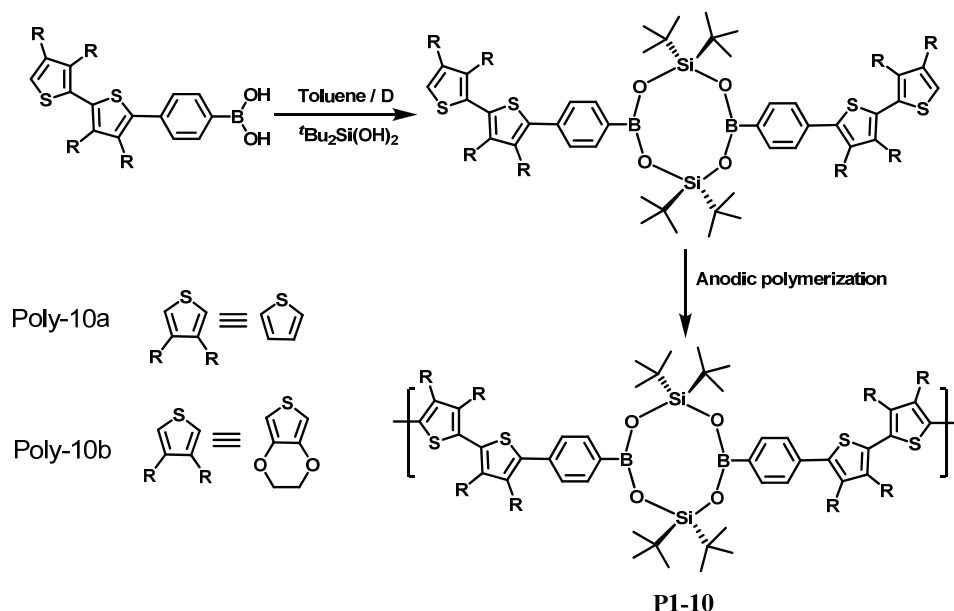
Scheme 1-8. Synthesis of P1-10 via electropolymerization

Most recently, Lee and coworkers have prepared two conjugated polymeric sensory materials through electropolymerization of bifunctional borasiloxane cage molecules, which were prepared via an efficient 2+2 cyclocondensation of arylboronic acids with di-^{t}butyl-dihydroxysilane. P1-10 exhibits a reversible colorimetric response towards amine vapor, which cannot be observed for the unfunctionalized PTs (**Scheme 1-8**).

In our group, the study in this subject started from a family of polymeric bithiophene-based Lewis acidic polymers with organoboron embedded in the main chain through metal exchange reaction (**Scheme 1-9**).[15] The polymers obtained showed interesting substituent-dependent photophysical properties: with phenyl (P1-11a), pentafluorophenyl

(P1-11b) and diphenylaminobithienyl (P1-11c) attached to boron, blue-green, green and red luminescence was observed, respectively. When substituted with the ferrocenyl groups, the polymer P1-11d is dark red in color and the luminescence is quenched. However, the stability of the polymers proved to be moderate, and the chain lengths varied for the polymers obtained from different reactions.
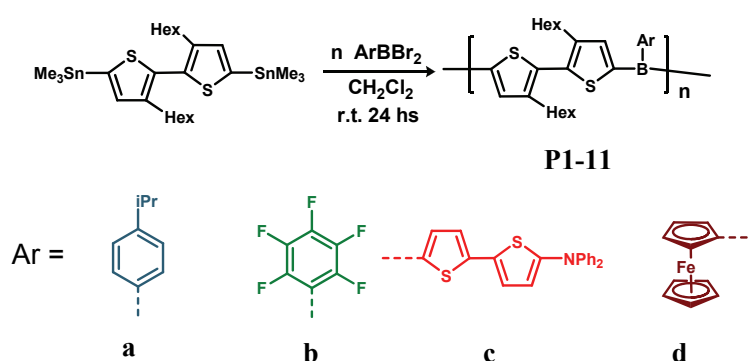
Scheme 1-9. Preparation of bithienylborane polymers through B / Sn exchange reactions

1.2 Fluorene-based main chain organoboron polymers

1.2.1 Introduction to fluorene-based conjugated polymers

Fluorene-based homo and copolymers have evolved as a major class of polymeric materials that have been intensively investigated and widely applied in materials science, for example, in PLEDs, OFETs, photovoltaics and chemical sensors, etc. According to prior literature reports, LEDs fabricated from fluorene homopolymers exhibit bright blue emission with efficiencies not reached when using other polymers.[16] Most importantly, the processability and the functionality of the polymers can be easily modified through

derivatizaion at the 9-potsitions, whereas the main chain electronic structure remains almost unaffected. By combining organoboron and fluorene moieties, we aimed to prepare a series of highly luminescent and tunable fluorenylborane polymers.

1.2.2 Synthesis and characterization of the fluorenylborane polymers

The preparation of fluorenylborane polymers took advantage of the high conversion of the Sn / B exchange reactions. Different from the previous procedure for the synthesis of bithiophene borane polymers, we first prepared two difunctional monomers, 2,7-bis(dibromoboryl)-9,9-dihexylfluorene (FlB$_2$) and 2,7-bis(trimethylstannyl)-9,9-dihexylfluorene (FlSn$_2$). Reaction of FlB$_2$ with FlSn$_2$ in CH$_2$Cl$_2$ was monitored by multinuclear NMR spectroscopy. After stirring at RT overnight, the volatile by-product Me$_3$SnBr was removed under high vacuum. A broad signal at 54 ppm in the ^{11}B NMR for the crude product PFBBr is consistent with the incorporation of boron into the polymer backbone. ^{1}H NMR spectroscopy confirms a linear polymer structure with the expected peak pattern. Compared to the reaction of FlSn$_2$ with BBr$_3$, which was studied initially, this process leads to much better control and higher selectivity without conversion of the remaining labile halide substituent on boron. PFBBr was not further studied because it is very sensitive to oxygen and moisture, whereas the high reactivity allows us to prepare a series of polymers by simple post-polymerization modification reactions.
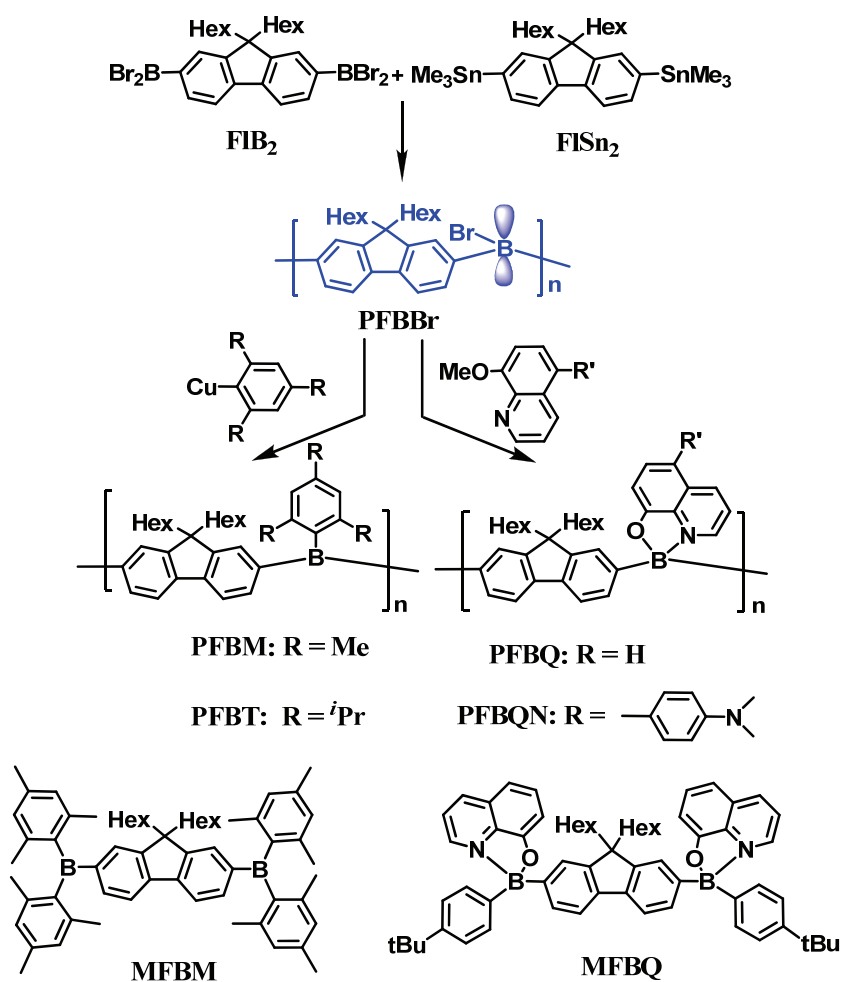
Scheme 1-10. Synthesis of PFBM, PFBT, PFBQ and PFBQN and chemical structures of MFBM and MFBQ
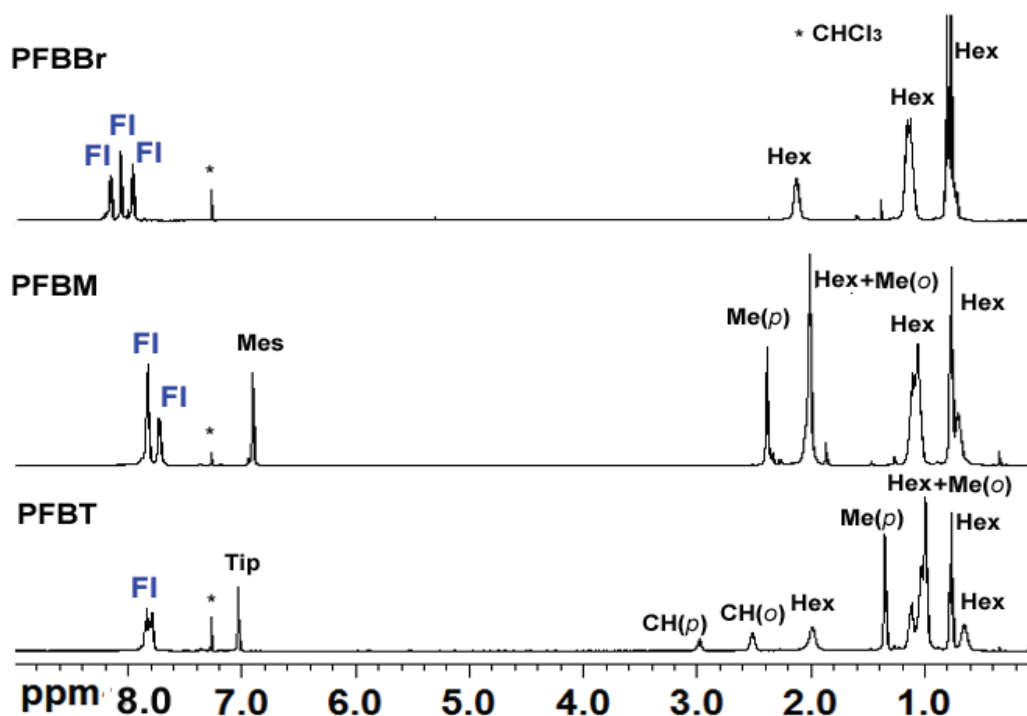
Figure 1-2. ^{1}H NMR comparison of PFBBr, PFBM and PFBT (in CDCl$_3$, referenced with CHCl$_3$ at 7.27 ppm)

Treatment of PFBBr with the mild nucleophilic reagents 2,4,6-trimethylphenyl copper (MesCu) and 2,4,6-triisopropylphenyl copper (TipCu) afforded two tri-coordinate organoboron polymers, PFBM and PFBT, respectively (**Scheme 1-10**). The bulky aryl groups were chosen because of their ability to stabilize triarylborane moieties through steric protection. [2,17-20] The polymers were purified by repeated precipitation from toluene into hexanes (PFBM, 70%) or acetone (PFBT, 80%), and isolated as pale yellow solids. Their ^{1}H NMR spectra show peak patterns that reflect the replacement of the Br substituents with the aryl groups. All the protons on the fluorene rings are upfield shifted and distinct signals for the aromatic protons on the pendant aryl groups are observed at

6.91 ppm for PFBM and 7.03 ppm for PFBT. Their integration is consistent with attachment of one aryl group to each fluorenylborane moiety (**Figure 1-2**). In the ^{11}B NMR spectrum, a single broad resonance emerged (PFBM, 59 ppm; PFBT, 57 ppm), which is slightly downfield from that of PFBBr and in the typical region for tri-coordinate arylboranes.

From the same universal polymeric precursor, two tetra-coordinate organoboron quinolate polymers, PFBQ and PFBQN, were obtained by simply reacting PFBBr with 8-methoxyquinoline (8MQ) or 4-(8-methoxyquinolin-5-yl)-N,N-dimethylaniline (8MQN) in CH_2Cl_2 (**Scheme 1-10**). The reactions took place at RT as evident by a rapid color change to bright yellow green and orange red, respectively. After purification by precipitation into methanol, PFBQ was isolated in 72% and PFBQN was isolated in 63% yield. In the ^{11}B NMR spectra, the resonance becomes narrower and upfield shifted to 10.3 ppm for PFBQ and 9.3 ppm for PFBQN, consistent with tetra-coordination of boron with the quinolato ligands (**Figure 1-3**).
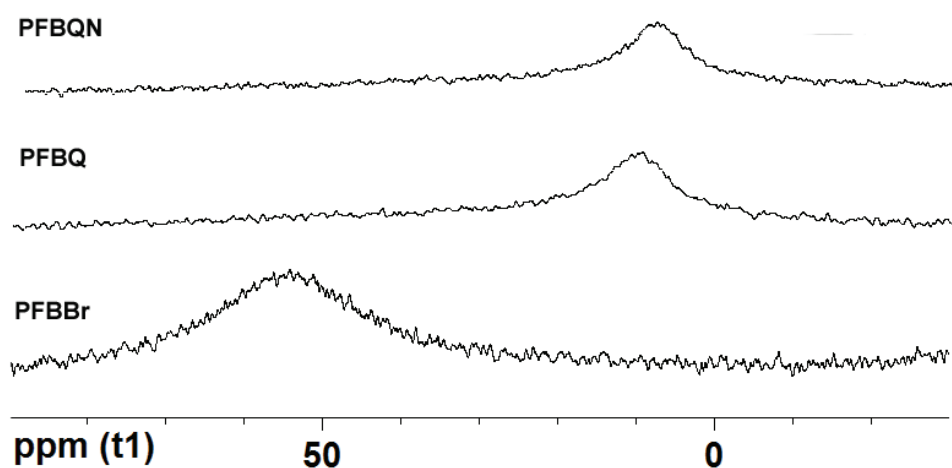
Figure 1-3. ^{11}B NMR comparison of PFBBr, PFBQ and PFBQN (in $CDCl_3$, referenced with $BF_3 \cdot Et_2O$)

1.2.3 **Polymer structure characterized by GPC and MALDI-TOF mass spectrometry**

All the polymers obtained are readily soluble in common organic solvents such as CH_2Cl_2, THF, toluene, etc. Their number average molecular weights (M_n) determined by GPC against PS standards vary from 7.9×10^3 for PFBM to 10.8×10^3 for PFBQN corresponding to a degree of polymerization of $DP_n = 16\text{-}19$.

The polymer structure for PFBQ and PFBQN was examined in detail by MALDI-TOF mass spectrometry. The mass spectrum acquired in the (+) reflector mode displays four main series of peaks with mass separation corresponding to the expected repeating unit of FBQ(N), which further confirms the formation of a linear polymer structure. By comparison of the isotope patterns with the calculated peak patterns, we were able to assign each independent series to polymer chains with fluorene, quinolato or Me end groups i.e., An = H-[FBQ(N)]$_n$, Bn = (N)QB-[FBQ(N)]$_n$, Cn = Me-[FBQ(N)]$_n$ and Dn = H-[FBQ(N)]$_n$F (Q = 8-oxaquinolato, QN = 4-(8-oxaquinolin-5-yl)-N,N-dimethylaniline, F = fluorenyl). The methyl end groups are due to a side reaction that involves methyl transfer from trimethylstannyl groups during the condensation reaction (**Figure 1-4**).
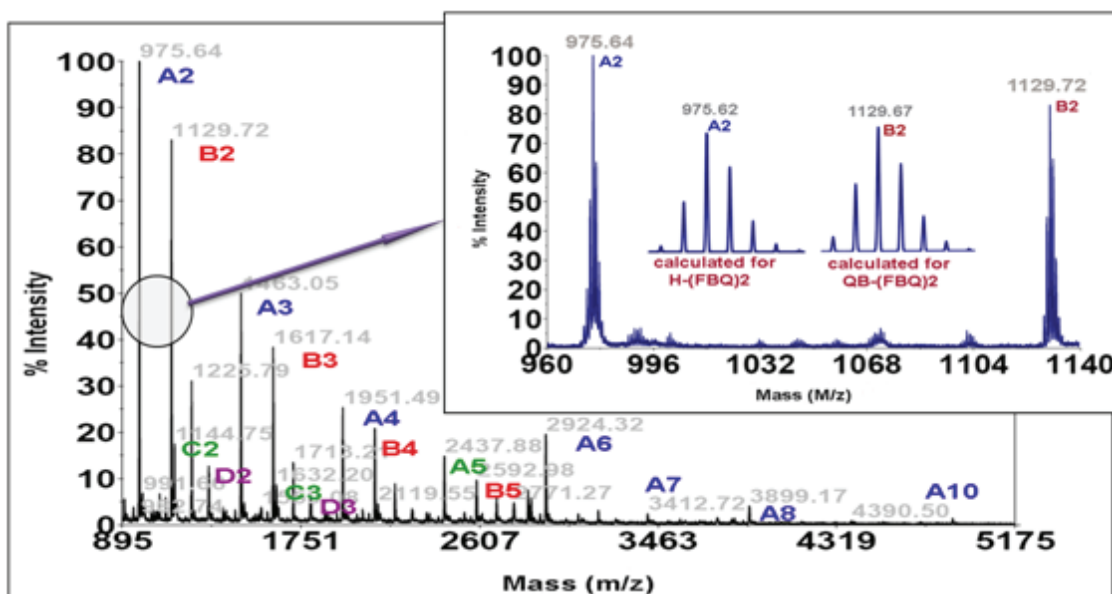
Figure 1-4. High resolution MALDI-TOF mass spectrum for PFBQ (acquired in (+) ion reflector mode, An = H-[FBQ]$_n$, Bn = QB-[FBQ]$_n$, Cn = Me-[FBQ]$_n$ and Dn = H-[FBQ]$_n$Fl (Q = 8-oxalquinolato)

1.2.4 Thermal behavior of the polymers

The thermal characteristics of the resulting polymers were studied by thermogravimetric analysis (TGA) and differential scanning calorimetry (DSC). All the polymers show good thermal stabilities and the thermal decomposition temperature ranges from 210 °C for PFBM to 360 °C for PFBQN (**Figure 1-5**). The environmental stabilities in the solid state and in solution were monitored by ^{1}H NMR spectroscopy. Desirable stabilities were found for PFBT, PFBQ and PFBQN without significant decomposition upon exposure to air for several weeks. However PFBM slowly degrades, indicating that a Tip group is required for optimal steric protection of the tri-coordinate boron ceter. The glass transition temperatures of T_g (onset) = 119 °C for PFBM, 130 °C

for PFBQ, and 153 °C for PFBQN are higher than that reported for poly(9,9-dihexylfluorene) (**Figure 1-6**).[21]
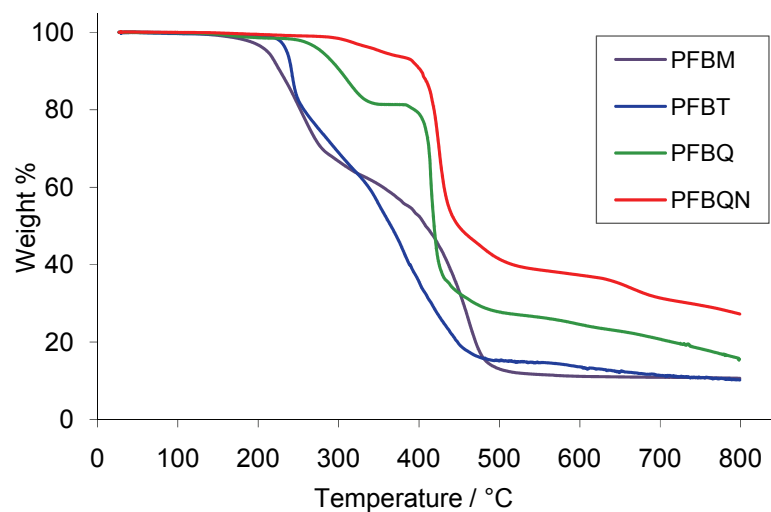
Figure 1-5. TGA traces of PFBM, PFBT, PFBQ and PFBQN (heating rate of 10 °C/min)
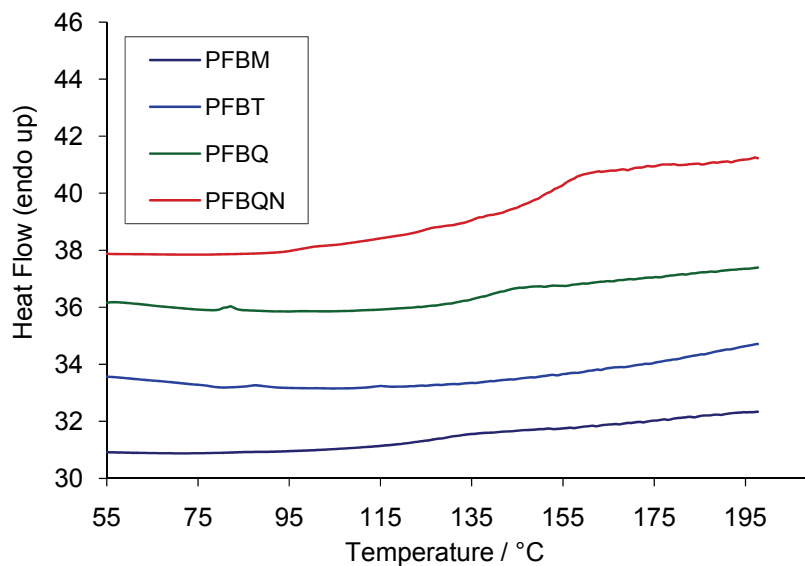
Figure 1-6. DSC plots for PFBM, PFBT, PFBQ and PFBQN (heating rate of 20 °C/min)

1.2.5   Photophysical properties in solution

The photophysical properties in solution were studied by UV-vis and fluorescence spectroscopy. Similar absorption and emission maxima were observed for PFBM and PFBT (**Figure 1-7**). They both display two vibronic absorption bands at 375 nm and 395 nm, which differ from the fluorene homopolymer's broad and featureless absorption. Compared to the absorption of parent dihexylfluorene, the absorption for PFBM and PFBT is strongly red-shifted (> 80 nm), but only a small shift (20 nm) was found relative to that of the model compound 2,7-bis(dimesitylboryl)-9,9-dihexylfluorene (MFBM) (**Figure 1-8**). Therefore the absorptions for PFBM and PFBT are attributed to $\pi-n_B{}^*$ charge transfer, while the conjugation through the polymer chain is only moderate due to the twisted structure of the triarylborane moieties. Both polymers are highly emissive in the blue-violet region (PFBM, $\Phi = 84\%$; PFBT, $\Phi = 81\%$ in CH_2Cl_2), and the emission bands almost perfectly mirror the absorptions with very small Stokes shifts, indicative of a highly rigid structure.[16]

As shown in **Figure 1-9**, the absorption and emission for PFBQ overlap with those of the model compound MFBQ, indicating that conjugation through tetra-coordinate boron center is interrupted. They both have a relatively weaker low energy absorption centered at 394 nm with a series of high energy absorption assigned to $\pi-\pi^*$ transitions and a single emission in the green region at $\lambda_{max} = 506$ nm ($\Phi = 21\%$ for PFBQ and $\Phi = 24\%$ for MFBQ). On the other hand, derivatization on the quinolato ring causes a dramatic change in the photophysical properties of the polymer. For example, with the electron donating dimethylaminophenyl group, PFBQN displays a distinctly red-shifted low

energy absorption at λ_{max} = 441 nm. At the same time, a weak red emission centered at 610 nm was observed (Φ = 0.1%) (**Figure 1-10**). This is consistent with the results for styrene polymers that contain these boron quinolate moieties as pendant groups.[23]
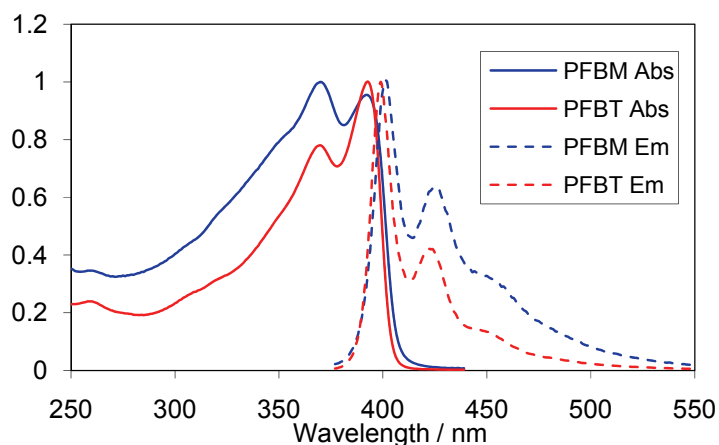
Figure 1-7. Comparison of UV-vis absorption and emission spectra for PFBM and PFBT (in CH_2Cl_2, normalized at λ_{max}, c = 5.77×10^{-7} M for PFBM and 5.91×10^{-7} M for PFBT, $\lambda_{exc, PFBM}$ = 370 nm, $\lambda_{exc, PFBT}$ = 371 nm)
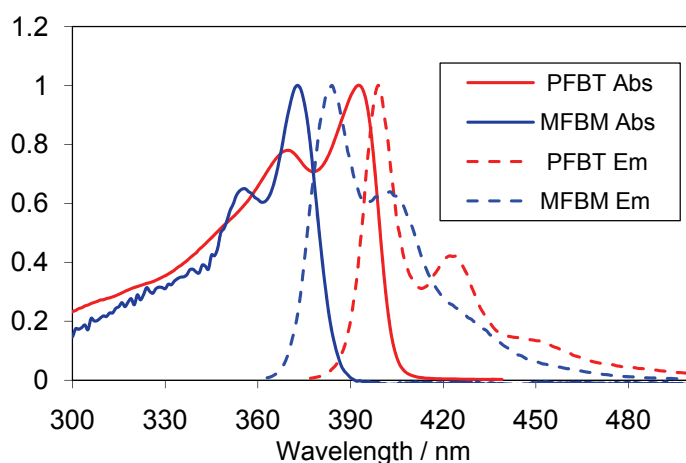
Figure 1-8. Comparison of UV-vis absorption and emission spectra for MFBM and PFBT (in CH_2Cl_2, normalized at λ_{max}, $c = 1.29 \times 10^{-6}$ M for MFBM and 5.91×10^{-7} M for PFBT, $\lambda_{exc, MFBM} = 356$ nm, $\lambda_{exc, PFBT} = 375$ nm)
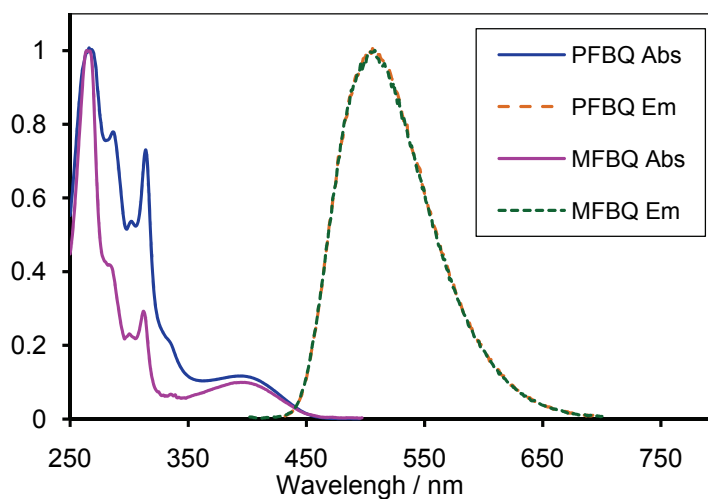
Figure 1-9. Comparison of UV-vis absorption and emission spectra for PFBQ and MFBQ (in CH_2Cl_2, normalized at λ_{max}, $c = 1.85 \times 10^{-5}$ M for PFBQ and 9.06×10^{-6} M for MFBQ, $\lambda_{exc, PFBQ} = 394$ nm, $\lambda_{exc, MFBQ} = 394$ nm)
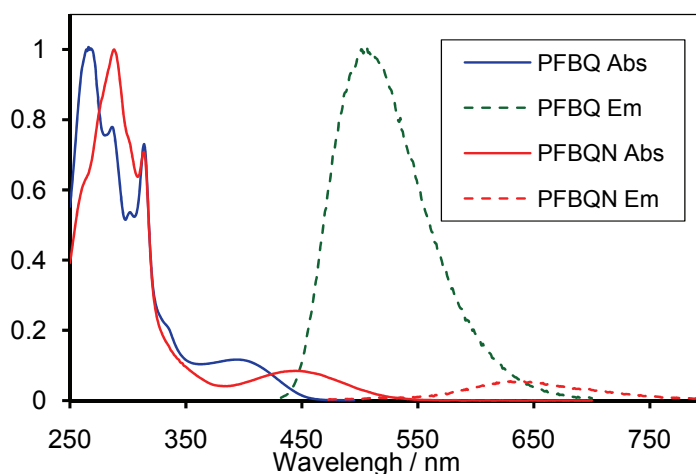
Figure 1-10. Comparison of UV-vis absorption and emission spectra for PFBQ and PFBQN (in CH_2Cl_2, normalized at λ_{max}, c = 1.85×10^{-5} M for PFBQ and 5.10×10^{-5} M for PFBQN, $\lambda_{exc, PFBQ}$ = 394 nm, $\lambda_{exc, PFBQN}$ = 444 nm)

Table 1-1. Summary of photophysical properties of polymers and models

	$\lambda_{Abs}{}^a$	$\varepsilon_{Abs}{}^a$	$\lambda_{em} (\lambda_{ex})^{a,}$	$\Phi^{a, b}$
PFBM	391 370	1.93×10^5 1.73×10^5	401 (370) 425 (370)	0.84
PFBT	394 371	1.83×10^5 1.15×10^5	399 (371) 423 (371)	0.81
PFBQ	394 313 302 286 264	4.97×10^3 3.04×10^4 2.28×10^4 3.41×10^4 5.10×10^4	506 (394) 504 (313) 338 (313)	0.21
PFBQN	444 314 288 275	1.05×10^3 8.84×10^3 1.25×10^4	639 (444)	<0.01
MFBM	373 356	9.00×10^4 5.82×10^4	384 (356) 401 (356)	0.72
MFBQ	395 313 300 284	8.39×10^3 2.47×10^4 1.19×10^4 8.46×10^4	508 (398)	0.24

^{a} Acquired in CH_2Cl_2, ^{b} referenced with diphenylanthracene (Φ = 0.91)

1.2.6 Electrochemical properties

The electron-accepting ability of PFBT was examined by cyclic voltammetry. The first quasi-reversible reduction occurs at –2.13 V vs. Fc/Fc$^+$ couple. The LUMO energy level calculated from the reduction onset is ca. 2.8 eV, which is about 0.6 eV lower than that of fluorene homopolymers.[16] A series of unresolved irreversible reduction waves

appeared at more negative potentials, reflecting the complexity of multiple-site reduction for the polymer. The observed enhanced electron affinity is highly desirable for applications in electronic device materials.[24, 25]
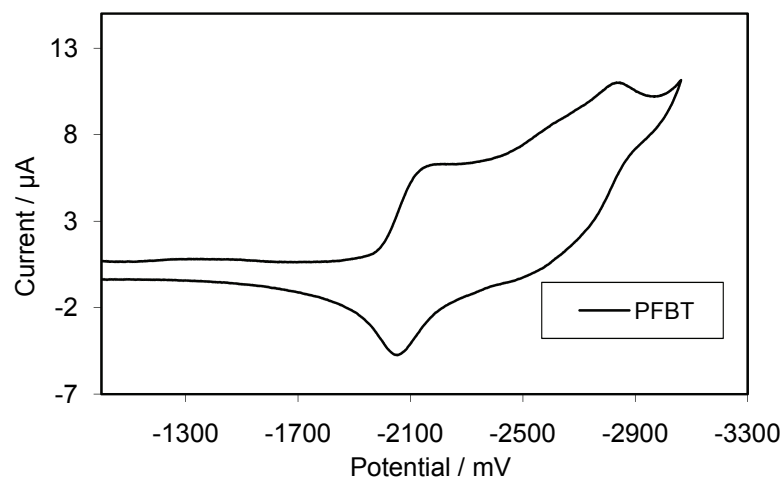
Figure 1-11. Cyclic voltammogram of PFBT (vs. Fc/Fc^+, 100 mV/min, 0.1 M $[Bu_4N]PF_6$ in THF)

1.2.7   Anion binding behavior of PFBT

The anion binding ability of PFBT was evaluated by UV-vis and fluorescence spectroscopy.   First, we examined the response of PFBT towards different anions in solution. A binding study showed that PFBT selectively binds to small anions, such as hydroxide, fluoride and cyanide. The original absorptions at 375 nm and 396 nm disappeared, while a series of high energy absorptions emerged in the short wavelength region (shorter than 330 nm) upon complexation with hydroxide, fluoride or cyanide (**Figure 1-12**). At the same time, the blue emission was quenched completely (**Figure 1-13**).

To further investigate the binding behavior of this multi-recognition-site system, quantitative titrations were also carried out for PFBT and MFBM. As shown in **Figure 1-14** and **Figure 1-15**, the spectral titration of MFBM with fluoride reveals a two-step binding process. In the first step (green plots), the original absorption and emission gradually decreased and a new red-shifted band formed in the longer wavelength region. Two isosbestic points were found at 290 nm and 380 nm. According to a previous study reported by Müllen et al.[26], the binding reaction predominately occurs at one boron site of each individual molecule, because the electron donating nature of the formed tetra-coordinate boron species reduces the electron affinity of the second boron site (**Scheme 1-11**). The red-shifted absorption and emission are attributed to charge transfer from the tetra-coordinate boron to the electron deficient tri-coordinate boron. In the second step (red plots), the fluoride started to bind to the remaining boron sites at higher ratio of fluoride to boron, since the first boron sites were consumed. The photophysical phenomena in this step include: the new absorption and emission bands formed in the first step gradually disappeared accompanied with the appearance of a series of high energy absorption bands at 260-330 nm.
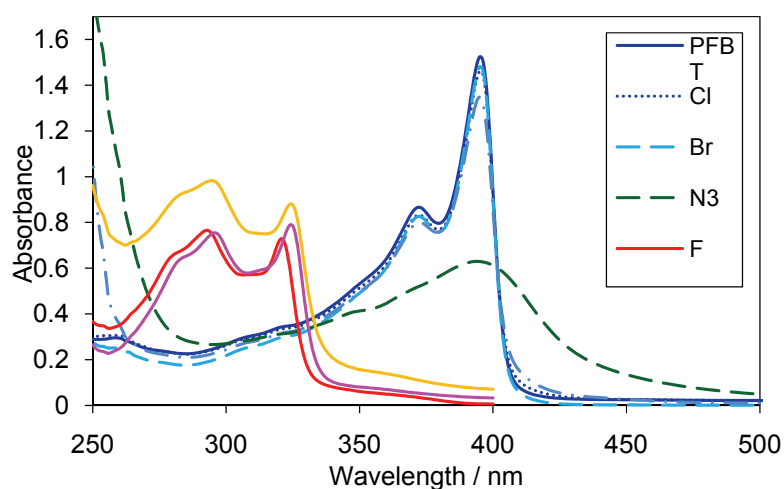
Figure 1-12. Effect of anion binding on the UV-vis absorption spectra of PFBT: solution of anion (0.10 M, 8.6 µL) were added to a solution of PFBT (in THF, 3.12 mL, 2.75×10^{-5} M per repeating unit)
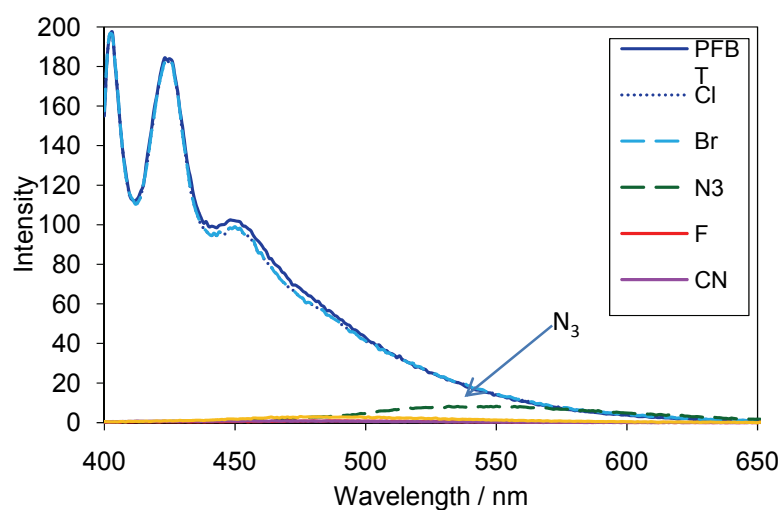
Figure 1-13. Effect of anion coordination on the emission spectra of PFBT: solution of anion (0.10 M, 8.6 µL) were added to a solution of PFBT (in THF, 3.12 mL, 2.75×10^{-5} M per repeating unit, $\lambda_{exc} = 392$ nm)
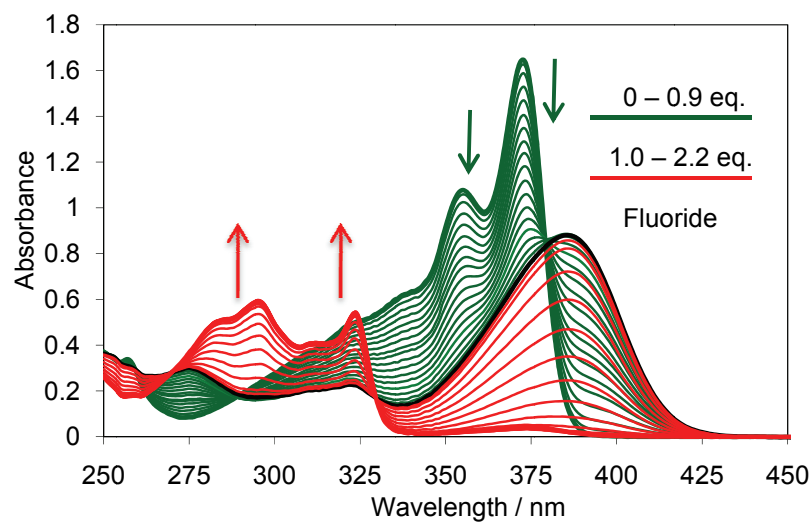
Figure 1-14. Quantitative titration of MFBM (in THF, 3.12 mL, 1.91×10^{-5} M per molecule) with fluoride (in THF, 1.19×10^{-3} M) monitored by UV-vis absorption spectroscopy
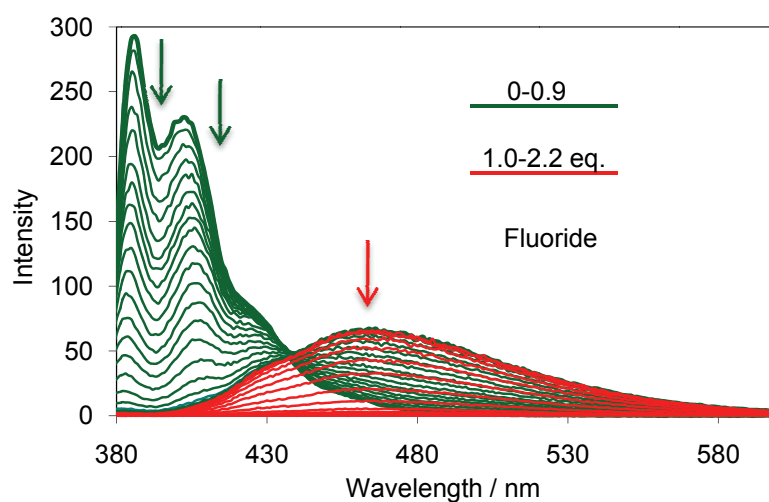
Figure 1-15. Quantitative titration of MFBM (in THF, 3.12 mL, 1.91×10^{-5} M per molecule) with fluoride (in THF, 1.19×10^{-3} M) monitored by fluorescence spectroscopy ($\lambda_{exc} = 375$ nm)
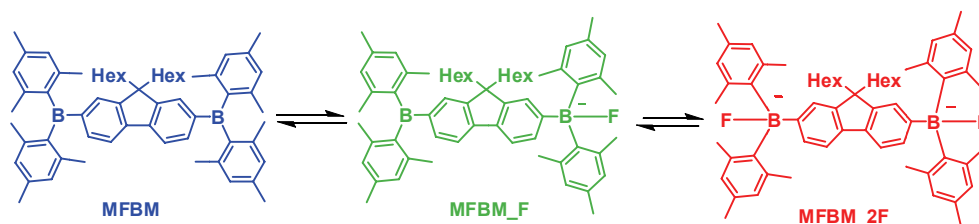
Scheme 1-11. Proposed step-wise binding process of MFBM with fluoride

Similar binding behavior was observed for PFBT. The initial binding process (up to ca. 0.8 eq. of fluoride, green plots) is believed to occur at alternating boron sites to form an alternating copolymer PFBT-F. The binding of the remaining boron sites took place at higher concentrations of fluoride and afforded the final product PFBT-2F (**Scheme 1-12**). It is important to note that the original fluorescence of PFBT was quenched at very low ratio of fluoride to boron (ca. 0.2 eq.), while it took almost 1.0 eq. of fluoride to quench the emission for MFBM (**Figure 1-16**, **1-17**). Förster resonance energy transfer effect (FRET)[27] might be responsible for this signal amplification effect since there is considerable spectral overlap between the absorption of the binding intermediate PFBT-F and the emission of the free polymer PFBT (**Figure 1-18**).
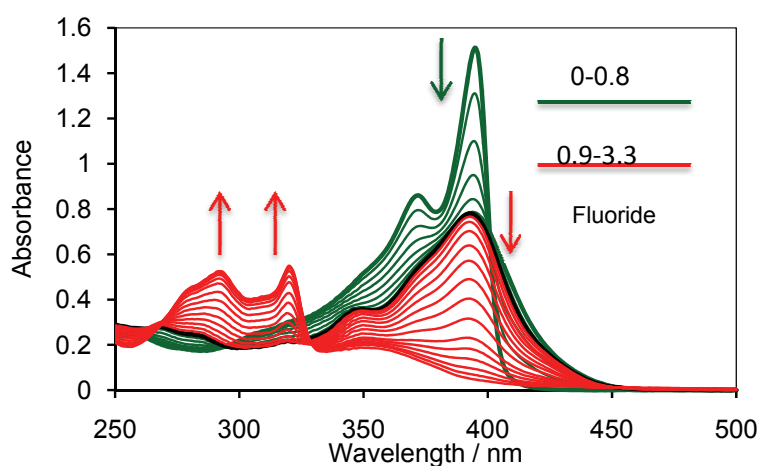
Figure 1-16. Quantitative titration of PFBT (in THF, 3.12 mL, 1.37×10^{-5} M per repeating unit) with fluoride (in THF, 8.56×10^{-4} M) monitored by UV-vis absorption spectroscopy
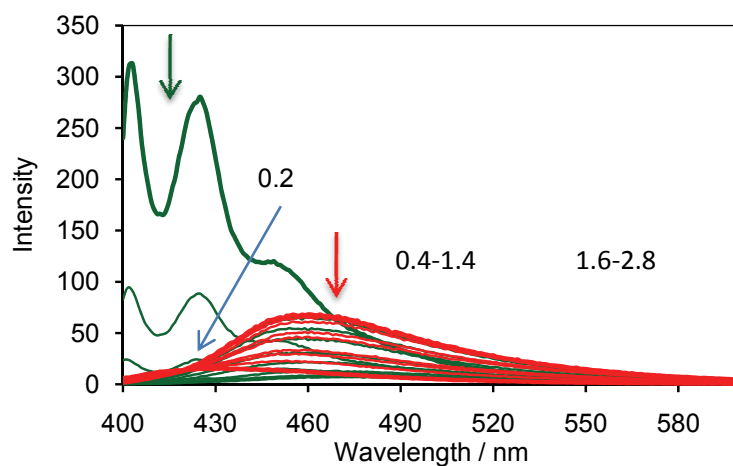
Figure 1-17. Quantitative titration of PFBT (in THF, 3.12 mL, 1.37×10^{-5} M per repeating unit) with fluoride (in THF, 8.56×10^{-4} M) monitored by fluorescence spectroscopy
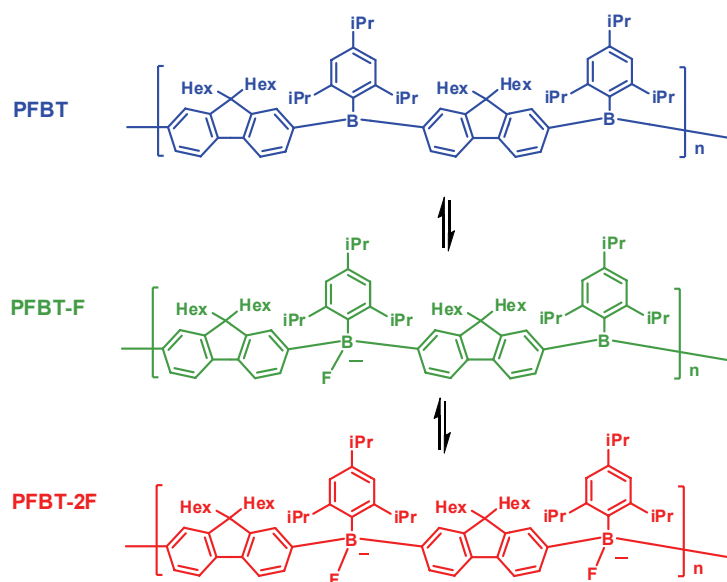
Scheme 1-12. Proposed step-wise binding process of PFBT with fluoride
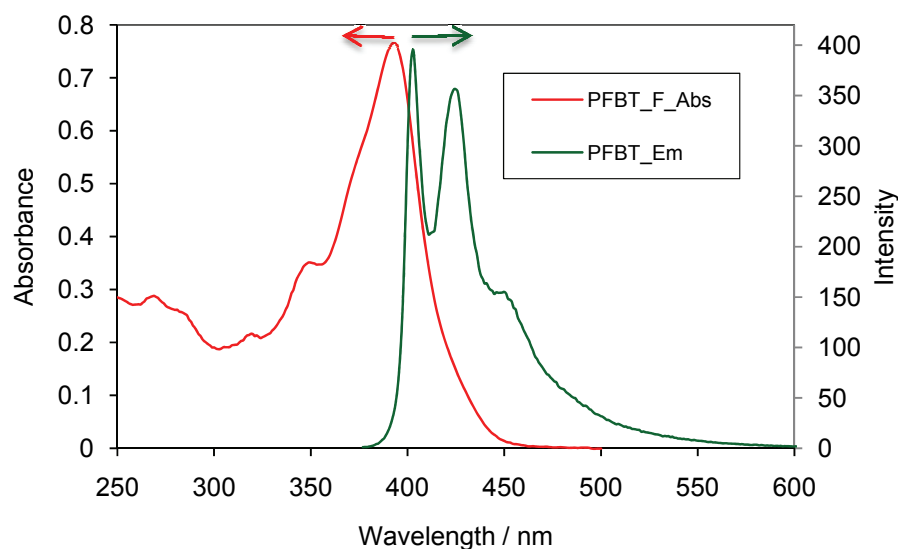
Figure 1-18. Overlay of the absorption of PFBT-F (at 0.8 eq.) and the emission of PFBT (at 0 eq.; extracted from the titration plots)

As shown in **Figure 1-13** and **1-14**, the absorption and emission spectra for the reaction of PFBT with azide are significantly different from the original spectra and those for the fluoride, cyanide and hydroxide complexes: the long wavelength absorption became lower, but no significant changes in the short wavelength region were found; the emission also decreased strongly and became red shifted, but it was not quenched completely. In fact, both the absorption and emission spectra resemble the fluoride titration plots for the intermediate PFBT-F at around 0.8 to 0.9 eq. of fluoride, which suggests that PFBT only partially binds to azide.

1.3 Main chain donor-π-acceptor type polymer

1.3.1 Introduction

Even though the efficiencies of organic semiconductors have been remarkably increased over the past few decades, they are generally lower than the efficiencies of crystalline silicon. Unbalanced charge transfer ability is one important reason that accounts for the low performance of these materials, since hole transport tends to be more favorable than electron transport for most organic π conjugated systems.[28-35] Multiple layer devices can effectively balance the hole and electron transport and injection. However, fabrication by solution processing turns out to be difficult since it is essential to ensure that as each layer is deposited, it doesn't dissolve the preceding layer. Another approach is to blend hole transport materials with electron transport materials including polymer and small molecule blends and all-polymer blends. A problem commonly encountered for blend systems is that undesirable phase separation always occurs leading to the formation of larger domains during storage and operation. To solve the above issues, researchers have become interested in bipolar or multifunctional polymers that possess both electron and hole transpor abilities. Moreover, introduction of a donor and acceptor moiety into one system can also effectively loer the band gap of materials. In this respect, a series of donor acceptor (D-A) type materials, which contain both electron donors, such as amino, thienyl, carbazyl (**Figure 1-19**) and electron acceptors, such as pyridinyl, quinolinyl, quinoxalinyl, benzothiadiazyl, oxadiazyl, triazyl, and cyano or fluoro substitued π systems (**Figure 1-20**), have been developed. [36, 37,38]
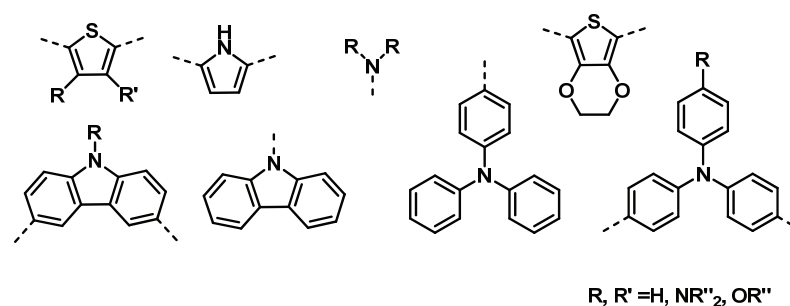
Figure 1-19. Electron donors used in bipolar CPs
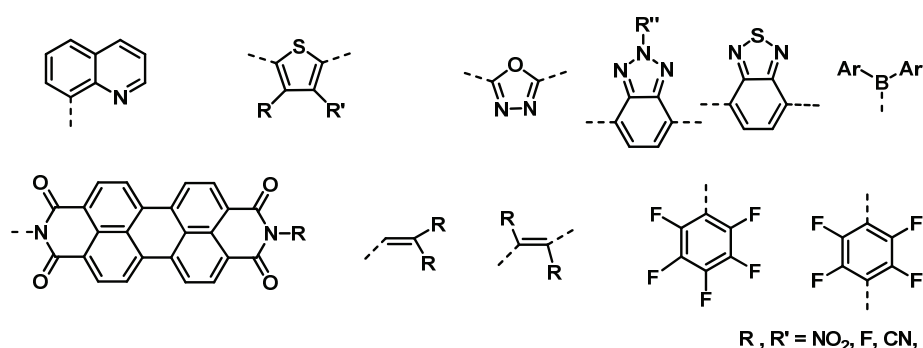
Figure 1-20. Electron acceptors used in bipolar CPs

Boron and nitrogen are from the same period in the periodic table, possessing an empty *p* orbital and a lone pair, respectively, which makes them a perfect D-A pair. A broad range of B-N centered molecular D-π-A materials have been developed.[46-55] Their optoelectronic properties are dominated by charge transfer from nitrogen to boron, which strongly depends on the geometry of the molecule, the linker between the donor and acceptor, the electronic effect of substituents, and the distance between the two centers. However, polymers based on N, B ambipolar systems are rare.[56-58] Lambert and coworkers recently reported on polycarbazole derivatives that feature pendant dimesitylboryl groups, but the molecular weights of the polymers were only moderate

(**Figure 1-20**).[58] We presented here the facile synthesis and properties of a new linear D-
π-A type polymer of comparatively high molecular weight that features electron rich
triarylamine groups alternating with electron deficient bifunctional arylborane moieties.
With both boron and nitrogen embedded in the main chain, highly efficient charge
transfer is expected.
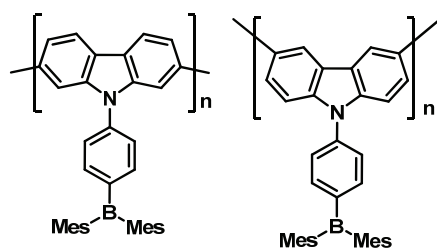
Figure 1-21. Examples of D-π-A type polymers based on N, B[58]

1.3.2 Synthesis and characterization of a main-chain donor-π-acceptor polymer: PNB$_2$

The main chain ambipolar polymer PNB$_2$ was prepared as shown in **Scheme 1-13**.
Using an organometallic polycondensation procedure[15,59] we reacted the ditin monomer
bis(4- trimethylstannylphenyl)mesitylamine (TPASn$_2$) with FlB$_2$. Selective Sn / B
exchange reaction was achieved in toluene solution to give the alternating copolymer
PNB$_2$Br$_2$ as confirmed by ^{1}HNMR analysis. The *ortho*-phenyl protons on the arylamine
were strongly down-field shifted relative to those of TPASn$_2$, and a subtle down-field
shift of the *meta*-phenyl protons and the mesityl protons was also observed as a result of
the electron-withdrawing effect of the adjacent borane groups. Polymer PNB$_2$Br$_2$ was not
further studied because it is very sensitive to oxygen and moisture. In order to sterically

protect the electron deficient boron centers, bulky Tip groups were introduced. Treatment

of PNB$_2$Br$_2$ with a slight excess of TipCu at elevated temperature afforded polymer PNB$_2$

as a yellow powdery solid in 53% isolated yield after precipitation into acetone. Polymer

PNB$_2$ exhibits good solubility in most common organic solvents such as CHCl$_3$, CH$_2$Cl$_2$,

THF, toluene and DMF, allowing for detailed investigation of its structure and properties.

In the ^{1}H NMR spectrum, all the aromatic proton signals experienced down-field shifts

compared to those of PNB$_2$Br$_2$, and a new signal emerged at 6.98 ppm that is assigned to

the *meta*-protons of the Tip group and confirmed successful attachment of the aromatic

pendant group to boron (**Figure 1-22**). In the ^{11}B NMR, a single broad resonance

appeared at 57 ppm, which is in the expected region for tricoordinate boron. M$_n$ was

determined by GPC against polystyrene standards to be 1.3×10^4 (PDI = 1.66)

corresponding to an average of ca. 15 repeating units, which is relatively high in

comparison to organoborane D-π-A type polymers prepared by other methods.[58] High

thermal stability of PNB$_2$ was confirmed by TGA, which revealed <5% weight loss up to

237 ºC.
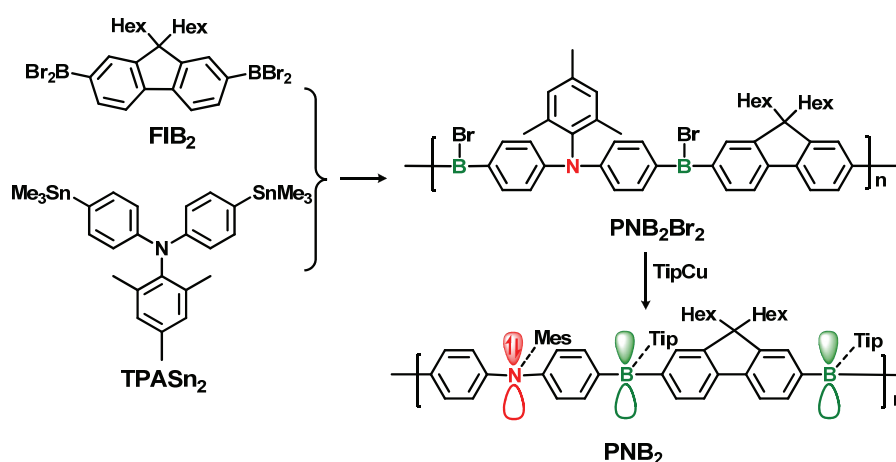
Scheme 1-13. Synthesis of PNB_2Br_2 and PNB_2
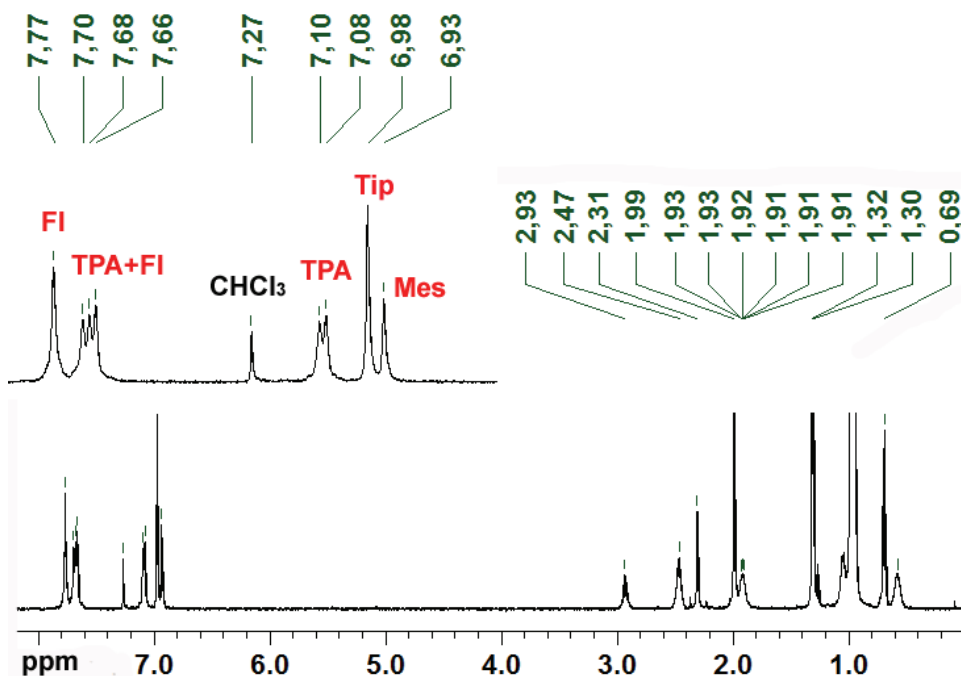
Figure 1-22. ^1H NMR of PNB_2 (in $CDCl_3$, referenced with $CHCl_3$ at 7.27 ppm)

1.3.3 Photophysical properties

To examine the effect of the alternating donor-π-acceptor structure in the polymer main chain on the photophysical properties, UV absorption and fluorescence spectra were acquired in different organic solvents and in the solid state. As shown in **Figure 1-23**, the lowest energy absorption band at 422 nm is only slightly shifted (< 10 nm) in different solvents. This relatively intense band is attributed to ITC from N to B; in comparison to the related molecular D-π-A systems [p-(dimesitylboryl)phenyl]diphenylamine (λ = 377 nm in hexane)[60] and 3,6-bis(dimesitylboryl)-N-butyl-carbazole (λ = 364 nm in hexane)[55]

the absorption is shifted to lower energy, presumably due to the presence of multiple organoborane acceptor sites. Other effects such as a certain degree of extended delocalization throughout the polymer main chain or Davydov splitting as a result of linear alignment of electric transition dipoles, may also play an important role. Indeed, the absorption maximum of PNB_2 is even lower in energy than that reported for the A-π-D-π-A species bis[p-(dimesitylboryl)phenyl]methylamine ($\lambda = 398$ nm in dioxane). Several additional, weaker absorption bands were observed in the range from 300-380 nm, and these are assigned to π-π* and π-n_B* transitions.
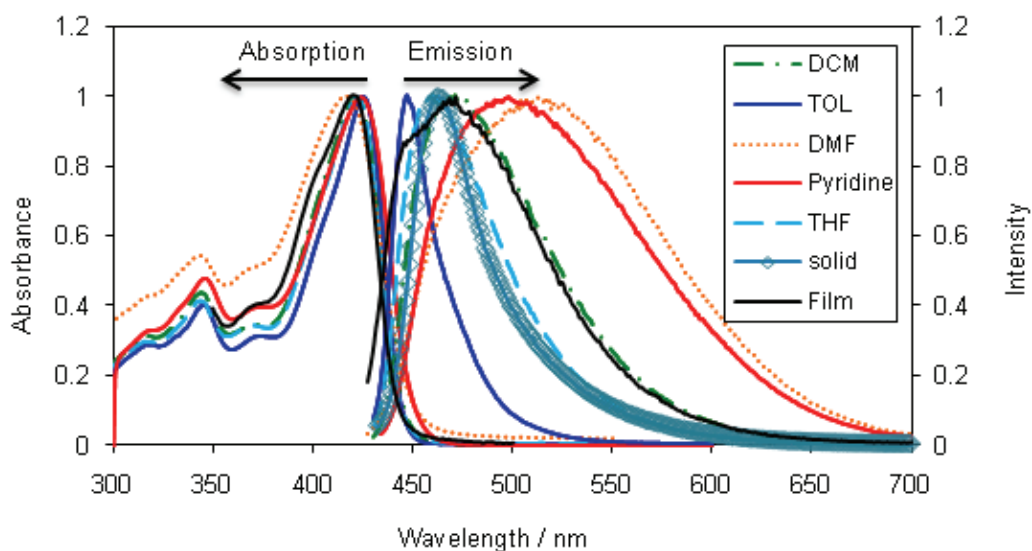
Figure 1-23. Absorption and emission spectra of PNB_2 in different organic solvents and in the solid state as thin film and powder (normalized at λ_{max}, $\lambda_{exc} = \lambda_{max,abs}$ for the solution samples, $\lambda_{exc} = 420$ nm for the solid samples)

Polymer PNB_2 was found to be highly emissive and, as expected for an ambipolar system, the emission wavelength strongly depends on the solvent. In toluene, a narrow

emission band was found in the blue region with a maximum at 442 nm ($\Phi = 75\%$), which was broadened and red shifted with increasing solvent polarity all the way to 510 nm in DMF ($\Phi = 21\%$). This solvatochromic effect can be attributed to a highly polarized structure of the excited state. Interestingly, upon precipitation from toluene into acetone a bright blue ($\lambda = 462$ nm) emissive powdery material was obtained. Strongly emissive organic solids have attracted much recent interest and especially the structural rigidity and charge transfer character of the emission can play an important role as discussed by Yamaguchi in a recent study on highly emissive borylated bithiophene derivatives.[61,62] A thin film of polymer PNB_2 was spin coated on a quartz slide and further studied. In the thin film state, the emission of PNB_2 was red-shifted to 472 nm relative to the powdery form (462 nm) and a somewhat lower quantum efficiency of $\Phi = 13\%$ was measured. The latter suggests that alignment of the polymer chains leads to a certain extent of luminescence quenching.

1.3.4 Electrochemical properties

We further investigated the ambipolar character of PNB_2 by cyclic voltammetry. In analogy to boron-based molecular D-π-A systems,[50,63] PNB_2 was readily reduced and oxidized electrochemically. Two reversible reduction processes occurred at –2.35 V and – 2.79 V, respectively, which are attributed to successive reduction of the two boron centers in each of the repeating units. The potential for the first reduction process is more negative than that determined for PFBT (–2.13 V vs. Fc/Fc$^+$ in THF/[Bu$_4$N]PF$_6$)[59], illustrating the electron donating effect of the additional amine moiety. However, in comparison to related molecular D-π-A compounds, [(2,5-dimethyl-4-

diphenylamino)phenyl]-dimesitylborane (–2.58 V vs. Fc/Fc$^+$ in THF/[Bu$_4$N]PF$_6$) and [4-(dimethylamino)phenyl]-dimesitylborane (–2.16 V vs. SCE in DMF corresponding to ca. –2.63 V vs. Fc/Fc$^+$)[64,65], reduction occurs at less negative potentials; we attribute this to a mutual π-acceptor effect of the two adjacent electron deficient boron centers in PNB$_2$. In an anodic scan in CH$_2$Cl$_2$/[Bu$_4$N]PF$_6$ as the solvent, an only partially reversible oxidation event was observed at 610 mV, which is higher than the potential of 470 mV reported for the respective molecular compound [(2,5-dimethyl-4-diphenylamino)phenyl]-dimesitylborane[63]. Again, the presence of two adjacent organoborane π-acceptor moieties in the polymer chain is likely responsible for this trend (**Figure 1-24**).
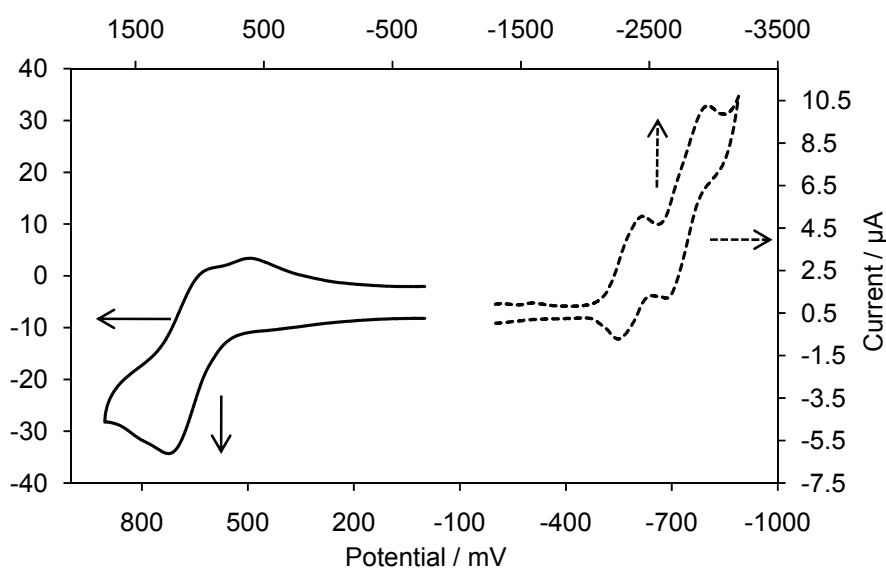
Figure 1-24. Cyclic voltammogram of PNB$_2$ (anodic scan, CH$_2$Cl$_2$ / 0.1 M Bu$_4$N[PF$_6$], 100 mV/s; cathodic scan, THF / 0.1 M Bu$_4$N[PF$_6$], 100 mV/s; reported relative to Fc/Fc$^+$ couple)

Table1-2. Summary of photophysical and electrochemical properties of PNB$_2$ and PFBT

	Red1 [a] (mV)	Red2 [a] (mV)	Ox1 [b] (mV)	UV(nm, solvent, $\varepsilon \times 10^4$)	Em (nm, solvent[c])	Φ (solvent[c])
PNB$_2$	-2350	-2793	670	425 (TOL, 8.09) 422 (THF, 7.34) 422 (DCM,7.99) 424 (Pyridine) 424 (DMF)	447 (TOL) 459 (THF) 468 (DCM) 498 (Pyridine) 510 (DMF)	0.75 (TOL) 0.54 (THF) 0.62 (DCM) 0.27 (Pyridine) 21 (DMF)
PFBT	-2130	-2700		394 (DCM, 18.4) 371 (DCM, 11.5)	399 (DCM) 423 (DCM) 447 (DCM)	0.81 (DCM)

[a] THF / 0.1 M Bu$_4$N[PF$_6$], 100 mV/s, referenced vs Fc/Fc$^+$ couple; [b] CH$_2$Cl$_2$ / 0.1 M Bu$_4$N[PF$_6$], 100 mV/s, referenced vs Fc/Fc$^+$ couple; [c] solvent polarity: [c] toluene 2.4, THF 4.0, DCM 3.1, pyridine 5.3, DMF 6.4

1.3.5 Anion binding behavior

Triarylboranes are also receiving much interest as probes and sensors for anions and other electron-rich small molecules.[49,64,65] Complexation of boron with anions typically leads to a distinct change in the photophysical properties, and polymeric species are particularly interesting because of the potential for mutual interactions between different binding sites. Hence, we examined the response of polymer PNB$_2$ towards different anions in solution via UV-vis and fluorescence measurements. Upon addition of an excess of fluoride or cyanide, the original absorption bands of PNB$_2$ in THF at 422 nm, 367 nm and 344 nm disappeared, while new bands appeared in the high-energy region from 270 nm to 330 nm (**Figure 1-25**). A significant difference in absorbance between the respective cyanide and fluoride complexes was observed, which might be due to subtle differences in the steric or electronic effect of the anions. Moreover, the original

emission at 459 nm was fully quenched when excited at 422 nm, and only a very weak blue shifted emission was observed when excited at the new absorption maximum (295 nm for the fluoride and 322 nm for the cyanide complex) (**Figure 1-26**). In contrast, none of the other anions studied (Cl^-, Br^- and NO_3^-) led to any significant changes to absorption or emission, indicating that the coordination of these larger anions to PNB_2 is unfavorable.
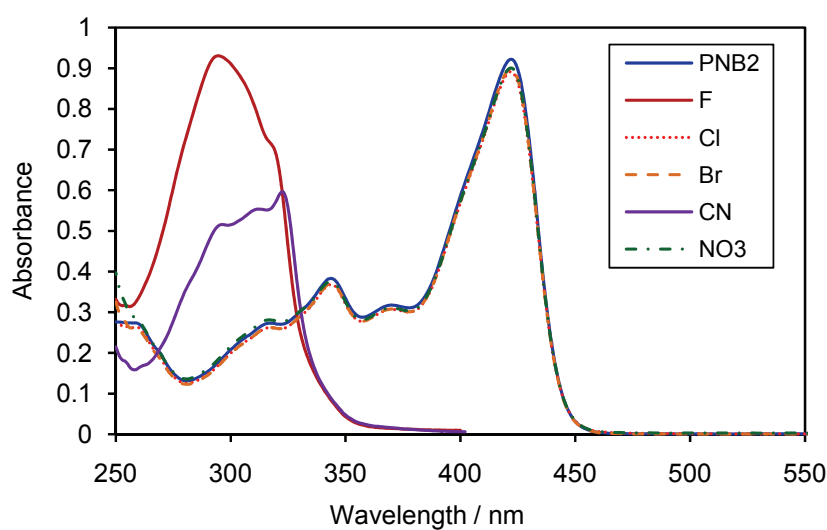
Figure 1-25. Response of PNB_2 towards F^-, Cl^-, Br^-, NO_3^- and CN^- examined by UV-vis absorption spectroscopy: solution of anion (in THF, 7.61×10^{-3} M, 100 μL) were added to a solution of PNB_2 (in THF, 1.22×10^{-5} M per repeating unit (2 boron sites), 3.12 mL)
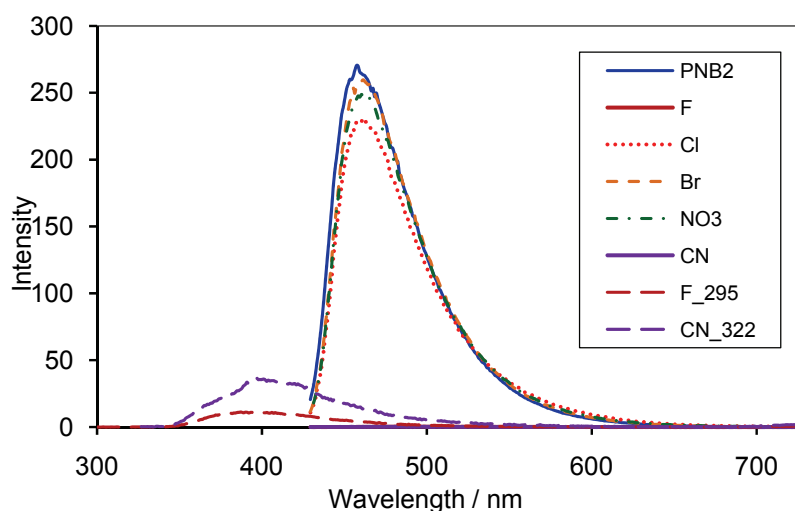
Figure 1-26. Response of PNB$_2$ towards F$^-$, Cl$^-$, Br$^-$, NO$_3^-$ and CN$^-$ examined by fluorescence spectroscopy: solution of anion (in THF, 7.61×10^{-3} M, 100 μL) were added to a solution of PNB$_2$ (in THF, 1.22×10^{-5} M per repeating unit (2 boron sites), 3.12 mL); excited at λ_{max} for free acid; F_295 and CN_322: excited at λ_{max} for the fluoride and cyanide complexes

Quantitative titration with CN$^-$ revealed a two-step binding process (**Scheme 1-14**, **Figure 1-27**, **1-28**). In the first step (up to ca. 1.0 eq. of CN$^-$, green plots), the CT band at 422 nm decreased in intensity and experienced a blue shift to ca. 405 nm, indicating that CT from N to B became higher in energy. It is reasonable to assume that CN$^-$ initially binds to one of the boron sites of the diborylfluorene moiety,[59] which should convert the chromophore from a [-A-π-D-π-A-π-]$_n$ system to a simple D-π-A system similar to that in [p-(dimesitylboryl)phenyl] -diphenylamine (λ = 377 nm).[60] However, a comparison of the absorption data with those of PFBT[59] after complexation of alternating boranes sites with one equivalent of CN$^-$ (λ = 392 nm) would suggest that CT from the newly formed tetra-coordinate borate to the remaining tri-coordinate borane sites also contributes to this

absorption band. In the second step (ca. 1.1 eq. to 3.0 eq., red plots), the intensity of this low energy band continued to decrease without any pronounced change in its position and a series of new bands appeared in the high-energy region (270 to 325 nm). As more and more of the remaining tri-coordinate borane sites are coordinated with CN^-, these π-π^* transitions become dominant. A quantitative analysis gave a binding constant of $\lg K_{11}$ = 7.4 for the first step and a considerably smaller number of $\lg K_{12}$ = 5.1 for the second step, consistent with a distinct negative cooperativity effect as a result of coulombic repulsion and possibly a certain degree of through-bond interactions between adjacent boron centers within the polymer chain. Consistent with the proposed two-step binding process are also the emission data. In the fluorescence spectra, the intensity for the emission at 459 nm decreased abruptly with a new red shifted band emerging at ca. 550 nm during addition of the first equivalent of CN^-. This new band became gradually more intense and shifted to 510 nm. The emergence of a low energy emission band upon complexation of alternating borane binding sites is consistent with recent reports by Wang et al and Müllen et al, who attribute such a behavior to CT between tricoordinated borane and tetracoordinate borate moieties attached to the same conjugated π-system.[66, 26] Moreover, for the all-boron analog PFBT, a similar CT emission was found after addition of one equiv of CN^-, albeit at a slightly shorter wavelength of 475 nm.[59] Upon addition of >1 equivalents of CN^- to PNB_2 the intensity of the CT emission band gradually decreased without any significant wavelength shift. An interesting aspect is the rapid decrease of the original emission band at 459 nm, which almost completely disappears after addition of >0.3 equiv of CN^-. We attribute this apparent amplified quenching effect,

which has been described also for other organoborane polymers [59, 67-70] to efficient energy

transfer to a small number of lower energy CT states that are only weakly emissive.
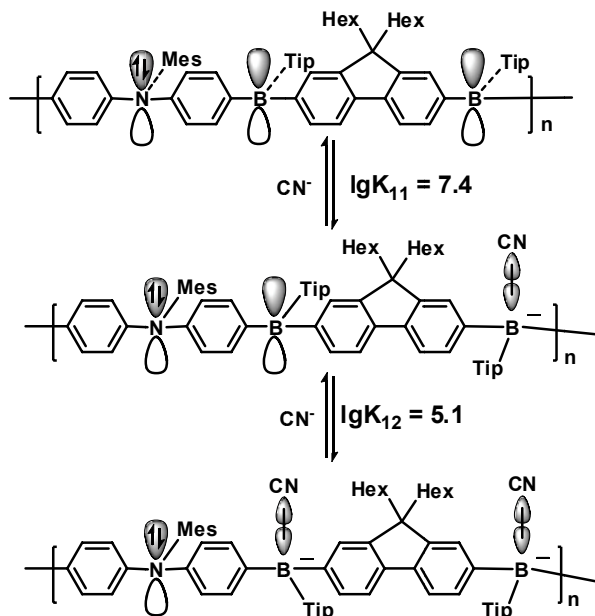
Scheme 1-14. Proposed step-wise complexation of PNB_2 with cyanide
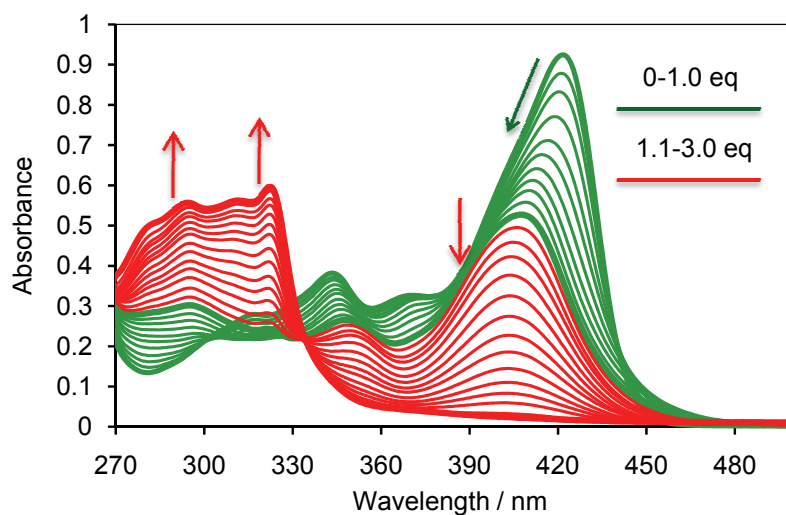
Figure 1-27. Titration of PNB_2 (in THF, 1.22×10^{-5} M per repeating unit (2 boron sites) with [^{n}Bu$_4$N]CN (1.52×10^{-3} M): green plots 0-1.0 eq. of cyanide, red plots 1.1-3.0 eq. of cyanide
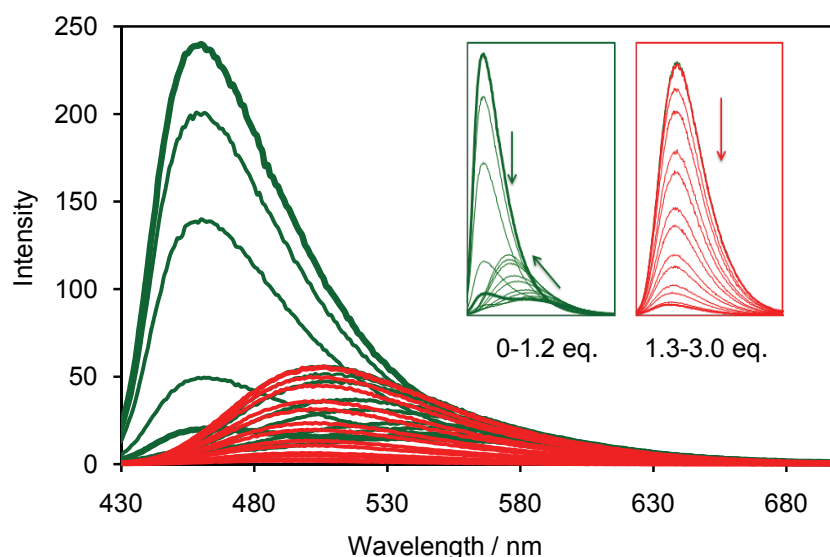
Figure 1-28. Titration of PNB_2 (in THF, 2.44×10^{-5} M per repeating unit (2 boron sites)) with [^{n}Bu$_4$N]CN (1.52×10^{-3} M): green plots 0-1.2 eq. of cyanide, red plots 1.3-3.0 eq. of cyanide

1.4 Conclusions

We have developed a new synthetic route to prepare a highly reactive main chain organoboron polymer PFBBr via an organometallic polycondensation reaction. Reaction of PFBBr with different nucleophiles gave two triarylborane polymers, PFBM and PFBT, and two tetracoordinative organoboron quinolate polymers, PFBQ and PFBQN. Electrochemical studies show that the first reduction in the cyclic voltammetry study corresponds to a LUMO energy level of ca. 2.8 eV, which is about 0.6 eV lower than that

of fluorene homopolymers. The observed enhanced electron affinity is highly desirable for applications in electronic device materials.

Through the same approach, we have also successfully incorporated both electron deficient borane and amine moieties into a polymer chain to afford a main chain ambipolar polymer PNB_2. PNB_2 shows good stability to air and moisture and is thermally stable up to 240 ºC. A phtophysical study reveals a pronounced charge transfer from the nitrogen center to the boron center. As expected for ambipolar compounds, PNB_2 exhibits strong solvatochromic fluorescence and can be reduced and oxidized electrochemically at moderate potentials.

With triarylborane embedded in the main chain, both PFBT and PNB_2 are promising for use as chemosensory materials for anions. Complexation studies showed that PFBT strongly binds to fluoride, cyanide and hydroxide, weakly binds to azide, but for anions such as chloride or bromide, no distinct changes in the absorption and emission spectra were found. Quantitative titration of PFBT and PNB_2 with fluoride and cyanide reveals two distinct binding regimes: the anions first bind to alternating borane sites, which leads to the appearance of a new CT emission, followed by complexation of the remaining borane sites with almost complete quenching of the emission. Interestingly an amplified fluorescence quenching effect was also observed, which might arise from effectively energy transfer to the less emissive charge transfer state.

1.5   Experimental section

Diphenylamine, BBr_3, tetrabutylammonium rhodanide and tetrabutylammonium fluoride (1.0 M in THF) were purchased from Aldrich, ^{n}BuLi (1.6 M in hexanes),

tetrabutylammonium bromide, tetrabutylammonium nitrate from Fisher Scientific, Me_3SnCl from Strem Chemical, tetrabutylammonium hydroxide (40% w/w in methanol) from Alfa Aesar, tetrabutylammonium chloride from Fluka, tetrabutylammonium iodide from MP Biomedical LLC and tetrabutylammonium azide from TCI. 2,7-Dibromo-9,9-dihexylfluorene,[71] mesityl copper,[72-74] tri-isopropylphenyl copper,[75] and 4-(8-methoxyquinolin-5-yl)-N,N-dimethylaniline[76,77] N,N-bis(4-bromophenyl)-2,4,6-trimethylaniline[78], triisopropylphenylcopper (TipCu)[79] were prepared according to literature procedures. All air- or moisture-sensitive reactions and manipulations were carried out under an atmosphere of pre-purified nitrogen using Schlenk techniques or an inert atmosphere glove box (mBraun). Ether solvents were distilled from Na / benzophenone prior to use. Hydrocarbon and chlorinated solvents were purified using a solvent purification system (Innovative Technologies, alumina / copper columns for hydrocarbon solvents), and chlorinated solvents were subsequently distilled from CaH_2 and degassed via several freeze-pump-thaw cycles.

GPC analyses were performed in THF (1 mL/min) using a Waters Breeze system equipped with a 717plus autosampler, a 1525 binary HPLC pump, a 2993 photodiode array detector, and a 2414 refractive index detector. Three styragel columns (Polymer Laboratories; 2×5 μm Mix-C and 5 μm Mix-D), which were kept in a column heater at 35 °C, were used for separation. The columns were calibrated with polystyrene standards (Polymer Laboratories).

GC-MS spectra were acquired on a Hewlett Packard HP 6890 Series GC system equipped with a series 5973 mass selective detector and a series 7683 injector. A temperature profile with a heating rate of 20 °C/min from 70 °C to 280 °C was used. The

MALDI-TOF measurements were performed on an Applied Biosystems 4700 Proteomics Analyzer in reflectron (+)-mode with delayed extraction. Benzo[a]pyrene was used as the matrix (20 mg/mL in toluene). The sample was dissolved in toluene (10 mg/mL), mixed with the matrix in a 1:10 ratio, and then spotted on the wells of a sample plate inside a glove box. Peptides were used for calibration (Des-Arg-Bradykinin (904.4681), Angiotensin I (1296.6853), Glu-Fibrinopeptide B (1570.6774), ACTH (clip 1-17) (2093.0867), ACTH (clip 18-39) (2465.1989), ACTH (clip 7-38) (3657.9294) with α-hydroxy-4-cyanocinnamic acid as the matrix.

UV-visible absorption data were acquired on a Varian Cary 500 UV-Vis / NIR spectrophotometer. The fluorescence data and quantum yields were measured on a Varian Cary Eclipse Fluorescence spectrophotometer with the same solutions as those used in the UV-visible measurements. 9,10-Diphenylanthracene[5] was used as the standard for determination of the quantum yields (Φ). Sample solutions were prepared using a microbalance (±0.1 mg) and volumetric glassware. The quantum yield was calculated by plotting a graph of integrated fluorescence intensity *vs* absorbance of at least four solutions with increasing concentration. The gradient of the graph is proportional to the quantum yield. The quantum yields were corrected for different solvent refractive indices according to the following formula, where η is the refractive indes of the solvent.

$$\Phi = \Phi_{standard} \times [\text{Gradient}_{compound} \times (\eta_{compound})^2] / [\text{Gradient}_{standard} \times (\eta_{standard})^2]$$

Binding constants for the complexation reaction of PNB$_2$ with anion were determined using program Hyperquad^{TM}. The UV-vis absorption titration data was used as the input file and every second wavelenth was selected. The wavelength ranges 280-320 nm and 340-440 nm were considered. The thin film sample for the solid state quantum yield

measurement was prepared by spin coating a polymer solution in toluene onto a quartz slide with a maximal absorbance of 0.3.

Cyclic voltammetry was carried out on a CV-50W analyzer from BAS. The three-electrode system consisted of an Au disk as working electrode, a Pt wire as secondary electrode and a Ag wire as the pseudo-reference electrode. The voltammograms were recorded with ca. 10^{-3} to 10^{-4} M solution in THF (reduction waves) or CH_2Cl_2 (oxidation waves) containing $Bu_4N[PF_6]$ (0.1 M) as the supporting electrolyte. The scans were referenced after the addition of a small amount of ferrocene (reduction cycles) or decamethylferrocene (oxidation cycles) as internal standard. The potentials are reported relative to the ferrocene/ferrocenium couple (0 mV) or decamethylferrocene/decamethylferrocenium ($-$548 mV).

Differential scanning calorimetry (DSC) measurements were performed on a Perkin Elmer Differential Scanning Calorimeter Pyris 1 system with ca. 10 mg of polymer and at a scan rate of 20 °C / min. The results reported are from the second heating cycle. TGA measurements were performed on a Perkin Elmer Pyris 1 Thermogravimetric Analyzer at a scan rate of 10 °C / min and up to 800 °C.

Preparation of 2,7-bis(trimethylsilyl)-9,9-dihexylfluorene (FlSi$_2$): 2,7-Dibromo-9,9-dihexylfluorene (7.26 g, 14.7 mmol) and TMEDA (7.0 mL, 46 mmol) were dissolved in diethyl ether (200 mL) and cooled to -78 °C, followed by slowly adding a solution of *n*-BuLi in hexanes (27.6 mL, 1.6 M, 44.1 mmol). The resulting yellow suspension was allowed to slowly warm up to RT and kept stirring for 1 h. After cooling back to -78 °C again, the reaction was quenched by addition of neat Me$_3$SiCl (4.82 g, 44.3 mmol) and kept stirring over night. After standard aqueous work-up, the product was obtained as a

white solid by crystallization from hot ethanol. Yield: 5.23 g (74%). ^{1}H NMR (499.893 MHz, CDCl$_3$): δ = 7.68 (d, 2H, ^3J = 7.5 Hz, Fl), 7.48 (m, 4H, Fl), 1.97 (m, 4H, Hex), 1.17-1.01 (m, 12H, Hex), 0.78 (t, 6H, ^3J = 7.0 Hz, Hex), 0.67 (br, 4H, Hex), 0.32 (s/d, 18H, ^2J (^{29}Si, ^{1}H) = 62 Hz Me$_3$Si); ^{13}C NMR (125.698 MHz, CDCl$_3$): δ = 150.3, 141.9, 139.3, 131.9, 127.9, 119.3, 55.1, 40.1, 31.5, 29.7, 23.8, 22.6, 14.2, 0.6. ^{29}Si NMR (99.25 MHz, CDCl$_3$): δ = –4.0; GC-MS: (t = 17.3 min), m/z: 478 [M$^+$].

Synthesis of 2,7-bis(dibromoboryl)-9,9-dihexylfluorene (FlB$_2$): At –35 °C, a solution of FlSi2 (2.00 g, 4.18 mmol) in 15 mL of CH$_2$Cl$_2$ was slowly added to a solution of BBr$_3$ (2.75 g, 11.0 mmol) in 2 mL of CH$_2$Cl$_2$. The reaction mixture was allowed to warm to RT and kept stirring for 2 h. The volatile materials were evaporated under high vacuum and the residue was crystallized from hexanes at –35 °C to give the pure product. Yield: 2.30 g (82%). ^{1}H NMR (499.893 MHz, CDCl$_3$): δ = 8.31 (dd, 2H, ^3J = 7.8 Hz, Fl), 8.23 (s, 2H, Fl), 7.89 (d, 2H, ^3J = 7.5 Hz, Fl), 2.10 (m, 4H, Hex), 1.15-0.98 (m, 12H, Hex), 0.77 (t, 6H, ^3J = 7.0 Hz, Hex), 0.65-0.55 (m, 4H, Hex); ^{13}C NMR (125.698 MHz, CDCl$_3$): δ = 152.2, 146.7, 138.3, 137.4, 132.3, 119.9, 55.8, 40.0, 31.6, 29.7, 24.0, 22.7, 14.2; ^{11}B NMR (CDCl$_3$, 160.3 MHz): δ = 57 ($w_{1/2}$ = 2500 Hz); elemental analysis calcd for C$_{25}$H$_{32}$B$_2$Br$_4$: C 44.57, H 4.79; found C 44.38, H 4.73%.

Synthesis of 2,7-bis(trimethylstannyl)-9,9-dihexylfluorene (FlSn$_2$): To a solution of 2,7-dibromo-9,9-dihexylfluorene (15.0 g, 30.5 mmol) and TMEDA (13.80 mL, 91.4 mmol) in 800 mL of ether at –78 ºC was added slowly *n*-BuLi in hexanes (57.1 mL, 1.6 M, 91.4 mmol). The mixture was allowed to warm up to RT and kept stirring for 1 h. After cooling back to –78 ºC, Me$_3$SnCl (20.10 g, 100.5 mmol) in 20 mL of ether was added. The reaction mixture was allowed to warm up to RT, kept stirring over night and

at last was quenched by addition of saturated buffer solution. After standard aqueous work-up, the crude product was re-crystallized from hot ethanol to give colorless crystals. Yield: 15.7 g (78%). ^{1}H NMR (499.893 MHz, CDCl$_3$): δ = 7.67 (d/d, 2H, ^{3}J (^{1}H, ^{1}H) = 7.5 Hz, ^{2}J (^{119}Sn, ^{1}H) = 16 Hz, Fl), 7.44 (dm, 4H, ^{3}J (^{119}Sn, ^{1}H) = 50 Hz, Fl), 1.95 (m, 4H, Hex), 1.15-1.05 (m, 12H, Hex), 0.78 (t, 6H, ^{3}J = 7.0 Hz, Hex), 0.71-0.65 (br, 4H, Hex), 0.33 (s/dd, 18H, ^{2}J ($^{117/119}$Sn, H) = 53/54 Hz, SnMe$_3$); ^{13}C NMR (125.698 MHz, CDCl$_3$): δ = 150.3, 141.5, 141.1, 134.1, 130.4, 119.4, 55.2, 40.2, 31.5, 29.8, 23.9, 22.7, 14.2, 9.1; ^{119}Sn NMR (CDCl$_3$, 186.4 MHz): δ = –25.2.

Synthesis of PFBBr: At –35 °C, a solution of FlSn2 (200 mg, 0.30 mmol) in 5 mL of CH$_2$Cl$_2$ was added to a solution of FlB2 (203 mg 0.30 mmol) in 10 mL of CH$_2$Cl$_2$. The mixture was allowed to warm up to room temperature and kept stirring for 4 h. The volatile materials were removed, and the residue was kept under high vacuum for 12 h. The light yellow solid product was studied by multinuclear NMR spectroscopy and used as outlined below in nucleophilic substitution reactions without further purification. ^{1}H NMR (499.893 MHz, CDCl$_3$): δ = 8.16 (d, 2H, ^{3}J = 7.5 Hz, Fl), 8.07 (s, 2H, Fl), 7.96 (d, ^{3}J = 7.5 Hz, Fl) 2.12 (br, 4H, Hex), 1.40-1.00 (m, 12H, Hex), 0.85-0.70 (m, 10H, Hex); ^{13}C NMR (125.698 MHz, CDCl$_3$): δ = 151.2, 145.3, 140.2, 137.7, 132.3, 120.4, 55.7, 40.5, 31.8, 30.0, 24.3, 22.8, 14.3; ^{11}B NMR (CDCl$_3$, 160.3 MHz): δ = 54 ($w_{1/2}$ = 6800 Hz).

Synthesis of PFBM: The reactive polymer PFBBr, prepared as described above from FlSn2 (200 mg, 0.30 mmol) and FlB2 (203 mg, 0.30 mmol), was re-dissolved in 10 mL of toluene, followed by addition of a solution of 2,4,6-trimethylphenyl copper (MesCu) (111 mg, 0.61 mmol) in toluene (5 mL). The mixture was heated to 120 °C and kept

stirring for 24 h. The precipitate (CuBr) that formed was removed by filtration through a glass frit. The solution was concentrated to 1 mL and precipitated into 100 mL of hexanes. A short neutral alumina column was used to completely remove trace amounts of copper compounds. The product was isolated by freeze-drying from benzene. Yield: 195 mg (70%). ^{1}H NMR (499.893 MHz, CDCl$_3$): δ = 7.83 (m, 4H, Fl), 7.73 (d, 2H, ^3J = 8.0 Hz, Fl), 6.91 (s, 2H, Ph), 2.39 (s, 3H, p-Me), 2.02 (br, 10H, o-Me/Hex), 1.20-1.00 (m, 12H, Hex), 0.80-0.60 (m, 10H, Hex); ^{13}C NMR (125.698 MHz, CDCl$_3$): δ = 151.0 (Mes), 144.6 (Fl), 143.4 (Fl), 142.4 (Fl), 138.5 (Mes), 137.4 (Fl), 132.2 (Fl), 128.4 (Mes), 127.4 (Mes), 120.1 (Fl), 55.4 (Fl), 40.5 (Hex), 31.8 (Hex), 29.9 (Hex), 24.2 (Hex), 23.0 (Hex), 22.7 (Mes^o), 21.5 (Mes^p), 14.2 (Hex-Me); ^{11}B NMR (CDCl$_3$, 160.3 MHz): δ = 59 ($w_{1/2}$ = 6400 Hz); GPC-RI (in THF against PS standards) M_n = 8.8×10^3, M_w = 14.1×10^3, PDI = 1.61; UV-Vis (CH$_2$Cl$_2$, 5.77×10^{-7} M): λ_{max} (ε, M^{-1} cm^{-1}) = 391 (1.93×10^5), 370 nm (1.73×10^5); fluorescence (CH$_2$Cl$_2$): $\lambda_{em,max}$ = 401, 425 nm (λ_{exc} = 370 nm, Φ = 84%); DSC (20 ºC/min, onset): T$_g$ = 119 ºC; TGA (N$_2$, 20 ºC/min): T$_{dec}$ = 212 ºC (onset), 10% residue at 800 ºC.

Synthesis of PFBT: The reactive polymer PFBBr, prepared as described above from FlSn2 (200 mg, 0.30 mmol) and FlB2 (203 mg, 0.30 mmol), was re-dissolved in 10 mL of toluene, and a solution of 2,4,6-triisopropylphenyl copper (TipCu) (194 mg, 0.62 mmol) was added. The mixture was heated to 120 °C and kept stirring for 48 h. A solid precipitate of CuBr was removed by filtration through a glass frit. The product was obtained as a light yellow solid after purification by repeated precipitation from THF into acetone (250 mL). A short neutral alumina column was used to completely remove trace amounts of copper compounds. The product was isolated by freeze-drying from benzene.

Yield: 260 mg, 80 %. ^{1}H NMR (499.893 MHz, CDCl$_3$): δ = 7.90-7.74 (m, 6H, Fl), 7.03 (s, 2H, Tip), 2.98 (pentet, 1H, p-CHMe$_2$), 2.51 (m, 2H, o-CHMe$_2$), 1.99 (br, 4H, Hex), 1.35 (d, 6H, ^{3}J = 7.0 Hz, p-CHMe$_2$), 1.20-0.90 (m, 24H, Hex/o-CHMe$_2$), 0.77 (t, 7.0 Hz, 6H, Hex), 0.65 (br, 4H, Hex); ^{13}C NMR (125.698 MHz, CDCl$_3$): δ = 150.8 (Fl), 149.0 (Tip^m), 148.6 (Tip^p), 144.4 (Fl), 142.9 (Fl), 141.3 (Tip-B), 137.6 (Fl), 132.3 (Fl), 120.2 (Fl), 119.8 (Tip^o), 55.4 (Fl), 40.7 (Hex), 35.7 (Tip), 34.5 (Tip), 31.9 (Hex), 30.0 (Hex), 24.4 (Tip^{m,p}-Me + Hex), 22.8 (Hex), 14.3 (Hex-Me); ^{11}B NMR (CDCl$_3$, 160.3 MHz): δ = 57 ($w_{1/2}$ = 8400 Hz); GPC-RI (in THF against PS standards) M_n = 10.4×10^3, M_w = 17.4×10^3, PDI = 1.68; UV-Vis (CH$_2$Cl$_2$, 5.91×10^{-7} M): λ_{max} (ε, M^{-1} cm^{-1}) = 394 (1.83×10^5), 371 nm (1.15×10^5); fluorescence (CH$_2$Cl$_2$, 5.91×10^{-7} M): $\lambda_{em,max}$ = 399, 423, 447 nm (λ_{exc} = 371 nm, Φ = 81%); TGA (N$_2$, 20 ºC/min): T$_{dec}$ = 237 ºC (onset), 10% residue at 800 ºC.

Synthesis of PFBQ: The reactive polymer PFBBr prepared as described above from FlSn2 (400 mg, 0.61 mmol) and FlB2 (407 mg, 0.61 mmol) was re-dissolved in 10 mL of CH$_2$Cl$_2$, and a solution of 8-methoxyquinoline (194 mg, 1.22 mmol) in 10 mL of CH$_2$Cl$_2$ was added. The reaction mixture was kept stirring over night and then concentrated to ca. 2 mL. The product was obtained as a yellow solid after purification by precipitation into a mixture of hexanes and CH$_2$Cl$_2$ (7:1, v:v). Yield: 421 mg, 72%. ^{1}H NMR (499.893 MHz, CDCl$_3$): δ = 8.55-8.45 (br, 1H, Qu), 8.42-8.35 (br, 1H, Qu), 7.72-7.60 (d, 2H, ^{3}J = 8.0 Hz, Fl), 7.62-7.45 (m, 5H, Fl/Qu), 7.28 (d, 2H, ^{3}J = 7.0 Hz, Fl), 7.21, (br, 2H, Qu), 1.90-1.75 (m, 4H, Hex), 1.15-0.85 (m, 12H, Hex), 0.85-0.55 (m, 10H, Hex); ^{13}C NMR (125.698 MHz, CDCl$_3$): δ = 159.3 (Qu), 150.2 (Fl), 145.6 (Fl), 140.7 (Fl), 139.2 (Qu), 138.6 (Qu), 137.9 (Qu), 133.1 (Fl), 130.6 (Qu), 128.6 (Fl), 127.0 (Qu), 122.8 (Qu), 118.7 (Fl),

112.2 (Qu), 109.8 (Qu), 54.9 (Fl), 40.4 (Hex), 31.8 (Hex), 29.9 (Hex), 24.1 (Hex), 22.7 9

(Hex), 14.3 (Hex-Me); ^{11}B NMR (CDCl$_3$, 160.3 MHz): δ = 10.3 ($w_{1/2}$ = 3200 Hz); GPC-

RI (in THF against PS standards) M_n = 7.9×10^3, M_w = 14.1×10^3, *PDI* = 1.78; UV-Vis

(CH$_2$Cl$_2$, 1.85×10^{-5} M): λ_{max} (ε, M^{-1} cm^{-1}) = 394 (4.97×10^3), 313 (3.04×10^4), 302

(2.28×10^4), 286 (3.41×10^4), 264 nm (5.10×10^4); fluorescence (CH$_2$Cl$_2$, 1.85×10^{-5} M):

$\lambda_{em,max}$ = 504, 338 nm (λ_{exc} = 313 nm, Φ = 21%); DSC (20 ºC/min, onset): T_g = 130 ºC;

TGA (N$_2$, 20 ºC/min): T_{dec} = 282 ºC / 420 ºC (onset), two-step degradation, 14% residue

at 800 ºC.

Synthesis of PFBQN: The reactive polymer PFBBr prepared as described above from

FlSn2 (400 mg, 0.61 mmol) and FlB2 (407 mg, 0.61 mmol) was re-dissolved in 10 mL of

CH$_2$Cl$_2$, and a solution of 4-(8-methoxyquinolin-5-yl)-N,N-dimethylaniline (339 mg,

1.22 mmol) in 5 mL of CH$_2$Cl$_2$ was added. The resulting red solution was kept stirring

over night. The product was purified by repeated precipitation from THF into methanol.

Yield: 476 mg, 63%. ^{1}H NMR (499.893 MHz, CDCl$_3$): δ = 8.56 (d, 1H, ^{3}J = 8.5 Hz, Qu),

8.48 (d, 1H, ^{3}J = 4.5 Hz, Qu), 7.62 (d, 1H, ^{3}J = 8.0 Hz, Qu), 7.58-7.45 (m, 5H, Fl/Qu),

7.37 (d, 2H, ^{3}J = 7.5 Hz, Ph), 7.32 (d, 2H, ^{3}J = 6.0 Hz, Fl), 7.26 (d, 1H, ^{3}J = 9.0 Hz, Qu),

6.66 (d, 2H, ^{3}J = 8.0 Hz, Ph), 3.02 (s, 6H, NMe$_2$), 1.90-1.75 (br, 4 H, Hex), 1.15-0.85 (m,

12H, Hex), 0.78-0.55 (m, 10H, Hex); ^{13}C NMR (125.698 MHz, CDCl$_3$): δ = 158.0 (Qu),

150.2 (Fl), 150.1 (Qu-Ph), 145.8 (Fl), 140.7 (Qu), 139.1 (Fl), 138.1 (Qu), 132.6 (Qu),

130.6 (Fl), 130.5 (Qu-Ph), 127.2 (Qu), 127.1 (Fl), 126.7 (Qu), 126.4 (Qu-Ph), 122.5 (Qu),

118.7 (Fl), 112.9 (Qu + Qu-Ph), 109.8 (Qu), 54.9 (Hex), 40.8 (NMe$_2$), 40.5 (Hex), 31.8

(Hex), 30.0 (Hex), 24.2 (Hex), 22.8 (Hex), 14.3 (Hex-Me); ^{11}B NMR (CDCl$_3$, 160.3

MHz): δ = 9.3 ($w_{1/2}$ = 3300 Hz); GPC-RI (in THF against PS standards) M_n = 10.8×10^3,

M_w = 18.2×10^3, *PDI* = 1.69; UV-Vis (CH$_2$Cl$_2$, 5.1×10^{-5} M): λ_{max} (ε, M^{-1} cm^{-1}) = 444 (1.05×10^3), 314 (8.84×10^3), 288 nm (1.25×10^4); fluorescence (CH$_2$Cl$_2$, 5.1×10^{-5} M): $\lambda_{em,max}$ = 639 nm (λ_{exc} = 439 nm, Φ = 0.1%); DSC (20 ºC/min, onset): T_g = 153 ºC; TGA (N$_2$, 20 ºC/min): T_{dec} = 357 ºC (onset), 27% residue at 800 ºC.

Synthesis of N,N-bis(4-(trimethylstannyl)phenyl)-2,4,6-trimethylaniline (TPASn$_2$): At −78 ºC, a solution of *n*-BuLi in hexanes (1.6M, 5.12mL) was slowly added to a solution of N,N-bis(4-bromophenyl)-2,4,6-trimethylaniline (1.46 g, 3.28 mmol) in 250 mL of ether. The mixture was allowed to warm up to r.t. and kept stirring for an additional 35 min. After cooling back to −78 ºC, the dilithiate intermediate formed was reacted with Me$_3$SnCl (1.63 g, 8.18 mmol) in 20 mL of ether. The reaction mixture was kept stirring over night and 70 mL of saturated buffer solution were then added. After standard aqueous work-up, the crude product was purified by repeated crystallization from ether and ethanol mixture (1v:2v). The product was collected as colorless crystals. Yield: 1.27 g (63%). ^{1}H NMR (499.9 MHz, CDCl$_3$): δ = 7.91 (d, 4H, ^{3}J = 8.0 Hz, Ph), 6.98 (d, 4H, Ph), 6.94 (s, 2H, Mes), 2.33 (s, 3H, ^{p}Me), 2.00 (s, 6H, ^{o}Me) 0.25 ppm (s/d, 18H, ^{2}J ($^{117/119}$Sn, H) = 53/54 Hz, SnMe$_3$); ^{13}C NMR (125.7 MHz, CDCl$_3$): δ = 146.2, 140.1, 137.9, 136.7, 132.8, 130.1, 129.2, 119.5, 21.3, 18.8, −9.3 ppm; ^{119}Sn NMR (CDCl$_3$, 186.4 MHz): δ = −26.4 ppm.

Synthesis of PNB$_2$Br$_2$ & PNB$_2$: TPASn$_2$ (100 mg, 0.16 mmol) was dissolved in 5 mL of toluene and cooled to −35 ºC, followed by addition of a pre-cooled solution of FlB$_2$ (110 mg 0.16 mmol) in 10 mL of toluene. The mixture was slowly warmed up to room temperature and kept stirring over night. The by-product Me$_3$SnBr was fully removed under high vacuum. The light yellow solid product was studied by ^{1}H NMR spectroscopy.

^{1}H NMR (499.9 MHz, CDCl$_3$): δ = 8.02-7.96 (m, 8H, Fl+Ph), 7.86 (d, ^{3}J = 7.5 Hz, 2H, Fl), 7.17 (d, 4H, ^{3}J = 7.5 Hz, Ph), 7.02 (s, 2H, Mes), 2.31 (s, 3H, ^{p}Me), 2.08 (m, 10H, ^{o}Me+Hex), 1.15-1.05 (m, 12H, Hex), 0.85-0.75 ppm (m, 10H, Hex). Without further purification, the crude material was re-dissolved in 10 mL of toluene, followed by addition of a solution of TipCu (105 mg, 0.39 mg) in 5 mL of toluene. The mixture was slowly heated to 115 °C and kept stirring for 2days. After cooling back to room temperature, the solid by-product was removed by passing the mixture through a short celite column. The clear filtrate was concentrated to less than 1 mL and precipitated into 100 mL of acetone. The product was collected as a yellow powder. Yield: 91 mg (53%).

^{1}H NMR (499.9 MHz, CDCl$_3$): δ = 7.77 (s, 4H, Fl), 7.68 (t, 4H, Fl+Ph), 7.10 (d, 4H, ^{3}J = 8.0Hz, Ph), 6.98 (s, 4H, Tip), 6.95 (s, 4H, Mes), 2.93 (m, 2H, ^{p}CH), 2.47 (m, 4H, ^{o}CH), 2.31 (s, 3H, ^{p}Me), 1.99 (s, 6H, ^{o}Me), 1.92 (br, 4H, Hex), 1.31 (d, 12H, ^{p}CHMe$_2$), 1.15-0.90 (m, 36H, ^{o}CHMe$_2$+Hex), 0.69 (t, 6H, ^{3}J = 3Hz, Hex), 0.58 ppm (br, 4H, Hex); ^{13}C NMR (125.7 MHz, CDCl$_3$): δ = 150.7, 148.9, 148.7, 148.3, 144.0, 142.8, 141.5, 140.1, 139.6, 137.5, 136.8, 136.0, 131.8, 130.2, 128.6, 120.1, 119.6, 118.8, 55.2, 40.5, 35.5, 34.4, 31.7, 29.8, 24.4, 24.3, 24.0, 22.8, 18.5, 14.2 ppm; ^{11}B NMR (CDCl$_3$, 160.3 MHz): δ = 56 ppm ($w_{1/2}$ = 8000 Hz); GPC-RI (in THF against polystyrene standards) Mn = 1.23×10^4, M_w = 2.85×10^4, PDI = 2.31; CV (CH$_2$Cl$_2$, 0.1M Bu$_4$N[PF$_6$], 100 mV/s, vs. Fc/Fc$^+$ couple): $E_{1/2}$(1) = 0.67 V (E_p = 111 mV); CV (THF, 0.1M Bu$_4$N[PF$_6$], 100 mV/s, vs. Fc/Fc$^+$ couple): $E_{1/2}$(1) = −2.35 V (E_p = 192 mV) and $E_{1/2}$(2) = −2.79 V (E_p = 322 mV); UV-Vis (CH$_2$Cl$_2$): λ_{max} (ε) = 422 (79 900), 344 nm (35 100 mol^{-1}·cm^{-1}) ; fluorescence

(CH$_2$Cl$_2$): $\lambda_{em,max}$ = 468 nm (λ_{exc} = 422 nm, Φ = 10%); TGA (N$_2$, 10 ºC/min): T$_{dec}$ = 237 ºC (onset), 6% residue at 800 ºC.

1.6   References

(1)   Corriu, R. J.-P.; Deforth, T.; Douglas, W. E.; Guerreroa, G.; Siebert, W. S. *Chem. Comm.* 1998, 963.

(2)   Matsumi, N.; Naka, K.; Chujo, Y. *J. Am. Chem. Soc.* 1998, *120*, 5112.

(3)   Matsumi, N.; Miyata, M.; Chujo, Y. *Macromolecules* 1999, *32*, 4467.

(4)   Sato, N.; Ogawa, H.; Matsumoto, F.; Chujo, Y.; Matsuyama, T. *Syn. Met.* 2005, *154*, 113.

(5)   Entwistle, C. D.; Batsanov, A. S.; Howard, J. A. K.; Fox, M. A.; Marder, T. B. *Chem. Comm.* 2004, 702.

(6)   Matsumi, N.; Chujo, Y.; Lavastre, O.; Dixneuf, P. H. *Organometallics* 2001, *20,* 2425.

(7)   Matsumoto, F.; Matsumi, N.; Chujo, Y. *Polym. Bull.* 2001, *46*, 257.

(8)   Lorbach, A.; Bolte, M.; Li, H.; Lerner, H.-W.; Holthausen, M. C.; Jäkle, F.; Wagner, M. *Angew. Chem. Int. Ed.* 2009, *48*, 4584.

(9)   Matsumi, N.; Naka, K.; Chujo, Y. *J. Am. Chem. Soc.* 1998, *120,* 10776.

(10)   Matsumi, N.; Umeyama, T.; Chujo, Y. *Polym. Bull.* 2000, *44*, 431.

(11)   Braunschweig, H.; Dirk, R.; Müller, M.; Nguyen, P.; Resendes, R.; Gates, D. P.; Manners, I. *Angew. Chem. Int. Ed.* 1997, *36*, 2338.

(12)   Heilmann, J. B.; Scheibitz, M.; Qin, Y.; Sundararaman, A.; Jäkle, F.; Kretz, T.; Bolte, M.; Lerner, H.-W.; Holthausen, M. C.; Wagner, M. *Angew. Chem. Int. Ed.* 2006, *45*, 920.

(13)   Heilmann, J. B.; Qin, Y.; Jäkle, F.; Lerner, H.-W.; Wagner, M. *Inorg. Chim. Acta* 2006, *359*, 4802.

(14)   Niu, W.; Smith, M. D.; Lavigne, J. J. *J. Am. Chem. Soc.* 2006, *128*, 16466.

(15)   Sundararaman, A.; Victor, M.; Varughese, R.; Jäkle, F. *J. Am. Chem. Soc.* 2005, *127*, 13748.

(16)   Neher, D. *Macromol. Rapid Commun.* 2001, *22*, 1365.

(17)   Entwistle, C. D.; Marder, T. B. *Chem. Mater.* 2004, *16*, 4574.

(18)   Jäkle, F. *Coord. Chem. Rev.* 2006, *250*, 1107.

(19)   Yamaguchi, S.; Wakamiya, A. *Pure Appl. Chem.* 2006, *78*, 1413.

(20)   Elbing, M.; Bazan, G. C. *Angew. Chem. Int. Ed.* 2008, *47*, 834.

(21)   Yu, W.; Pei, J.; Huang, W.; Heeger, A. J. *Adv. Mater.* 2000, *12*, 828.

(22)   Jung, B.-J.; Lee, J.-I.; Chu, H.-Y.; Do, L.-M.; Shim, H.-K. *Macromolecules* 2002, *35*, 2282.

(23)   Qin, Y.; Kiburu, I.; Shah, S.; Jäkle, F. *Macromolecules* 2006, *39*, 9041.

(24)   Li, H.; Sundararaman, A.; Venkatasubbaiah, K.; Jäkle, F. *J. Am. Chem. Soc.* 2007, *129*, 5792.

(25)   Yamaguchi, I.; Choi, B. J.; Koizumi, T. A.; Kubota, K.; Yamamoto, T. *Macromolecules* 2007, *40*, 438.

(26)   Zhao, G.; Baumgarten, M.; Müllen, K. *J. Am. Chem. Soc.* 2008, *130*, 12477.

(27)   Principles of Fluorescence Spectroscopy; 2nd ed.; Lakowicz, J. R.; Plenum Publishing Corporation, 1999.

(28)   Braun, D.; Heeger, A. J. *Appl. Phys. Lett.* 1991, *58*, 1982.

(29)   Kraft, A.; Burn, P. L.; Holmes, A. B.; Bradley, D. D. C.; Friend, R. H.; Martens, J. H. F. *Synth. Met.* 1993, *72*, 4163.

(30)   Antomiadis, H.; Abkowitz, M. A.; Hsieh, B. R. *Appl. Phys. Lett.* 1994, *65*, 2030.

(31)   Meyer, H.; Haarer, D.; Naarmann, H.; Hörhold, H. H. *Phys. Rev.B* 1995, *52*, 2587.

(32)   Blom, P. W. M.; de Jong, M. J. M.; Vleggaar, J. J. M. *Appl. Phys. Lett.* 1996, *68*, 3308.

(33)   Yang, Y.; Pei, Q.; Heeger, A. J. *J. Appl. Phys.* 1996, *79*, 934.

(34)   Martens, H. C. F.; Huiberts, J. N.; Blom, P. W. M. *Appl. Phys. Lett.* 2000, *77*, 1852.

(35)   Wöhrle, D.; Meissner, D. *Adv. Mater.* 1991, *3*, 129.

(36)   Meier, H. *Angew. Chem. Int. Ed.* 2005, *44*, 2482.

(37)   Günes, S.; Neugebauer, H.; Sariciftci, N. S. *Chem. Rev.* 2007, *107*, 1324.

(38)   Li, Y.; Zou, Y.; *Adv. Mater.* 2008, *20*, 2952.

(39)   Devasagayaraj, A.; Tour, J. M. *Macromolecules* 1999, *32*, 6425.

(40)   Blouin, N.; Michaud, A.; Gendron, D.; Wakim, S.; Blair, E.; Neagu-Plesu, R.; Belletête, M.; Durocher, G.; Tao, Y.; Leclerc, M. *J. Am. Chem. Soc.* 2008, *130*, 732.

(41)   Peng, Q.; Park, K.; Lin, T.; Durstock, M.; Dai, L. *J. Phys. Chem. B* 2008, *112*, 2801.

(42)   Bürgi, L.; Turbiez, M.; Pfeiffer, R.; Bienewald, F.; Kirner, H.-J.; Winnewisser, C. *Adv. Mater.* 2008, *20*, 2217.

(43)   Zaumseil, J.; Sirringhaus, H. *Chem. Rev.* 2007, *107*, 1296.

(44)   Huang, F.; Chen, K.-S.; Yip, H.-L.; Hau, S. K.; Acton, O.; Zhang, Y.; Luo, J.; Jen, A. K.-Y. *J. Am. Chem. Soc.* 2009, *131*, 13886.

(45)   Zhang, K.; Tao, Y.; Yang, C.; You, H.; Zou, Y.; Qin, J.; Ma, D. *Chem. Mater.* 2008, *20*, 7324.

(46)   Yuan, Z.; Collings, J. C.; Taylor, N. J.; Marder, T. B.; Jardin, C.; Halet, J.-F. *J. Solid State Chem.* 2000, *154*, 5.

(47)   Entwistle, C. D.; Marder, T. B.; *Angew. Chem. Int. Ed. En.* 2002, *41*, 2927.

(48)   Entwistle, C. D.; Marder, T. B. *Chem. Mater.* 2004, *16*, 4574.

(49)   Hudson, Z. M.; Wang, S. *Acc. Chem. Res.* 2009, *42*, 1584.

(50)   Shirota, Y.; Kinoshita, M.; Noda, T.; Okumoto, K.; Ohara, T. *J. Am. Chem. Soc.* 2000, *122*, 11021.

(51)   Doi, H.; Kinoshita, M.; Okumoto, K.; Shirota, Y. *Chem. Mater.* 2003, *15*, 1080.

(52)   Sundararaman, A.; Varughese, R.; Li, H.; Zakharov, L. N.; Rheingold, A. L.; Jäkle, F.; Organometallics 2007, *26*, 6126.

(53)   Stahl, R.; Lambert, C.; Kaiser, C.; Wortmann, R.; Jakober, R. *Chem. Eur. J.* 2006, *12*, 2358.

(54)   Bai, D.; Liu, X.; Wang, S. *Chem. Eur. J.* 2007, *13,* 5713.

(55)   Cao, D.; Liu, Z.; Li, G.; Liu, G.; Zhang, G. *J. Mol. Struct.* 2008, *874,* 46.

(56)   Branger, C.; Lequan, M.; Lequan, R. M.; Large, M.; Kajzar, F. *Chem. Phys. Lett.* 1997, *272*, 265.

(57)   Mutaguchi, D.; Okumoto, K.; Ohsedo, Y.; Moriwaki, K.; Shirota, Y. *Org. Electron.* 2003, *4,* 49.

(58)   Reitzenstein, D.; Lambert, C. *Macromolecules* 2009, *42,* 773.

(59)   Li, H.; Jäkle, F. *Angew. Chem. Int. Ed.* 2009, *48*, 2313.

(60)   Doty, J. C.; Babb, B.; Glogowski, M. E.; Williams, J. L.; Grisdale, P. J.; *J. Organomet. Chem.* 1972*,* 38.

(61)   Wakamiya, A.; Mori, K.; Yamaguchi, S. *Angew. Chem. Int. Ed.* 2007, *46*, 4273.

(62)   Elbing, M.; Bazan, G. C. *Angew. Chem. Int. Ed.* 2008, *47*, 834.

(63)   Stahl, R.; Lambert, C.; Kaiser, C.; Wortmann, R.; Jakober, R. *Chem. Eur. J.* 2006, *12*, 2358.

(64)   Jia, W. L.; Feng, X. D.; Bai, D. R.; Lu, Z. H.; Wang, S. N.; Vamvounis, G.; *Chem. Mater.* 2005, *17*, 164.

(65)   Li, F.; Jia, W.; Wang, S.; Zhao, Y.; Lu, Z.-H. *J. Appl. Phys.* 2008, *103*, 034509.

(66)   Zhao, S.-B.; Wucher, P.; Hudson, Z. M.; McCormick, T. M.; Liu, X.-Y.; Wang, S.; Feng, X.-D.; Lu, Z.-H. *Organometallics* 2008, *27,* 6446.

(67)   Miyata, M.; Chujo, Y. *Polym. J.* 2002, *34*, 967.

(68)   Sundararaman, A.; Victor, M.; Varughese, R.; Jäkle, F. *J. Am. Chem. Soc* 2005, *127*, 13748.

(69)   Bonifacio, V. D. B.; Morgado, J.; Scherf, U. *J. Polym. Sci. Part A, Polym. Chem.* 2008, *46*, 2878.

(70)   Liu, W.; Pink, M.; Lee, D. *J. Am. Chem. Soc.* 2009, *131*, 8703.

(71)   Ranger, M.; Rondeau, D.; Leclerc, M. *Macromolecules*, 1997, 30, 7686.

(72)   Tsuda, T.; Yazawa, T.; Watanabe, K.; Fujii, T.; Saegusa, T. *J. Org. Chem.* 1981, *46*, 192.

(73)   Gambarotta, S.; Floriani, C.; Chiesi-Villa, A.; Guastini, C. *J. Chem. Soc., Chem. Commun.* 1983, 1156.

(74)   Eriksson, H.; Håkansson, M. *Organometallics* 1997, *16*, 4243.

(75)   Nobel, D.; van Koten, G.; Spek, A. L. *Angew. Chem.* 1989, *101*, 211.

(76)   Gershon, H.; McNeil, M. W.; Schulman, S. G. *J. Org. Chem.* 1972, *37*, 4078.

(77)   Pohl, R.; Montes, V. A.; Shinar, J.; Anzenbacher Jr., P. *J. Org. Chem.* 2004, *69*, 1723.

(78)   Hooper, M. W.; Utsunomiya, M.; Hartwig, J. F. *J. Org. Chem.* 2003, *68*, 2861.

(79)   Nobel, D.; van Koten, G.; Spek, A. L. *Angew. Chem.* 1989, *101*, 211.

(80)   Handbook of Photochemistry; 3rd ed.; Montalti, M.; Credi, A.; Prodi, L.; Gandolfi, M. T., Eds.; Taylor & Francis: New York, 2006.

Chapter 2. Diarylboryl Functionalized Bithiophene-Based Homo- and Copolymers

We have demonstrated a series of main-chain organoboron CPs based on fluorene in the previous chapter, which exhibit interesing luminescent properties and are potential

candidates for sensory materials. Polythiophenes (PTs) represent another important class of organic semiconducting materials. Unlike fluorene-based CPs, for which incorporation of substituent groups at the 9-position has little effect on the main-chain conformation and electronic structures, PTs tend to change their conformation upon modification with different substituents at the β-position(s) of the thiophene rings through steric or electronic interactions. Therefore, the second part of this thesis is focused on the structure-property relationship of organoborane functionalized PTs including: i) the influence of dimesitylboryl functionality on the electronic structure of PTs, ii) tuning of the electronic and structural properties by introducing redox active ferrocenylboryl groups and iii) the influence of copolymerization of bis(dimesitylboryl)-bithiophene with different aromatic molecules on the photophysical and electrochemical properties.

2.1 Introduction to PTs

Recent research on PTs has been mainly focused on their semiconducting, conducting, luminescence and sensing properties and covers a wide range of areas from electronic and optoelectronic devices to chemical and biological sensors. The successful applications of PTs in materials science arise from the great diversity of thiophene-based chemical structures. They can be easily modified at the α position, β position and even at the sulphur atom itself, and thus the processability and electronic structure can be fine-tuned through the chemical structure variation.[1-3]

However, unsubstituted PT is an insoluble and infusible material, which means that it hardly has any practical applications. The solubility can be greatly enhanced by the substituent groups at the β position(s). In fact, substitution at the β-position of the

thiophene ring not only confers processability to PTs, but can also be used to refine their electro-optical properties through electronic and steric interactions. In addition, PTs with different functionalities can be prepared through post-polymerization modifications or direct polymerization of the functional thiophene monomers. Several substituent groups that have been used to modify the processability, optical and electrical properties of PTs are summarized here.

2.1.1 Long alkyl groups: to improve the solubility, to insulate conjugated chains and to control the conjugation

Polymerization of asymmetric 3-substituted thiophene results in three different types of coupling patterns along the polymer chain i.e., head to tail (HT), head to head (HH) and tail to tail (TT) (**Figure 2-1**). Common polymerization methods including oxidative polymerization and metal catalyzed polycondensation afford all three possible types of isomers. Although HT coupling is somewhat preferred due to steric and electronic effects, the presence of a small amount of HH coupling generally leads to twisted conformations with concomitant loss of conjugation.

Head to tail (HT)   **Head to head (HH)**   **Tail to tail (TT)**
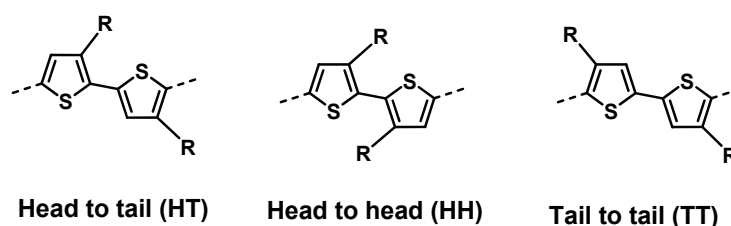
Figure 2-1. Three coupling patterns for poyl(3-substituted thiophene)

The first regioregular poly(3-alkylthiophene) rrPAT was synthesized by McCullough et al.[1,2] As shown in **Scheme 2-1**, the reaction relies on the regiospecific metallation of

2-bromo-3-R-thiophene with lithium diisopropylamide (LDA) at 5-position. After transformation into the Grignard derivative, the monomer was polymerized by using Kumada cross-coupling reaction to afford a rrPAT. Since then, several other cross coupling methods were also reported for preparation of rrP3AT, including Stille[3] and Suzuki[4] coupling. Rieke et al. also demonstrated the synthesis of rrP3AT by use of reactive "Rieke Zinc" species.[5,6] The regioregular structure effectively improves planarization of the backbone and well-defined, organized three-dimensional polycrystalline structures can be achieved during the solid state assembly. This brings about not only the development of a wide variety of new functional PTs, but also a dramatic enhancement in the electrical properties of rrP3ATs.[7,8]

LDA = lithium diisopropylamide
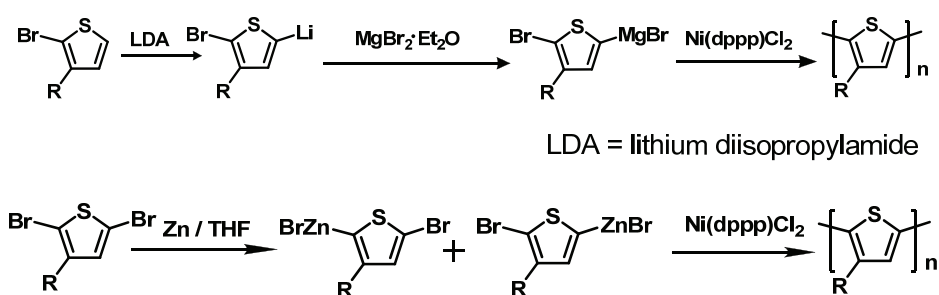
Scheme 2-1. McCullough and Rieke routes to rrPAT

Although the substitution on the thiophene rings can improve the solubility of the PTs, bulky side chains on PATs may cause an undesirable conformation change of the backbone and reduce the conjugation and electronic conductivity. For example, poly(3-cyclohexylthiophene) (**P2-1**) (**Figure 2-2**) prepared by Wegner and coworkers was much less conjugated (80 nm blue shift) in the solid state relative to rrP3HT.[9] Consequently, the conductivity in the doped state is much lower than that for rrP3HT. Similarly, a PT containing annulated cyclohexyl ring, poly(3,4-cyclohexylthiophene) (**P2-2**) (**Figure 2-**

2), also exhibits lower conductivity.[10] But when the bulky group is far enough removed from the backbone, then the conjugation is relatively unaffected as illustrated in a study by Guillerez and coworkers.[11]

P2-1   **P2-2**
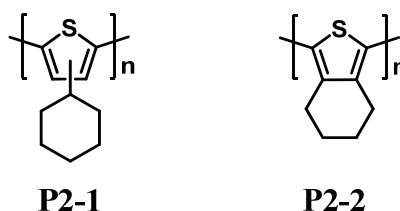
Figure 2-2. Chemical structures of **P2-1** and **P2-2**

On the other hand, by using different numbers and different sizes of substituents on the thiophene rings, one is able to control the conjugation length and tune the absorption and emission of the materials. Andersson et al. have prepared a family of polymers (**P2-3** to **P2-11**), as shown in **Figure 2-3**, to achieve electroluminescence covering the whole visible spectrum.[12] Such wide variation in the emission color of homopolymers is remarkable and cannot be achieved with other CPs (except via copolymer approaches).[13] This is because the PT emission color closely relies on the effective conjugation length determined by the twist angle between the thiophene units.
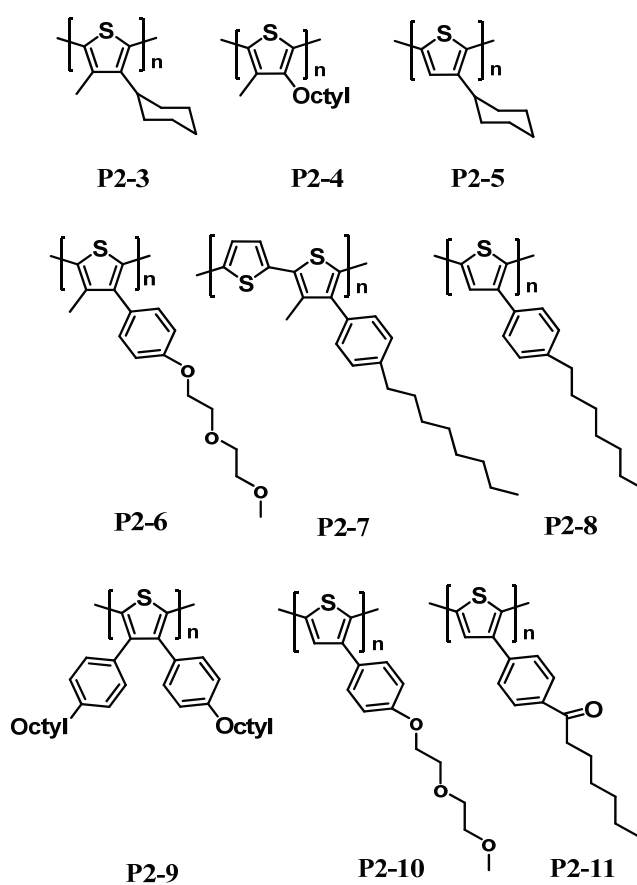
Figure 2-3. Tuning of the electroluminescence of PTs via substituent groups
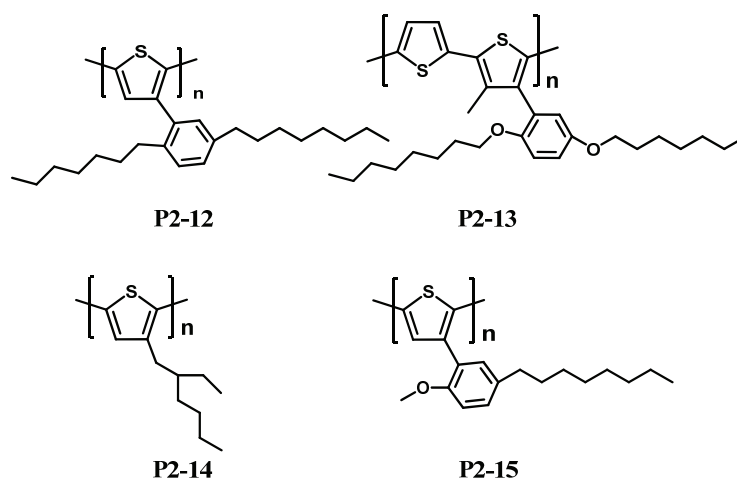
Figure 2-4. Examples of PTs with sterically demanding side chains

Another reason to introduce bulky side chain is to prevent close contact between the conjugated chains, namely to insulate the polymer main chains. The interactions between the conjugated chains may lead to undesirable non-radiative recombination of excited states and increase the chance for luminescence quenching, which is responsible for the luminescence intensity decrease when going from solutions to thin films of PTs. For example, McCullough et al. have prepared polymer **P2-12**, with a bulky dioctylphenyl group as the side chain.[14] Such an arrangement resulted in a very high luminescence quantum yield in both solution and thin film forms because the long alkyl chains effectively separate the conjugated chains in all three dimensions. PTs with other substituent groups shown in **Figure 2-4** gave relatively lower photoluminescence efficiencies compared to **P2-12**. For polymers **P2-14** and **P2-15**, the side chains are less bulky, so the main chains were separated by a shorter distance. The chain-chain separation for **P2-13** is smaller because of the presence of unsubstituted thiophenes.

P2-16   **P2-17**
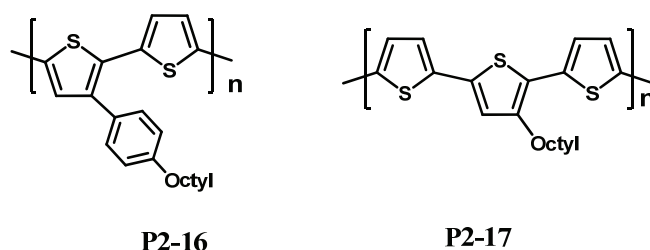
Figure 2-5. Examples of PTs with low density of side chains

Although increasing the size or the number of side chains on PTs can lead to high luminescence quantum yields in the solid state, low density of side chains may be required in other cases. As shown in the previous studies, when all the thiophene rings are substituted to give good processability in the undoped state, the stability of the doped polymer is dramatically decreased,[15-17] and a thermal dedoping process is encountered. In

contrast, unsubstituted PTs are stable in both undoped and doped states.[18,19] Thus, it is desirable to prepare substituted PTs with low density of side chains without compromising the solubility. For instance, copolymerization of 3-methylthiophene and 3-octylthiophene gave a polymer with higher stability against thermal dedoping than the homopolymer of 3-octylthiophene, P3OT.[20,21] And also a better way to lower the concentration of the side chains along the polymer backbone is to directly polymerize mono-substituted thiophene dimer, trimer or tetramer.[22] The obtained polymers **P2-16** and **P2-17** shown in **Figure 2-5** exhibited similar processability and mechanical properties as P3OT.

2.1.2 Heteroatom containing side chains as sensing elements

The ability of PTs to change their color and electrical conductivity in response to various analytes makes them ideal candicates for sensory materials. The side chains, in this respect, are introduced as sensing probes or analyte receptors. They are commonly heteratom containing groups including open long alkoxy chains (**P2-19**, **P2-25**), annulated oligo(oxyethylene) groups (**P2-18**, **P2-20**, **P2-22**, **P2-23**), crown ether derivatives (**P2-21)**, calixarene (**P2-24**) and thymine (**P2-16**) functional groups, etc. Representative structures of these polymers[23,24] are shown in **Figure 2-6**.

P2-18 **P2-19** **P2-20** **P2-21**

P2-22 **P2-23**

P2-24 **P2-25** **P2-26**
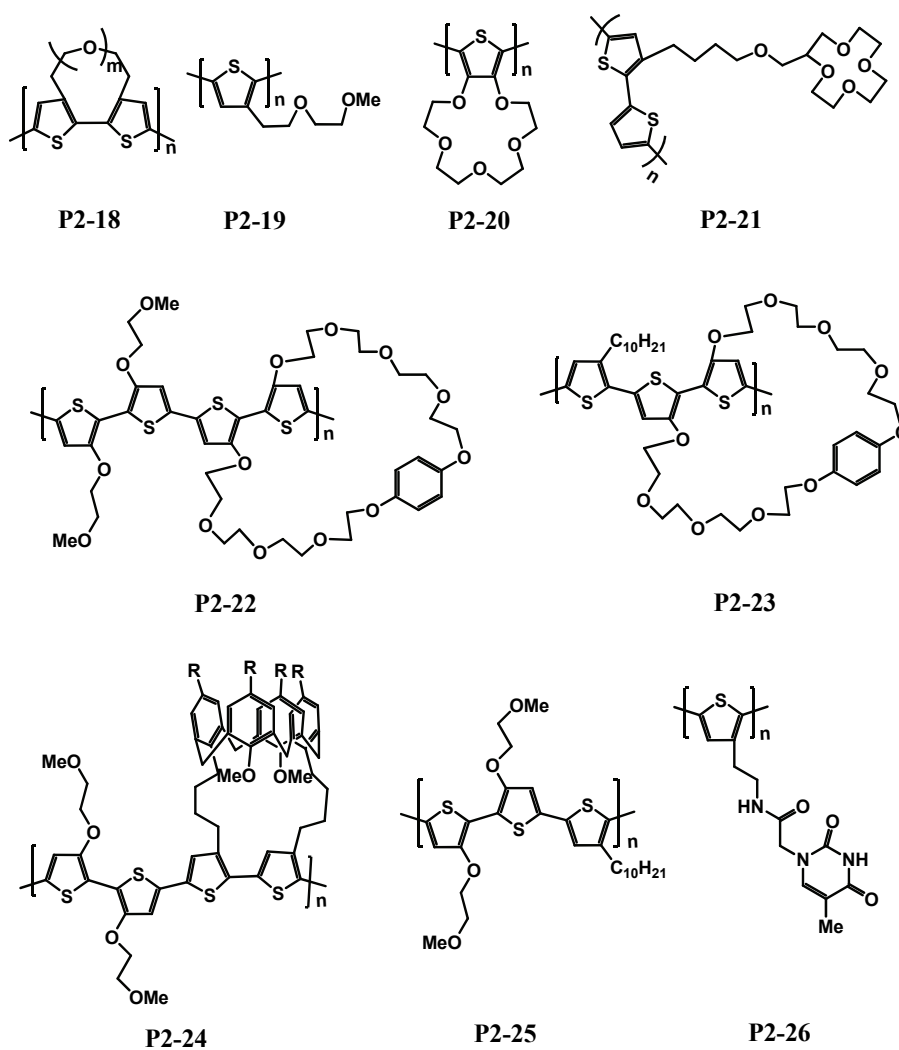
Figure 2-6. Representative examples of PTs possessing molecular recognition properties

P2-27 **P2-28** **P2-29**
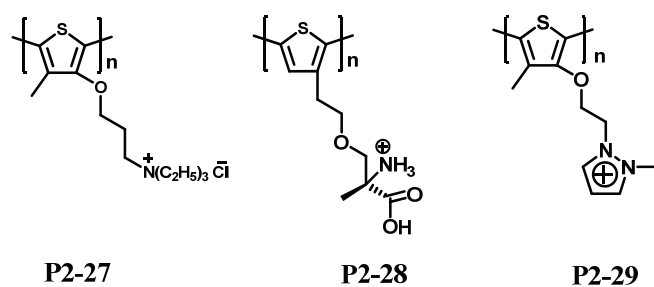
Figure 2-7. Chemical structure of some cationic PTs

As important sensory materials, PTs can also be exploited in biosensors for the detection of biological molecules. In this regard, utilization of water-soluble conjugated polymers would be more useful for *in situ* detection, therefore different cationic side chains were introduced (**Figure 2-7**).[25,26] Mixing ssDNA with cationic polythiophenes (**P2-27**, **P2-28**, **P2-29**) leads to the formation of stable aggregates containing an optical (chromic) transducer and a DNA probe, which can be used to detect oligonucleotides. When they bind to artificial nucleic acid ligands (aptamers), PTs can also be used as protein sensors. In both cases, no chemical modification is required for either probes or analytes, which is greatly advantageous.[27]

2.1.3 Conjugated side chains to improve the absorption and lower the band gap

The carrier mobility of conjugated polymers plays a critical role in high performance polymer solar cells. Compared to the high mobility for the intramolecular charge transport along the polymer chain, interchain hopping tends to be much slower, which can be overcome in the materials with two or three-dimensional conjugated structures. In addition, multi-dimensional conjugation can also effectively lower the band-gap and broaden the absorption spectra of the polymers. For example, two soluble polythiophenes, **P2-30** and **P2-31** (**Figure 2-8**), bearing conjugated side chains, were synthesized via Grignard methathesis (GRIM) method by Li et al.[28] The vinylene and acetylene linkers here reduce the steric hindrance between the main chain and the side chain, which results in smaller energy gaps due to a better co-planarity in comparison with phenyl groups directly attached at the β position.[29]
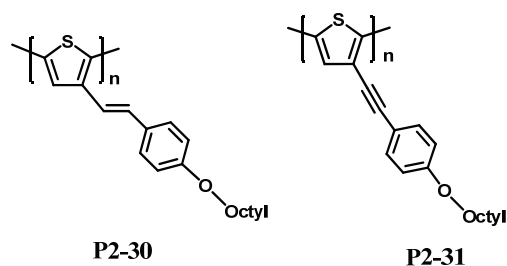
Figure 2-8. Examples of PTs with conjugated side chain

Bo and coworkers have prepared several PTs with electron-donating carbazole side chains via Stille coupling reaction.[30] The polymers exhibit broad absorptions in the visible region. Remarkably, the phase separation for blends with [6,6]-phenyl-C_{61}-butyric acid methyl ester ($PC_{61}BM$) was minimized due to the steric hindrance effect of the rigid side chains that attached to the conjugated main chain. A photovoltaic cell fabricated from the three-component copolymer **P2-32** (**Scheme 2-2**) and $PC_{61}BM$ gave a power conversion efficiency of 0.86%.
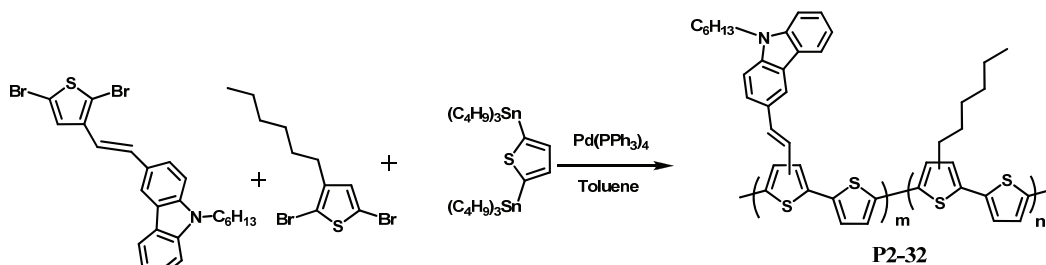
Scheme 2-2 Synthesis of PTs with carbazole containing conjugated side chains
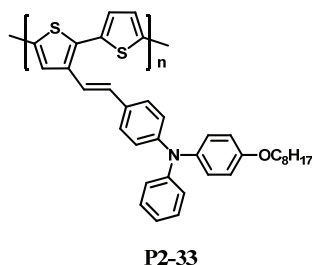
P2-33

Figure 2-9. Examples of PTs with triphenylamine-containing conjugated side chains

Polythiophene **P2-33** with electron-donating triphenylamine derivatives attached through a vinylene linker (**Figure 2-9**) have also been published by Li and coworkers.[31] A broad absorption from 350 nm to 640 nm was found. The power conversion efficiency of the polymer solar cell based on the **P2-33**/$PC_{61}BM$ (1:1, w/w) blend was 0.21%. The hole mobility for an FET based on **P2-33** was 1.6×10^{-4} cm^2 V^{-1}. While substituted with another electron-donating group, phenothiazine-vinylene group, **P2-34** exhibited an absorption covering a broader range (from 250 nm to 650 nm) and the hole mobility based on an FET measurement was improved to 6.8×10^{-3} $cm^2 S^{-1} V^{-1}$ (**Figure 2-10**).[32]

P2-34
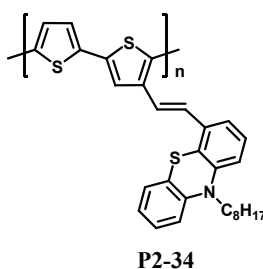
Figure 2-10. PT with conjugated phenothiazine-vinylene side chains

To systematically investigate the influence of the conjugated side chains on the photophysical properties of PTs, Li and coworkers have prepared a family of PTs with different length and different density of conjugated side chains along the main chains. All the polymers shown in **Figure 2-11** exhibit two bands attributed to the absorption of the conjugated side chain and distorted main chain, respectively. The study shows that the high energy absorption band becomes red shifted by increasing the side chain length, while lowering the ratio of the substituted thiophene causes the low energy absorption band to become more intense and red-shifted.[33]
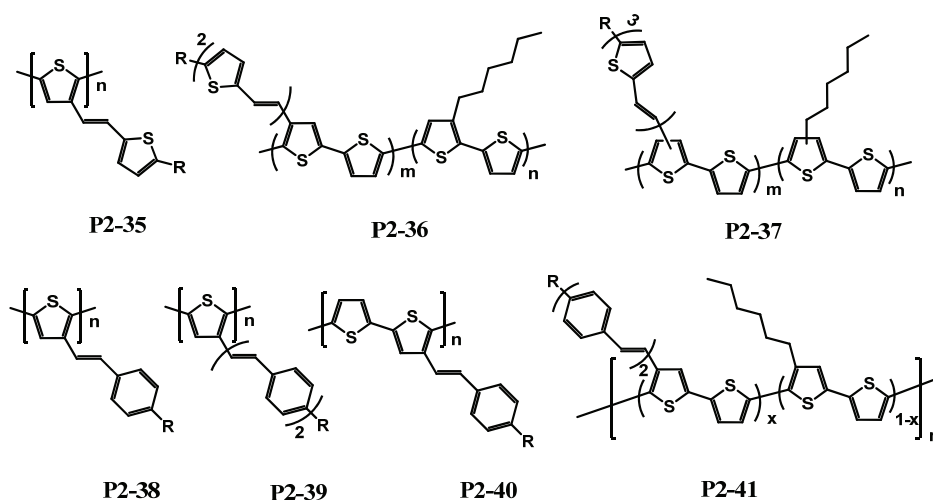
Figure 2-11. PTs with conjugated thienylenevinylene and phenylvinylene side chains

Recently, Chen et al. have reported the synthesis of two-dimensional PTs with conjugated oligothiophene side chains attached to the polythiophene main chain, **P2-42a** and **P2-42b** (**Figure 2-12**).[34] Thin film transistor measurements indicated that **P2-42a** and **P2-42b** have a hole mobility of 3.5×10^{-4} and 4.6×10^{-3} cm^{2}S^{-1}V^{-1}, respectively. A polymer solar cell comprising **P2-42a** and 6,6-phenyl-C$_{71}$ butyric acid methylester (PC$_{71}$BM) (1w/3w) exhibits a promising power conversion efficiency of 2.5%.
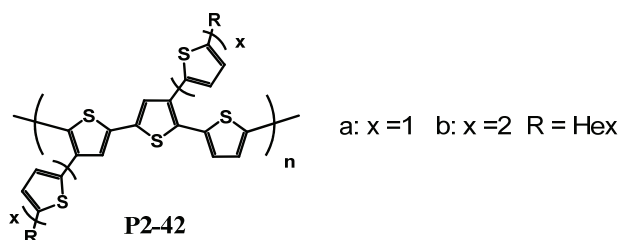
Figure 2-12. Examples of two-dimensional conjugated PTs

Dependent on the applications, other types of functional groups are also introduced. For example, PTs with pendant hydroxyl groups can be used as reactive intermediates for developing other functional polythiophene derivatives.[35] Studies showed that acid-base

equilibria can also influence the conformation of the polymer backbone in polythiophene derivatives, which has been applied to prepare several pH sensitive sensors **P2-43**, **P2-44** and **P2-45** (**Figure 2-13**). Additionally, fused ring systems, which represent another specific type of PT derivatives, have been widely used for developing ambipolar CPs and low band gap CPs.[36]

P2-43   **P2-44**   **P2-45**
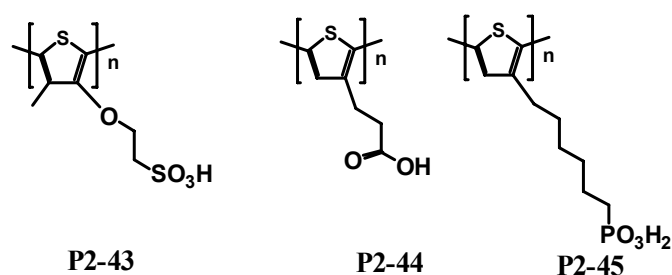
Figure 2-13. Examples of pH sensitive PTs

2.2   Diarylboryl functionalized polythiophenes

2.2.1 Synthesis and characterization

For most organic π-conjugated systems, hole transport is more favorable than electron transport, which leads to unbalanced charge injection and transfer. Therefore, development of acceptor-type materials with good electron transport ability has become one of the most essential topics in the area of organic semiconductors. One of the most effective strategies to prepare acceptor-type materials is to introduce electron-withdrawing groups. As mentioned in the general introduction, triarylboryl groups are important functionalites that feature both Lewis acidity and electron-accepting character. And the empty *p* orbital of boron allows for extended conjugation with adjacent π−systems. In this regard, a polythiophene functionalized with organoborane, PTBM, has

been prepared previously via a new polymer modification strategy by Anand Sundararaman as shown in **Scheme 2-3**.[37] The silylated polymer PTSi was prepared in 60% yield by Stille-type polycondensation. Treatment of PTSi (M_w = 14 000, M_n = 20 000, PDI = 1.88) with BBr_3 quantitatively converted the $SiMe_3$ groups to the BBr_2 groups to form PTBBr. Bulky Mes groups were subsequently introduced to sterically protect the Lewis acidic boron centers by reacting PTBBr with MesCu at elevated temperature and polymer PTBM was obtained in 50% yield. Similarly, a quarterthiophene model QTBM was synthesized by treating QTBBr with 4 eq. of MesCu.

The absorption maxima of QTSi and QTBM are found at 357 and 412 nm, respectively, corresponding to excitation from the HOMO to LUMO levels. For QTBM, an additional band is observed at 340 nm, which is primarily due to excitation to a cross-conjugated state (LUMO+2) with orbital contributions from the central bithiophene moieties and two $BMes_2$ fragments (**Figure 2-14**). The polymers display very similar absorptions that are red shifted by about 25 to 30 nm, indicative of moderately extended conjugation. PTBM has a red emission (617 nm, Φ = 3%), which is strongly shifted relative to the orange emission of PTSi (554 nm, Φ = 10%) thereby confirming the significant decrease of the LUMO energy level upon boryl substitution.
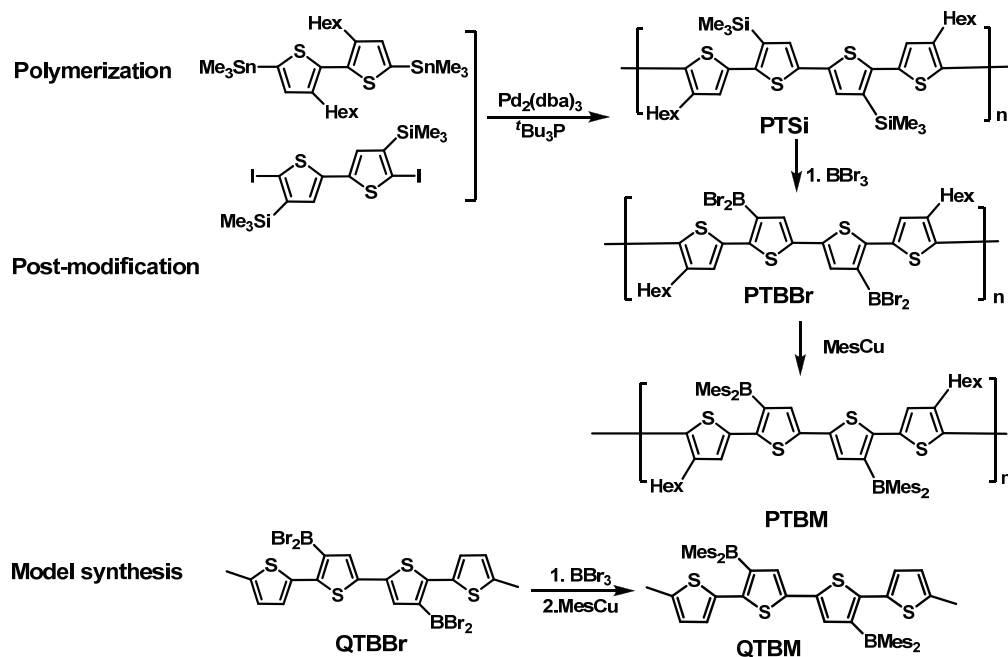
Scheme 2-3 Synthesis of PTBM and QTBM
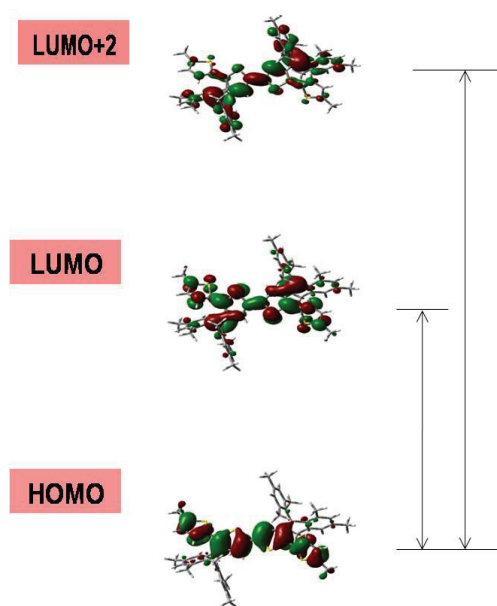
Figure 2-14. Calculated orbital plots for QTBM (Gauss03 program, B3LPY/ 6-31G(d))

In THF, both PTBM and the model QTBM show two quasi-reversible reduction events that occur at considerably lower potentials than for the silylated species. This further proves that the LUMO energy levels are lowered by boryl substitution.

2.2.1 Anion binding behavior

The ability of triarylboranes to change their color or luminescent properties upon exposure to different anions makes them potential candidates for sensory materials. The anion recognition ability of PTBM in THF was evaluated by UV-vis and fluorescence spectroscopy after addition of a ten-fold excess of respective anion in THF solution. The studies showed that PTBM selectively binds to OH^-, F^- or CN^-, but doesn't show any affinity for other bigger anions such as Cl^-, Br^-. Upon binding to OH^-, F^- or CN^-, the high energy band at around 342 nm in the UV-vis spectrum disappeared. Relative to the original low energy band at $\lambda_{max} = 441$ nm, a red shifted band for the F^- complex and a blue shifted band for the CN^- and OH^- complexes were observed at $\lambda_{max} = 455$, 416 and 424 nm, respectively. At the same time, a blue shifted emission was observed for all the anion complexes. The emission for the F^- and CN^- complexes is relatively more intense than that for OH^- complex, but, most importantly, they all are more intense than the original emission for PTBM (**Figure 2-15, 2-16**). As for the reaction of PTBM with N_3^-, the changes in the absorption and emission bands are not as distinctive as for the reaction with F^-, CN^- and OH^-, which indicates that the complexation reaction is not as favorable and that PTBM is only partially complexed with N_3^- under the experimental conditions chosen.
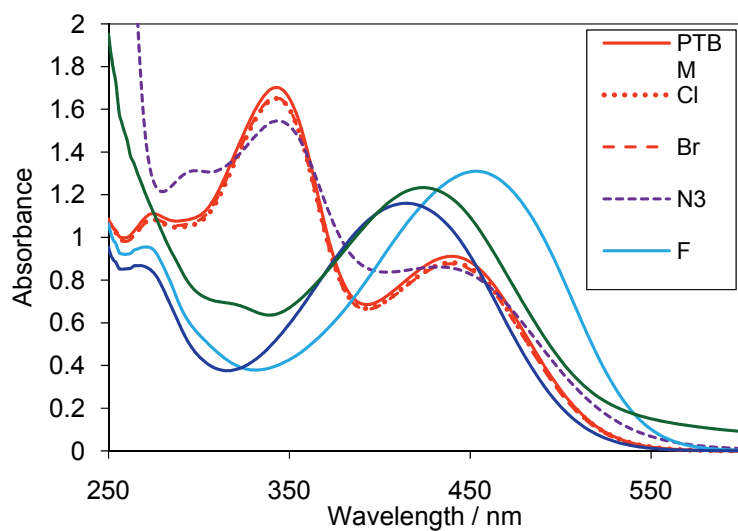
Figure 2-15. Coordination of PTBM (in THF, 3.22×10^{-5} M for the molecules) with different anions (in THF, 10 eq., 0.04 M) examined by UV-vis spectroscopy
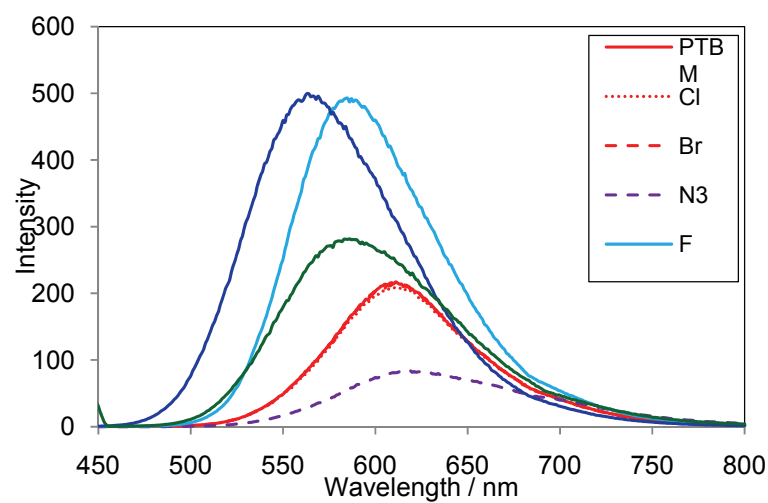
Figure 2-16. Coordination of PTBM (in THF, 3.22×10^{-5} M for the molecules) with different anions (in THF, 10 eq., 0.04 M) examined by fluorescence spectroscopy (λ_{exc} = 441 nm)
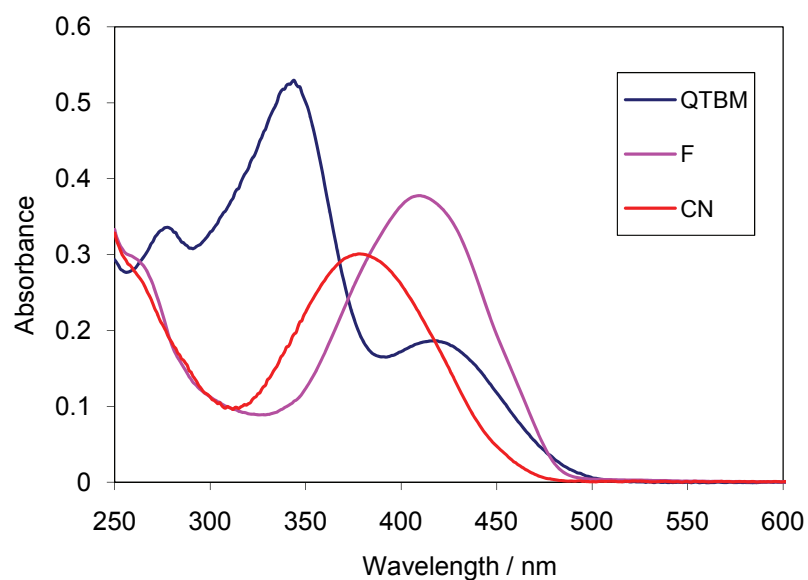
Figure 2-17. Coordination of QTBM (in THF, 5.71×10^{-5} M for moleucles) with different

anions (in THF, 10 eq., 0.02 M) examined by UV-vis absorption spectroscopy
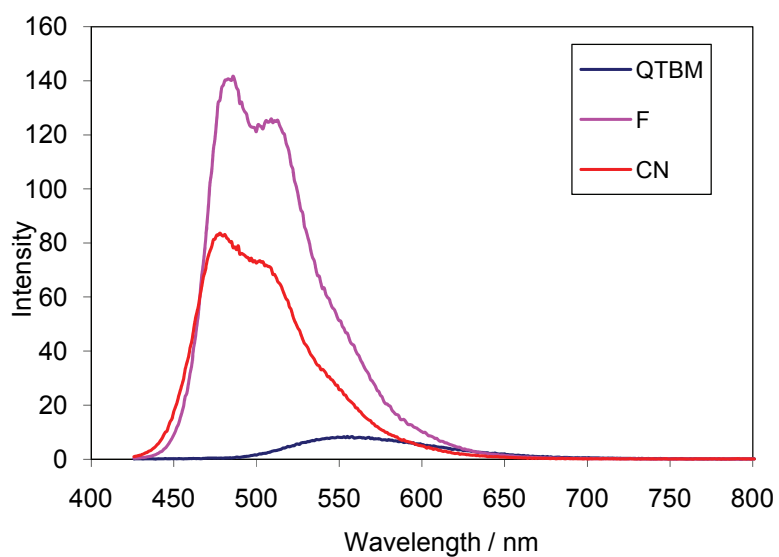
Figure 2-18. Coordination of QTBM (in THF, 5.71×10^{-5} M per molecule) with different

anions (in THF, 10 eq., 0.02 M) examined by fluorescence spectroscopy (λ_{exc} = 412 nm)
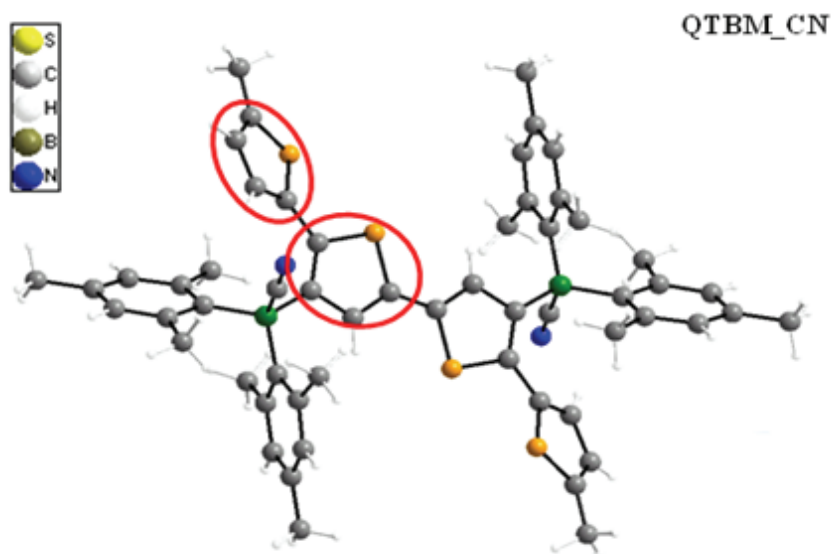
Figure 2-19. Plot of the single crystal structure of QTBM-CN complex (crystallized from THF/Hexanes, tetrabutylammonium cations are omitted for clarity, interplanar angle for Th(central)//Th(terminal) = 31°)

Figure 2-20. Plot of the single crystal structure of QTBM-F complex (crystallized from THF/Hexanes, potassium/18crown6 cations and THF solvent molecules are omitted for clarity, interplanar angle for Th(central)//Th(terminal) = 16°)

Table 2-1. Selected Geometric Parameters of QTBM-F and QTBM-CN

	QT-Mes$_2$-F	QTBM-CN	QTBM[37]
Th^B // Th^B	0	0	0
Th^B // Th^{Me}	16.0 °	31.0 °	15.2 °
Th^B // Mes (c)	83.7 °	78.6 °	79.63 °
Th^B // Mes (t)	67.1 °	59.4 °	70.19 ° (Mes)
Mes // Mes	83.9 °	85.4 °	84.34 ° (Mes/Mes)
C$_{22}$-C$_{23}$	1.457 Å	1.462 Å	1.456 Å
C$_{19}$-C$_{19A}$	1.448 Å	1.457 Å	1.450 Å
B-C(N) or F	1.637 Å	1.461 Å	N/A
B-C$_1$	1.672 Å	1.667 Å	1.572 Å
B-C$_{10}$	1.659 Å	1.679 Å	1.576 Å
B-C$_{21}$	1.653 Å	1.660 Å	1.568 Å
C$_{10}$BC$_{21}$	116.5 °	119.2 °	120.9 °
C$_{10}$BC$_1$	115.5 °	110.7 °	122.9 °
C$_1$BC$_{21}$	107.2 °	109.2 °	116.2 °

Mes = mesityl ring, Th^B = boron-substituted thiophene ring, Th^{Me} = methyl-substituted thiophene ring, Mes (c) = Mes group facing central thiophene ring, Mes (t) = Mes group facing terminal thiophene ring.

As noticed in **Figures 2-15** and **2-16**, there is a significant spectral difference between the F$^-$ complex and the CN$^-$ complex, which seemed worthy further investigation. We first focused on the quaterthiophene derivative QTBM, which is a simple model for PTBM. The binding study demonstrated that QTBM also showed different absorption and emission upon binding to F$^-$ and CN$^-$ (**Figure 2-17, 2-18**).

To probe whether the conformation changed when coordinated with different anions, we acquired single crystal X-ray data for the F⁻ and the CN⁻ complexes. The single crystal X-ray structures show that the F⁻ complex adopts a better coplanar conformation with an inter-planar angle of 16º between the central thiophene and the terminal thiophene (**Figure 2-20**), while the inter-planar angle is 31º for the CN⁻ complex (**Figure 2-19**). Therefore, this would suggest that the relatively more twisted main chain structure of the CN⁻ complex increases the energy band gap and leads to a blue shift in the absorption spectrum. However, given that the solid state and solution conformations may be quite different, theoretical studies will be necessary to further confirm this tentative explanation.
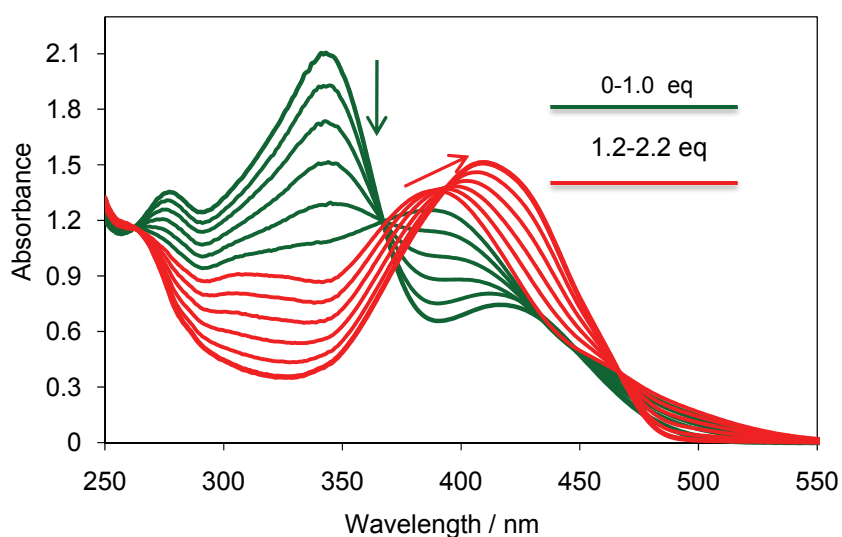
Figure 2-21. Titration of QTBM (in THF, 5.71×10^{-5} M for molecuels) with fluoride (7.13×10^{-3} M) monitored by UV-vis absorption spectroscopy
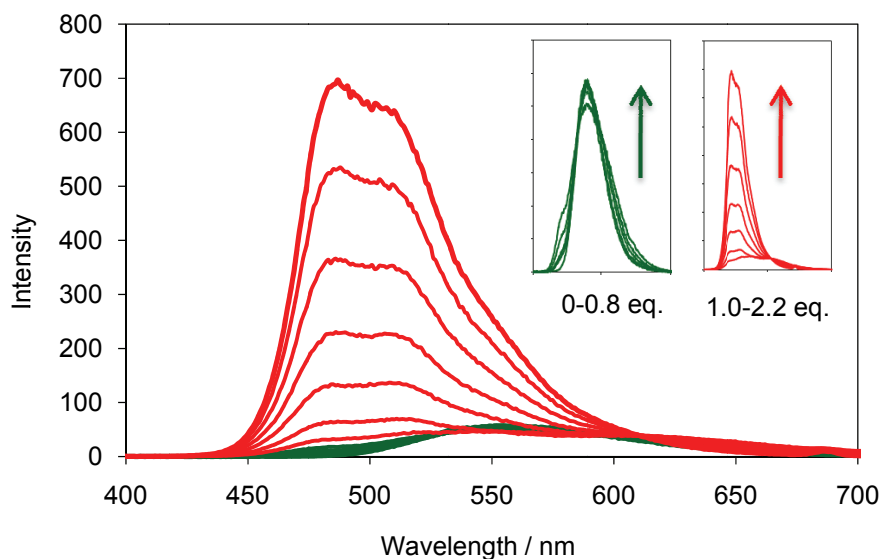
Figure 2-22. Titration of QTBM (in THF, 5.71×10^{-5} M per molecule) with fluoride (7.13×10^{-3} M) monitored by fluorescence spectroscopy ($\lambda_{exc} = 412$ nm): green plots 0-0.8 eq. of cyanide, red plots 1.0-2.2 eq. of fluoride

As described in the previous chapter, titration of the model compound MFBM provides a facile means to understand the coordination mechanism of polymer PFBT with fluoride. The similarity in the absorption spectra between them illustrates a two-step binding process, while significant differences in the emission titration spectra suggest a signal amplification effect for the polymer. Following what we did for PFBT and MFBM, we carried out a spectral titration for PTBM and QTBM, respectively.

Quantitative titration of QTBM with fluoride monitored by UV-vis absorption spectroscopy shows a two–step coordination behavior, which suggests successive binding of fluoride to the two boron centers connected by one bithienylene unit (**Figure 2-21**). In the first step (up to ca. 1.0 eq., green plots), the original high energy band at $\lambda_{max} = 340$ nm gradually decreased with an isosbestic point found at 370 nm; the low energy band at

λ_{max} = 416 nm increased in intensity with a simultaneous blue shift. In the second step (from ca. 1.2 to ca. 2.2 eq., red plots), the low energy absorption band, which was blue shifted to λ_{max} = 388 nm in the first step, changed its shifting direction and became red shifted with a small increase in the absorbance. The final position for this band was found at λ_{max} = 408 nm. The same process was monitored by fluorescence spectroscopy, which shows that no significant change in the emission wavelength occurred within the initial ca. 0.8 eq. of fluoride (**Figure 2-22**, green plots). Starting from ca. 1.0 eq, a blue shifted band appeared at λ_{max} = 485 nm with a shoulder and became more and more intense until no more change was observed at ca. 2.2 eq of fluoride (**Figure 2-22**, red plots).

As shown in **Figure 2-23**, coordination of PTBM with fluoride also proceeded in a stepwise fashion: the first step is from 0 to ca.1.0 eq. of fluoride (green plots) and the second step is from ca. 1.2 eq. to ca. 2.2 eq. (red plots). Unexpectedly, the titration spectra are quite different from those for QTBM in the first step. For clarity, the absorption plots at ca. 1.0 eq. of fluoride for PTBM and QTBM were extracted, which are supposed to be closest to that for the mono-fluoride intermediates, PTBM-F and QTBM-F (**Figure 2-29**, **2-30**). As shown in **Figure 2-25**, the low energy band for PTBM-F is much broader than that for QTBM-F, reminiscent of overlap of different absorption bands, while this difference in the spectral shape is not so distinctive for PFBT-F and MFBM-F (**Figure 2-28**). For model compounds MFBM and QTBM, coordination of one boron center with fluoride produces only one type of intermediate, respectively (**Figure 2-27**, **2-29**). This is also true for the main chain polymer PFBT, in which coordination of alternating boron centers with fluoride yields only one type of structure –[Fl-B-Fl-B(F)]-

(**Figure 2-26**). Therefore, absorption spectra for the intermediates MFBM-F and PFBT-F are quite similar and no band broadening is observed. However, for the side chain boron-modified polymer intermediate PTBM-F, there are three possible substitution patterns including: -[T(BF)T(B)T(Hex)T(Hex)T(BF)T(B)]-,   -[T(BF)T(B)T(Hex)T(Hex)T(B)T(BF)]-   and   -[T(B)T(BF)T(Hex)T(Hex)T(BF)T(B) (**Figure 2-30)**. As mentioned in the introduction, the main chain conformation and electronic structure of PTs closely relate to the electronic and steric effects of the side chain. The presence of three different substitution patterns might be responsible for the band broadening for the PTBM-F intermediate.
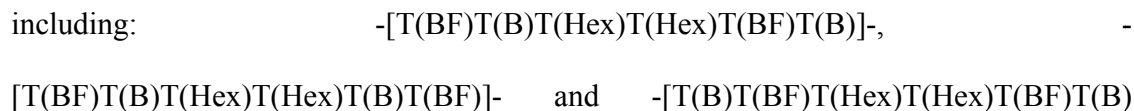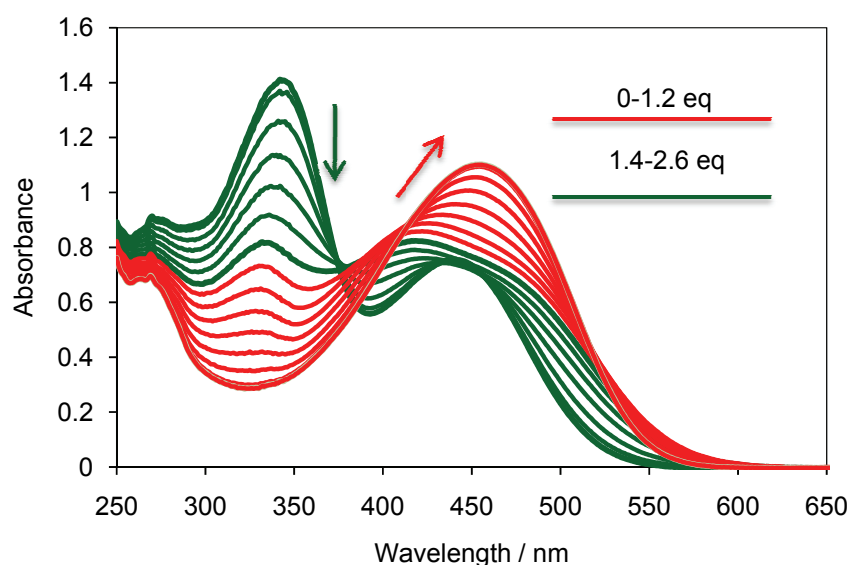
Figure 2-23. Titration of PTBM (in THF, 3.22×10^{-5} M for the repeating units) with fluoride (4.31×10^{-3} M) monitored by UV-vis absorption spectroscopy: green plots 0-1.2 eq. of cyanide, red plots 1.4-2.6 eq. of fluoride
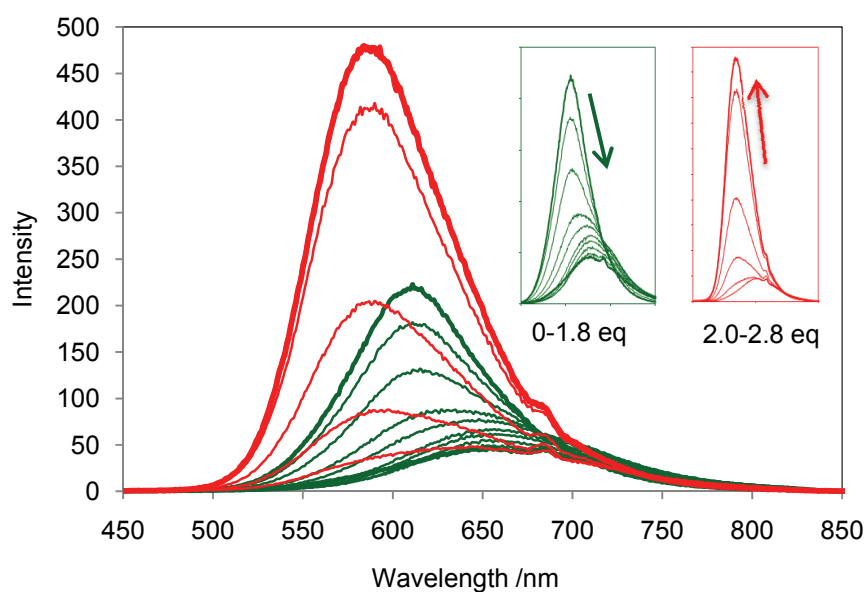
Figure 2-24. Titration of PTBM (in THF, 3.22×10^{-5} M for the repeating units) with fluoride (4.31×10^{-3} M) monitored by fluorescence spectroscopy ($\lambda_{exc} = 441$ nm): green plots 0-1.8 eq. of cyanide, red plots 2.0-2.8 eq. of fluoride
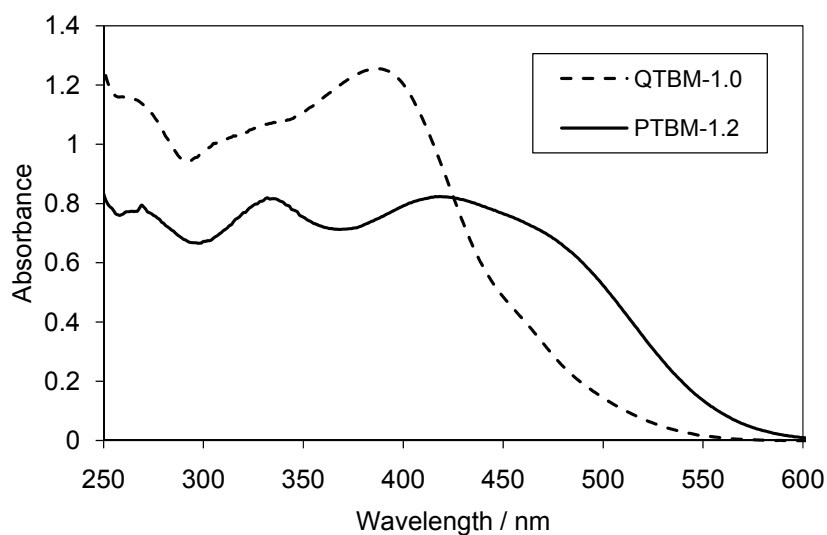
Figure 2-25. UV-vis absorption spectra for QTBM-F and PTBM-F (extracted from the titration plot at ca.1.0 eq. of fluoride for QTBM and 1.2 eq. of fluoride for PTBM)
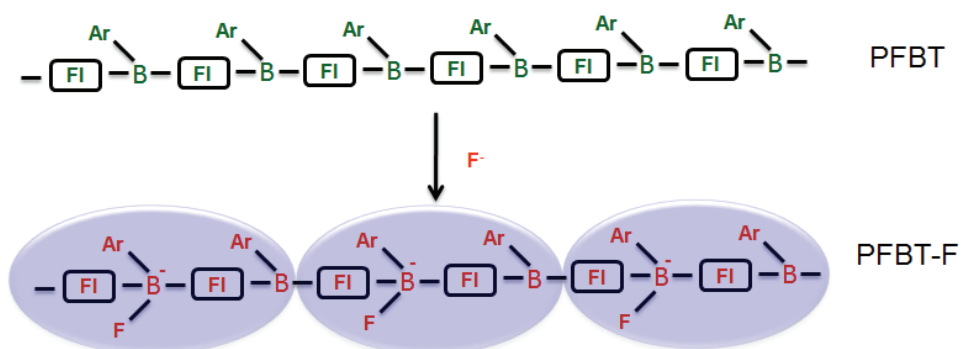
Figure 2-26. Coordination of fluoride with PFBT at alternating boron sites to form the proposed intermediate PFBT-F with one type of structure: -[Fl-B-Fl-B(F)]- (Fl = fluorene)
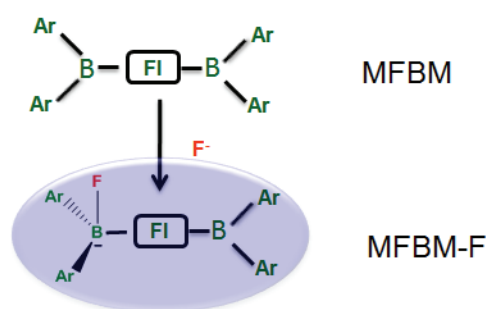
Figure 2-27. Coordination of fluoride to MFBM at one boron site to form the proposed intermediate MFBM-F (Fl = fluorene)
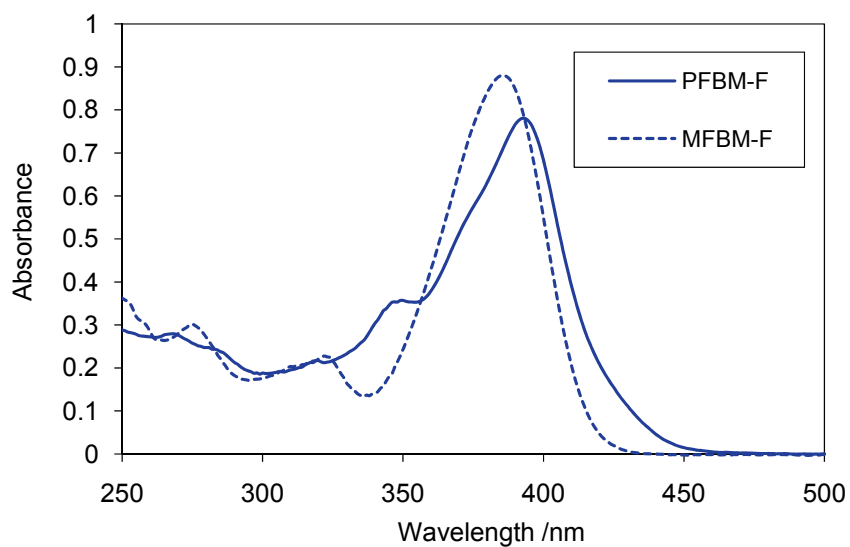
Figure 2-28. UV-vis absorption spectra for MFBM-F and PFBT-F (extracted from the titration plot at ca. 0.9 eq. of fluoride)
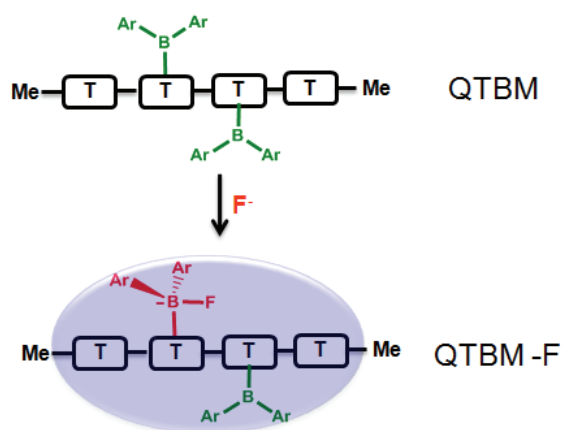
Figure 2-29. Schematic illustration of the coordination of fluoride to one boron site of QTBM to form the proposed intermediate QTBM-F (T = thiophene)

In the fluorescence spectra of PTBM (**Figure 2-24**), the initial emission band at 610 nm gradually decreased upon fluoride addition, accompanied with a gradual red shift. In the second step starting from ca. 2.0 eq to ca. 2.8 eq., the emission became blue-shifted

and the intensity started to increase upon addition of more fluoride until no further change was observed. The final emission for the fluoride complex is centered at 587 nm.
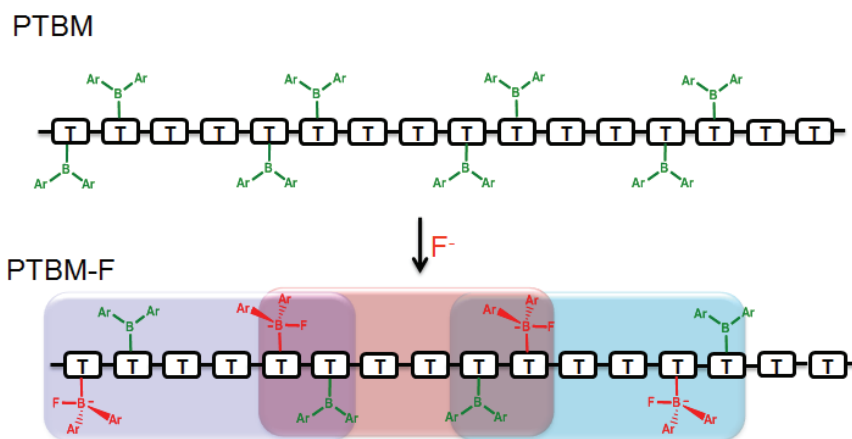
Figure 2-30. Schematic illustration of the coordination of fluoride to PTBM to alternating boron sites to form the proposed intermediate PTBM-F with three different substitution patterns: -[T(BF)T(B)T(Hex)T(Hex)T(BF)T(B)]-, -[T(BF)T(B)T(Hex)T(Hex)T(B)T(BF)]- and -[T(B)T(BF)T(Hex)T(Hex)T(BF)T(B) (T = thiophene)

2.3 Ferrocenylborane functionalized quaterthiophenes and polythiophenes

2.3.1 Introduction

Functionalization of polythiophene with diarylboryl groups provides interesting photophysical and electrochemical properties. With the borane moieties at the lateral positions, two substituents on each boron center are subject to change, which allows us to further tune the electronic and structural properties. Ferrocene is noted for its unusual

reactivity and distinctive redox properties. The iron center in ferrocene can undergo facile one-electron oxidation at moderate potential to form a stable ferrocenium cation. In this section, we will demonstrate two PTs modified with organoborane functionalities carrying one redox active ferrocenyl group and one sterically different Ar group (Ar = Mes or Tip). The structure-property relationship and electrochemical properties for the polymers and their respective model quaterthiophene compounds will be discussed in detail.

2.3.2 Synthesis and characterization

As shown in **Scheme 2-4**, ferrocenylborane substituted quater- and polythiophenes were prepared in a two-step modification reaction. Treatment of QTBBr and PTBBr, with 2 eq. of FcSnMe$_3$ (Fc = ferrocenyl) at RT for 12 h in CH$_2$Cl$_2$, under the conditions applied, leads to attachment of only one ferrocenyl group to each boryl moiety. The excellent selectivity of this reaction was confirmed by ^{1}H NMR of the intermediate B(Br)Fc-substituted oligo- and polythiophenes. In a second step, MesCu or TipCu were added and the mixture was kept at 110 °C for 48 h. The purpose of installing the bulky aryl group as a second substituent is to increase the stability of the polymer toward air and moisture.[38,39]
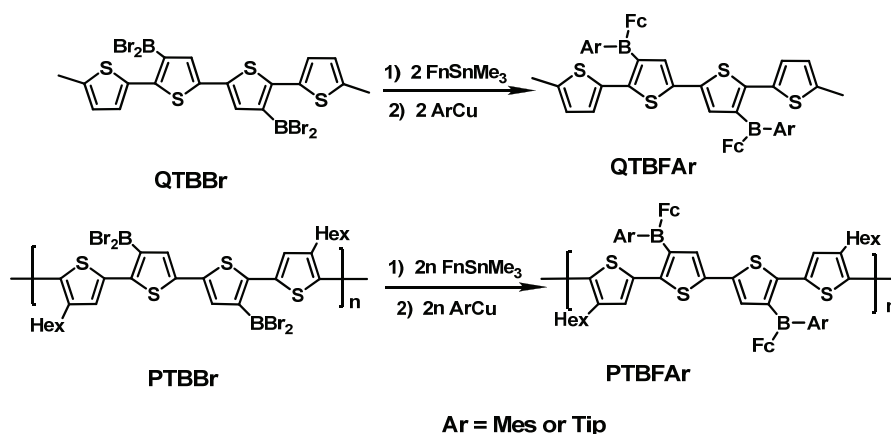
Scheme 2-4 Synthesis of QTBFAr and PTBFAr (QTBFM: Ar = Mes, QTBFT: Ar = Tip)

2.3.3 Molecular weight determination

The polymer structure was characterized by gel permeation chromatography (GPC) and MALDI-TOF analysis. The absolute molecular weights of PTBFM and PTBFT were examined by GPC coupled with an in-line multi angle laser light scattering (GPC-MALLS) detector. Weight average molecular weights of $M_w = 2.06 \times 10^4$ with a PDI of 1.88 for PTBFM and $M_w = 5.08 \times 10^4$ with a PDI of 1.60 for PTBFT were determined. MALDI-TOF analysis with benzo[a]pyrene as the matrix was used to further confirm the polymer structure and to study the nature of the end groups. The spectrum of PTBFM shows three major series of peaks that correspond to linear polymers with the expected [Th$_4$Hx$_2$(BMesFc)$_2$] (Hx = n-hexyl) repeating units (**Figure 2-31**, **Table 2-2**). Polymers with a number of repeating units of n = 3-11 could be clearly identified in the spectrum. The most intense peaks (Series A) correspond to polymers with H- and -CH$_3$ end groups, where the dihexylbithiophene end group is capped with a proton and the diborylbithiophene end group is capped with a methyl group. This is consistent with the

structure of the precursor polymer, for which we found series with H-, -CH$_3$ (and a smaller amount of CH$_3$Th$_2$Si$_2$-, -CH$_3$) end groups as a result of methyl group transfer as a mode of polymer termination in the Stille-type polycondensation reaction.[37] The other two less intense series are due to (i) the presence of an additional boryl group (BMesFc) instead of a proton, presumably at the 2-position of the terminal thiophene group (Series B) (ii) and the loss of one boryl group within the polymer chain (Series C). We rationalize this behavior by reaction of the terminal acidic thiophene proton with BBr$_3$ under generation of a –BBr$_2$ terminus, which leads to polymers with one additional functional group. The concomitant release of HBr in turn may induce protiodesilylation at the disilylbithiophene fragments of the same or another polymer, with formation of Me$_3$SiBr and a polymer chain that is lacking one of the functional groups.
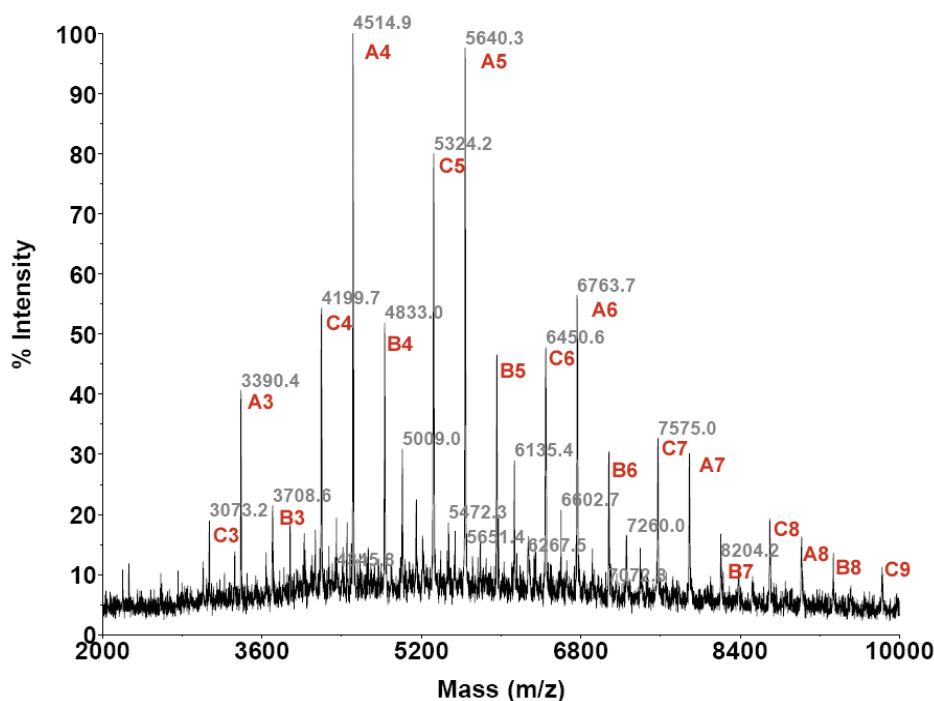
Figure 2-31. MALDI-TOF mass spectrum of **PTBFM** recorded in (+)-reflector mode

Table 2-2. Summary of MALDI-TOF data: comparison of experimental data with theoretical data

Structure / $n =$		**3**	**4**	**5**	**6**	**7**	**8**
H-(Th$_2$Hx$_2$Th$_2$B$_2$)$_n$-CH$_3$	Calcd	3390.0	4515.3	5639.7	6765.0	7890.3	9014.7
(An)	Observed	3390.4	4514.9	5640.3	6763.7	7890.2	9017.4
MesFcB-(Th$_2$Hx$_2$Th$_2$B$_2$)$_n$-	Calcd	3704.1	4829.4	5953.8	7079.1	8203.4	9329.8
CH$_3$ (Bn)	Observed	3703.2	4833.0	5958.5	7083.9	8204.2	9334.0
H-(Th$_2$Hx$_2$Th$_2$B$_2$)$_n$-CH$_3$	Calcd	3074.9	4200.2	5324.6	6449.9	7574.3	8699.5
- loss of BMesFc (Cn)	Observed	3073.2	4199.7	5324.2	6450.6	7574.9	8697.5

2.3.4 NMR characterization

The polymers and their models were also examined by multinuclear NMR spectroscopy (**Table 2-2**). The observation of a broad ^{11}B NMR resonance at 60 to 67 ppm for each of the compounds is consistent with the formation of triarylborane functional groups. The attachment of two different aryl groups to boron is reflected in the ^{1}H NMR spectra, which show three signals in the region of 4 to 5 ppm in a 5:2:2 intensity ratio, in agreement with attachment of the mono-substituted ferrocenyl groups. The phenyl proton signals are found at about 6.6 ppm for QTBFM and PTBFM, while they resonate at about 6.9 ppm for QTBFT and PTBFT. Peak integration of the methyl and isopropyl groups in the region from 3.0 to 0.8 ppm supports the attachment of one Mes or Tip and one ferrocenyl group to each boryl moiety. The protons on the borylated thiophene rings are downfield shifted to about 8.20 ppm for QTBFM / PTBFM and even 8.40 ppm for QTBFT / PTBFT, in stark contrast to the BMes$_2$-functionalized materials

(ca. 6.9 ppm). A slight upfield shift of the protons on the adjacent alkylthiophene moieties for P(Q)TBFM (6.24 to 6.33 ppm) and a stronger shift for QTBFT / PTBFT (5.77 to 6.22 ppm) are also noticeable. These pronounced ring current effects suggest distinct conformational changes as a result of variations in the substitution pattern on boron.

Table 2-3. Comparison of selected ^{11}B and ^{1}H NMR data

	^{11}B NMR (ppm)	Th^{B} (ppm)	Th$^{Me/Hex}$ (ppm)	*m*-Ph (ppm)
QTBFM	67	8.21	6.33, 6.28	6.63
PTBFM	60	8.27	6.24	6.65
QTBFT	67	8.40	6.22, 5.77	6.91
PTBFT	58	8.44	5.90	6.92
QTBM[37]	69	6.89	6.53	6.68
PTBM[37]	62	6.94	6.48	6.69

To further examine these conformational peculiarities we acquired H,H-NOESY NMR data for all new compounds (**Figure 2-32**). Similar chemical shifts and cross coupling patterns were observed for each of the individual polymers and their respective model compounds, suggesting that the polythiophenes adopt similar conformations as the quaterthiophene model compounds (**Table 2-3**). Cross-peaks between the *ortho*-protons of the boron-substituted Cp ring (Cp^{B}) and the protons on the free Cp rings with those of the boron-substituted thiophene rings (Th^{B}) are observed in all cases. For QTBFT / PTBFT, these cross peaks are of similar intensity. However, in contrast, the cross-peak between Cp^{B} and Th^{B} for QTBFM / PTBFM is much more intense than that between the protons of the free Cp and Th^{B}, suggesting that the thiophene protons are closer to the

substituted Cp rings than the free Cp rings. No cross-peak was observed between the free Cp protons and the terminal thiophene protons, which indicates that the ferrocenyl groups are facing to the center of each molecule. These observations are consistent with two distinct conformations for QTBFM and QTBFT as illustrated in **Figure 2-33**.
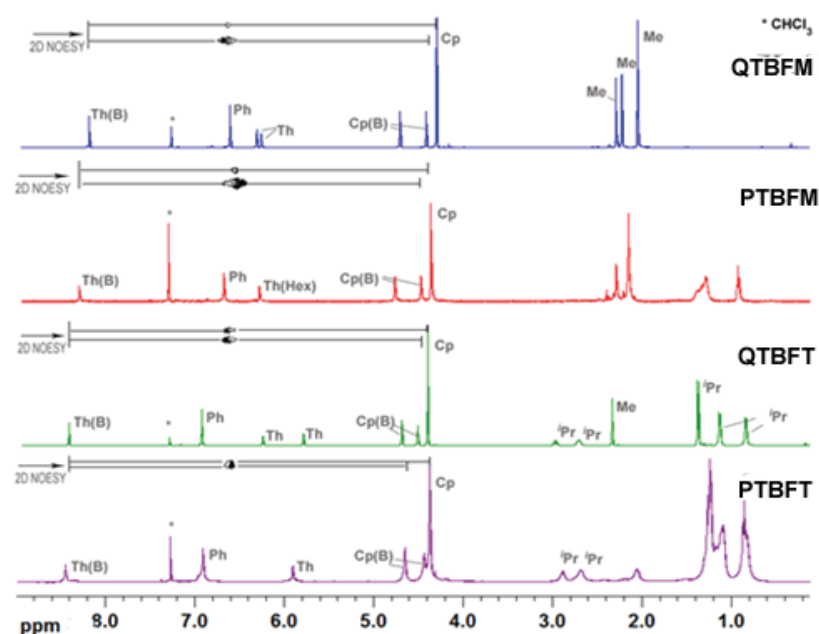
Figure 2-32. Comparison of 1D 1H NMR and 2D H,H-NOESY NMR (in CDCl$_3$; * corresponds to the CHCl$_3$ solvent signal)
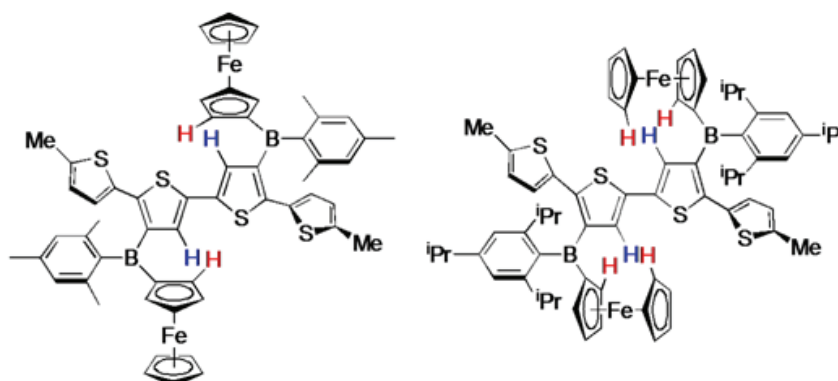
Figure 2-33. The different conformations adopted by **QTBFM** and **QTBFT**; thiophene and ferrocene protons that show strong NOE signals are emphasized.

2.3.5 X-ray crystal structure of the QTBFM and QTBFT

To compare the conformations adopted by the oligothiophenes in solution with those in the solid state we acquired single crystal X-ray diffraction data for both QTBFM and QTBFT. The crystal structure of QTBFM in **Figure 2-34** shows a surprisingly different conformation in comparison to that previously found for QTBM.[37] In stark contrast to the almost coplanar arrangement of the four thiophene rings in QTBM, the terminal rings for QTBFM are strongly tilted with respect to the (coplanar) internal bithiophene unit (dihedral angles Th^B // Th^{Me} 61.0°). As expected, the arrangement of the aryl groups on boron is also quite different. The bulky Mes groups stand almost orthogonal to the thiophene (69.9°) and Cp rings (78.1°). However, the Cp rings of the ferrocenyl moieties make a rather small angle of only 30.2° with the internal thiophene rings, consistent with the conformation deduced from our solution NMR studies. This conformation should favor cross-conjugation through the Cp rings rather than the terminal thiophene rings. To estimate the possible overlap between the empty p-orbital on boron and the conjugated Cp^B and Th^B rings, we determined the dihedral angles with the best plane made of boron and the three boron-bound ipso-carbon atoms (BC_3); relatively small angles of BC_3 // Th^B 15.2° and BC_3 // Cp^B 19.1° suggest that extended conjugation through the tricoordinate boron center should be very favorable. This conjugation in turn is likely further extended to the iron centers as the boryl groups are slightly bent out of the Cp plane toward the Fe atoms (tilt angle Cp^B_{CENT}-C19-B1 172.55). This tilting effect has been shown by Wagner

and Holthausen in a density functional theory (DFT) study of $FcBH_2$ to be due to a delocalized interaction between the electron-deficient boron, the Cp ring, and the electron-rich iron.[40] Consistent with strong electronic coupling between boron and the ferrocenyl moiety is also that the B-C bond length to the Cp ring of B1-C19 1.553(3) Å is relatively short in comparison to that to the thiophene ring (B1-C3 1.570(3) Å) and even more so the long distance to the mesityl group (B1-C10 1.580(3) Å). Another unusual feature of the structure of QTBFM is the almost coplanar arrangement of the terminal thiophene rings and the B-Mes substituents.

Substitution with the even bulkier Tip groups in QTBFT leads to three significant changes to the molecular conformation (**Table 2-4, Figure 2-35**): (i) the four thiophene rings adopt a more coplanar conformation with a smaller dihedral angle Th^B // Th^{Me} of 46.3º between the terminal and internal thiophenes. This effect should favor extended conjugation through the oligothiophene chain; (ii) the dihedral angles between the Cp^B, Th^B, and Tip rings on the same boron atom are considerably larger than those for QTBFM; remarkably, the Tip group stands almost orthogonal to both the Th^B and the Cp^B rings, and the ferrocene moieties rotate into a position that places the free Cp rings close to the internal thiophene rings as already deduced from the solution NOE experiments; (iii) the dihedral angle between each of the aromatic rings attached to boron relative to the BC_3 plane becomes larger. These observations suggest that the empty p orbital on boron participates less effectively in extended p-π conjugation in the presence of the bulkier Tip substituent in QTBFT than in QTBFM.
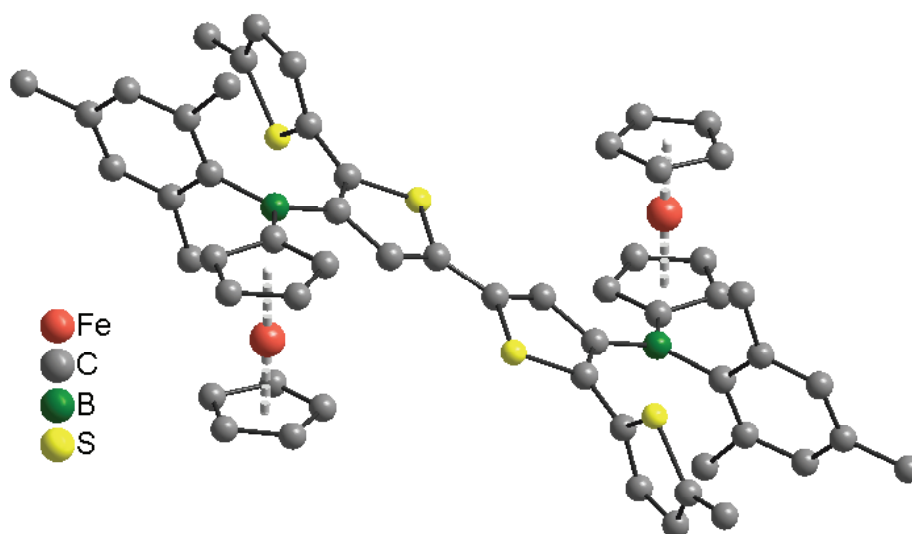
Figure 2-34. Plot of the single crystal X-ray structure of QTBFM
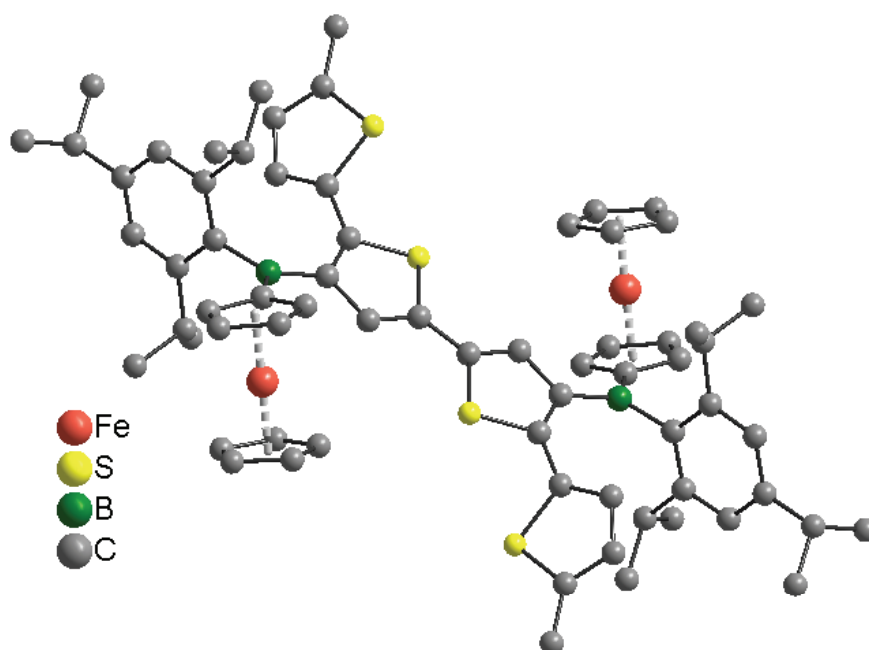
Figure 2-35. Plot of single crystal X-ray structure of QTBFT

Table 2-4. Selected Geometric Parameters of **QTBFM** and **QTBFT**

	QTBFM	QTBFT	QTBM[37]
Th^B // Th^B	0	0	0
Th^B // Th^{Me}	61.0 °	46.3 °	15.2 °
Th^B // Mes or Tip	69.9 °	81.9 °	79.63 °
Th^B // Cp^B or Mes	30.2 °	44.7 °	70.19 ° (Mes)
Tip // Cp^B or Mes	78.1 °	89.6 °	84.34 ° (Mes/Mes)
BC_3 // Th^B	15.2 °	25.7 °	41.13 °
BC_3 // Cp^B or Mes	19.1 °	24.9 °	52.63 ° (Mes)
BC_3 // Mes or Tip	65.0 °	82.1 °	45.79 °
Th^{Me} // Mes or Tip	29.9 °	41.3 °	65.43 °
Cp^B_{CENT}-^iC-B	172.6 °	174.7 °	N/A

Mes = mesityl ring, Tip = tri-isopropylphenyl ring, BC_3 = best plane made of boron and the three boron-bound ipso-carbon atoms, Th^B = boron-substituted thiophene ring, Th^{Me} = methyl-substituted thiophene ring, Cp^B = boron-substitutend Cp ring.

We conclude that the lower steric demand of only one Mes group in QTBFM allows for alignment of the Fc-B-Th-Th-B-Fc fragment, which should favor cross-conjugation with electronic delocalization between the Cp rings and the central bithiophene moiety via the empty *p* orbital on boron. Replacement of the Mes groups with the even bulkier Tip groups in QTBFT to some extent disfavors this conjugation pathway, but leads to a more planar structure of the quaterthiophene backbone. This trend is taken one step further when two Mes groups are attached to each boron center in QTBM, which leads to an almost coplanar arrangement of the entire oligothiophene chain, but a strong twist of the boron substituents.

2.3.6 Photophysical properties

An obvious feature of the ferrocenyl derivatives is their deep red color, which is due to relatively intense absorption bands at around 490 to 510 nm ($\varepsilon = 96$ cm^{-1}M^{-1} at 442 nm

for ferrocene in cyclohexane[44]) (**Table 2-4**). These absorptions are not observed for QTBM and PTBM[37], and they are in a typical region of bands for ferrocenylboranes that are generally attributed to d-d transitions with considerable charge transfer character (**Figure 2-36**).[41] In the case of the polymers this band overlaps with one of several more intense higher energy absorptions, the origin of which could be either the ferrocene or oligothiophene moieties. We find the second-lowest energy band at longer wavelength for the polymers than for the quaterthiophenes, which suggests that it is due to the conjugated oligo- / polythiophene chromophores, consistent with our prior observations for the silylated precursors (QT-SiMe$_3$, 357 nm; PTSi, 382 nm) and the BMes$_2$-substituted species (QTBM, 412 nm; PTBM, 441 nm).[37] This band is slightly more bathochromic by ca. 25 to 30 nm for the derivatives with the bulkier Tip groups in comparison to the systems with Mes substituents. While it is difficult to draw quantitative conclusions, the more planar structure adopted by the quaterthiophene backbone in the case of the Tip derivative seen in the X-ray structure of QTBFT may be responsible at least in part.
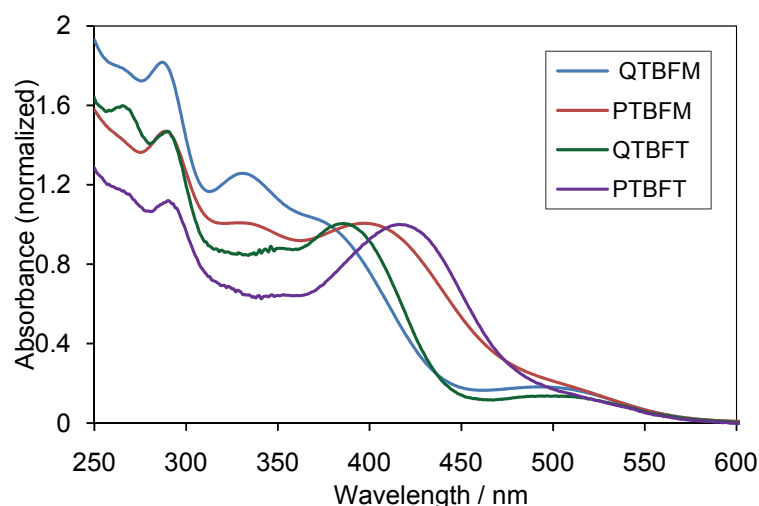
Figure 2-36. UV-vis absorption spectra (CH$_2$Cl$_2$, normalized to second lowest energy band)

2.3.7 Electrochemical properties

The electronic structure of the oligo- and polythiophenes was further studied by cyclic voltammetry. For all of the compounds two well-separated quasi-reversible redox waves were found at around –2.4 V and –2.6 V, which correspond to reduction of the two boron centers attached to the adjacent thiophenes (Figures **2-37**, **2-38**). The redox splitting is in the order of ΔE = 0.14 to 0.24 V, suggesting significant electronic communication through the bithiophene bridge. The polymers show consistently larger redox splittings than the quaterthiophene derivatives and are reduced at comparatively lower potential (by 50 mV for PTBFM and 120 mV for PTBFT), thereby highlighting the role of extended conjugation through the polythiophene main chain. In addition to these boron-centered processes, we find two reversible one-electron process at ca. 0.12 to 0.16 V that is attributed to oxidation of the ferrocene moieties. In contrast to the boron redox, two separate waves could not be resolved (**Table 2-5**). In the case of QTBFT, two additional quasi-reversible oxidation peaks are detected at higher potentials (957 and 1152 mV), while for the other compounds only one irreversible process is observed. This process likely corresponds to oxidation of the thiophene moieties and the bulkier Tip group helps to stabilize the polycationic species formed (**Figure 2-39**).
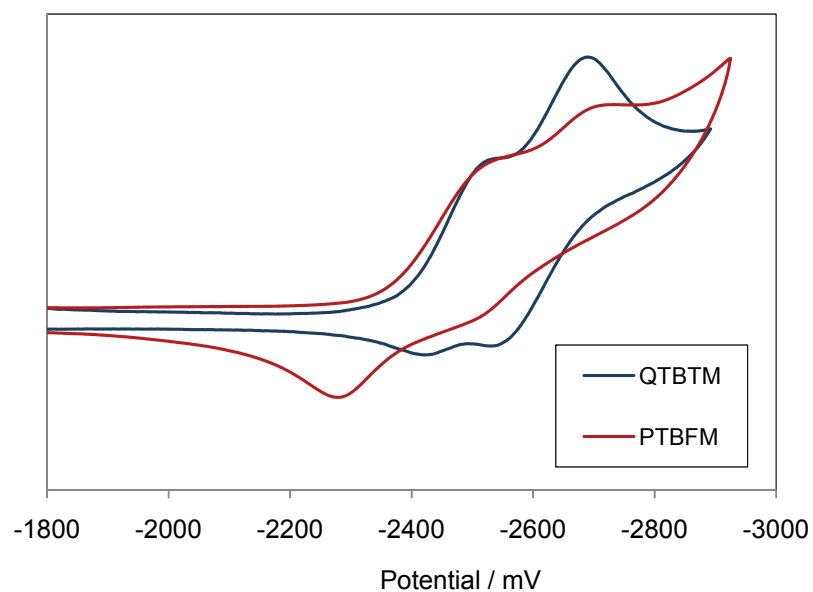
Figure 2-37. Cyclic Voltammogram of QTBFM and PTBFM (in THF, 0.1 M $Bu_4N[PF_6]$, 100 mV/s, vs Fc/Fc^+ couple)
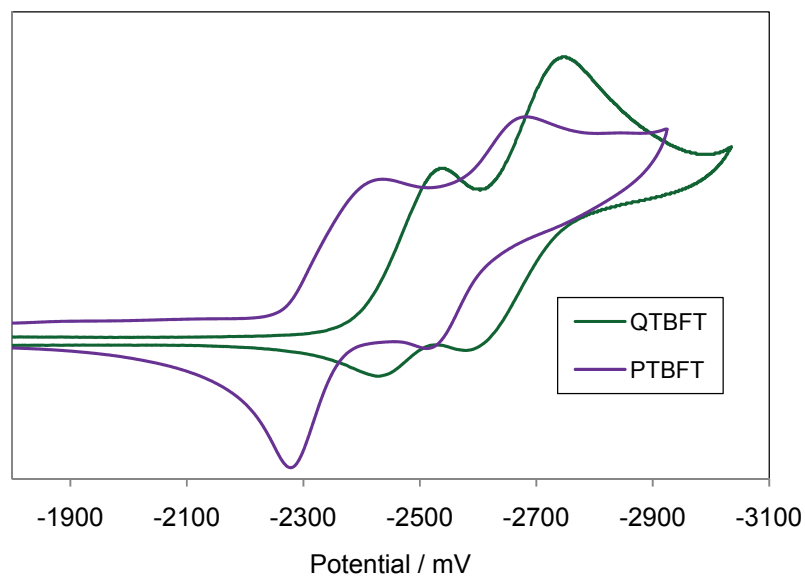
Figure 2-38. Cyclic Voltammogram of QTBFT and PTBFT (in THF, 0.1 M $Bu_4N[PF_6]$, 100 mV/s, vs Fc/Fc^+ couple)
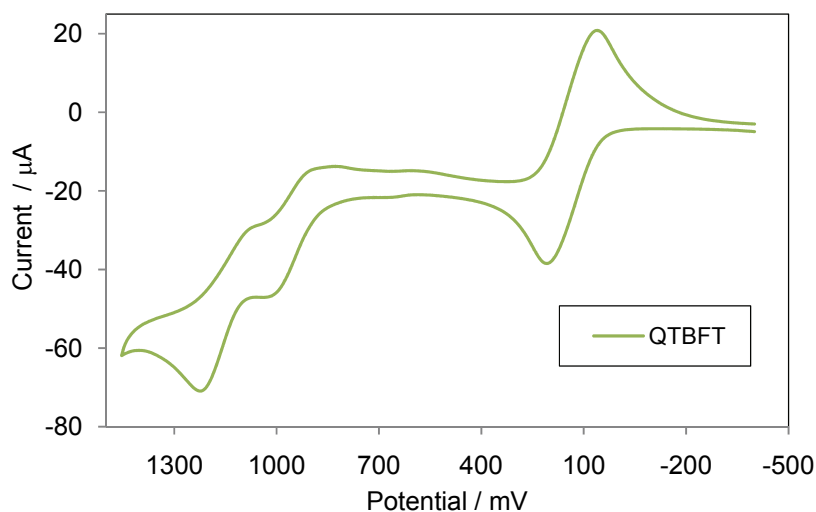
Figure 2-39. Cyclic Voltammogram of QTBFT (in CH_2Cl_2 / 0.05 M $Bu_4N[B(C_6F_5)_4]$, 100 mV/s, vs Fc/Fc$^+$ couple)

Table 2-5. Comparison of UV-visible absportion and cyclic voltammetry (CV) data

	λ_{max} (nm) (ε) [a]	$E_{1/2}$ (mV), (ΔE_p) (oxidation) [b]	$E_{1/2}$ (mV), (ΔE_p) (reduction) [c]
QTBFM	287 (38291) 326 (26900) 376 (21670) 490 (3900)	119 (172) 890 (319)	-2477 (96) -2613 (137)
PTBFM	289 (45205) 334 (31000) 401 (31000) 498 (2915)	154 (128) 882 [d]	-2412 (223) -2612 (185)
QTBFT	290 (34800) 386 (24300) 501 (8210)	135 (148) 957 (174) 1152 (143)	-2480 (110) -2660 (168)
PTBFT	290 (37700) 416 (34000) 511 (5108)	163 (238) 987 (286)	-2360 (158) -2600 (181)

[a] In CH_2Cl_2; [b] In CH_2Cl_2/0.05 M $Bu_4N[B(C_6F_5)_4]$, 100 mV/s, referenced vs. $Cp^*_2Fe/Cp^*_2Fe^+$ couple (-610 mV); [c] In THF/0.1M $Bu_4N[PF_6]$, 100 mV/s, referenced vs. $Cp^*_2Fe/Cp^*_2Fe^+$ (-548 mV); [d] from square wave voltammogram in CH_2Cl_2/0.05 M $Bu_4N[B(C_6F_5)_4]$, 100 mV/s, referenced vs. vs. $Cp^*_2Fe/Cp^*_2Fe^+$(-610 mV).

2.4 Dimesitylboryl functionalized conjugated copolymers

2.4.1 Introduction

As previously documented, homopolymers made of common organic aromatic molecules such as benzene, thiophene, fluorene and carbazole have been extensively investigated in organic semiconductors. However, the overall performance is still lower than that of the inorganic counterparts, although it also relates to supramolecular organization and solid state packing, and there is still room for future optimization. The improvement for simple homopolymers made of single organic π-system modified with solubilising groups is limited because of their inherent properties for each type of organic molecules. For instance, thiophene homopolymers have been widely used in organic solar cells with power conversion efficiencies reaching around 5%. However, as calculated, P3HT is only capable of absorbing 46% of the available solar photons. Polyfluorene derivatives also show promising features with power conversion efficiencies up to 4.2%, but they are negatively influenced by relatively high energy gap and low carrier mobility. Therefore, rational modification to optimize the electronic and structural properties at the lateral position or in the main chain is very desirable. Since we have demonstrated side chain modification in the last section, here we are going to discuss a series of dimesitylboryl functionalized bithiophene copolymer alternating with different organic π building blocks including fluorene, carbazole and triphenylamine derivatives. The effect of the main chain skeleton on the electronic structure and the optical properties of the polymers have been studied in detail.

2.4.2 Synthesis of alternating copolymers

A series of silylated bithiophene-based alternating copolymers were prepared by using standard Suzuki coupling reaction (**Scheme 2-5**). Precipitation of the crude materials from toluene into acetone afforded PFT-Si as a yellow powder in 65% isolated yield, PCT-Si as a pale yellow powder in 74% yield and PTT-Si as yellow powder in 57% yield. Their number average molecular weights (M_n) were determined by gel permeation chromatography (GPC) in THF against polystyrene standards to be 1.35×10^4, 6.19×10^3 and 1.47×10^4 for PFT-Si, PCT-Si and PTT-Si, respectively, corresponding to an average of ca. 21, 10 and 25 repeating units. Treatment of the silylated polymers with a slight excess of BBr_3 gave the respective dibromoboryl-substituted polymers. The Si/B exchange reaction was monitored by ^{1}H NMR spectroscopy. For PFT-Si and PCT-Si, the reaction proceeded smoothly and the trimethylsilyl signals in the ^{1}H NMR spectra completely disappeared. However, the reaction of PTT-Si with BBr_3 did not go to completion, because of precipitation of the poorly soluble dibromoborylated product. The air-sensitive BBr_2-functionalized polymers were directly reacted with MesCu to replace the bromo substituents with two bulky Mes groups, which strongly enhanced the chemical stability. The boron polymers, PFT-B, PCT-B, and PTT-B, were obtained as yellow powdery solids after precipitation into hexanes and freeze-drying from benzene solution. They show good stability and are well soluble in common organic solvents such as THF, chloroform, toluene and dichloromethane, etc, which allowed us to fully characterize their chemical structure and electronic properties.
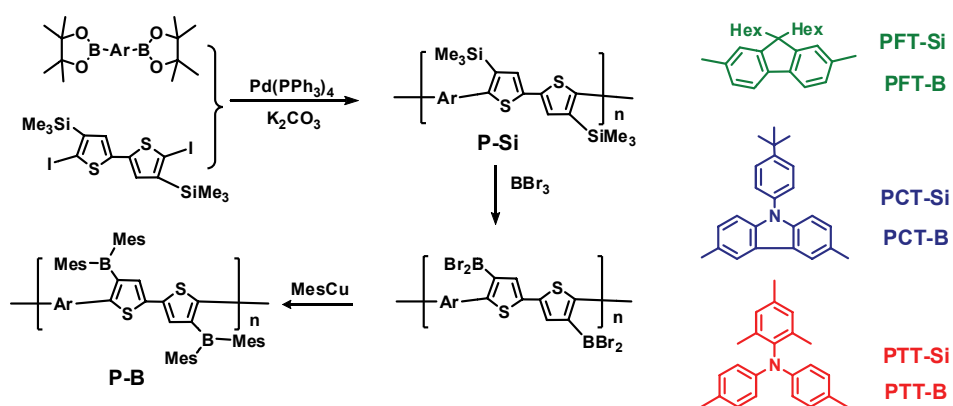
Scheme 2-5. Synthesis of silylated precursors and borylated polymers
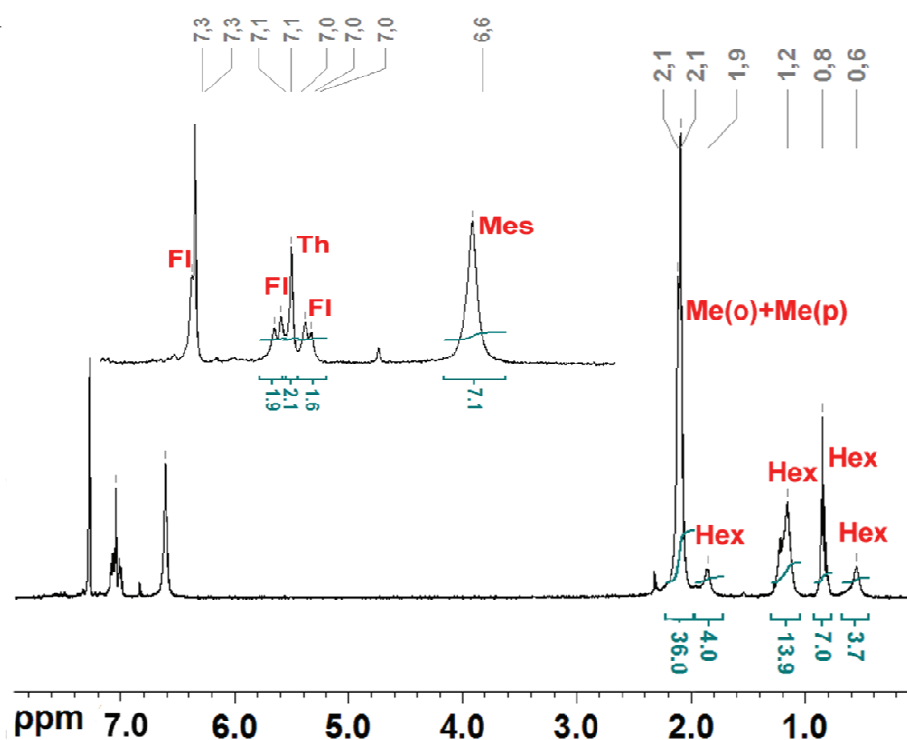
Figure 2-40. ¹H NMR spectrum of PFT-B
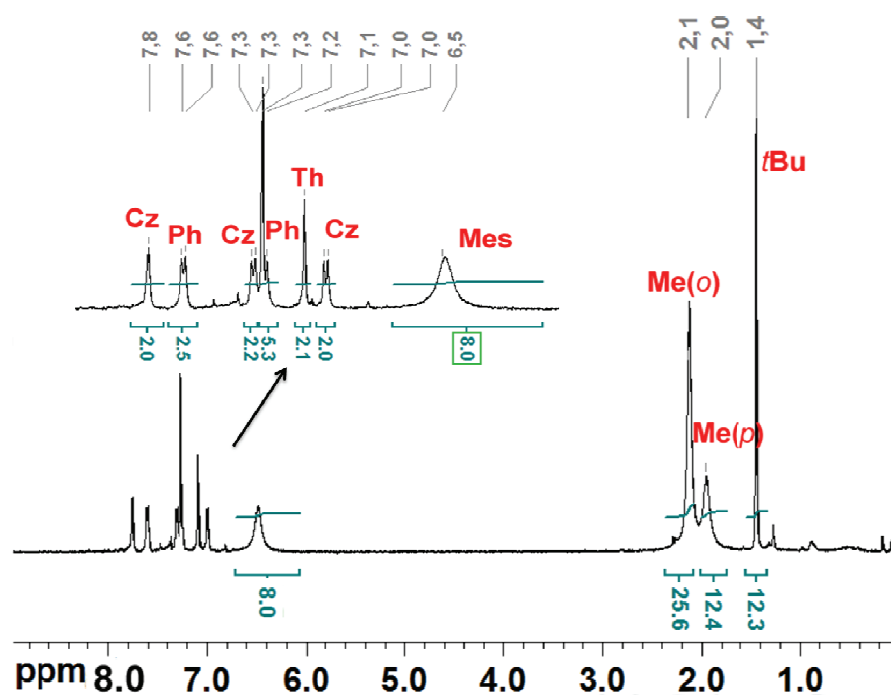
Figure 2-41. ^{1}H NMR spectrum of PCT-B
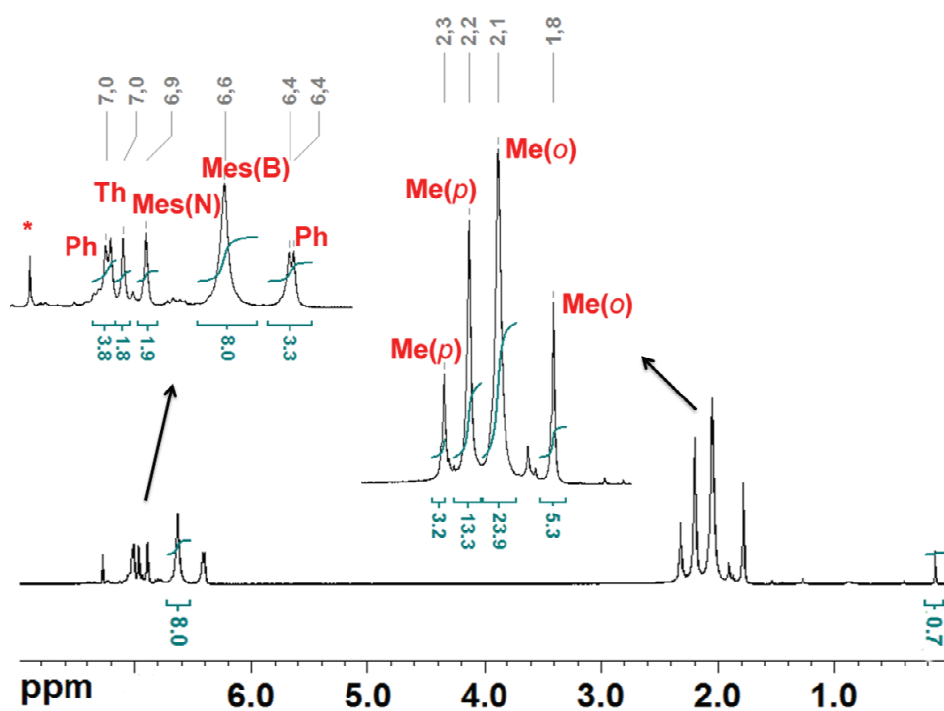
Figure 2-42. ^{1}H NMR spectrum of PTT-B

In the ^{1}H NMR spectra of polymers PFT-B, PCT-B and PTT-B, a new set of peaks for the Mes groups appeared at around 6.6, 2.2 and 2.0 ppm. The degree of functionalization based on ^{1}H NMR is >97% for PFT-B and PCT-B (**Figure 2-40**, **2-41**), but for PTT-B integration of the Mes signal at 6.63 ppm (8H) and the SiMe$_3$ signal at 0.14 ppm (0.84H) indicates that the conversion for the Si / B exchange reaction is less efficient (**Figure 2-42**). A broad resonance in the ^{11}B NMR spectra at 50 to 60 ppm further confirms the formation of the tricoordinate borane species. With an electron rich comonomer as the second building block, the ^{11}B NMR signals of PCT-B and PTT-B experience up-field shifts to 52 and 54 ppm relative to that of PFT-B at 61 ppm. The number average molecular weights (M$_n$) measured by GPC vary from 1.0×10^4 to 2.5×10^4, corresponding to an average of ca. 10 repeating units for PCT-B, 21 for PFT-B, and 26 for PTT-B. Both the degree of polymerization (DP$_n$) and the polydispersity (PDI) are consistent with those of the respective silicon precursors (**Table 2-6**).

Table 2-6. Molecular weight and thermal properties of the polymers

Sample	PFT-Si	PFT-B	PCT-Si	PCT-B	PTT-Si	PTT-B
Yield /%	65	52	74	48	57	47
M$_w$^{a}	2.52×10^4	4.04×10^4	1.36×10^4	2.03×10^4	2.37×10^4	5.61×10^4
M$_n$^{a}	1.35×10^4	2.19×10^4	6.19×10^3	1.04×10^4	1.47×10^4	2.53×10^4
PDI^b	1.86	1.85	2.19	1.95	1.61	2.22
DP$_n$ ^{c}	21.2	22.0	10.2	10.9	24.8	26.7
T$_{dec}$/°C^d, % residue^e	376, 10	256, 11	376, 6	285, 4	367, 9	293, 5

^{a} Molecular weight determined by GPC against polystyrene standards in THF. ^{b} polydispersity, $PDI = M_w/M_n$. ^{c} number average degree of polymerization based on GPC

analysis. ^{d} Thermal decomposition temperature determined by TGA under nitrogen at 10 ºC/min, based on 5% weight loss. ^{e} At 800 ºC.

The polymeric structures of the copolymers PFT-Si, PCT-Si and PCT-B were further confirmed by MALDI-TOF mass spectroscopy. A single set of peaks -[nM]- up to 12 repeating units was clearly identified in the mass spectra acquired in (+) reflector mode. By comparison with calculated isotopic patterns, the peaks for PCT-Si correspond to polymer chains with formula $-[Th_2Si_2Cz]_n-$ (**Figure 2-43**), while for PCT-B, beside the main set of peaks -[nM]- assigned to $-[Th_2B_2Cz]_n-$, one extra set of small peaks (nM-B) is found next to each main peak (**Figure 2-44**). The mass difference between them is 249.2 Da corresponding to one $BMes_2$ group; therefore, they are assigned to polymer chains that lost one $BMes_2$ group. Multiple series (four) of peaks are detected for PFT-Si with the An series assigned to $Th_2Si_2-[FlTh_2Si_2]_n-H$ and the Bn series assigned to H-$[FlTh_2Si_2]_n-H$ (**Figure 2-45**). We were not able to obtain a spectrum of sufficient quality for PFT-B.
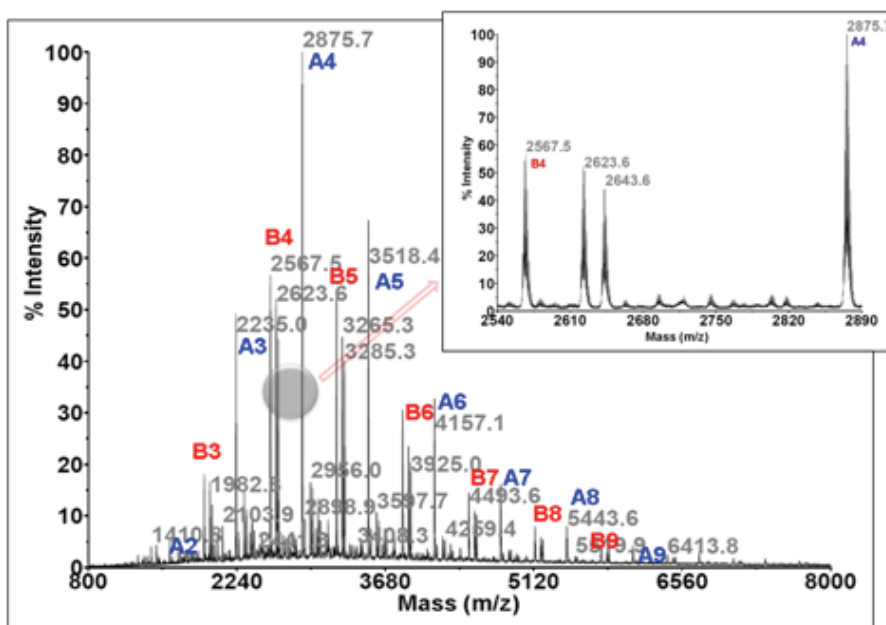
Figure 2-43. MALDI-TOF mass spectrum for **PFT-Si** acquired in (+) ion reflector mode

(An = Th_2Si_2-$[FlTh_2Si_2]_n$-H; Bn = H-$[FlTh_2Si_2]_n$-H)
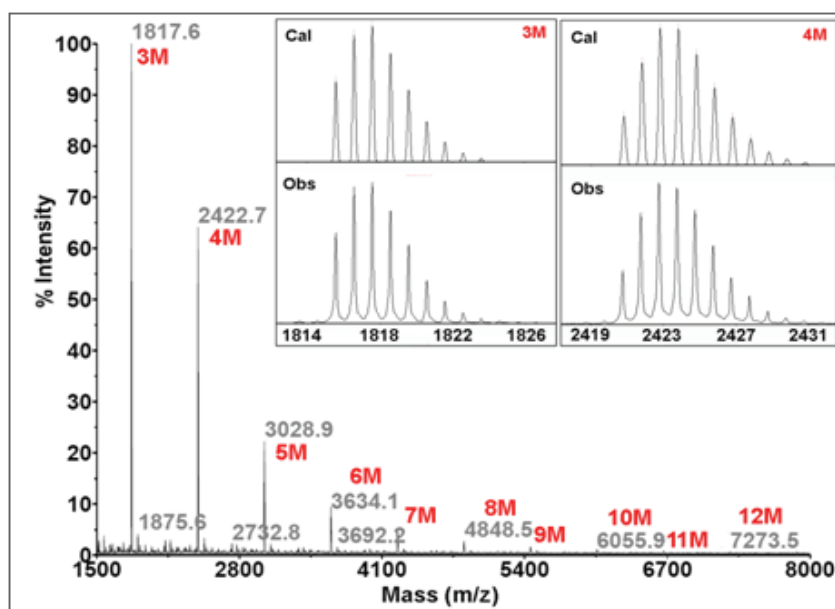
Figure 2-44. MALDI-TOF mass spectrum for **PCT-Si** acquired in (+) ion reflector mode

(nM = $[CzTh_2Si_2]_n$)
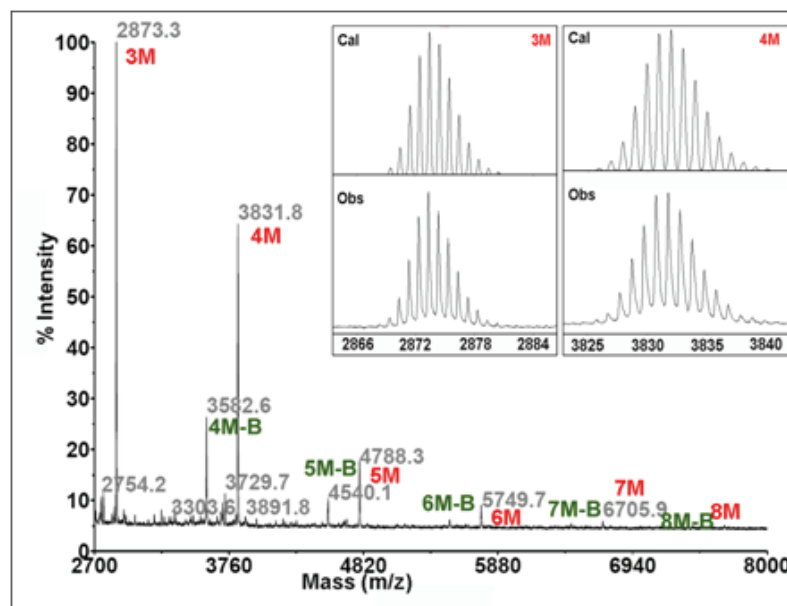
Figure 2-45. MALDI-TOF mass spectrum for **PCT-B** acquired in (+) ion reflector mode ($nM = [CzTh_2B_2]_n$; $nM-B = [CzTh_2B_2]_n -BMes_2$)

2.4.3 Thermal behavior of the polymers
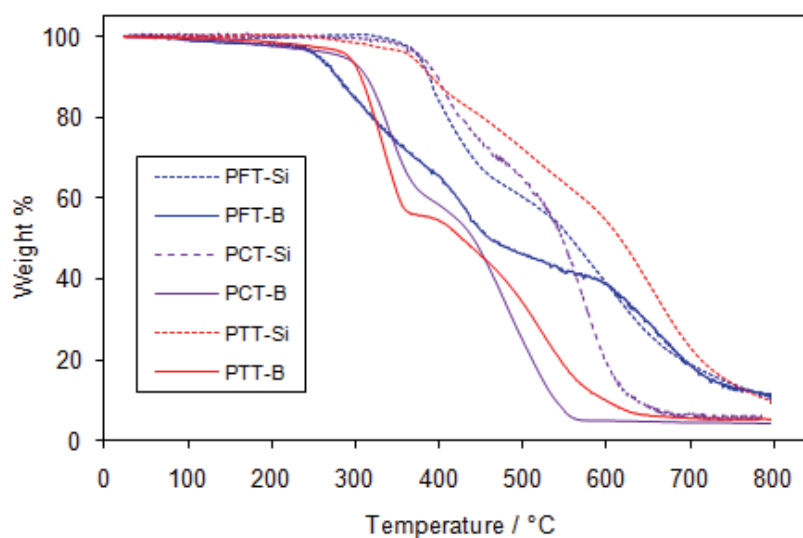
Figure 2-46. TGA traces for alternating copolymers (heating rate: 10 °C /min)

As outlined in **Table 2-5**, all the polymers obtained exhibit good thermal stabilities. A study by thermal gravimetric analysis (TGA) shows that they are all thermally stable up

to >250 °C. In comparison, modification with diarylboryl functional groups decreases the thermal stabilities and the borylated polymers decomposed at relatively lower temperature than their respective precursors (**Figure 2-46**).

2.4.4 Photophysical properties of the polymers

The photophysical properties of the organoborane polymers and their silylated precursors were examined by UV-Vis absorption and fluorescence spectroscopy. As shown in **Figure 2-47**, for the silyl-substituted polymers a single absorption is found in the region from 300 nm to 450 nm. This band is strongly red-shifted by ca. 70 nm when going to the respective borylated polymers PFT-B, PCT-B, and PTT-B. In addition, a new high-energy band emerges at about 335 nm, independent of the structure of the conjugated main chain skeleton. Therefore, this band is assigned to the 3,3'-bis(dimesitylboryl)-2,2'-bithiophene (Th_2B_2) chromophore. Based on our previous theoretical calculations on the borylated quaterthiophene species, QTBM (**Figure 2-48**), this transition is likely due to excitation into a cross conjugation state that involves contributions from the central bithiophene moietiy and the dimesitylboryl side groups.
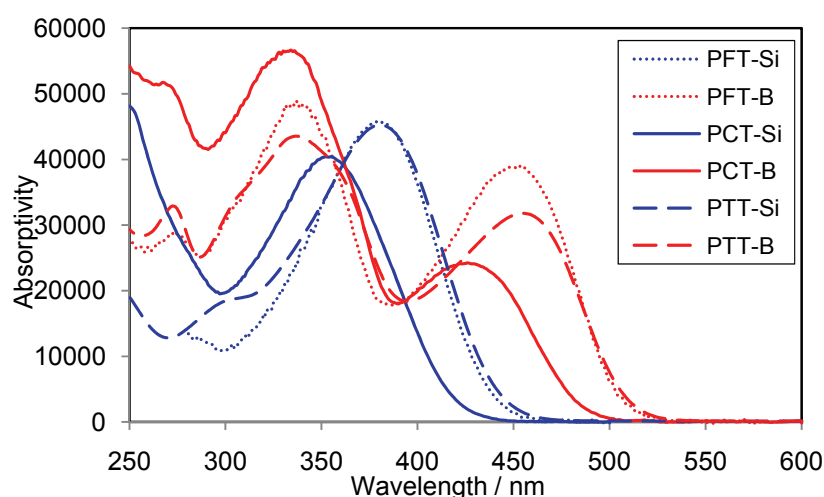
Figure 2-47. UV-vis absorption spectra (in CH$_2$Cl$_2$, ca. 1×10^{-5} to 1×10^{-6} M per repeat unit)

A comparison of the respective silylated and borylated polymers provides insight into the effect of the electronic structure of the co-monomer. The fluorene- and triarylamine-containing polymers PFT-Si and PTT-Si exhibit quite similar absorption characteristics. However, the absorption maximum at around 380 nm is red shifted by about 25 nm relative to that for PCT-Si at 355 nm. Similarly, the low energy absorption bands for PFT-B and PTT-B centered at around 454 nm are red-shifted by about 32 nm in comparison to that for PCT-B. Interesting is also to compare these results with our prior data for the all-thiophene polymers PTSi and PTBM.[43] The lowest energy absorptions for silylated PTSi and borylated PTBM are similar to those of the carbazole polymers PCT-Si and PCT-B, respectively, but considerably higher energy than those of the fluorene and triarylamine polymers. The optical band gaps were calculated from the absorption onset to be 2.45 eV for PFT-B, 2.55 eV for PCT-B, and 2.42 eV for PTT-B. They are by about 0.4 eV smaller than those for the silylated polymers, respectively, further reflecting the effect of functionalization with dimesitylboryl groups. The carbazole-based polymers show comparatively larger optical band gaps than the fluorene- or triarylamine polymers (**Table 2-7**). In addition, no significant wavelength shift in the absorption spectrum was observed for polymers PCT-B and PTT-B in different solvents varying from CH$_2$Cl$_2$, THF to pyridine.
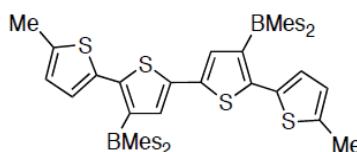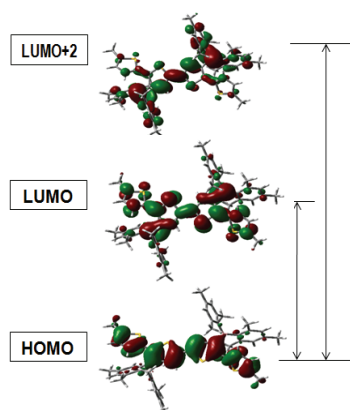
Figure 2-48. Calculated orbital plots for QTBM generated from Gaussview (scaling radii of 75%, isovalue of 0.02, performed with the Gaussian03 program using hybrid density functional B3LYP with the basis set of 6-31G(d))

All polymers are fluorescent and their emission spectra are illustrated in **Figure 2-49**. The silylated polymers emit in the blue green region with maxima ranging from 468 to 493 nm. Upon borylation, a single emission band emerges in the green region with a maximum at 533 nm for PFT-B, 527 nm for PCT-B, and 546 nm for PTT-B. These bands are red shifted by about 50 nm relative to those of the silylated polymers, which again is attributed to the electronic effect of the Mes_2B π-acceptor functionalities. However, in contrast to what we found from the absorption spectra, all the copolymers emit at much shorter wavelength than the thiophene polymers PT-Si and PTBM (PTSi, 554 nm; PTBM, 617 nm). This may suggest that electronic delocalization in the excited state is much more pronounced for the polythiophenes than the copolymers with fluorene, carbazole, or triarylamine moieties. Generally, the quantum efficiencies are considerably lower for the borylated polymers in comparison to the silylated polymers. This is likely related to the lower optical gap for the organoboron polymers, which favors non-radiative decay.

Measurements in different organic solvents (CH$_2$Cl$_2$, THF to pyridine) showed no apparent difference, suggesting no marked solvatochromic effect. Additionally, thin films exhibited similar absorption and emission profiles as summarized in **Table 2-7**, indicating that interchain aggregation and excimer formation are not favourable for this type of polymers.

Table 2-7. Photophysical and electrochemical properties of the polymers

Sample	PFT-Si	PFT-B	PCT-Si	PCT-B	PTT-Si	PTT-B
$E^{0'}{}_{Red}$/mV[a]	-2478 -2711(ir)	-2262 -2445	-2635 -2876 -3125	-2362 -2534	-2648 -2992	-2343 -2519
$E^{0'}{}_{Ox}$ /mV[b]	600 (623)[b] 964	560 (624)[b] 944	500 584	472 612 828	380 (375)[b] 704 932	392 (378)[b] 748 944
λ_{abs}/nm ($\varepsilon/\times10^4 M^{-1}cm^{-1}$)[c]	380 (4.58)	453 (3.96) 337 (4.85)	355 (4.05)	422 (2.49) 334 (5.68)	381 (4.52)	455 (3.17) 337 (4.35)
λ_{em}/nm[c]	484 (380)	533 (453)	468 (355)	527 (422)	493 (381)	546 (455)
Optical band gap[d]	2.84	2.45	2.96	2.55	2.79	2.42
Φ_{fl}[e]	0.19	0.07	0.10	0.02	0.14	0.04

λ_{abs}/nm^{f}	379	443 340	357	431 344	376	445 340
$\lambda_{em}/nm^{f,g}$	481	536	487	509	488	548

[a] In THF/ 0.1M $Bu_4N[PF_6]$, 100 mV/s, referenced vs. Fc/Fc^+ couple; [b] from square wave voltammogram in CH_2Cl_2/ 0.1M $Bu_4N[PF_6]$, 100 mV/s, referenced vs. Fc/Fc^+ couple; [c] In CH_2Cl_2; [d] Calculated from the absorption onset; [e] referenced vs. diphenylanthracene; [f] Thin film; [g] excited at $\lambda_{abs,max}$.
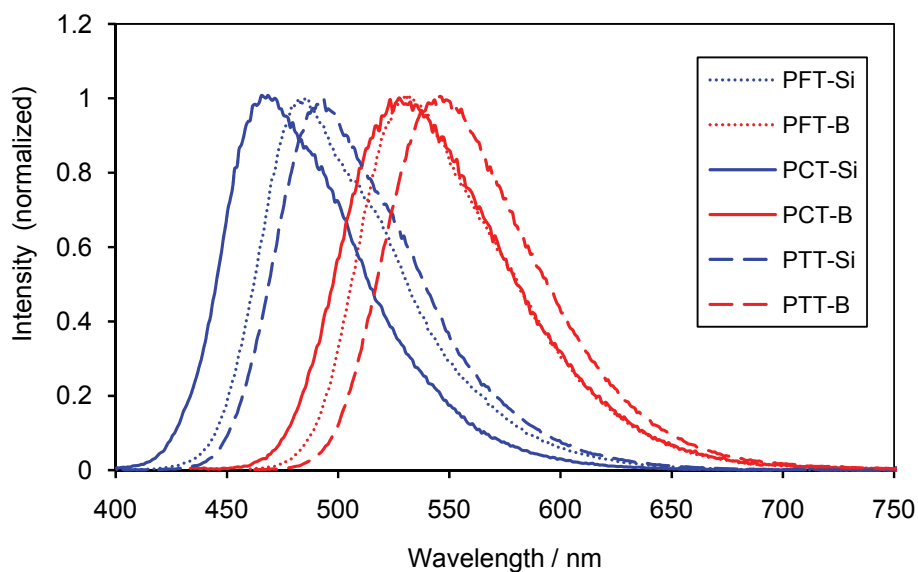
Figure 2-49. Fluorescence spectra of PFT-Si, PCT-Si, PTT-Si, PFT-B, PCT-B and PTT-B (in CH_2Cl_2, ca. 1×10^{-5} to 1×10^{-6} M per repeat unit, normalized at λ_{max})
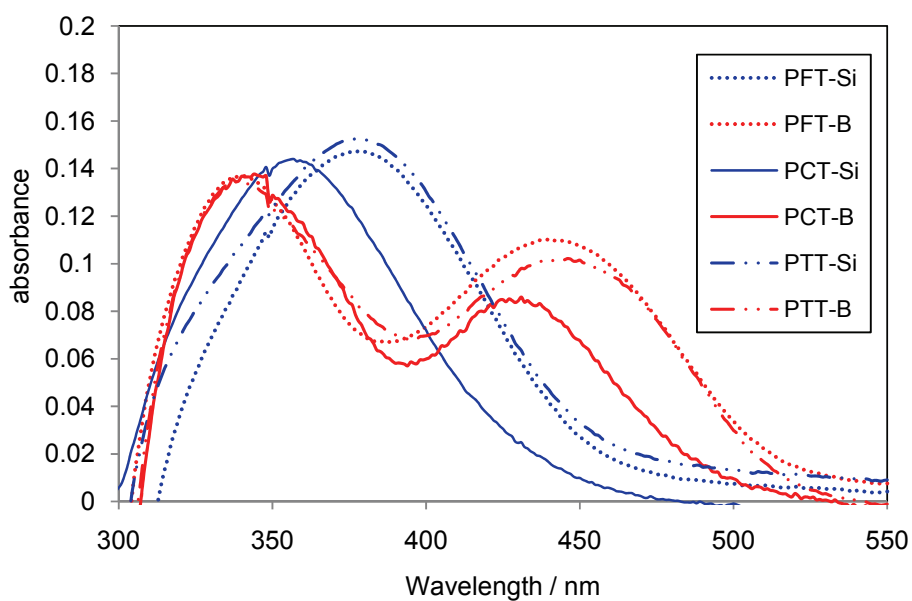
Figure 2-50. UV-vis absorption spectra for thin films of PFT-Si, PCT-Si, PTT-Si, PFT-B, PCT-B and PTT-B
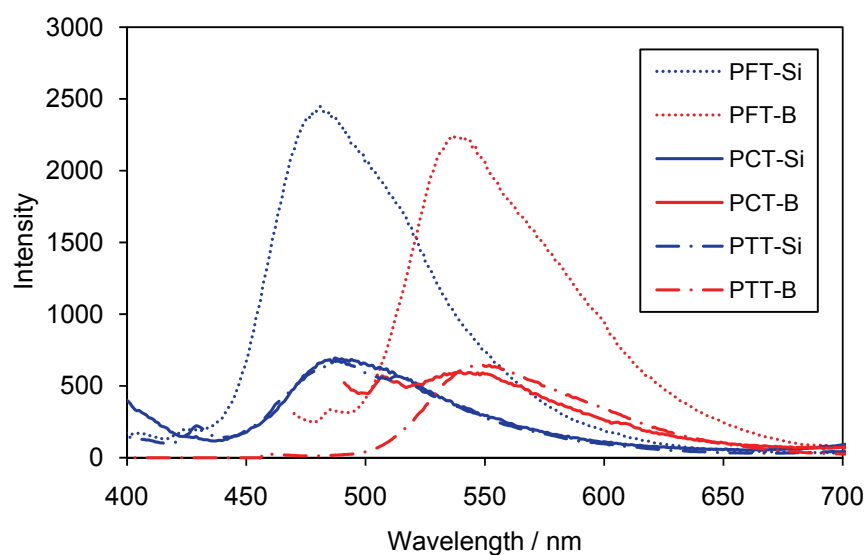
Figure 2-51. Fluorescence spectra for thin films of PFT-Si, PCT-Si, PTT-Si, PFT-B, PCT-B and PTT-B (excited at $\lambda_{max,abs}$)

2.4.5 Electrochemical properties of the polymers

The electrochemical properties were studied by cyclic voltammetry and square wave voltammetry. Two quasi-reversible cathodic waves were observed for all three boron polymers, which correspond to successive reduction of the two boron centers connected by the bithiophene moieties. The difference in the redox potential for the two waves varies from 176 eV for PTT-B to 183 eV for PFT-B, which is slightly smaller than what we found for PTBM (230 mV). The first reduction occurs at significantly less negative potential than that for the silicon polymers ($\Delta E > 200$ mV), which further illustrates that the LUMO energy level is lowered by attachment of the electron withdrawing Mes_2B functionalities. The LUMO energy levels are also affected by the nature of the conjugated main chain skeleton, although the effect is less pronounced. With the relatively more electron rich nitrogen containing co-monomers, PCT-B and PTT-B are reduced at more negative potentials than PFT-B. This trend also holds for polymers PFT-Si, PCT-Si and PTT-Si.

In contrast to what we find for the reduction processes, the oxidation potentials for the polymers are not strongly influenced by the nature of the side chain substituents. The potential differences are less than 30 mV between the boron polymers and the silicon precursors. A reversible oxidation wave due to oxidation of the triarylamine moieties is found at 380 mV for PTT-Si and 392 mV for PTT-B with two additional unresolved oxidation waves at higher potentials. This second feature is also found for the other polymers and attributed to oxidation of the conjugated polymer main chain.
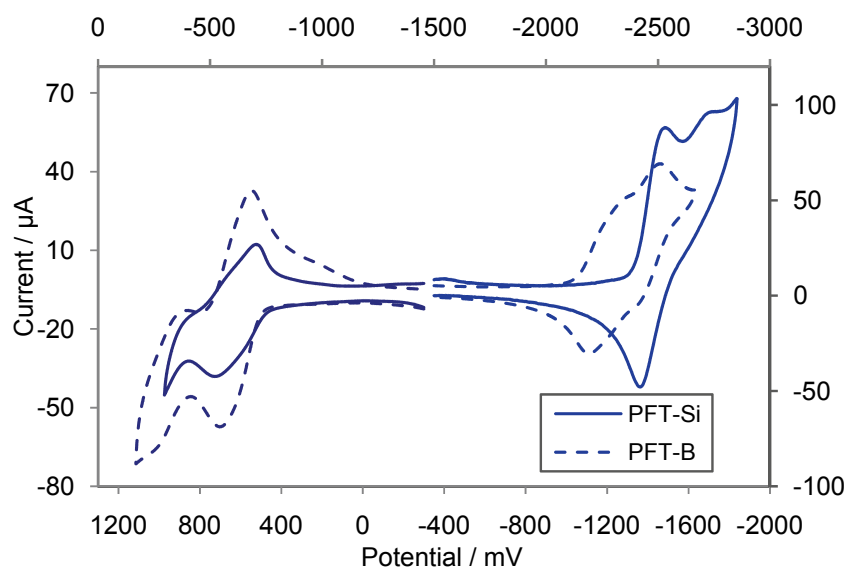
Figure 2-52. Cyclic voltammogram of PFT-Si and PFT-B (anodic scan: CH_2Cl_2 / 0.1 M $Bu_4N[PF_6]$, 100 mV/s; cathodic scan: THF / 0.1 M $Bu_4N[PF_6]$, 100 mV/s; reported relative to Fc/Fc$^+$ couple)
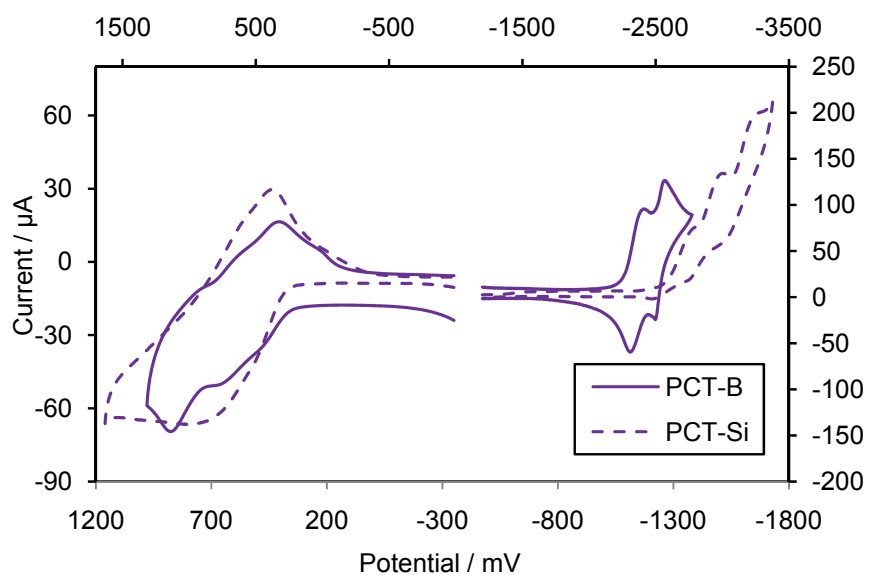
Figure 2-53. Cyclic voltammogram of PCT-Si and PCT-B (anodic scan: CH_2Cl_2 / 0.1 M $Bu_4N[PF_6]$, 100 mV/s; cathodic scan: THF / 0.1 M $Bu_4N[PF_6]$, 100 mV/s; reported relative to Fc/Fc^+ couple)
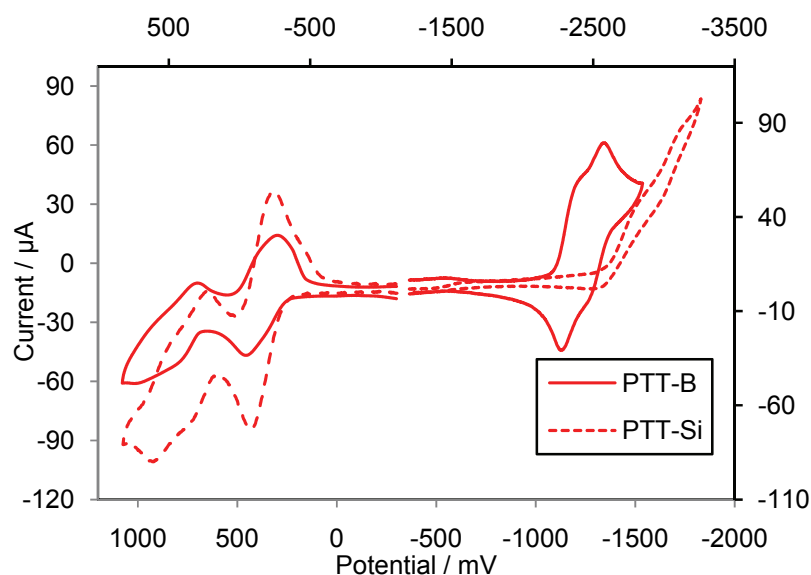
Figure 2-54. Cyclic voltammograms of PTT-Si and PTT-B (anodic scan: CH_2Cl_2 / 0.1 M $Bu_4N[PF_6]$, 100 mV/s; cathodic scan: THF / 0.1 M $Bu_4N[PF_6]$, 100 mV/s; reported relative to Fc/Fc^+ couple)

2.5 Conclusions

Acceptor type diarylboryl functionalized polythiophene was first prepared by Anand Sundararaman through a post-polymerization modification route. We have performed complexation studies that show the resulting polymer PTBM exhibits good selectivity towards different anions. It strongly binds to fluoride, cyanide and hydroxide ions, and partially binds to azide, but showed no affinity to other anions such as chloride, bromide, and nitrate. Interestingly, binding to fluoride and cyanide led to different photophysical

phenomena, which, on the basis of complexation studies for a quterthiophene model with fluoride and cyanide and single crystal X-ray structures for their complexes, might be due to differences in the conformation of the thiophene main chain.

Ferrocenylboryl groups were also introduced through a two-step modification reaction with $FcSnM_3$ and ArCu (Ar =Mes or Tip). The bulky Tip group dramatically improved the chemical stability of the borane polymers, while interesting electrochemical properties were brought up by the redox active ferrocenyl groups. Clear structure-property relationships for the polymers have been deduced by 1D and 2D NMR, single crystal X-ray structures for the models and electrochemical and photophysical results.

To further gain insight into how the chemical structure influences the electronic properties, a series of alternating copolymers involving fluorene, carbazole and triphenylamine derivatives have been prepared through standard Suzuki coupling reaction followed by post-polymerization borylation. Photophysical and electrochemical studies indicated that the energy gap became much narrower for the borylated polymers than that for their respective silylated precursors, due to the fact that the LUMO energy levels are lowered by the dimesitylboryl groups but the HOMO remains unchanged. In addition, electron rich carbazole and triphenylamine moieties embedded in the main chain slightly increase the HOMO energy levels of PCT-B and PTT-B.

2.6 Experimental section

Fluorene, carbazole, diphenylamine and BBr_3 were purchased from Aldrich, ^nBuLi (1.6 M in hexanes) from Fisher Scientific, Me_3SnCl from Strem Chemical. N,N-bis(4-bromophenyl)-2,4,6-trimethylaniline[46], mesitylcopper (MesCu)[47] and 2,7-dibromo-9,9'-

dihexylfluorene[48], 2,2'-(9,9-dihexyl-fluorene-2,7-diyl)bis(4,4,5,5-tetramethyl-1,3,2-dioxaborolane) (Fl(BPin)$_2$)[49] 9-(4-tert-butylphenyl)-3,6-bis(4,4,5,5-tetramethyl-1,3,2-dioxaborolan-2-yl)-carbazole (Cz(BPin)$_2$)[49], 2,4,6-trimethyl-N,N-bis(4-(4,4,5,5-tetramethyl-1,3,2-dioxaborolan-2-yl)phenyl)aniline (TPA(BPin)$_2$)[49] (5,5'-diiodo-2,2'-bithiophene-4,4'-diyl)bis(trimethylsilane) (T$_2$I$_2$)[43], QTBBr[37], PTBBr[37], and 2-trimethylstannylferrocene[50] were prepared according to literature procedures. All air or moisture-sensitive reactions and manipulations were carried out under an atmosphere of pre-purified nitrogen using Schlenk techniques or an inert atmosphere glove box (mBraun). Ether solvents were distilled from Na / benzophenone prior to use. Hydrocarbon and chlorinated solvents were purified using a solvent purification system (Innovative Technologies, alumina / copper columns for hydrocarbon solvents), and chlorinated solvents were subsequently distilled from CaH$_2$ and degassed via several freeze-pump-thaw cycles.

All 499.9 MHz ^{1}H, 125.7 MHz ^{13}C, and 160.4 MHz ^{11}B NMR spectra were recorded at ambient temperature on a Varian INOVA spectrometer equipped with a boron-free 5 mm dual broadband gradient probe (Nalorac, Varian Inc., Martinez, CA). Solution ^{1}H and ^{13}C NMR spectra were referenced internally to solvent signals. ^{11}B NMR spectra were acquired with boron-free quartz NMR tubes and referenced externally to BF$_3$ · Et$_2$O (δ = 0).

GPC analyses were performed in THF (1 mL/min) using a Waters Breeze system equipped with a 717plus autosampler, a 1525 binary HPLC pump, a 2993 Photodiode Array Detector, and a 2414 refractive index detector. For separation the samples were passed through a series of styragel columns (Polymer Laboratories; two columns 5 μm /

Mixed-C), which were kept in a column heater at 35 °C. The columns were calibrated with polystyrene standards (Polymer Laboratories). Multi-angle laser light scattering (MALLS) experiments were performed at 690 nm (30 mW linear polarized GaAs laser) using a Wyatt Dawn EOS instrument in-line with the GPC; the differential refractive indices dn/dc was calculated from in-line GPC-MALLS mode with the Wyatt Astra software assuming 100% mass recovery.

MALDI-TOF measurements were performed on an Applied Biosystems 4800 Proteomics Analyzer in reflectron (+) mode with delayed extraction. Benzo[α]pyrene was used as the matrix (10 mg/mL in toluene). Samples were prepared in toluene (10 mg/mL), mixed with the matrix in a 1:10 ratio, and then spotted on the wells of a sample plate inside a glove box. Peptides were used for calibration (Des-Arg-Bradykinin (904.4681), Angiotensin I (1296.6853), Glu-Fibrinopeptide B (1570.6774), ACTH (clip 1-17) (2093.0867), ACTH (clip 18-39) (2465.1989), ACTH (clip 7-38) (3657.9294) with α-hydroxy-4-cyanocinnamic acid as the matrix).

UV-visible absorption data were acquired on a Varian Cary 500 UV-Vis / NIR spectrophotometer. The fluorescence data and quantum yields were measured on a Varian Cary Eclipse Fluorescence spectrophotometer with the same solutions as those used in the UV-visible measurements. 9,10-diphenylanthracene was used as the standard for determination of the quantum yields (Φ). Sample solutions were prepared using a microbalance (±0.1 mg) and volumetric glassware. The quantum yield was calculated by plotting a graph of integrated fluorescence intensity vs absorbance of at least four solutions with increasing concentration. The gradient of the graph is proportional to the

quantum yield. The formula used to calculate the absolute quantum yield is $\Phi = \Phi$ standard $\times$ Gradient $_{compound}$ / Gradient $_{standard}$.

Cyclic voltammetry was carried out on a CV-50W analyzer from BAS. The three-electrode system consisted of an Au disk as working electrode, a Pt wire as secondary electrode and a Ag wire as the reference electrode. The voltammograms were recorded with ca. 10^{-3} M solutions in THF (reduction waves) or CH_2Cl_2 (oxidation waves) containing 0.1 M $Bu_4N[PF_6]$ (reductions scans) or 0.05 M $Bu_4N[B(C_6F_5)_4]$ (oxidation scans) as the supporting electrolyte. The scans were referenced after the addition of a small amount of ferrocene or decamethylferrocene as internal standard. The potentials are reported relative to the ferrocene/ferrocenium couple (-610 mV for $Cp^*_2Fe/Cp^*_2Fe^+$ in CH_2Cl_2 / 0.05 M $Bu_4N[B(C_6F_5)_4]$, -552 mV for $Cp^*_2Fe/Cp^*_2Fe^+$ in CH_2Cl_2 / 0.1 M $Bu_4N[PF_6]$ and -548 mV for $Cp^*_2Fe/Cp^*_2Fe^+$ in THF / 0.1 M $Bu_4N[PF_6]$). Elemental analyses were obtained from Quantitative Technologies Inc., Whitehouse, NJ.

X-ray diffraction intensities of QTBM-CN, QTBM-F and QTBFT were collected on a Bruker SMART APEX CCD diffractometer. Crystallographic data and details of the X-ray diffraction experiment and crystal structure refinement are given in Apendix. SADABS[51] absorption correction was applied and the structures were solved using direct methods and completed by subsequent difference Fourier syntheses and refined by full matrix least-squares procedures on reflection intensities (F^2). All non-hydrogen atoms were refined with anisotropic displacement coefficients. The H atoms were placed at calculated positions and were refined as riding atoms. All software and sources scattering factors are contained in the SHELXTL (6.14) program package.[52]

Caution! BBr$_3$ is toxic and corrosive and should be handled appropriately with great care. Fluorinated grease was used for ground glass joints in reactions involving BBr$_3$.

Synthesis of QTBM-F complex: A solution of **QTBM** (50 mg, 0.059 mmol) in 5 mL of THF was slowly added to a mixture of KF (30 mg, 0.51 mmol) and 18-crown-6 (34.0, 0.129 mmol) in THF while stirring. The reaction mixture was stirred at RT for 12 h followed by the removal of the solvent. The residue was washed with 2×10 mL of hexanes and then with 2 mL of dry ether. Clear yellow-orange crystals were obtained by layering the THF solution of the crude product with hexanes. Yield: 42 mg (48%). For **QTBM-F**: ^{1}H NMR (CD$_3$CN, 499.9 MHz): δ = 6.58 (s, 8H, Mes), 6.51 (br, 2H, Th), 6.40 (br, 2H, Th), 6.25 (br, 2H, Th), 3.55 (s, 48H, CH$_2$), 2.36 (s, 6H, Me), 2.19 (s, 24, *o*-Me), 1.96 (s, 12H, *p*-Me); ^{11}B NMR (CDCl$_3$, 160.3 MHz): δ = 4.7 (w$_{1/2}$ = 960 Hz).

Synthesis of QTBM-CN complex: A solution of **QTBM** (50 mg, 0.059 mmol) in 5 mL of THF was slowly added to a solution of ^{n}Bu$_4$NCN (30 mg, 0.51 mmol) in THF while stirring. The reaction mixture was stirred at RT for 12 h followed by the removal of the solvent. The residue was washed with 2×10 mL of hexanes and then with 2 mL of dry ether. Clear yellow-orange crystals were obtained by layering the CH$_2$Cl$_2$ solution of the crude product with hexanes. Yield: 47 mg (58%). For **QTBM-CN**: ^{1}H NMR (CD$_3$CN, 499.9 MHz): δ = 6.58 (s, 8H, Mes), 6.51 (br, 2H, Th), 6.40 (br, 2H, Th), 6.25 (br, 2H, Th), 3.07 (m, 16H, CH$_2$), 2.36 (s, 12H, *p*-Me), 2.19 (s,24, *o*-Me), 2.14 (s, 6H, Me), 1.59 (m, 16H, CH$_2$), 1.35 (m, 16H, CH$_2$), 0.96 (m, 24H, CH$_3$),; ^{11}B NMR (CDCl$_3$, 160.3 MHz): δ = -16 (w$_{1/2}$ = 160 Hz); Analysis calcd for C$_{88}$H$_{128}$B$_2$N$_4$S$_4$: C 75.94, H 9.27, N 4.03%; found C 75.25, H 9.58, N 4.35%.

Synthesis of QTBFM: **QTBBr** (100 mg, 0.143 mmol) in 5 mL of CH_2Cl_2 was treated with $FcSnMe_3$ (100 mg, 0.29 mmol) in 5 mL of CH_2Cl_2 and kept stirring for 12 h. Me_3SnBr was removed by repeatedly dissolving the crude materials in toluene and drying under high vacuum. Selective attachment of the ferrocenyl groups was confirmed by ^1H NMR (CDCl$_3$, 499.9 MHz): δ = 7.56 (s, 2H, Th-H8,8'), 6.95 (d, ^3J = 2.5 Hz, 2H, Th-H3,3'), 6.58 (br, 2H, Th-H4,4'), 4.76 (br, 4H, Cp-H2,5), 4.37 (br, 4H, Cp-H3,4), 4.20 (s, 10H, C$_5$H$_5$), 2.42 (s, 6H, Me). Without further purification, the product was re-dissolved in 8 mL of toluene and (MesCu)$_5$·toluene (63 mg, 0.31 mmol "MesCu") in 5 mL of toluene was added slowly and the reaction mixture was kept stirring at 100 °C for 24 h. A precipitate (CuBr) formed, which was removed by filtration through a fritted glass disk. All volatile components were removed under high vacuum and the product was crystallized from toluene at –35 °C. Yield: 82 mg (58%). For **QTBFM**: ^1H NMR (CDCl$_3$, 499.893 MHz): δ = 8.21 (s, 2H, Th^B-H), 6.63 (s, 4H, Mes-H), 6.33 (d, ^3J = 3.0 Hz, 2H, Th^{Me}-H), 6.28 (d, ^3J = 3.0 Hz 2H, Th^{Me}-H), 4.73 (pst, ^3J = 2.0 Hz, 4H, Cp-H2,5), 4.44 (pst, ^3J = 2.0 Hz, 4H, Cp-H3,4), 4.32 (s, 10H, C$_5$H$_5$), 2.32 (s, 6H, Me), 2.26 (s, 6H, p-Me), 2.08 (s, 12H, o-Me); ^{13}C NMR (CDCl$_3$, 125.7 MHz): δ = 145.9, 145.5, 142.7, 141.1, 139.0, 137.0, 136.1, 133.5, 132.9, 128.5, 127.2, 124.8 (Th-C, Mes-C), 77.9 (Cp-C), 76.7 (Cp-C$_i$), 74.7 (Cp-C), 69.7 (C$_5$H$_5$), 23.6 (o-Me), 21.3 (p-Me), 15.2 (Me); ^{11}B NMR (CDCl$_3$, 160.3 MHz): δ = 67 (w$_{1/2}$ = 3000 Hz); UV-Vis (CH$_2$Cl$_2$): λ_{max} = 326 (ε = 26900), 376 (ε = 21670), 494 nm (ε = 3900); MALDI-TOF: m/z = 986.2166 (calcd for $^{12}C_{56}{}^1H_{52}{}^{11}B_2{}^{32}S_4{}^{56}Fe_2$ 986.1837). Analysis calcd for $C_{56}H_{52}B_2Fe_2S_4$: C 68.18, H 5.31; found C 67.90, H 5.38%.

Synthesis of Polymer PTBFM: A solution of PTBBr prepared from BBr$_3$ (324 mg, 1.3 mmol) and PTSi (320 mg, 1.0 mmol of SiMe$_3$ groups) in 15 mL of CH$_2$Cl$_2$ was treated with FcSnMe$_3$ (506 mg, 1.45 mmol) in 5 mL of CH$_2$Cl$_2$ and kept stirring for 12 h. The reaction solution was concentrated under high vacuum to 3 mL and then precipitated into 500 mL of hexanes and washed twice with hexanes. Selective formation of the ferrocenyl-substituted product was confirmed by ^{1}H NMR (CDCl$_3$, 499.9 MHz): δ = 7.60 (s, 2H, B$_2$Th$_2$-H3,3'), 6.92 (s, 2H, Hx$_2$Th$_2$-H7,7'), 4.72 (br, 4H, Cp-H2,5), 4.35 (br, 4H, Cp-H3,4), 4.19 (br, 10H, C$_5$H$_5$), 2.29 (br, 4H, Hex), 1.4-1.2 (m, 8H, Hex-CH$_2$), 1.2-1.1 (m, 4H, Hex-CH$_2$), 1.1-1.0 (m, 4H, Hex-CH$_2$), 0.87 (t, ^{3}J = 6.5 Hz, 6H, Hex-CH$_3$). Without further purification, the product was redissolved in 15 mL of toluene, (MesCu)$_5$·toluene (302 mg, 1.48 mmol "MesCu") in 5 mL of toluene was added slowly, and the reaction mixture was kept stirring at 100 °C for 24 h. A solid precipitate (CuBr) formed and was removed by filtration through a fritted glass disk. The reaction solution was concentrated under high vacuum to 2 mL and then precipitated into 500 mL of cold hexanes. The red powdery product was washed with cold hexanes and dried under high vacuum for 12 h. Yield: 0.32 g (57 %). For PTBFM: ^{1}H NMR (CDCl$_3$, 499.893 MHz): δ = 8.27 (s, 2H, Th^B-H), 6.65 (s, 4H, Mes-H), 6.24 (s, 2H, Th^{Hex}-H), 4.74 (br, 4H, Cp-H2,5), 4.45 (br, 4H, Cp-H3,4), 4.34 (br, 10H, C$_5$H$_5$), 2.20 (br s, 6H, *p*-CH$_3$), 2.12 (br s, 12H, *o*-CH$_3$), 1.4-1.2 (m, 20H, Th-HxCH$_2$), 0.80 (t, ^{3}J = 6.5 Hz, 4H, Hexyl-Me); ^{13}C NMR (CDCl$_3$, 125.7 MHz): δ = 145.6, 142.8, 142.0, 139.1, 137.0, 136.2, 135.0, 133.6, 129.36, 129.55, 127.50 (Th-C, Mes-C), 77.9 (Cp-C), 74.7 (Cp-C), 69.68 (C$_5$H$_5$), Cp-C$_i$ not observed, 23.7 (*o*-CH$_3$), 21.6 (*p*-CH$_3$), 32.0, 30.4, 29.5, 28.6, 22.9, 14.4 (hexyl); ^{11}B NMR (CDCl$_3$, 160.3 MHz): δ = 60 ($w_{1/2}$ = 4000 Hz); GPC-RI (in THF against PS

standards) M_w = 14527, *PDI* = 1.54; GPC-MALLS (THF, dn/dc = 0.198 mL/g): M_w = 20,650, *PDI* = 1.88; UV-Vis (CH$_2$Cl$_2$ ε corresponding to quaterthiophene repeating units): λ_{max} = 334 (ε = 31000), 401 (ε = 31000), 498 nm (shoulder, ε = 5830); TGA (N$_2$, 20 °C / min): T_{dec} = 220 °C (onset, 80% weight loss at 900 °C). Analysis calcd for (C$_{33}$H$_{35}$B$_1$Fe$_1$S$_2$)$_n$: C 70.22, H 6.61; found C 69.26, H 6.38%.

Synthesis of QTBFT: FcSnMe$_3$ (100 mg, 0.29 mmol) in 5 mL of CH$_2$Cl$_2$ was added to QTBBr (100 mg, 0.14 mmol) in 5 mL of CH$_2$Cl$_2$. The solution turned red immediately and was kept stirring for 12 h at RT. After the solvent was evaporated, the crude materials were repeatedly dissolved in toluene and dried under high vacuum to remove completely Me$_3$SnBr. Formation of the ferrocene-substituted intermediate was confirmed by ^{1}H NMR. Without further purification, the crude product was re-dissolved in 8 mL of toluene and a solution of 2,4,6-triisoproylphenyl copper (TipCu) (92 mg, 0.35 mmol) in 5 mL of toluene was added. The reaction mixture was kept stirring at 110 °C for 48 h. The solid by-product CuBr was removed by filtration through a fritted glass disk. All volatile components were removed under high vacuum and the crude product was crystallized from a mixture of toluene and hexanes at –35 °C to afford a red microcrystalline solid. Yield: 121 mg (73%). For **QTBFT**: ^{1}H NMR (CDCl$_3$, 499.9 MHz): δ = 8.40 (s, 2H, Th^B-H), 6.91 (s, 4H, Mes-H), 6.22 (br, d, ^3J = 2.5 Hz, 2H, Th^{Me}-H), 5.77 (d, ^3J = 3.5 Hz, 2H, Th^{Me}-H), 4.66 (br, 4H, Cp-H2,5), 4.48 (br, 4H, Cp-H3,4), 4.37 (s, 10H, C$_5$H$_5$), 2.93 (septet, 2H, p-^{i}Pr), 2.67 (m, 4H, o-^{i}Pr), 2.30 (s, 6H, Me), 1.33 (d, ^3J = 7.0 Hz, 12H, p-^{i}Pr), 1.09 (d, ^3J = 6.0 Hz, 12H, o-^{i}Pr), 0.80 (d, ^3J = 6.0 Hz, 12H, o-^{i}Pr); ^{13}C NMR (CDCl$_3$, 125.7 MHz): δ = 149.2, 148.9, 146.2, 144.6, 143.9, 141.2, 135.3, 134.4, 133.5, 129.0, 125.6, 120.7 (aromatic C), 78.4 (Cp-C), 78.1 (Cp-C), 73.7 (Cp-C), 69.7 (C$_5$H$_5$), 35.4

(^{o}CHMe$_2$), 34.7 (^{p}CHMe$_2$), 30.0, 25.1, 24.7, 23.9, 15.2 (Th-CH$_3$); ^{11}B NMR (CDCl$_3$, 160.3 MHz): δ = 67 (w$_{1/2}$ = 4800 Hz); UV-Vis (CH$_2$Cl$_2$): λ_{max} = 290 (ε = 34800), 386 (ε = 24300), 501 nm (ε = 8210); CV (THF): $E_{1/2}$ = –2.48 V (ΔE_p = 110 mV); $E_{1/2}$ = –2.66 V (ΔE_p = 168 mV); CV (CH$_2$Cl$_2$): $E_{1/2}$ = 135 mV (ΔE_p = 148 mV), $E_{1/2}$ = 957 mV (ΔE_p = 174 mV), $E_{1/2}$ = 1.15 V (ΔE_p = 142 mV); MALDI-TOF: m/z = 1154.3606 (calcd for ^{12}C$_{68}$^{1}H$_{76}$^{11}B$_2$^{32}S$_4$^{56}Fe$_2$ 1154.3734). Analysis calcd for C$_{68}$H$_{76}$B$_2$Fe$_2$S$_4$: C 70.72, H 6.63; found: C 70.81, H 6.19.

Synthesis of Polymer PTBFT: A solution of **PTBBr** was prepared from BBr$_3$ (100 mg, 0.39 mmol), **PTSi** (100 mg, 0.31 mmol of SiMe$_3$ groups) and FcSnMe$_3$ (158 mg, 0.45 mmol) as described above. The product was analyzed by ^{1}H NMR (CDCl$_3$, 499.9 MHz): δ = 7.60 (s, 2H, B$_2$Th$_2$-H3,3'), 6.92 (s, 2H, Hx$_2$Th$_2$-H7,7'), 4.72 (br, 4H, Cp-H2,5), 4.35 (br, 4H, Cp-H3,4), 4.19 (br, 10H, C$_5$H$_5$), 2.29 (br, 4H, Hex), 1.4-1.2 (m, 8H, Hex-CH$_2$), 1.2-1.1 (m, 4H, Hex-CH$_2$), 1.1-1.0 (m, 4H, Hex-CH$_2$), 0.87 (t, ^{3}J = 6.5 Hz, 6H, Hex-CH$_3$). The crude product was re-dissolved in 5 mL of toluene, a solution of TipCu (123 mg, 0.46 mmol) in 3 mL of toluene was added, and the reaction mixture was kept stirring at 110 °C for 48 h. A solid precipitate (CuBr) formed and was removed by filtration through a fritted glass disk. The filtrate was concentrated under high vacuum to 1 mL and then precipitated into 100 mL of cold hexanes. A red precipitate formed, which was washed with hexanes twice and freeze-dried from benzene to afford a powdery red product. Yield: 120 mg (60 %). For **PTBFT**: ^{1}H NMR (CDCl$_3$, 499.9 MHz): δ = 8.44 (s, 2H, B$_2$Th$_2$-H3,3'), 6.91 (s, 4H, Mes-H), 5.90 (s, 2H, Hx$_2$Th$_2$-H7,7'), 4.65 (br, 4H, Cp-H2,5), 4.43 (br, 4H, Cp-H3,4), 4.37 (br, 10H, C$_5$H$_5$), 2.88 (br, 2H, p-^{i}Pr), 2.67 (br, 4H, o-

^{i}Pr), 2.05 (br, 4H, Hex), 1.4-0.9 (m, 40H, Hex-CH$_2$,^{i}Pr-CH$_3$), 0.90-0.75 (m, 18H, Hex-CH$_3$,^{i}Pr-CH$_3$); ^{13}C NMR (CDCl$_3$, 125.7 MHz): δ = 149.0, 148.8, 145.5, 144.6, 144.0, 142.6, 135.8, 135.5, 134.7, 130.8, 130.0, 120.8, (aromatic C), 78.4 (Cp-C), 73.7 (Cp-C), 69.7 (C$_5$H$_5$), Cp-C$_i$ not observed, 35.5 (Tip-CH), 34.4 (Tip-CH), 32.1 (Hex), 30.8 (Hex), 29.2 (Hex), 28.9 (Hex), 25.0 (Tip-CH$_3$), 24.3 (Tip-CH$_3$), 22.8 (Hex), 14.4 (Hex); ^{11}B NMR (CDCl$_3$, 160.3 MHz): δ = 58 ($w_{1/2}$ = 5120 Hz); GPC-RI (in THF against PS standards) M_w =24063, M_n =14600, PDI = 1.65; GPC-MALLS (THF, dn/dc = 0.171 mL/g): M_w = 50,800, PDI = 1.60; UV-Vis (CH$_2$Cl$_2$, ε corresponding to quaterthiophene repeating units): λ_{max} = 290 (ε = 37700), 416 (ε = 34000), 511 nm (shoulder, ε = 5108). TGA (N$_2$, 10 °C / min): T_{dec} = 236 °C (onset, 87% weight loss at 800 °C); CV (THF): $E_{1/2}$ = –2.36 V (ΔE_p = 158 mV); $E_{1/2}$ = –2.60 (ΔE_p = 181 mV); CV (CH$_2$Cl$_2$): $E_{1/2}$ = 156 mV (ΔE_p = 182 mV), $E_{1/2}$ = 928 mV (ΔE_p = 265 mV), $E_{1/2}$ = 1.23 V (irreversible).

Preparation of PFT-Si: An equimolar quantity of T$_2$I$_2$ (0.96 g, 1.71 mmol) and Fl(BPin)$_2$ (1.00 g, 1.71 mmol) were dissolved in 5 mL of toluene, Pd(PPh$_3$)$_4$ (39.6 mg, 0.034 mmol) was added and the mixture was transferred into a reaction tube, followed by addition of 4.5 mL of a degassed solution of aqueous K$_2$CO$_3$ (2.0 M). The reaction mixture was slowly heated to 110 ºC and kept stirring at that temperature for 2 days. The mixture was then cooled back to room temperature and the catalyst residue was removed by passing the organic layer through a short plug of alumina. The yellow filtrate was concentrated to 2 mL and precipitated into 150 mL of acetone. The product was isolated as yellow powder and dried under high vacuum at 50 ºC. Yield: 0.70 g, 65%. ^{1}H NMR (499.9 MHz, CDCl$_3$): δ = 7.76 (d, ^{3}J = 8.5 Hz, 2H, Fl), 7.49 (m, 4H, Fl), 7.22 (s, 2H, Th), 2.05 (br, 4H, Hex), 1.2-1.0 (m, 12H, Hex), 0.79 (t, ^{3}J = 7.5 Hz, 6H, Hex), 0.68 (br, 4H,

Hex), 0.20 ppm (s, 18H, SiMe$_3$); ^{13}C NMR (125.7 MHz, CDCl$_3$): δ = 151.2, 141.0, 139.0, 136.7, 135.4, 130.8, 129.0, 124.4, 119.7, 55.7 (Fl), 41.0 (Hex), 31.8 (Hex), 29.9 (Hex), 24.0 (Hex), 22.8 (Hex), 14.2 (Hex), 0.8 ppm (Si(CH$_3$)$_3$); ^{29}Si NMR (99.3 MHz, CDCl$_3$): δ = −8.1 ppm; GPC-RI (in THF against polystyrene standards) M_w = 2.52×10^4, M_n = 1.35×10^4, PDI = 1.86; UV-Vis (CH$_2$Cl$_2$, 3.39×10^{-6} M): λ_{max} (ε, M^{-1}cm^{-1}) = 380 nm (4.58×10^4); fluorescence (CH$_2$Cl$_2$, 3.39×10^{-6} M): $\lambda_{em,max}$ = 484 nm (λ_{exc} = 376 nm, Φ = 10%); TGA (N$_2$, 10 ºC/min): T$_{dec}$ = 376 ºC (onset), 10% residue at 800 ºC.

Preparation of PFT-B: At −35 ºC, a solution of PFT-Si (200 mg, 0.31 mmol) in 4 mL of CH$_2$Cl$_2$ was added dropwise to a solution of BBr$_3$ (194 mg, 0.77 mmol) in 2 mL of CH$_2$Cl$_2$. A green solution formed, which was gradually warmed up to room temperature and kept stirring overnight. The volatile materials were evaporated under high vacuum. Without further purification, the crude product was re-dissolved in 5 mL of toluene and mixed with a solution of MesCu (273 mg, 1.50 mmol) in 5 mL of toluene. The reaction mixture was slowly heated to 110 ºC and kept stirring at that temperature for 2 days. After cooling back to room temperature, the solid by-product (CuBr) was removed by passing the mixture through a fritted glass funnel, followed by a short plug of alumina. The filtrate was concentrated to less than 1 mL and precipitated into 50 mL of cold hexanes. The final product was obtained by freeze-drying from benzene as a yellow solid. Yield: 160 mg, 52%. ^{1}H NMR (499.9 MHz, CDCl$_3$): δ = 7.28 (s, 2H, Fl), 7.07 (d, ^{3}J = 7.5 Hz, 2H, Fl), 7.04 (s, 2H, Th), 7.01 (d, ^{3}J = 7.5 Hz, 2H, Fl), 6.61 (br, 8H, Mes), 2.12 (s, 12H, ^{p}Me), 2.09 (s, 24H, ^{o}Me), 1.86 (br, 4H, Hex), 1.3-1.0 (m, 12H, Hex), 0.85 (t, 6H, ^{3}J = 7.0 Hz, Hex), 0.56 ppm (br, 4H, Hex); ^{13}C NMR (125.7 MHz, CDCl$_3$): δ = 155.6, 150.8, 147.4, 142.5 (Mes), 140.7 (Mes), 140.2, 138.9 (Mes), 136.0, 134.0, 131.8, 129.4,

128.4 (Mes), 122.5, 118.2, 55.1, 40.2, 31.7, 29.9, 23.4×2 (^{o}Me+Hex) , 22.9, 21.3, 14.3; ^{11}B NMR (160.3 MHz, CDCl$_3$): δ = 61 ppm (w$_{1/2}$ = 6240 Hz); GPC-RI (in THF against PS standards) M_w = 4.04×10^4, M_n = 2.19×10^4, PDI = 1.85; UV-Vis (CH$_2$Cl$_2$, 1.57×10^{-6} M): λ_{max} (ε, M^{-1} cm^{-1}) = 453 nm (3.96×10^4), 337 nm (4.85×10^4); fluorescence (CH$_2$Cl$_2$, 1.57×10^{-6} M): $\lambda_{em,max}$ = 533 nm (λ_{exc} = 453 nm, Φ = 7.3%); TGA (N$_2$, 10 ºC/min): T$_{dec}$ = 256ºC (onset), 11% residue at 800 ºC.

Preparation of PCT-Si: Polymer PCT-Si was prepared in the same manner as described for PFT-Si by using Cz(BPin)$_2$ (490.6 mg, 0.89 mmol), T$_2$I$_2$ (500 mg, 0.89 mmol), Pd(PPh$_3$)$_4$ (21.0 mg, 0.018 mmol) and 2.5 mL of aqueous K$_2$CO$_3$ solution (2.0 M). The product was isolated as a pale yellow powder. Yield: 400 mg, 74%. ^{1}H NMR (499.9 MHz, CDCl$_3$): δ = 8.25 (s, 2H, Cz), 7.65 (d, ^{3}J = 8.0 Hz, 2H, Cz), 7.56 (m, 4H, Ph), 7.46 (d, ^{3}J = 8.5 Hz, 2H, Cz), 7.22 (s, 2H, Th), 1.45 (s, 9H, tBu), 0.19 ppm (s, 18H, SiMe$_3$); ^{13}C NMR (125.7 MHz, CDCl$_3$): δ = 151.2, 151.0, 141.5, 138.7, 136.7, 134.8, 130.7, 128.4, 128.3, 127.1, 126.7, 123.1, 121.8, 109.9, 35.1 (^{t}Bu), 31.7 (^{t}Bu), 0.9 ppm (SiMe$_3$); ^{29}Si NMR (99.3 MHz, CDCl$_3$): δ = −7.8 ppm; GPC-RI (in THF against PS standards) M_w = 1.36×10^4, M_n = 6.19×10^3, PDI = 2.19; UV-Vis (CH$_2$Cl$_2$, 1.30×10^{-5} M): λ_{max} (ε, M^{-1} cm^{-1}) = 355 nm (4.05×10^4); fluorescence (CH$_2$Cl$_2$, 1.30×10^{-5} M): $\lambda_{em,max}$ = 468 nm (λ_{exc} = 355 nm, Φ = 10.1% relative to DPA); TGA (N$_2$, 10 ºC/min): T$_{dec}$ = 376 ºC (onset), 6% residue at 800 ºC.

Preparation of PCT-B: Polymer PCT-B was prepared in the same manner as described for PFT-B using PCT-Si (100 mg, 0.17 mmol), BBr$_3$ (107 mg, 0.42 mmol) and MesCu (147 mg, 0.81 mmol). The product was obtained as yellow powder. Yield: 76 mg,

48%. ^{1}H NMR (499.9 MHz, CDCl$_3$): δ = 7.76 (s, 2H, Cz), 7.60 (d, ^{3}J = 8.5 Hz, 2H, Ph), 7.31 (d, ^{3}J = 8.0 Hz, 2H, Cz), 7.26 (d, ^{3}J = 7.0 Hz, 2H, Ph), 7.09 (s, 2H, Th), 7.00 (d, ^{3}J = 8.0 Hz, 2H, Cz), 6.49 (br, 8H, Mes), 2.13 (br, 24H, ^{o}Me), 1.96 (br, 12H, ^{p}Me), 1.44 ppm (s, 9H, t-Bu); ^{13}C NMR (125.7 MHz, CDCl$_3$): δ = 156.6, 150.6, 146.9, 142.4 (Mes), 140.8, 140.5 (Mes), 138.3 (Mes), 135.7, 135.0, 131.8 (Mes), 128.3, 127.7, 127.1, 127.0, 126.2, 122.8, 121.6, 108.6, 35.0 (^{t}Bu), 31.7 (^{t}Bu), 23.5 (^{o}Me), 21.1 ppm (^{p}Me); ^{11}B NMR (160.3 MHz, CDCl$_3$): δ = 56 ppm (w$_{1/2}$ = 8000 Hz); GPC-RI (in THF against PS standards) M_w = 2.03×10^4, M_n = 1.04×10^4, PDI = 1.95; UV-Vis (CH$_2$Cl$_2$, 1.73×10^{-6} M): λ_{max} (ε, M^{-1} cm^{-1}) = 422 (2.49×10^4), 330 nm (5.68×10^4); fluorescence (CH$_2$Cl$_2$, 1.73×10^{-6} M): $\lambda_{em,max}$ = 527 nm (λ_{exc} = 422 nm, Φ = 2.0%); TGA (N$_2$, 10 ºC/min): T$_{dec}$ = 284 ºC (onset), 4% residue at 800 ºC.

Preparation of PTT-Si: Polymer PTT-Si was prepared in the same manner as described for PFT-Si by using T$_2$I$_2$ (500 mg, 0.89 mmol), TPA(BPin)$_2$ (481 mg, 0.89 mmol), Pd(PPh$_3$)$_4$ (7.4 mg, 0.0064 mmol) and 2.5 mL of aqueous solution of K$_2$CO$_3$ (2.0 M). The product was isolated as yellow powder. Yield: 302 mg, 57%. ^{1}H NMR (499.9 MHz, CDCl$_3$): δ = 7.31 (d, ^{3}J = 8.5 Hz, 4H, Ph), 7.12 (s, 2H, Th), 7.02 (d, ^{3}J = 8.5 Hz, 4H, Ph), 6.99 (s, 2H, Mes), 2.36 (s, 3H, ^{p}Me), 2.05 (s, 6H, ^{o}Me), 1.34 (s, 0.82H, PinB end group), 0.15 ppm (s, 18H, SiMe$_3$); ^{13}C NMR (125.7 MHz, CDCl$_3$): δ = 150.4, 146.0, 139.9, 138.5, 137.7, 137.3, 135.3, 130.8, 130.5, 130.3, 128.9, 119.3, 25.1 (PinB end group), 23.8 (PinB end group), 21.3 (^{p}Me), 18.8 (^{o}Me), 0.7 ppm (SiMe$_3$); ^{29}Si NMR (99.3 MHz, CDCl$_3$): δ = –8.1 ppm; GPC-RI (in THF against PS standards) M_w = 2.37×10^4, M_n = 1.47×10^4, PDI = 1.61; UV-Vis (CH$_2$Cl$_2$, 3.03×10^{-5} M): λ_{max} (ε, M^{-1}cm^{-1}) = 381 nm

(4.52×10^4); fluorescence (CH_2Cl_2, 3.03×10^{-5} M): $\lambda_{em,max}$ = 493 nm (λ_{exc} = 381 nm, Φ = 13.2%); TGA (N_2, 10 ºC/min): T_{dec} = 367 ºC (onset), 9% residue at 800 ºC.

Preparation of PTT-B: At –35 ºC, a solution of PTT-Si (100 mg, 0.17 mmol) in 10 mL of toluene was added to a solution of BBr_3 (95 mg, 0.38 mmol) in 2 mL of CH_2Cl_2. A dark green solution formed, which was gradually warmed up to room temperature and kept stirring for 24 h. The mixture was concentrated under high vacuum, such that a small amount of solvent remained (it is difficult to re-dissolve the compound when it is fully dried). After adding more toluene (2 ml), the intermediate was mixed with a solution of MesCu (140 mg, 0.77 mmol) in 5 mL of toluene. The reaction mixture was heated to 110 ºC and kept stirring for 2 days. After cooling to room temperature, the solid by-product (CuBr) was removed by passing the mixture through a fritted glass funnel, followed by a short plug of alumina. The filtrate was concentrated to less than 1 mL and precipitated into 50 mL of cold hexanes. The final product was obtained by freeze-drying from benzene as a yellow solid. Yield: 76 mg, 47%. ^{1}H NMR (499.9 MHz, $CDCl_3$): δ = 7.01 (d, ^3J = 8.0 Hz, 4H, Ph), 6.97 (s, 2H, Th), 6.89 (s, 2H, Mes-N), 6.63 (s, 8H, Mes-B), 6.42 (d, ^3J = 8.5 Hz, Ph), 2.32 (s, 3H, ^pMe), 2.20 (s, 12H, ^pMe), 2.05 (s, 24H, ^oMe), 1.78 (s, 6H, ^oMe), 0.14 ppm (0.84H, 4.7% residual $SiMe_3$); ^{13}C NMR (125.7 MHz, $CDCl_3$): δ = 155.5, 147.4, 145.6, 142.5 (Mes), 140.7 (Mes), 139.5, 138.4 (Mes), 137.7, 137.2, 135.6, 131.2, 130.0, 128.3 (Mes), 128.1, 118.4, 23.4 (Me), 21.5 (Me), 21.3 (Me), 18.4 (Me), 0.7 ($SiMe_3$) ppm; ^{11}B NMR (160.3 MHz, $CDCl_3$): δ = 54 ppm ($w_{1/2}$ = 6400 Hz); GPC-RI (in THF against PS standards) M_w = 5.61×10^4, Mn = 2.53×10^4, PDI = 2.22; UV-Vis (CH_2Cl_2, 1.57×10^{-6} M): λ_{max} (ε, $M^{-1}cm^{-1}$) = 455 (3.17×10^4), 337 (4.35×10^4), 273 nm (3.28×10^4);

fluorescence (CH$_2$Cl$_2$, 1.78×10^{-5} M): $\lambda_{em,max}$ = 546 nm (λ_{exc} = 455 nm, Φ = 4.1%); TGA (N$_2$, 10 ºC/min): T$_{dec}$ = 293 ºC (onset), 5% residue at 800 ºC.

2.7 References

(1)   McCullough, R. D.; Lowe, R. D. *J. Chem. Soc., Chem. Commun.* **1992**, 70.

(2)   McCullough, R. D.; Lowe, R. D.; Jayaraman, M.; Anderson, D. L. *J. Org. Chem.* **1993**, *58*, 904.

(3)   McCullogh, R. D.; Ewbank, P. C.; Loewe, R. S. *J. Am. Chem. Soc.* **1997**, *119*, 633.

(4)   Guillerez, S.; Bidan, G. *Synth. Met.* **1998**, *93*, 123.

(5)   Chen, T. A.; Rieke, R. D. *J. Am. Chem. Soc.* **1992**, *114*, 10087.

(6)   Chen, T.-A.; Wu, X.; Rieke, R. D. *J. Am. Chem. Soc.* **1995**, *117*, 233.

(7)   Loewe, R. S.; Khersonsky, S. M.; McCullough, R. D. *Adv. Mater.* **1999**, *11*, 250.

(8)   Osaka, I.; McCullough, R. D. *Acc. Chem. Res.* **2008**, *41*, 1202.

(9)   Goedel, W. A.; Somanathan, N. S.; Enkelmann, V.; Wegner, G. *Macromol. Chem.* **1992**, *193*, 1195.

(10)   Somanathan, N.; Wegner, G. *Synth. Met.* **1995**, *75*, 123.

(11)   Bidan, G.; Guillerez, S.; Sorokin, V.; *Adv. Mater.* **1996**, *8*, 157.

(12)   Andersson, M. R.; Thomas, O.; Mammo, W.; Svensson, M.; Theanderc, M.; Inganäsc, O. *J. Mater. Chem.* **1999**, *9*, 1933.

(13)   Perepichka, I. F.; Perepichka, D. F.; Meng, H.; Wudl, F. *Adv. Mater.* **2005**, *17*, 2281.

(14)   Andersson, M. R.; Berggren, M.; Olinga, T.; Hjertberg, T.; Inganäs, O.;
         Wennerström, O. *Synth. Met.* **1997**, *85*, 1383.

(15)   Gustavsson, G.; Inganäs, O.; Nilsson, J. O.; Liedberg, B. *Synth Met* **1998**, *26*, 297.

(16)   Loponen, M. T.; Taka, T.; Laakso, J.; Väkiparta, K.; Suuronen, K.; Valkeinen, P.;
         Österholm, J.-E. *Synth. Met.* **1991**, *41*, 479.

(17)   Loponen, M. T.; Salaneck, W. R.; Österholm, J.-E.; Laakso, J. *Synth. Met.* **1988**,
         22, 395.

(18)   Tourillon, G.; Garnier, F.; *J. Electrochem. Soc.* **1983**, *130*, 2042.

(19)   Österholm, J.-E.; Passiniemi, P. *Synth. Met.* **1997**, *18*, 213.

(20)   Pei, Q.; Inganäs, O.; Österholm, J.-E.; Laakso, J. *Polymer* **1993**, *34*, 247.

(21)   Elsenbaumer, R. L.; Jen, K. Y.; Miller, G. G.; Shacklette, L. W. **1987**, *18*, 277.

(22)   Andersson, M. R.; Pei, Q.; Hjertberg, T.; Inganäs, O.; Wenneröstrm, O.;
         Österholm, J.-E. *Synth. Met.* **1993**, *55*, 1227.

(23)   Goldenberg, L. M.; Bryce, M. R.; Petty, M. C. *J. Mater. Chem.* **1999**, *9*, 1957.

(24)   Thomas III, S. W.; Joly, G. D.; Swager, T. M. *Chem. Rev.* **2007**, *107*, 1339.

(25)   Ho, H.-A.; Boissinot, M.; Bergeron, M. G.; Corbeil, G.; Doré, K.; Boudreau, D.;
         Leclerc, M. *Angew. Chem. Int. Ed.* **2002**, *41*, 1548.

(26)   Nilsson, K. P. R.; Inganäs, O. *Nat. Mater.* **2003**, *2*, 419.

(27)   Ho, H.-A.; Najari, A.; Leclerc, M. *Acc. Chem. Res.* **2008**, *41*, 168.

(28)   Zhou, E.; Hou, J.; Yang, C.; Li, Y. *J. Polym. Sci. Part A, Polym. Chem*, **2006**, *44*,
         2214.

(29)   Andersson, M. R.; Mammo, W.; Olinga, T.; Svensson, M.; Theander, M.;
         Inganäs, O. *Synth Met* **1999**, *101*, 11.

(30)   Li, W.; Han, Y.; Chen, Y.; Li, C.; Li, B.; Bo, Z. *Macromol. Chem. Phys.* **2010**, *211*, DOI: 10.1002/macp.200900641.

(31)   Zoua, Y.; Sang, G.; WeipingWua; Liu, Y.; Li, Y. *Synth. Met.* **2009**, *159*, 182.

(32)   Zou, Y.; Wu, W.; Sang, G.; Yang, Y.; Liu, Y.; Li, Y. *Macromolecules* **2007**, *40*, 7231.

(33)   Li, Y.; Zou, Y. *Adv. Mater.* **2008**, *20*, 2952.

(34)   Yu, C.-Y.; Ko, B-T.; Ting, C.; Chen C.-P. *Sol. Energ. Mat.Sol. C.* **2009**, *98*, 613.

(35)   Kim, H.-C.; Kim, J.-S.; Baek, S.; Ree, M. *Macromolecular Research* **2006**, *14*, 173.

(36)   McCullough, R. D. *Adv. Mater.* **1998**, *10*, 93.

(37)   Li, H.; Sundararaman, A.; Venkatasubbaiah, K.; Jäkle, F. *J. Am. Chem. Soc.* **2007**, *129*, 5792.

(38)   Entwistle, C. D.; Marder, T. B. *Angew. Chem. Int. Ed.* **2002**, *41*, 2927.

(39)   Entwistle, C. D.; Marder, T. B. *Chem. Mater.* **2004**, *16*, 4574.

(40)   Scheibitz, M.; Bolte, M.; Bats, J. W.; Lerner, H.-W.; Nowik, I.; Herber, R. H.; Krapp, A.; Lein, M.; Holthausen, M.; Wagner, M. *Chem. Eur. J.* **2005**, *11*, 584.

(41)   Gamboa, J. A.; Sundararaman, A.; Kakalis, L.; Lough, A. J.; Jäkle, F. *Organometallics* **2002**, *21*, 4169.

(42)   Flanagan, J. B.; Margel, S.; Bard, A. J.; Anson, F. C. *J. Am. Chem. Soc.* **1978**, *100*, 4248.

(43)   Li, H.; Sundararaman, A.; Venkatasubbaiah, K.; Jäkle, F. *J. Am. Chem. Soc.* **2007**, *129*, 5792.

(44)   *Advances in Photochemistry*; Pitts,Jr. J. N.; Hammond, G. S. and Noyes,Jr. W. A.; New York, **1971**, 8, 227-244.

(45)   Li, H.; Jäkle, F. *Macromol. Rapid Commun.* **2010**, in press

(46)   Hooper, M. W.; Utsunomiya, M.; Hartwig, J. F. *J. Org. Chem.* **2003**, *68*, 2861.

(47)   Tsuda, T.; Yazawa, T.; Watanabe, K.; Fujii, T.; Saegusa, T. *J. Org. Chem.* **1981** *46*, 192.

(48)   Li, H.; Jäkle, F. *Angew. Chem. Int. Ed.* **2009**, *48*, 2313.

(49)   Ranger, M.; Rondeau, D.; Leclerc, M. *Macromolecules* **1997**, *30*, 7686.

(50)   Guillaneux, D.; Kagan, H. B. *J. Org. Chem.* **1995**, *60*, 2502.

(51)   Sheldrick, G.M. (1998), SADABS (2.01), Bruker/Siemens Area Detector Absorption Correction Program, Bruker AXS, Madison, Wisconsin, USA

(52)   Sheldrick, G., Bruker XRD, Madison, WI.

Chapter 3. A Facile Route to Organoboron Quinolate Polymers Through Boron-Induced Ether Cleavage

3.1 Introduction

Since the first efficient organic light-emitting diode (OLED) based on Alq$_3$ was reported by Tang and van Slyke,[1,2] many studies have focused on metal or metalloid complexes with 8-hydroxyl quinoline (8HQ) and related ligands. A variety of metals or metalloids have been used to form complexes with 8HQ, including main group elements such as Li, Be, Mg, Ga, In, B, Al and transition metals such as Sc, Yb, Zn.[3-18] Among them, molecular organoboron quinolates and related chelate complexes turned out to be promising and often exhibited good thermal stability and efficient luminescence due to the increased bond covalency of the boron to ligand bonds.[19-23]

We are interested in polymeric materials since they often offer advantages over molecular materials in their solution processabilty, allowing for low cost manufacture and large scale application.[24,25] Several approaches are available specifically for the synthesis of organoboron quinolate polymers.

3.1.1 Post-polymerization modification

Post-polymerization modification methods are often advantageous owing to the high conversion and mild conditions of the complexation reaction of the boron centers with

quinoline ligands. The method requires a preformed polymer support, to which metal centers or quinolinol ligands are attached. They are subsequently subject to post modification to form organoboron quinolate polymers. For instance, Weck et al have reported a soluble styrene polymer with quinoline ligands attached, which serves as versatile precursors to form polymers with various pendant 8-hydroxyquinoline metal complexes (**Scheme 3-1**). [26]
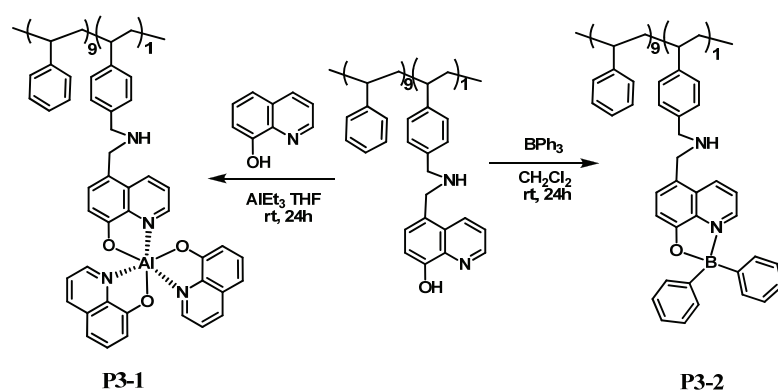
Scheme 3-1. Synthesis of organoboron quinolate polymers via post-polymerization modification
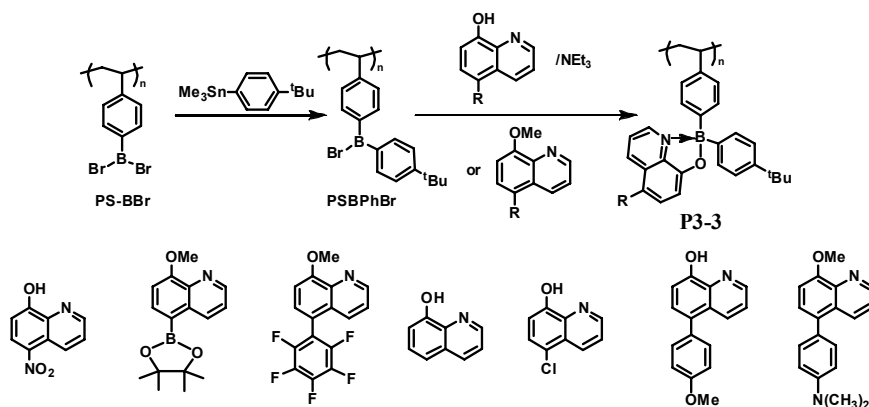
Scheme 3-2. Luminescence tuning of organoboron quinolate polymers through post-polymerization modification

Different from their ligand-first approach, Jäkle and coworkers have developed a metal-first method.[27,28] The polymeric metal containing precursor is prepared via a controlled free radical polymerization technique, atom transfer radical polymerization (ATRP), which leads to well-defined structure and narrow PDIs. Most importantly, the luminescence of the polymers can be easily tuned by simply varying the quinoline ligands in the last step. Polymers with emission colors varying from blue, green to red have been achieved (**Scheme 3-2**).[27]

The polymeric precursor can also be prepared through a transition metal catalyzed polycondensation route as illustrated by Chujo et al.[29] Chelation with BPh$_3$ afforded a novel quinoline-linked main chain organoboron quinolate polymer with a significantly red shifted emission (**Scheme 3-3**).
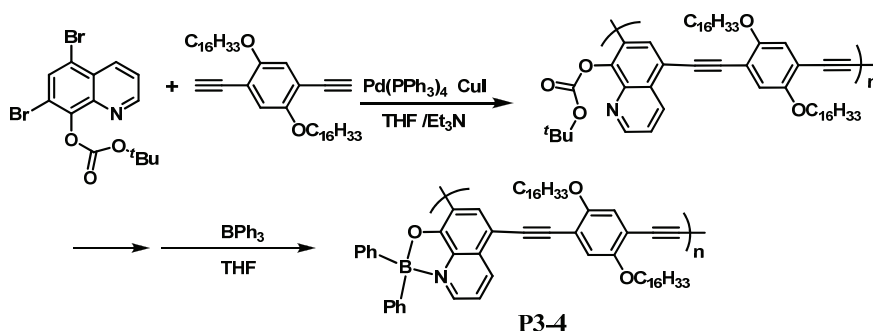
Scheme 3-3. Main chain organoboron quinolate polymer linked on quinoline

3.1.2 Direct polymerization using transition metal-catalyzed coupling reactions

Alternatively, organoboron quinolate polymers can also be obtained by one step transition metal catalyzed polycondensation reaction as studied by Chujo and coworkers.[29-32] As shown in **Scheme 3-4**, the polymerization is based on the Sonogashira-Hagihara coupling reaction,[33,34] which involves the use of a preformed

difunctional organoboron quinolate monomer. The polymers obtained exhibited efficient

charge transfer character and intense blue emission was observed. Moreover, the method

is tolerant to different functional groups and applicable to a variety of monomers. Several

analogous organoboron 8-aminoquinolate-coordinate polymers (**Scheme 3-5**)[35],

organoboron quinoline-8-thiolate and quinoline-8-selenolate complexes (**Scheme 3-6**)[36]

were also created. As evident from these studies, variation of the substituent groups on

quinoline ring or switch of the chelating atoms can further enrich the luminescent

properties of these materials.
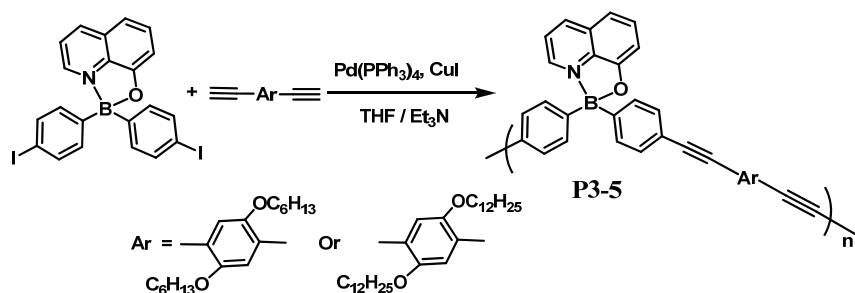
Scheme 3-4. Synthesis of main chain organoboron quinolate polymers via Sonogashira-Hagihara coupling reaction
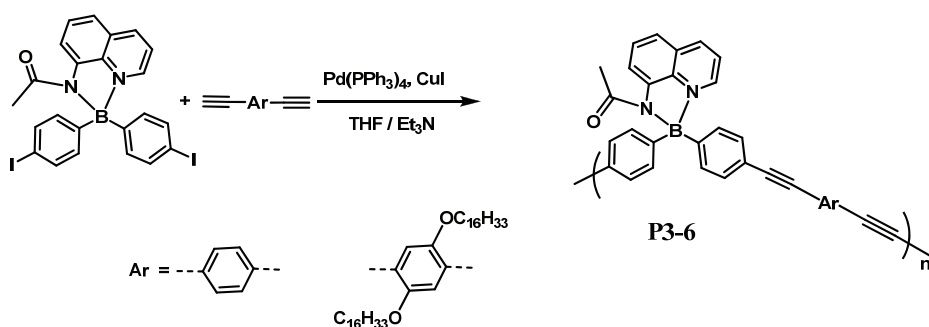
Scheme 3-5. Synthesis of organoboron 8-aminoquinolate-coordinate polymers
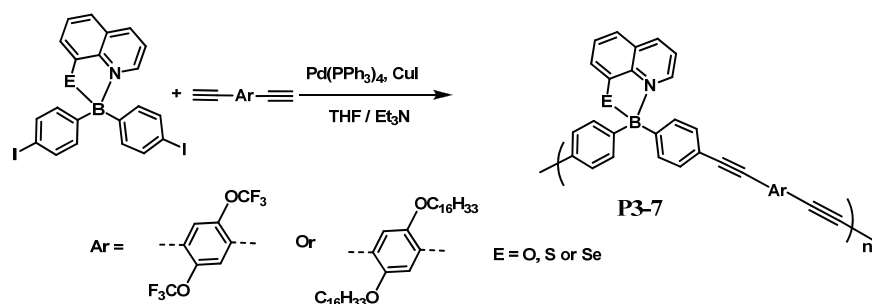
Scheme 3-6. Organoboron quinoline-8-thiolate and quinoline-8-selenolate main chain polymers

3.2 Results and discussion

Recently, Wang and Cui have reported a family of linear or star-shaped molecules prepared from polyfunctional ligands (**Figure 3-1**).[21] Compared to the mono-boron compounds, the multi-boron compounds exhibit dramatically enhanced thermal stability due to increased intermolecular interactions. A unique temperature and concentration dependent effect was also observed for B5. Inspired by these exceptional properties, we have prepared a new type of polymeric architecture with both the quinolato ligands and boron centers embedded into the main chain, which was achieved by a simple one-step procedure that involves metal-free boron-induced ether cleavage reactions.
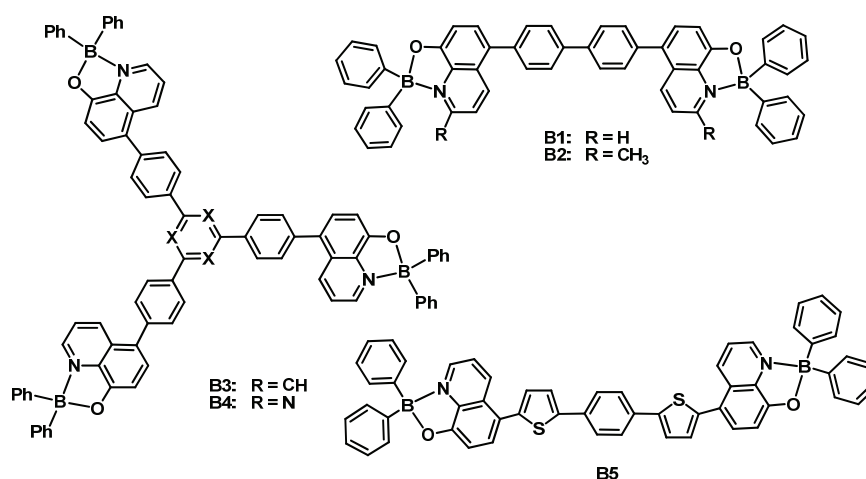
Figure 3-1. Di- or tri-topic organoboron quinolate molecules[21]

3.2.1 Synthesis of P1 and P2

As shown in **Scheme 3-7**, the bifunctional organoborane monomer 2,7-bis((*t*-butylphenyl)bromoboryl)-9,9-dihexylfluorene (B1) was prepared by reaction of 2,7-bis(dibromoboryl)-9,9-dihexylfluorene (FlB$_2$) with 2 equiv of 1-trimethylstannyl-4-*t*-butylbenzene, which led to selectively replacement of one Br substituent on each boron atom as confirmed by ^{1}H NMR analysis. The monomer B1 was purified by repeated recrystallization from hexanes at –35 °C.
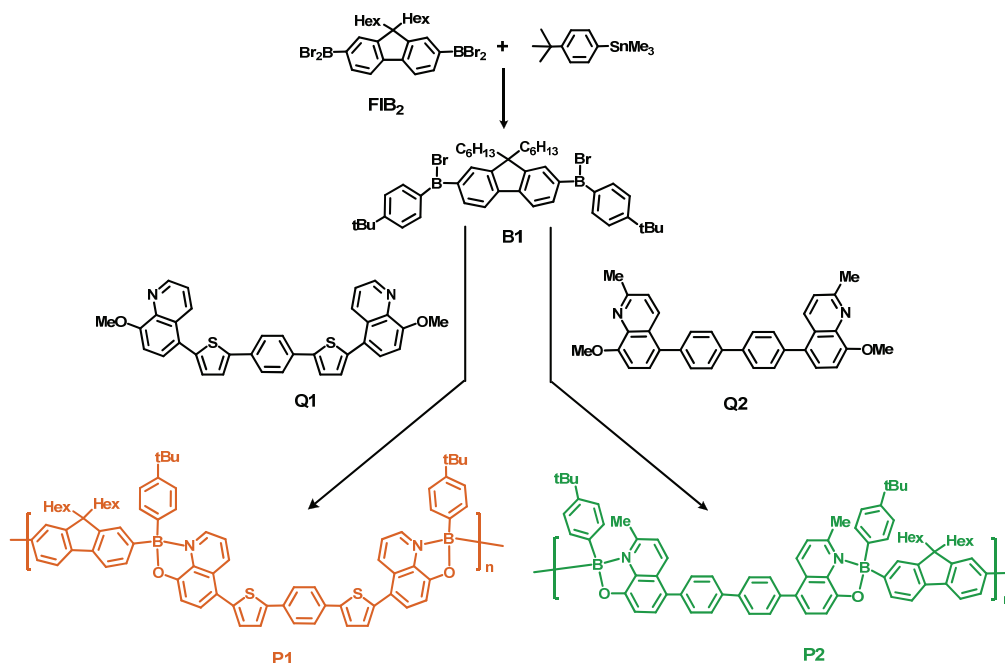
Scheme 3-7. Synthesis of P1 and P2

The organoboron quinolate polymers P1 and P2 were prepared under mild conditions by simply mixing the bifunctional boron monomer B1 at RT with the methoxy-protected bifunctional quinolato monomers Q1 and Q2, respectively, followed by stirring for 24 h (**Scheme 3-7**). The volatile by-product MeBr was easily removed under high vacuum. The polymers were purified by adding hexanes to a solution of the crude material in CH$_2$Cl$_2$, which led to precipitation of the products. P1 was isolated as an orange solid in 59% yield and P2 as a yellow solid in 66% yield.

3.2.2 Polymer structure characterization by NMR spectroscopy

The chemical structure of the polymers was confirmed by 1D multi-nuclear NMR spectroscopy and 2D ^{1}H NMR. ^{11}B NMR resonances at 11 ppm for P1 and at 12 ppm for P2, respectively, which are in the typical region of tetra-coordinate boron compounds,

confirm the attachment of the quinolato groups to boron. For both P1 and P2 the protons of the fluorene and *tert*-butylphenyl moieties experience a strong upfield shift upon chelation by the electron-donating quinolato ligands (**Figure 3-2**). Most of the signals for the quinolato moieties and the aromatic bridging groups do not significantly change upon boron coordination. A notable exception is the pronounced downfield shift of one of the quinolato protons in P2 from 8.24 to 8.55 ppm, which is similar to the chemical shift observed for the respective diboron species B2 (8.61 ppm)[21] and likely a result of ring current effects. Importantly, all the major signals can be readily assigned to the expected polymer structures based on 2D NMR experiments (**Figure 3-3**, **3-4**), indicative of clean transformations through boron-induced ether cleavage reactions. The absence of additional signals also suggests that the concentration of end groups is small and hence the polymers are either cyclic or of fairly high molecular weight.
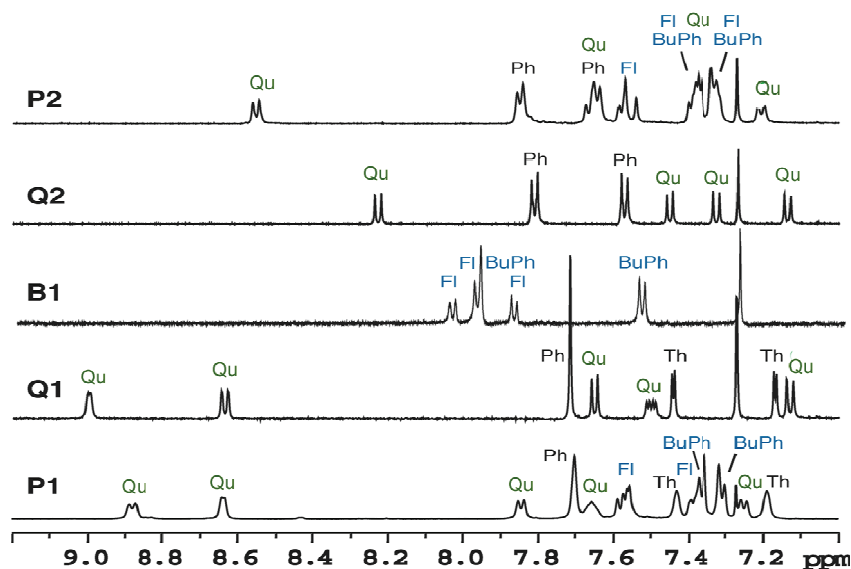
Figure 3-2. ^{1}H NMR comparison made to B1, Q1, Q2, P1 and P2 (in CDCl$_3$, aromatic region)
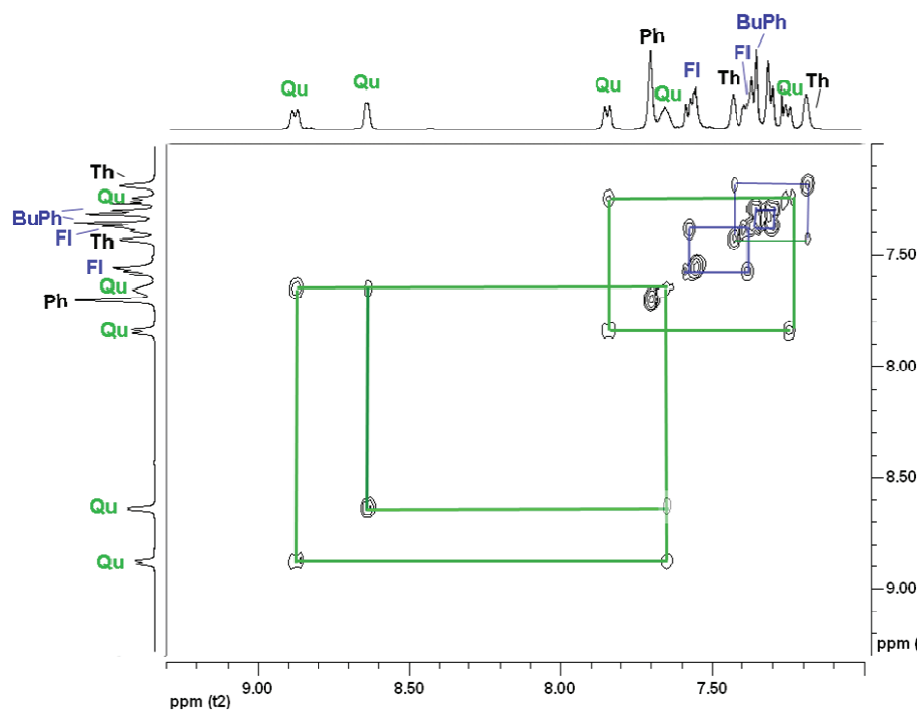
Figure 3-3. ^{1}H, ^{1}H- COSY spectrum of P1 (in CDCl$_3$, aromatic region)
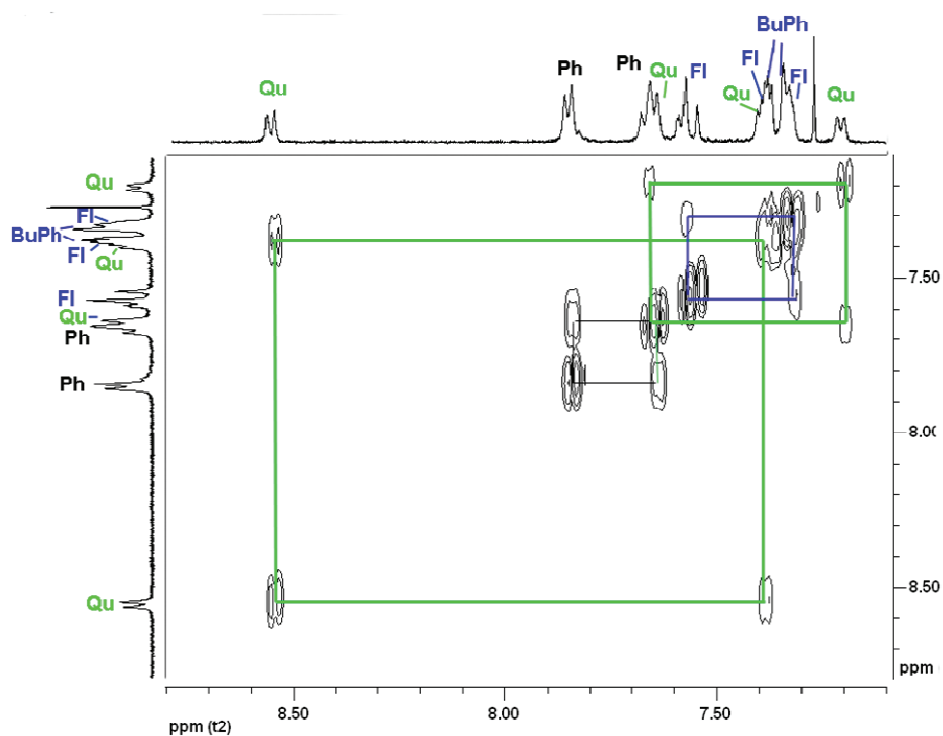
Figure 3-4. ^{1}H, ^{1}H- COSY spectrum of P2 (in CDCl$_3$, aromatic region)

3.2.3 Molecular weight determination

Gel permeation chromatography with in-line multi-angle laser light scattering (GPC-MALLS) detection in THF gave weight-average molecular weights of $M_w = 1.72 \times 10^4$ (PDI = 1.20) for reprecipitated samples of P1 and $M_w = 1.66 \times 10^4$ (*PDI* = 1.24) for P2. These results indicate that for each polymer an average of ca. 25 quinolato moieties are embedded into the polymer chains. We further examined the polymers by high-resolution matrix-assisted laser desorption ionization – time of flight (MALDI-TOF) mass spectrometry. For both polymers P1 (**Figure 3-5**) and P2 (**Figure 3-6**), we were able to detect two different series of peaks, both of which show the expected repeating units and a chain length of up to n = 6. A more detailed analysis suggested that the two different series, An and Bn, correspond to fragments with a quinolatoborane moiety at one chain end and a fluorene moiety at the other chain end. The difference between the first series An and the second series Bn is that An corresponds to protonated species $[\{RU\}_nH]^+$ (RU = repeating unit), while loss of a *tert*-butylphenyl group is observed for Bn $[\{RU\}_n–tBuPh]^+$.
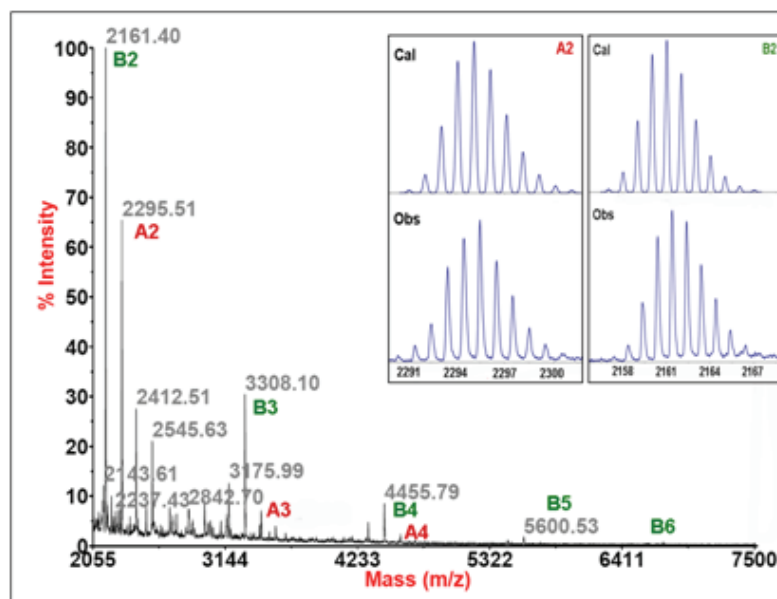
Figure 3-5. MALDI-TOF mass spectrum of P1 (acquired in positive reflector mode, An = $[\{RU\}_nH]^+$ (RU = repeating unit), Bn = $[\{RU\}_n - {}^tBuPh]^+$)
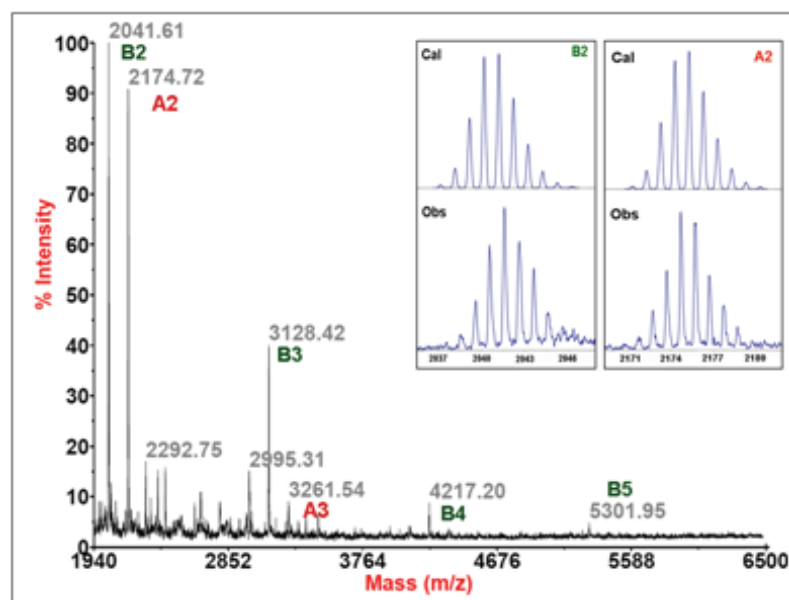
Figure 3-6. MALDI-TOF mass spectrum of P2 (acquired in positive reflector mode, An = $[\{RU\}_nH]^+$ (RU = repeating unit), Bn = $[\{RU\}_n - {}^tBuPh]^+$)

3.2.4 Thermal properties

P1 and P2 are stable both as solids and in solution for extended periods of time. The polymers also show good thermal stability based on thermogravimetric analysis (TGA). The onset of the thermal degradation of **P1** was determined to be 326 °C and that of **P2** to be 318 °C.
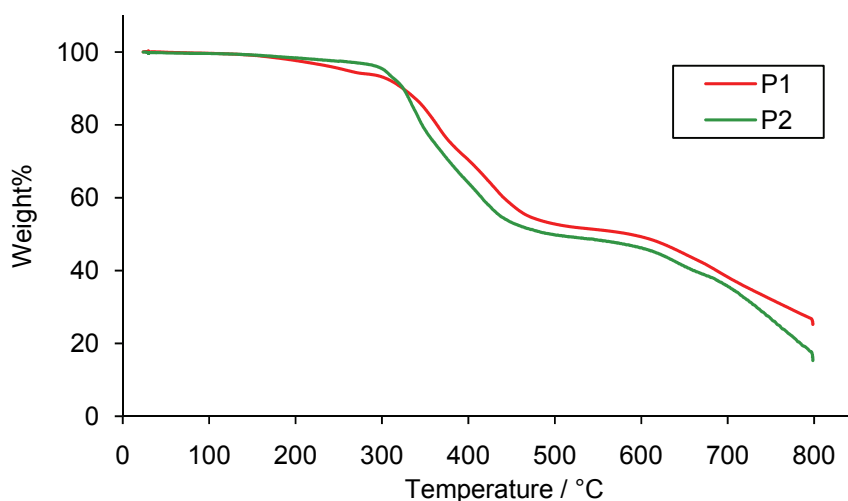
Figure 3-7. Thermal stability of P1 and P2 examined by TGA (10 °C /min)

3.2.5 Photophysical properties

The photophysical properties were studied by UV-visible spectroscopy and fluorescence measurements, and the data were supported by density functional theory (DFT) calculations on molecular model systems. The UV-vis absorption spectra of the two polymers in CH_2Cl_2 are shown in **Figure 3-8**. Solutions of P1 in CH_2Cl_2 are orange colored and those of **P2** are yellow. The lowest energy absorption bands are almost identical to those of the respective bifunctional species B5 and B2 reported by Wang's group[21] and therefore likely due to quinolato ligand-based transitions. For instance, P2

shows a maximum at 411 nm that is red-shifted by only ca. 5 nm relative to that of B2. Polymer P1 shows a band (shoulder) at ca. 443 nm (430 nm for B5) and a higher energy maximum at 367 (366 nm for B5). The latter band was tentatively attributed to an electronic transition that involves the bridging moiety. The red-shift of this band for P1 relative to P2 (ca. 311 nm) is consistent with the higher degree of conjugation of the Th-C_6H_4-Th linker in comparison to the biphenyl group.[21] The observation that the polymer absorptions are similar to those reported for the bifunctional species further confirms the structural integrity of the polymers with organoboron quinolato chromophores bridging the organic aromatic linkers. At the same time it strongly suggests that extended electronic communication throughout the polymer chain is very limited, due to tetracoordination of the boron moieties.
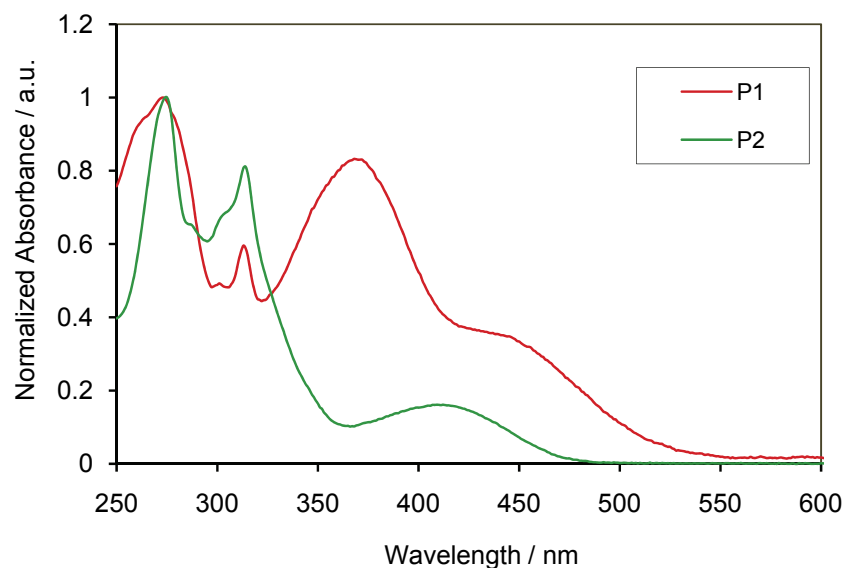
Figure 3-8. UV-visible spectra of P1 (1.04×10^{-6} M repeat units, excited at 443 nm) and P2 (4.0×10^{-7} M repeat units, excited at 411 nm)

To further confirm the assignments of the absorptions bands for P1 and P2, we performed DFT calculations on the molecular model systems M1 and M2 (**Figure 3-9**). Coordination of the quinolato groups leads to generation of a stereogenic center at boron and only the structures of the R,R-isomers of M1 and M2 were optimized. As reported for other organoboron quinolate complexes, the lowest unoccupied molecular orbital (LUMO) is primarily localized on the pyridyl moiety of the quinolato groups. However, the highest occupied molecular orbital (HOMO) for M1 and M2 is different in that for M1 the electron density is delocalized on the aromatic Th-C_6H_4-Th linker with contributions from the phenolate part of the quinolate moiety, while for M2 it is found on the pendant fluorene moieties. The reverse situation is observed for the HOMO-2, which is localized on the fluorene moieties for M1 and the biphenyl linker / phenolate π-system for M2. This implies that the HOMO and HOMO-2 exchange positions when going from M1 with its highly delocalized bridging π-system to M2 with its twisted biphenyl linker.

Time-dependent DFT calculations demonstrate that the lowest energy absorptions indeed correspond primarily to a HOMO to LUMO transition. This transition is therefore characterized by charge transfer from the conjugated quinolate linker (for M1) and the fluorene moieties (for M2) to the pyridyl ring of the quinolato moiety. This is different from the parent compound Ph_2BQ and related organoboron quinolate species, for which the HOMO-LUMO transition typically corresponds to a quinolate-centered charge transfer from the phenolate to the pyridyl moiety. However, it is consistent with studies on organoboron quinolate complexes where organic π-systems with extended delocalization are attached in 5-position of the quinolate ligand.[4,7] For instance, attachment of a benzothiophene group leads to a strong orbital contribution from the

benzothiophene moiety to the HOMO level, while the LUMO remains centered on the quinolato ligand.[4] Finally, for both M1 and M2, the higher energy band can be assigned to excitation into the LUMO+2, a π^* orbital centered on the bridging aromatic linker.

As noted in the introduction, the unusual emission properties of the bifunctional species B5 in part prompted us to investigate the respective polymeric materials. The photoluminescence spectra of P1 and P2 in CH_2Cl_2 solution (ca. 1×10^{-6} to 1×10^{-7} M) are presented in **Figure 3-10**. Independent of the excitation wavelength and concentration, P2 emits yellow light at a wavelength of $\lambda_{em} = 536$ nm. The emission of P2 is reminiscent of that of a 5-naphthyl-substituted Ph_2BQ derivative, which was reported to emit at 534 nm with a quantum efficiency of 11%. Noteworthy is also that the emission is only slightly red shifted compared to the molecular species B2 ($\lambda_{em} = 528$ nm)[21] and the quantum efficiency of 19% is also similar to that of B2 (23%).

M1: A = Charge transfer , B = π-π* transition
M2: A = charge transfer, B = charge transfer
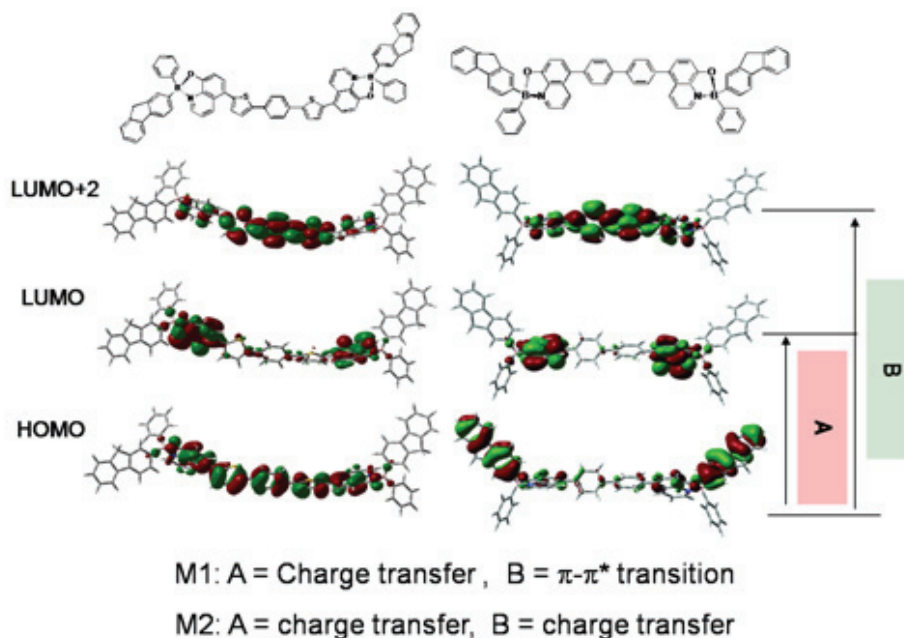
Figure 3-9. Computed (Gaussian03) orbital plots for M1 and M2 (B3LYP 6-31G(d))

The emission of P1 is excitation wavelength dependent. When excited at 443 nm, a single emission band was observed at $\lambda_{em} = 611$ nm. This band correlates reasonably well with that found by Wang[21] for B5 at concentrations $>5 \times 10^{-5}$ M ($\lambda_{em} = 593$ nm) and the relatively low quantum efficiency of ca. 1% is also similar to that of the molecular species. Wang reported that at very low concentrations of B5 the emission was centered at $\lambda_{em} = 462$ nm.[21] We found that excitation into the higher energy band of P1 at 367 nm led to dual emission at $\lambda_{em} = 470$ and 611 nm. Moreover, the lower energy band became relatively more intense with increasing concentration (**Figure 3-11**). This suggests that excimer formation, as postulated for the molecular species,[21] occurs also for the polymeric material at high concentrations.[15] Thus, despite the incorporation of the organoboron quinolate moieties into the polymeric structure alignment of the chromophores is still possible and an interesting concentration dependent emission behavior due to excimer formation was realized.
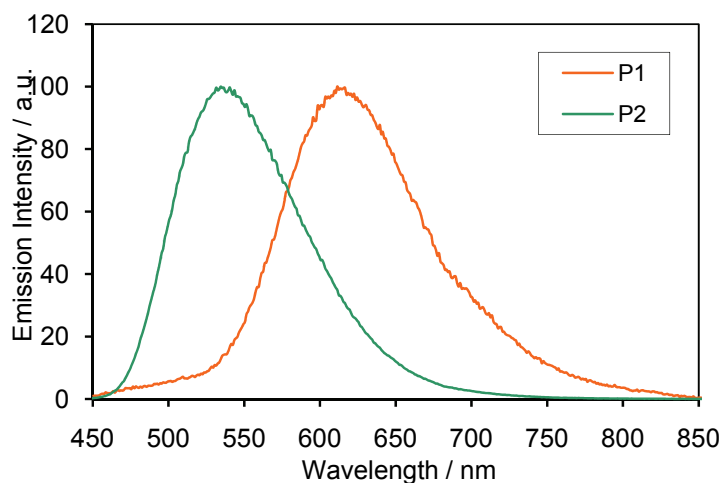
Figure 3-10. Emission spectra of P1 (1.04×10^{-6} M per repeating unit, excited at 443 nm) and P2 (4.0×10^{-7} M repeat units, excited at 411 nm)
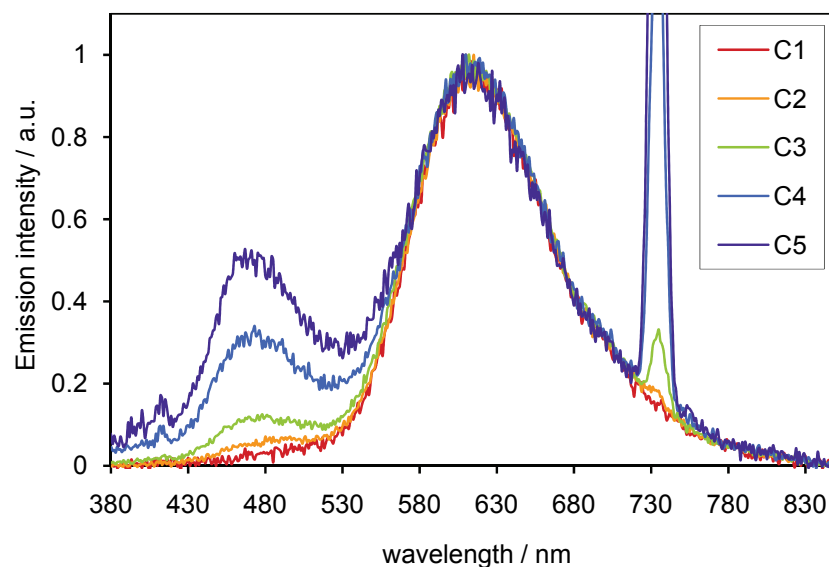
Figure 3-11. Concentration dependence of the emission of P1 (concentration of repeat units: c1 = 2.73 × 10^{-5} M, c2 = 1.36 × 10^{-5} M, c3 = 6.80 × 10^{-6} M, c4 = 1.70 × 10^{-6} M, c5 = 8.5 × 10^{-7} M; λ_{exc} = 367 nm (the signal at 734 nm is due to the half-harmonic of the excitation pulse))

3.3 Conclusions

Boron-induced ether cleavage reactions serve as an exceptionally mild, transition metal-free method for the preparation of organoboron quinolate polymers with both the boron and quinolato ligands embedded into the polymer main chain. Two polymers with different π-conjugated linkers were prepared. Both of theses polymers are readily soluble in common organic solvent and thermally stable to >300°C. The photoluminescence properties can be tuned by varying the conjugated bridge connecting the quinolato groups. In fact, the degree of conjugation of the linker critically influences the nature of the frontier orbitals as demonstrated by DFT calculations for molecular model systems. With

the highly delocalized Th-C$_6$H$_4$-Th linker, the lowest energy absorption corresponds to intramolecular charge transfer (ICT) from this conjugated linker to the pyridyl moiety. In contrast, with a less delocalized biphenyl linker, ICT occurs from the fluorene moiety of the diboron monomer to the pyridyl rings based on time-dependent DFT calculations on molecular model systems. Another interesting phenomenon that is also attributed to the presence of the extended conjugated π-system is that the Th-C$_6$H$_4$-Th linker leads to a concentration dependent emission behavior as a result of aggregation phenomena.

3.4 Experimental section

Synthesis of 2,7-bis(4-*t*-butylphenylbromoboryl)-9,9-dihexylfluorene (B1): At −35 °C, a solution of 1-trimethylstannyl-4-*tert*-butylbenzene (230 mg, 0.74 mmol) in 10 mL of CH$_2$Cl$_2$ was added to a solution of 2,7-bis(dibromoboryl)-9,9-dihexylfluorene (251 mg, 0.37 mmol) in 5 mL of CH$_2$Cl$_2$. The mixture was allowed to warm up to room temperature and kept stirring for 4 h. The volatile materials were removed under high vacuum and the residue was purified by crystallization from hexanes at −35 °C. Yield: 210 mg, 72%. ^{1}H NMR (CDCl$_3$): δ = 8.07 (d, 2H, ^{3}J=7.5 Hz, Fl), 8.00 (m, 6H, ^{3}J=8.6 Hz, Ph and Fl), 7.90 (d, 2H, ^{3}J=8.0 Hz, Fl), 7.55 (d, 4H, ^{3}J=8.0 Hz, Ph), 2.07 (m, 4H, Hex-CH$_2$), 1.41 (s, 18H, t-Bu), 1.06-1.20 (br, 12H, Hex-CH$_2$), 0.81 (t, 6H, ^{3}J=7.0 Hz, Hex-CH$_3$), 0.74 (br, 4H, Hex-CH$_2$); ^{13}C NMR (CDCl$_3$): δ = 157.1, 151.3, 145.0, 140.1, 138.1, 137.4, 137.1, 132.2, 125.2, 120.2, 55.6, 40.1, 35.4, 31.7, 31.3, 29.8, 24.2, 22.9, 14.3; ^{11}B NMR (CDCl$_3$): δ = 66 ($w_{1/2}$ = 2380 Hz).

Polymerization of B1 and Q1: Synthesis of P1. A solution of **Q1** (15 mg, 0.027 mmol) in 10 mL of CH$_2$Cl$_2$ was added to a solution of **B1** (21.1 mg, 0.027 mmol) in 5

mL of CH_2Cl_2 and the mixture was kept stirring overnight. The volatile materials were removed under high vacuum. The crude material was dissolved in 5 mL of CH_2Cl_2, and the product was precipitated by addition of 10 mL of hexanes. The polymer was obtained as an orange powdery solid by freeze-drying from benzene. Yield: 18.0 mg, 59%. ^{1}H NMR ($CDCl_3$): δ = 8.86 (d, 2H, [3]J=8 Hz, Qu), 8.64 (br, 2H, Qu), 7.85 (d, 2H, [3]J=8 Hz, Qu), 7.70 (s, 4H, Ph), 7.66 (d, 2H, [3]J=6 Hz, Qu), 7.58 (d, 2H, [3]J=8 Hz, Fl), 7.55 (br d, 2H, [3]J=3 Hz, Fl), 7.44 (br, 2H, Th), 7.39-7.35 (m, 6H, tBuPh and Fl), 7.30 (d, 4H, [3]J=8 Hz, tBuPh), 7.25 (d, 2H, [3]J=8 Hz, Qu), 7.19 (br, 2H, Th), 1.87 (br, 4H, Hex), 1.30 (s, 18H, tBu), 1.20-0.95 (br, 12H, Hex), 0.82-0.60 (br, 10H, Hex); ^{13}C NMR ($CDCl_3$): δ = 159.3, 150.4, 149.9, 145.3, 144.1, 143.9, 140.7, 139.8, 138.1, 137.8, 134.1, 133.6, 132.3, 130.3, 127.6, 127.0, 126.4, 124.7, 124.0, 123.3, 118.8, 118.4, 109.9, 54.9, 40.3, 34.6, 31.6, 31.6, 29.9, 24.2, 22.8, 14.3; ^{11}B NMR ($CDCl_3$): δ = 11 ($w_{1/2}$ = 2100 Hz); GPC-RI: M_w = 2.07 × 10^4, PDI = 1.90; GPC-MALLS (THF, dn/dc = 0.272 mL/g): M_w = 1.72 × 10^4, PDI = 1.20; UV-Vis (CH_2Cl_2, 2.1 × 10^{-6} M repeat units): λ_{max} = 367, 443 nm; fluorescence (CH_2Cl_2, 2.1 × 10^{-6} M repeat units): $\lambda_{em,max}$ = 470, 611 nm (λ_{exc} = 367 nm), Φ = 0.9%; TGA (N_2, 20 °C/min): T_{dec} = 326 °C (onset).

Polymerization of B1 and Q2: Synthesis of P2. A solution of **B1** (102.7 mg, 0.137 mmol) in 10 mL of CH_2Cl_2 was added to a solution of **Q2** (68.5 mg, 0.137 mmol) in 10 mL of CH_2Cl_2 and kept stirring over night. The volatile materials were removed under high vacuum. The crude material was dissolved in 20 mL of CH_2Cl_2, and the polymer was precipitated by addition of 40 mL of hexanes. A second fraction was obtained by addition of an additional 20 mL of hexanes. The polymer was isolated by freeze-drying from benzene as a yellow powdery solid that was kept under high vacuum for 24 h.

Yield: 98 mg, 66%. ^{1}H NMR (CDCl$_3$): δ = 8.55 (d, 2H, ^{3}J=8 Hz, Qu), 7.85 (d, 4H, ^{3}J=8 Hz, Ph), 7.70-7.60 (m, 6H, Qu and Ph), 7.60-7.52 (m, 4H, Fl), 7.42-7.28 (m, 12H, Fl and tBuPh and Qu), 7.21 (d, 2H, ^{3}J=8 Hz, Qu), 2.57 (s, 6H, Qu-CH$_3$), 1.85 (br, 4H, Fl-CH$_2$), 1.33 (s, 18H, tBu), 1.20-1.00 (br, 12H, Hex), 0.9-0.6 (m, 10H, Hex); ^{13}C NMR (CDCl$_3$): δ = 153.6, 148.5, 145.1, 144.7, 135.8, 134.8, 133.3, 133.1, 128.3, 127.2, 126.5, 125.5, 124.0, 123.9, 124.7 120.6, 120.5, 120.3, 119.7, 113.9, 104.9, 49.9, 35.6, 29.7, 26.0, 26.7, 25.1, 19.2, 17.9, 16.4, 9.4; ^{11}B NMR (160.3 MHz): δ = 12 ($w_{1/2}$ = 2400 Hz); GPC-RI for fraction 1: M_w = 2.72 × 10^4, PDI = 1.56; for fraction 2: M_w = 1.26 × 10^4, PDI = 1.40; GPC-MALLS for fraction 1: (THF, dn/dc = 0.207 mL/g) M_w = 1.66 × 10^4, PDI = 1.24; for fraction 2: (THF, dn/dc = 0.200 mL/g) M_w = 9.82 × 10^3, PDI = 1.30; UV-Vis (CH$_2$Cl$_2$, 5.3 × 10^{-6} M repeat units): λ_{max} = 411 nm; fluorescence (CH$_2$Cl$_2$, 5.3 × 10^{-6} M repeat units): $\lambda_{em,max}$ = 536 nm (λ_{exc} = 314 nm), Φ = 19%; TGA (N$_2$, 20 ºC/min): T_{dec} = 318 ºC (onset); elemental analysis calcd for {C$_{77}$H$_{80}$B$_2$N$_2$O$_2$}$_n$: C 85.07, H 7.42, N 2.58%; found C 83.93, H 6.99, N 2.57%.

3.5 References

(1)   Tang, C. W.; VanSlyke, S. A. *Appl. Phys. Lett.* 1987, *51*, 913.

(2)   Tang, C. W.; VanSlyke, S. A.; Chen, C. H. *J. Appl. Phys.* 1989, *65*, 3610.

(3)   Jang, H.; Do, L. M.; Kim, Y.; Zyung, T.; Do, Y. *Synth. Met.* 2001, *121*, 1667.

(4)   Matsumura, M.; Akai, T. *Jpn. J. Appl. Phys.* 1996, *35*, 5357.

(5)   Burrows, P. E.; Shen, Z.; Bulovic, V.; McCarty, D. M.; Forrest, S. R.; Cronin, J. A.; Thompson, M. E. *J. Appl. Phys.* 1996, *79*, 7991.

(6)   Sapochak, L. S.; Padmaperuma, A.; Washton, N.; Endrino, F.; Schmett, G. T.; Marshall, J.; Fogarty, D.; Burrows, P. E.; Forrest, S. R. *J. Am. Chem. Soc.* 2001, *123*, 6300.

(7)   Hamada, Y.; Sano, T.; Fujita, M.; Fujii, T.; Nishio, Y.; Shibata, K. *J. Appl. Phys.* 1993, *32*, L514.

(8)   Shoji, E.; Miyatake, K.; Hlil, A. R.; Hay, A. S.; Maindron, T.; Jousseaume, V.; Dodelet, J. P.; Tao, Y.; D'lorio, M. *J. Polym. Sci. Part A: Polym. Chem.* 2003, *41*, 3006.

(9)   Pohl, R.; Montes, V. A.; Shinar, J.; Anzenbacher Jr., P. *J. Org. Chem.* 2004, *69*, 1723.

(10)   Montes, V. A.; Li, G.; Pohl, R.; Shinar, J.; Anzenbacher Jr., P., *Adv. Mater.* 2004, *16*, 2001.

(11)   Pohl, R.; Anzenbacher Jr, P. *Org. Lett.* 2003, *5*, 2769.

(12)   Cheng, J.-A.; Chen, C. H. *J. Mater. Chem.* 2005, *15*, 1179.

(13)   Cheng, J.-A.; Chen, C. H.; Yang, H. *Chem. Phys. Lett.* 2004, *397*, 302.

(14)   Zheng, X.; Wu, Y.; Sun, R.; Zhu, W.; Jiang, X.; Zhang, Z.; Xu, S. *Thin Solid Films* 2005, *478*, 252.

(15)   Jaafari, A.; Ouzeau, V.; Ely, M.; Rodriguez, F.; Yassar, A.; Aaron, J. J.; Benalloul, P.; Barthou, C. *Syn. Met.* 2004, *147*, 175.

(16)   Sapochak, L. S.; Benincasa, F. E.; Schofield, R. S.; Baker, J. L.; Riccio, K. K. C.; Fogarty, D.; Kohlmann, H.; Ferris, K. F.; Burrows, P. E. *J. Am. Chem. Soc.* 2002, *124*, 6119.

(17)   Donze, N.; Pechy, P.; Gratzel, M.; Schaer, M.; Zuppiroli, L. *Chem. Phys. Lett.* 1999, *315*, 405.

(18)   Burrows, P. E.; Sapochak, L. S.; McCarty, D. M.; Forrest, S. R.; Thompson, M. E. *Appl. Phys. Lett.* 1994, *64*, 2718.

(19)   Wu, Q.; Esteghamatian, M.; Hu, N.-X.; Popovic, Z.; Enright, G.; Tao, Y.; D'Iorio, M.; Wang, S. *Chem. Mater.* 2000, *12*, 79.

(20)   Cui, Y.; Liu, Q.-D.; Bai, D.-R.; Jia, W.-L.; Tao, Y.; Wang, S. *Inorg. Chem.* 2005, *44*, 601.

(21)   Cui, Y.; Wang, S. *J. Org. Chem.* 2006, *71*, 6485.

(22)   Kappaun, S.; Rentenberger, S.; Pogantsch, A.; Zojer, E.; Mereiter, K.; Trimmel, G.; Saf, R.; Möller, K. C.; Stelzer, F.; Slugovc, C. *Chem. Mater.* 2006, *18*, 3539.

(23)   Qin, Y.; Kiburu, I.; Venkatasubbaiah, K.; Shah, S.; Jäkle, F. *Org. Lett.* 2006, *8*, 5227.

(24)   Bao, Z.; Rogers, J. A.; Katz, H. E. *J. Mater. Chem.* 1999, *9*, 1895.

(25)   Calvert, P. *Chem. Mater.* 2001, *13*, 3299.

(26)   Wang, X.-Y.; Weck, M. *Macromolecules* 2005, *38*, 7219.

(27)   Qin, Y.; Kiburu, I.; Shah, S.; Jäkle, F. *Macromolecules* 2006, *39*, 9041.

(28)   Qin, Y.; Cheng, G.; Parab, K.; Achara, O.; Jäkle, F. *Macromolecules* 2004, *37,* 7123.

(29)   Nagata, Y.; Otaka, H.; Chujo, Y. *Macromolecules* 2008, *41*, 737.

(30)   Nagata, Y.; Chujo, Y. *Macromolecules* 2007, *40,* 6.

(31)   Nagata, Y.; Chujo, Y. *Macromolecules* 2008, *41*, 2809.

(32)   Nagata, Y.; Chujo, Y. *Macromolecules* 2008, *41*, 3488.

(33)   Sonogashira, K.; Tohda, Y.; Hagihara, N. *Tetrahedron Lett.* 1975, *16*, 4467.

(34)   Takahashi, K.; Kuroyama, Y.; Sonogashira, K. *Synthesis* 1980, 627.

(35)   Nagata, Y.; Chujo, Y. *Macromolecules* 2008, *41*, 3488.

(36)   Tokoro, Y.; Nagai, A.; Kokado, K.; Chujo, Y. *Macromolecules* 2009, *42*, 2988.

(37)   Li, H.; Jäkle, F. *Angew. Chem. Int. Ed.* 2009, *48*, 2313.

Appendix

Appendix 1. The following tables are supplementary materials for the X-ray crystal structures of compound **QTBM-CN** and **QTBM-F**. The data of fractional atomic coordinates and equivalent isotropic displacement parameters, anisotropic displacement parameters, bond lengths and bond angles are listed.

Crystal Data and Structure Refinement Details for QTBM-CN and QTBM-F

	QTBM-CN	QTBM-F
Empirical formula	C88 H128 B2 N4 S4	C94 H136 B2 F2 K2 O16 S4
M_r	1391.80	1788.09
T, K	100(2)	100(2)
Wavelength, Å	1.54178	1.54178
Crystal system	Triclinic	Triclinic
Space group	P-1	P -1
a, Å	11.6855(3)	10.7612(1)
b, Å	12.0398(3)	11.4101(2)
c, Å	16.0851(5)	21.9383(3)
α, °	78.460(2)	89.5585(9)
β, °	74.957(2)	88.1985(8)
γ, °	70.046(2)	63.2907(7)
V, Å^3	2038.73(10)	2405.04(6)
Z	1	1
ρ_{calc}, g/cm^{-3}	1.134	1.235
μ(CuKα),mm^{-1}	1.405	2.210

F(000)	758	958
Crystal size, mm^3	0.47 x 0.19 x 0.17	0.33 x 0.28 x 0.17
θ range, °	3.94 to 66.95	4.03 to 71.03
Index ranges	-13<=h<=13	-12<=h<=12
	-14<=k<=13	-13<=k<=13
	-18<=l<=16	-25<=l<=25
Reflections collected	16584	23466
Independent reflections	6549 [R(int) = 0.0300]	8064 [R(int) = 0.027]
Absorption correction	Numerical	Numerical
Refinement method	Full-matrix least-squares on F^2	Full-matrix least-squares on F^2
Data / restraints / parameters	6549 / 0 / 454	8064 / 0 / 552
Goodness-of-fit on F^2	1.052	1.03
Final R indices [I>2σ(I)][a]	R1 = 0.0438, wR2 = 0.1120	R1 = 0.044, wR2 = 0.111
R indices (all data) [a]	R1 = 0.0531, wR2 = 0.1183	R1 = 0.056, wR2 = 0.118
Peak/hole (eÅ^{-3})	0.347 and -0.271	0.73 and -0.40

Fractional Atomic Coordinates (×10^4) and Equivalent Isotropic Displacement Parameters (Å^2×10^3) of QTBM-CN where U(eq) = (1/3)$\sum_j U^{ij} a_i a_j a_i . a_j$

	x	y	z	U(eq)
S(1)	6591(1)	5043(1)	448(1)	21(1)

C(1)	7053(2)	1051(2)	2501(1)	20(1)
B(1)	5820(2)	2235(2)	2340(1)	20(1)
N(1)	5420(2)	3543(1)	3691(1)	26(1)
S(2)	9184(1)	4219(1)	948(1)	24(1)
C(2)	8205(2)	662(2)	1919(1)	21(1)
N(2)	5520(2)	7198(1)	3054(1)	26(1)
C(3)	9151(2)	-350(2)	2157(1)	24(1)
C(4)	9035(2)	-1014(2)	2964(1)	25(1)
C(5)	7911(2)	-648(2)	3537(1)	25(1)
C(6)	6929(2)	334(2)	3318(1)	22(1)
C(7)	8561(2)	1235(2)	997(1)	25(1)
C(8)	10074(2)	-2091(2)	3213(2)	36(1)
C(9)	5751(2)	552(2)	4010(1)	26(1)
C(10)	4633(2)	1802(2)	2287(1)	21(1)
C(11)	4795(2)	1082(2)	1641(1)	23(1)
C(12)	3843(2)	668(2)	1571(1)	26(1)
C(13)	2696(2)	924(2)	2130(1)	28(1)
C(14)	2516(2)	1640(2)	2755(1)	27(1)
C(15)	3425(2)	2103(2)	2827(1)	24(1)
C(16)	5979(2)	762(2)	956(1)	26(1)
C(17)	1663(2)	496(2)	2049(2)	36(1)
C(18)	3002(2)	2975(2)	3489(1)	34(1)
C(19)	5344(2)	4678(2)	335(1)	19(1)
C(20)	5150(2)	3755(2)	954(1)	20(1)
C(21)	6006(2)	3294(2)	1525(1)	19(1)
C(22)	6857(2)	3924(2)	1323(1)	20(1)
C(23)	7941(2)	3813(2)	1662(1)	22(1)

C(24)	8182(2)	3495(2)	2481(1)	25(1)
C(25)	9326(2)	3616(2)	2532(1)	25(1)
C(26)	9979(2)	4011(2)	1765(1)	26(1)
C(27)	11194(2)	4264(2)	1575(1)	31(1)
C(28)	5528(2)	2978(2)	3158(1)	21(1)
C(29)	6229(2)	6266(2)	3686(1)	29(1)
C(30)	6888(2)	6735(2)	4171(1)	33(1)
C(31)	7980(2)	5748(2)	4473(2)	36(1)
C(32)	7599(2)	4720(2)	5051(2)	42(1)
C(33)	6386(2)	7770(2)	2353(1)	28(1)
C(34)	7606(2)	6911(2)	1951(1)	32(1)
C(35)	8301(2)	7529(2)	1152(1)	32(1)
C(36)	7756(2)	7761(2)	351(1)	35(1)
C(37)	4537(2)	8206(2)	3519(1)	28(1)
C(38)	3498(2)	7867(2)	4195(1)	30(1)
C(39)	2498(2)	8983(2)	4521(1)	31(1)
C(40)	1504(2)	8690(2)	5272(2)	38(1)
C(41)	4946(2)	6528(2)	2652(1)	28(1)
C(42)	4108(2)	7271(2)	2034(1)	31(1)
C(43)	3326(2)	6558(2)	1900(1)	30(1)
C(44)	2567(2)	7184(2)	1210(2)	34(1)

Bond Lengths [Å] and Angles [deg] of QTBM-CN (Symmetry transformations used to generate equivalent atoms: #1 -x+1,-y+1,-z)

S(1)-C(19)	1.7193(19)	C(13)-C(14)	1.382(3)
S(1)-C(22)	1.7535(18)	C(13)-C(17)	1.507(3)
C(1)-C(2)	1.414(3)	C(14)-C(15)	1.396(3)
C(1)-C(6)	1.423(3)	C(15)-C(18)	1.516(3)
C(1)-B(1)	1.679(3)	C(19)-C(20)	1.375(3)
B(1)-C(28)	1.637(3)	C(19)-C(19)#1	1.448(4)
B(1)-C(21)	1.662(3)	C(20)-C(21)	1.429(3)
B(1)-C(10)	1.667(3)	C(21)-C(22)	1.385(3)
N(1)-C(28)	1.154(3)	C(22)-C(23)	1.461(3)
S(2)-C(26)	1.731(2)	C(23)-C(24)	1.370(3)
S(2)-C(23)	1.7497(19)	C(24)-C(25)	1.418(3)
C(2)-C(3)	1.403(3)	C(25)-C(26)	1.362(3)
C(2)-C(7)	1.521(3)	C(26)-C(27)	1.495(3)
N(2)-C(37)	1.523(2)	C(29)-C(30)	1.520(3)
N(2)-C(29)	1.524(2)	C(30)-C(31)	1.526(3)
N(2)-C(41)	1.524(3)	C(31)-C(32)	1.515(3)
N(2)-C(33)	1.531(2)	C(33)-C(34)	1.518(3)
C(3)-C(4)	1.381(3)	C(34)-C(35)	1.534(3)
C(4)-C(5)	1.381(3)	C(35)-C(36)	1.517(3)
C(4)-C(8)	1.513(3)	C(37)-C(38)	1.516(3)
C(5)-C(6)	1.398(3)	C(38)-C(39)	1.530(3)
C(6)-C(9)	1.510(3)	C(39)-C(40)	1.521(3)
C(10)-C(11)	1.419(3)	C(41)-C(42)	1.516(3)
C(10)-C(15)	1.420(3)	C(42)-C(43)	1.526(3)
C(11)-C(12)	1.400(3)	C(43)-C(44)	1.519(3)
C(11)-C(16)	1.514(3)		
C(12)-C(13)	1.380(3)	C(19)-S(1)-C(22)	92.18(9)

C(2)-C(1)-C(6)	115.32(16)	C(11)-C(10)-C(15)	114.80(18)
C(2)-C(1)-B(1)	128.01(16)	C(11)-C(10)-B(1)	119.06(17)
C(6)-C(1)-B(1)	116.67(16)	C(15)-C(10)-B(1)	126.13(18)
C(28)-B(1)-C(21)	99.54(14)	C(12)-C(11)-C(10)	121.96(18)
C(28)-B(1)-C(10)	113.48(15)	C(12)-C(11)-C(16)	115.64(18)
C(21)-B(1)-C(10)	109.24(15)	C(10)-C(11)-C(16)	122.33(18)
C(28)-B(1)-C(1)	104.29(15)	C(13)-C(12)-C(11)	122.3(2)
C(21)-B(1)-C(1)	119.16(16)	C(12)-C(13)-C(14)	116.52(19)
C(10)-B(1)-C(1)	110.66(15)	C(12)-C(13)-C(17)	122.4(2)
C(26)-S(2)-C(23)	92.88(10)	C(14)-C(13)-C(17)	121.0(2)
C(3)-C(2)-C(1)	120.99(17)	C(13)-C(14)-C(15)	122.96(19)
C(3)-C(2)-C(7)	112.93(17)	C(14)-C(15)-C(10)	121.34(19)
C(1)-C(2)-C(7)	126.07(16)	C(14)-C(15)-C(18)	114.90(18)
C(37)-N(2)-C(29)	111.09(15)	C(10)-C(15)-C(18)	123.71(18)
C(37)-N(2)-C(41)	111.98(16)	C(20)-C(19)-S(1)	110.03(14)
C(29)-N(2)-C(41)	105.37(14)	C(19)#1-C(19)-S(1)	120.77(18)
C(37)-N(2)-C(33)	106.39(14)	C(22)-C(21)-C(20)	109.86(16)
C(29)-N(2)-C(33)	111.50(16)	C(22)-C(21)-B(1)	129.32(17)
C(41)-N(2)-C(33)	110.61(16)	C(20)-C(21)-B(1)	120.61(16)
C(4)-C(3)-C(2)	123.06(18)	C(21)-C(22)-C(23)	133.37(17)
C(3)-C(4)-C(5)	116.56(17)	C(21)-C(22)-S(1)	111.99(14)
C(3)-C(4)-C(8)	122.24(19)	C(23)-C(22)-S(1)	114.58(13)
C(5)-C(4)-C(8)	121.20(18)	C(24)-C(23)-C(22)	132.18(18)
C(4)-C(5)-C(6)	122.28(18)	C(24)-C(23)-S(2)	109.59(15)
C(5)-C(6)-C(1)	121.70(18)	C(22)-C(23)-S(2)	118.13(14)
C(5)-C(6)-C(9)	114.59(17)	C(23)-C(24)-C(25)	113.18(18)
C(1)-C(6)-C(9)	123.71(16)	C(26)-C(25)-C(24)	114.52(19)

C(25)-C(26)-C(27)	129.54(19)	C(33)-C(34)-C(35)	111.45(16)
C(25)-C(26)-S(2)	109.77(16)	C(36)-C(35)-C(34)	113.82(19)
C(27)-C(26)-S(2)	120.69(15)	C(38)-C(37)-N(2)	115.99(16)
N(1)-C(28)-B(1)	173.16(19)	C(37)-C(38)-C(39)	110.22(16)
C(30)-C(29)-N(2)	114.84(16)	C(40)-C(39)-C(38)	112.43(17)
C(29)-C(30)-C(31)	111.41(18)	C(42)-C(41)-N(2)	116.39(15)
C(32)-C(31)-C(30)	113.1(2)	C(41)-C(42)-C(43)	109.47(16)
C(34)-C(33)-N(2)	115.35(15)	C(44)-C(43)-C(42)	112.77(17)

Anisotropic Displacement Parameters (Å^2 x 10^3) of QTBM-CN

	U11	U22	U33	U23	U13	U12
S(1)	24(1)	18(1)	22(1)	2(1)	-7(1)	-9(1)
C(1)	25(1)	17(1)	22(1)	-1(1)	-8(1)	-10(1)
B(1)	22(1)	19(1)	19(1)	1(1)	-5(1)	-7(1)
N(1)	27(1)	26(1)	25(1)	-4(1)	-4(1)	-9(1)
S(2)	24(1)	25(1)	24(1)	1(1)	-6(1)	-10(1)
C(2)	24(1)	18(1)	23(1)	-3(1)	-7(1)	-11(1)
N(2)	35(1)	18(1)	26(1)	-1(1)	-7(1)	-7(1)
C(3)	23(1)	21(1)	29(1)	-5(1)	-5(1)	-8(1)
C(4)	25(1)	19(1)	33(1)	0(1)	-10(1)	-8(1)
C(5)	32(1)	21(1)	25(1)	4(1)	-10(1)	-12(1)
C(6)	25(1)	19(1)	24(1)	-1(1)	-7(1)	-11(1)

C(7)	26(1)	22(1)	26(1)	-3(1)	-2(1)	-7(1)
C(8)	30(1)	28(1)	40(1)	6(1)	-8(1)	-4(1)
C(9)	30(1)	25(1)	22(1)	4(1)	-5(1)	-10(1)
C(10)	27(1)	16(1)	21(1)	4(1)	-9(1)	-7(1)
C(11)	28(1)	17(1)	24(1)	5(1)	-10(1)	-8(1)
C(12)	35(1)	17(1)	30(1)	1(1)	-15(1)	-9(1)
C(13)	31(1)	20(1)	37(1)	7(1)	-17(1)	-12(1)
C(14)	24(1)	26(1)	31(1)	5(1)	-9(1)	-9(1)
C(15)	24(1)	24(1)	24(1)	3(1)	-8(1)	-7(1)
C(16)	34(1)	21(1)	25(1)	-4(1)	-8(1)	-8(1)
C(17)	34(1)	30(1)	51(2)	1(1)	-18(1)	-16(1)
C(18)	22(1)	46(1)	34(1)	-14(1)	-2(1)	-9(1)
C(19)	20(1)	17(1)	22(1)	-4(1)	-4(1)	-6(1)
C(20)	21(1)	16(1)	23(1)	-3(1)	-4(1)	-6(1)
C(21)	21(1)	15(1)	21(1)	-4(1)	-3(1)	-5(1)
C(22)	24(1)	16(1)	20(1)	1(1)	-5(1)	-5(1)
C(23)	24(1)	17(1)	24(1)	-1(1)	-4(1)	-7(1)
C(24)	23(1)	22(1)	29(1)	1(1)	-7(1)	-8(1)
C(25)	27(1)	25(1)	25(1)	0(1)	-11(1)	-8(1)
C(26)	26(1)	21(1)	29(1)	0(1)	-8(1)	-6(1)
C(27)	29(1)	35(1)	33(1)	3(1)	-11(1)	-15(1)
C(28)	18(1)	20(1)	23(1)	3(1)	-4(1)	-7(1)
C(29)	38(1)	19(1)	28(1)	1(1)	-10(1)	-7(1)
C(30)	42(1)	28(1)	30(1)	1(1)	-10(1)	-12(1)
C(31)	39(1)	35(1)	33(1)	-5(1)	-9(1)	-8(1)
C(32)	49(2)	32(1)	42(2)	0(1)	-16(1)	-7(1)
C(33)	38(1)	21(1)	26(1)	0(1)	-8(1)	-11(1)

C(34)	37(1)	24(1)	32(1)	0(1)	-7(1)	-8(1)
C(35)	34(1)	24(1)	37(1)	-4(1)	-5(1)	-11(1)
C(36)	44(1)	28(1)	31(1)	-3(1)	-2(1)	-13(1)
C(37)	37(1)	18(1)	29(1)	-4(1)	-7(1)	-6(1)
C(38)	39(1)	23(1)	28(1)	-1(1)	-9(1)	-9(1)
C(39)	36(1)	26(1)	30(1)	-4(1)	-11(1)	-6(1)
C(40)	40(1)	34(1)	36(1)	-4(1)	-6(1)	-8(1)
C(41)	36(1)	19(1)	30(1)	-5(1)	-7(1)	-10(1)
C(42)	37(1)	22(1)	33(1)	-3(1)	-9(1)	-9(1)
C(43)	32(1)	24(1)	32(1)	-8(1)	-2(1)	-8(1)
C(44)	36(1)	32(1)	34(1)	-9(1)	-6(1)	-10(1)

Fractional Atomic Coordinates (×10^4) and Equivalent Isotropic Displacement Parameters (Å^2×10^3) of QTBM-F where U(eq) = (1/3)$\sum_j$U^{ij}a$_i$a$_j$a$_i$.a$_j$

	x	y	z	U(eq)
S(1)	6961(1)	8818(1)	4497(1)	20(1)
K(1)	5000	5000	5000	31(1)
C(1B)	1267(3)	3079(3)	1365(1)	40(1)
C(1D)	794(4)	7931(4)	20(2)	70(1)
C(1)	2847(2)	10685(2)	3043(1)	19(1)
B(1)	4396(3)	9390(2)	2987(1)	19(1)
O(1)	2392(2)	5360(2)	4573(1)	32(1)
C(1A)	1219(3)	6191(3)	4945(1)	33(1)

F(1)	5252(1)	9652(1)	2528(1)	21(1)
O(1C)	8429(3)	-254(3)	1269(1)	80(1)
S(2)	9430(1)	7671(1)	3533(1)	26(1)
K(2)	0	5000	0	34(1)
C(2B)	-283(3)	3763(3)	1474(1)	35(1)
C(2D)	1947(4)	8312(4)	75(2)	68(1)
C(2)	1676(2)	10606(2)	3319(1)	21(1)
C(2A)	2370(3)	4150(3)	4430(1)	39(1)
O(2)	4850(2)	3019(2)	4380(1)	34(1)
C(3B)	-2288(3)	5754(3)	1323(1)	30(1)
C(3D)	3232(4)	7073(4)	-49(2)	71(1)
C(3)	392(2)	11719(2)	3389(1)	23(1)
O(3)	7493(2)	2869(2)	4584(1)	32(1)
C(3A)	3632(3)	3334(3)	4039(1)	38(1)
O(4)	1555(2)	2822(2)	728(1)	38(1)
C(4B)	-2788(3)	7080(3)	1043(1)	32(1)
C(4D)	2847(5)	6040(4)	165(2)	80(1)
C(4)	193(2)	12947(2)	3209(1)	24(1)
C(4A)	6080(3)	2141(3)	4051(1)	33(1)
O(5)	-819(2)	5038(2)	1215(1)	29(1)
C(5B)	-3196(3)	8137(3)	87(1)	45(1)
C(5)	1336(2)	13047(2)	2948(1)	24(1)
C(5A)	7282(3)	1747(3)	4460(1)	32(1)
O(6)	-2689(2)	6924(2)	396(1)	35(1)
C(6B)	3010(3)	2142(3)	586(1)	47(1)
C(6)	2632(2)	11952(2)	2862(1)	20(1)
C(6A)	8687(3)	2565(3)	4938(1)	33(1)

O(7)	1422(3)	6512(2)	23(1)	74(1)
C(7)	1753(2)	9335(2)	3562(1)	28(1)
C(8)	-1202(2)	14141(2)	3294(1)	32(1)
C(9)	3772(2)	12231(2)	2570(1)	27(1)
C(10)	4402(2)	8020(2)	2719(1)	19(1)
C(11)	4022(2)	8044(2)	2103(1)	22(1)
C(12)	4229(2)	6898(2)	1797(1)	26(1)
C(13)	4810(2)	5681(2)	2073(1)	26(1)
C(14)	5120(2)	5651(2)	2681(1)	24(1)
C(15)	4910(2)	6784(2)	3004(1)	21(1)
C(16)	3370(3)	9306(2)	1744(1)	27(1)
C(17)	5074(3)	4445(3)	1728(1)	39(1)
C(18)	5266(3)	6570(2)	3673(1)	28(1)
C(19)	5215(2)	9736(2)	4695(1)	20(1)
C(20)	4430(2)	9863(2)	4196(1)	20(1)
C(21)	5164(2)	9268(2)	3642(1)	19(1)
C(22)	6585(2)	8679(2)	3737(1)	19(1)
C(23)	7769(2)	7957(2)	3323(1)	20(1)
C(24)	7846(2)	7425(2)	2758(1)	22(1)
C(25)	9218(2)	6800(2)	2501(1)	25(1)
C(26)	10201(2)	6845(2)	2861(1)	24(1)
C(27)	11730(3)	6326(3)	2737(1)	32(1)
C(1C)	7261(3)	416(3)	1670(2)	53(1)
C(4C)	9644(4)	-375(5)	1555(2)	73(1)
C(3C)	9215(5)	421(6)	2106(2)	106(2)
C(2C)	7784(4)	700(4)	2255(2)	68(1)

Bond Lengths [Å] and Angles [deg] of QTBM-F

S(1)-C(19)	1.733(2)	S(2)-C(26)	1.730(2)
S(1)-C(22)	1.753(2)	S(2)-C(23)	1.743(2)
K(1)-O(2)	2.7165(17)	K(2)-O(7)#2	2.775(3)
K(1)-O(2)#1	2.7165(17)	K(2)-O(7)	2.775(3)
K(1)-O(3)	2.8215(18)	K(2)-O(5)#2	2.7754(16)
K(1)-O(3)#1	2.8215(18)	K(2)-O(5)	2.7755(16)
K(1)-O(1)	2.8366(17)	K(2)-O(4)#2	2.8099(17)
K(1)-O(1)#1	2.8366(17)	K(2)-O(4)	2.8100(17)
K(1)-C(18)#1	3.478(2)	K(2)-O(6)#2	2.8473(17)
C(1B)-O(4)	1.426(3)	K(2)-O(6)	2.8473(17)
C(1B)-C(2B)	1.501(4)	C(2B)-O(5)	1.423(3)
C(1D)-O(7)	1.447(4)	C(2D)-C(3D)	1.486(5)
C(1D)-C(2D)	1.496(6)	C(2)-C(3)	1.400(3)
C(1)-C(6)	1.414(3)	C(2)-C(7)	1.509(3)
C(1)-C(2)	1.419(3)	C(2A)-C(3A)	1.499(4)
C(1)-B(1)	1.659(3)	O(2)-C(4A)	1.427(3)
B(1)-F(1)	1.462(3)	O(2)-C(3A)	1.428(3)
B(1)-C(21)	1.653(3)	C(3B)-O(5)	1.429(3)
B(1)-C(10)	1.672(3)	C(3B)-C(4B)	1.494(4)
O(1)-C(1A)	1.425(3)	C(3D)-C(4D)	1.483(6)
O(1)-C(2A)	1.429(3)	C(3)-C(4)	1.376(3)
C(1A)-C(6A)#1	1.492(4)	O(3)-C(5A)	1.426(3)
O(1C)-C(4C)	1.418(4)	O(3)-C(6A)	1.426(3)
O(1C)-C(1C)	1.419(4)	O(4)-C(6B)	1.425(3)

C(4B)-O(6)	1.427(3)	C(6B)-C(5B)#2	1.501(4)
C(4D)-O(7)	1.423(5)	C(6)-C(9)	1.522(3)
C(4)-C(5)	1.392(3)	C(6A)-C(1A)#1	1.492(4)
C(4)-C(8)	1.514(3)	C(10)-C(15)	1.412(3)
C(4A)-C(5A)	1.492(4)	C(10)-C(11)	1.421(3)
C(5B)-O(6)	1.415(3)	C(11)-C(12)	1.396(3)
C(5B)-C(6B)#2	1.501(4)	C(11)-C(16)	1.514(3)
C(5)-C(6)	1.401(3)		
C(12)-C(13)	1.384(4)	O(2)-K(1)-O(2)#1	180
C(13)-C(14)	1.380(3)	O(2)-K(1)-O(3)	61.22(5)
C(13)-C(17)	1.512(3)	O(2)#1-K(1)-O(3)	118.78(5)
C(14)-C(15)	1.402(3)	O(2)-K(1)-O(3)#1	118.78(5)
C(15)-C(18)	1.518(3)	O(2)#1-K(1)-O(3)#1	61.22(5)
C(19)-C(20)	1.370(3)	O(3)-K(1)-O(3)#1	180.000(1)
C(19)-C(19)#3	1.447(4)	O(2)-K(1)-O(1)	60.80(5)
C(20)-C(21)	1.427(3)	O(2)#1-K(1)-O(1)	119.20(5)
C(21)-C(22)	1.388(3)	O(3)-K(1)-O(1)	120.76(5)
C(22)-C(23)	1.457(3)	O(3)#1-K(1)-O(1)	59.24(5)
C(23)-C(24)	1.368(3)	O(2)-K(1)-O(1)#1	119.20(5)
C(24)-C(25)	1.420(3)	O(2)#1-K(1)-O(1)#1	60.80(5)
C(25)-C(26)	1.360(3)	O(3)-K(1)-O(1)#1	59.24(5)
C(26)-C(27)	1.493(3)	O(3)#1-K(1)-O(1)#1	120.76(5)
C(1C)-C(2C)	1.513(5)	O(1)-K(1)-O(1)#1	180
C(4C)-C(3C)	1.451(5)	O(2)-K(1)-C(18)#1	86.85(6)
C(3C)-C(2C)	1.453(6)	O(2)#1-K(1)-C(18)#1	93.15(6)
		O(3)-K(1)-C(18)#1	94.13(5)
C(19)-S(1)-C(22)	92.03(10)	O(3)#1-K(1)-C(18)#1	85.88(5)

O(1)-K(1)-C(18)#1	93.95(5)	O(7)-K(2)-O(4)#2	75.46(7)
O(1)#1-K(1)-C(18)#1	86.05(5)	O(5)#2-K(2)-O(4)#2	61.37(5)
O(4)-C(1B)-C(2B)	108.6(2)	O(5)-K(2)-O(4)#2	118.63(5)
O(7)-C(1D)-C(2D)	107.0(3)	O(7)#2-K(2)-O(4)	75.47(7)
C(6)-C(1)-C(2)	115.7(2)	O(7)-K(2)-O(4)	104.53(7)
C(6)-C(1)-B(1)	122.27(19)	O(5)#2-K(2)-O(4)	118.63(5)
C(2)-C(1)-B(1)	121.9(2)	O(5)-K(2)-O(4)	61.37(5)
F(1)-B(1)-C(21)	105.72(17)	O(4)#2-K(2)-O(4)	180
F(1)-B(1)-C(1)	108.90(17)	O(7)#2-K(2)-O(6)#2	99.34(7)
C(21)-B(1)-C(1)	107.17(17)	O(7)-K(2)-O(6)#2	80.66(7)
F(1)-B(1)-C(10)	102.32(17)	O(5)#2-K(2)-O(6)#2	61.16(5)
C(21)-B(1)-C(10)	116.52(18)	O(5)-K(2)-O(6)#2	118.84(5)
C(1)-B(1)-C(10)	115.49(18)	O(4)#2-K(2)-O(6)#2	120.97(5)
C(1A)-O(1)-C(2A)	112.0(2)	O(4)-K(2)-O(6)#2	59.03(5)
C(1A)-O(1)-K(1)	114.84(14)	O(7)#2-K(2)-O(6)	80.67(7)
C(2A)-O(1)-K(1)	112.74(14)	O(7)-K(2)-O(6)	99.33(7)
O(1)-C(1A)-C(6A)#1	108.3(2)	O(5)#2-K(2)-O(6)	118.84(5)
C(4C)-O(1C)-C(1C)	109.0(3)	O(5)-K(2)-O(6)	61.16(5)
C(26)-S(2)-C(23)	93.07(11)	O(4)#2-K(2)-O(6)	59.03(5)
O(7)#2-K(2)-O(7)	180.00(6)	O(4)-K(2)-O(6)	120.97(5)
O(7)#2-K(2)-O(5)#2	102.21(7)	O(6)#2-K(2)-O(6)	179.998(1)
O(7)-K(2)-O(5)#2	77.79(7)	O(5)-C(2B)-C(1B)	108.9(2)
O(7)#2-K(2)-O(5)	77.79(7)	C(3D)-C(2D)-C(1D)	104.1(3)
O(7)-K(2)-O(5)	102.21(7)	C(3)-C(2)-C(1)	121.3(2)
O(5)#2-K(2)-O(5)	180	C(3)-C(2)-C(7)	116.6(2)
O(7)#2-K(2)-O(4)#2	104.54(7)	C(1)-C(2)-C(7)	122.1(2)

O(1)-C(2A)-C(3A)	108.8(2)	C(5B)-O(6)-C(4B)	112.5(2)
C(4A)-O(2)-C(3A)	111.60(19)	C(5B)-O(6)-K(2)	115.53(15)
C(4A)-O(2)-K(1)	116.50(14)	C(4B)-O(6)-K(2)	111.48(14)
C(3A)-O(2)-K(1)	117.47(14)	O(4)-C(6B)-C(5B)#2	108.1(2)
O(5)-C(3B)-C(4B)	109.0(2)	C(5)-C(6)-C(1)	121.4(2)
C(4D)-C(3D)-C(2D)	103.6(4)	C(5)-C(6)-C(9)	115.4(2)
C(4)-C(3)-C(2)	122.5(2)	C(1)-C(6)-C(9)	123.2(2)
C(5A)-O(3)-C(6A)	112.73(19)	O(3)-C(6A)-C(1A)#1	108.1(2)
C(5A)-O(3)-K(1)	111.20(14)	C(4D)-O(7)-C(1D)	108.0(3)
C(6A)-O(3)-K(1)	116.15(14)	C(4D)-O(7)-K(2)	125.2(2)
O(2)-C(3A)-C(2A)	109.1(2)	C(1D)-O(7)-K(2)	125.8(2)
C(6B)-O(4)-C(1B)	112.4(2)	C(15)-C(10)-C(11)	115.3(2)
C(6B)-O(4)-K(2)	116.32(15)	C(15)-C(10)-B(1)	127.63(19)
C(1B)-O(4)-K(2)	113.32(14)	C(11)-C(10)-B(1)	116.53(19)
O(6)-C(4B)-C(3B)	108.2(2)	C(12)-C(11)-C(10)	121.4(2)
O(7)-C(4D)-C(3D)	105.2(3)	C(12)-C(11)-C(16)	116.5(2)
C(3)-C(4)-C(5)	117.0(2)	C(10)-C(11)-C(16)	122.0(2)
C(3)-C(4)-C(8)	121.7(2)	C(13)-C(12)-C(11)	122.4(2)
C(5)-C(4)-C(8)	121.3(2)	C(14)-C(13)-C(12)	116.8(2)
O(2)-C(4A)-C(5A)	108.3(2)	C(14)-C(13)-C(17)	121.6(2)
C(2B)-O(5)-C(3B)	111.46(18)	C(12)-C(13)-C(17)	121.6(2)
C(2B)-O(5)-K(2)	112.82(13)	C(13)-C(14)-C(15)	122.3(2)
C(3B)-O(5)-K(2)	113.53(13)	C(14)-C(15)-C(10)	121.5(2)
O(6)-C(5B)-C(6B)#2	108.0(2)	C(14)-C(15)-C(18)	114.9(2)
C(4)-C(5)-C(6)	122.1(2)	C(10)-C(15)-C(18)	123.5(2)
O(3)-C(5A)-C(4A)	108.8(2)	C(20)-C(19)-C(19)#3	129.8(3)

C(20)-C(19)-S(1)	109.42(16)		C(25)-C(26)-S(2)	109.89(17)
C(19)#3-C(19)-S(1)	120.8(2)		C(27)-C(26)-S(2)	121.09(18)
C(19)-C(20)-C(21)	116.9(2)		O(1C)-C(1C)-C(2C)	107.8(3)
C(22)-C(21)-C(20)	109.37(19)		O(1C)-C(4C)-C(3C)	108.0(3)
C(22)-C(21)-B(1)	126.93(19)		C(4C)-C(3C)-C(2C)	107.8(3)
C(20)-C(21)-B(1)	123.54(19)		C(3C)-C(2C)-C(1C)	104.2(3)
C(24)-C(23)-S(2)	109.43(16)		C(21)-C(22)-C(23)	131.1(2)
C(22)-C(23)-S(2)	119.39(16)		C(21)-C(22)-S(1)	112.26(16)
C(23)-C(24)-C(25)	113.5(2)		C(23)-C(22)-S(1)	116.60(16)
C(26)-C(25)-C(24)	114.1(2)		C(24)-C(23)-C(22)	131.2(2)
C(25)-C(26)-C(27)	129.0(2)			

Anisotropic Displacement Parameters ($\text{Å}^2 \text{x } 10^3$) of QTBM-F

		U22	U33	U23	U13	U12
S(1)	18(1)	22(1)	18(1)	-2(1)	-1(1)	-6(1)
K(1)	38(1)	36(1)	24(1)	-2(1)	-3(1)	-22(1)
C(1B)	44(2)	40(2)	23(1)	7(1)	-1(1)	-8(1)
C(1D)	68(3)	51(2)	78(3)	-21(2)	-10(2)	-16(2)
C(1)	20(1)	22(1)	14(1)	-1(1)	-2(1)	-8(1)
B(1)	19(1)	19(1)	17(1)	1(1)	0(1)	-8(1)
O(1)	40(1)	31(1)	32(1)	3(1)	-5(1)	-22(1)
C(1A)	37(2)	45(2)	25(1)	5(1)	-6(1)	-25(1)
F(1)	20(1)	21(1)	20(1)	0(1)	1(1)	-8(1)
O(1C)	55(2)	140(3)	46(1)	-22(2)	11(1)	-47(2)

S(2)	18(1)	32(1)	25(1)	-5(1)	0(1)	-10(1)
K(2)	35(1)	32(1)	22(1)	4(1)	5(1)	-3(1)
C(2B)	45(2)	32(2)	22(1)	6(1)	2(1)	-13(1)
C(2D)	78(3)	64(2)	58(2)	-8(2)	-1(2)	-28(2)
C(2)	22(1)	22(1)	18(1)	-2(1)	-2(1)	-9(1)
C(2A)	43(2)	33(2)	49(2)	7(1)	-17(1)	-24(1)
O(2)	40(1)	33(1)	32(1)	1(1)	-10(1)	-19(1)
C(3B)	30(1)	37(2)	22(1)	-4(1)	5(1)	-15(1)
C(3D)	77(3)	75(3)	52(2)	-22(2)	4(2)	-27(2)
C(3)	21(1)	29(1)	19(1)	0(1)	1(1)	-11(1)
O(3)	39(1)	35(1)	29(1)	4(1)	-6(1)	-23(1)
C(3A)	47(2)	31(1)	40(2)	2(1)	-18(1)	-21(1)
O(4)	37(1)	37(1)	25(1)	5(1)	2(1)	-4(1)
C(4B)	31(1)	33(1)	28(1)	-4(1)	8(1)	-9(1)
C(4D)	89(3)	57(2)	82(3)	-6(2)	-50(2)	-20(2)
C(4)	21(1)	26(1)	18(1)	-1(1)	-1(1)	-4(1)
C(4A)	47(2)	29(1)	29(1)	1(1)	-4(1)	-21(1)
O(5)	31(1)	29(1)	23(1)	1(1)	4(1)	-10(1)
C(5B)	42(2)	31(2)	42(2)	7(1)	9(1)	2(1)
C(5)	25(1)	20(1)	22(1)	2(1)	0(1)	-7(1)
C(5A)	43(2)	31(1)	29(1)	1(1)	0(1)	-21(1)
O(6)	38(1)	28(1)	27(1)	1(1)	5(1)	-5(1)
C(6B)	37(2)	41(2)	40(2)	15(1)	2(1)	2(1)
C(6)	21(1)	22(1)	16(1)	0(1)	-1(1)	-8(1)
C(6A)	35(2)	38(2)	28(1)	3(1)	-3(1)	-18(1)
O(7)	74(2)	57(2)	86(2)	-5(1)	-26(2)	-24(1)

C(7)	24(1)	26(1)	33(1)	-1(1)	7(1)	-10(1)
C(8)	24(1)	29(1)	31(1)	6(1)	3(1)	-2(1)
C(9)	26(1)	20(1)	34(1)	2(1)	3(1)	-8(1)
C(10)	15(1)	21(1)	19(1)	-2(1)	2(1)	-6(1)
C(11)	19(1)	24(1)	22(1)	-2(1)	2(1)	-9(1)
C(12)	28(1)	34(1)	19(1)	-4(1)	3(1)	-17(1)
C(13)	25(1)	24(1)	31(1)	-10(1)	11(1)	-12(1)
C(14)	19(1)	19(1)	32(1)	1(1)	5(1)	-7(1)
C(15)	16(1)	22(1)	24(1)	0(1)	1(1)	-7(1)
C(16)	33(1)	29(1)	19(1)	1(1)	-5(1)	-12(1)
C(17)	54(2)	32(2)	36(2)	-11(1)	14(1)	-24(1)
C(18)	35(1)	23(1)	27(1)	5(1)	-5(1)	-13(1)
C(19)	21(1)	19(1)	21(1)	-1(1)	0(1)	-8(1)
C(20)	18(1)	18(1)	22(1)	0(1)	-1(1)	-7(1)
C(21)	19(1)	17(1)	21(1)	0(1)	0(1)	-8(1)
C(22)	22(1)	17(1)	18(1)	-1(1)	-2(1)	-8(1)
C(23)	18(1)	18(1)	23(1)	2(1)	-2(1)	-8(1)
C(24)	20(1)	20(1)	23(1)	-2(1)	-1(1)	-7(1)
C(25)	26(1)	21(1)	23(1)	-2(1)	3(1)	-7(1)
C(26)	24(1)	19(1)	29(1)	-1(1)	4(1)	-9(1)
C(27)	23(1)	30(1)	40(1)	-5(1)	6(1)	-11(1)
C(1C)	46(2)	57(2)	51(2)	-7(2)	11(2)	-19(2)
C(4C)	43(2)	128(4)	51(2)	-15(2)	7(2)	-40(2)
C(3C)	85(3)	187(6)	72(3)	-59(3)	19(2)	-84(4)
C(2C)	63(2)	73(3)	60(2)	-15(2)	9(2)	-24(2)

Appendix 2 The following tables are supplementary materials for the X-ray crystal structure of compound **QTBFT**. The data of fractional atomic coordinates and equivalent isotropic displacement parameters, anisotropic displacement parameters, bond lengths and bond angles are listed.

Crystal Data and Structure Refinement Details for QTBFT

	QTBFT
Empirical formula	C82 H92 B2 Fe2 S4
M_r	1339.12
T, K	100(2)
Wavelength, Å	1.54178
Crystal system	Triclinic
Space group	P-1
a, Å	9.7770(3)
b, Å	11.5826(4)
c, Å	16.0262(5)
α, °	81.645(2)
β, °	75.3130(10)
γ, °	83.325(2)
V, Å^3	1730.94(10)
Z	1
ρ_{calc}, g/cm^{-3}	1.285
μ(CuKα),mm^{-1}	4.818
F(000)	710
Crystal size, mm^3	0.10 x 0.09 x 0.08

		2.87 to 66.97
θ range, °		2.87 to 66.97
Index ranges		-11<=h<=11
		-13<=k<=13
		-17<=l<=19
Reflections collected		13131
Independent reflections		5627 [R(int) = 0.0458]
Absorption correction		Numerical
Refinement method		Full-matrix least-squares on F^2
Data / restraints / parameters		5627 / 0 / 414
Goodness-of-fit on F^2		0.999
Final R indices [I>2σ(I)][a]		R1 = 0.0475, wR2 = 0.1073
R indices (all data) [a]		R1 = 0.0761, wR2 = 0.1197
Peak/hole (eÅ^{-3})		0.500 and -0.273

Fractional Atomic Coordinates (×10^4) and Equivalent Isotropic Displacement Parameters (Å^2×10^3) of QTBFT where U(eq) = (1/3)$\sum_j$U^{ij}a$_i$a$_j$a$_i$.a$_j$

	x	y	z	U(eq)
Fe(1)	6227(1)	3459(1)	6827(1)	23(1)
S(1)	2390(1)	9053(1)	9027(1)	28(1)
S(2)	3487(1)	6530(1)	9893(1)	24(1)
B(1)	3982(4)	5742(3)	7391(3)	21(1)
C(1)	459(4)	10993(3)	8826(3)	37(1)
C(2)	905(4)	9737(3)	8714(2)	27(1)

C(3)	286(4)	8982(3)	8379(2)	27(1)
C(4)	996(3)	7839(3)	8372(2)	22(1)
C(5)	2171(3)	7728(3)	8699(2)	23(1)
C(6)	3132(3)	6706(3)	8867(2)	21(1)
C(7)	3904(3)	5860(3)	8364(2)	20(1)
C(8)	4746(3)	5076(3)	8852(2)	20(1)
C(9)	4651(3)	5305(3)	9675(2)	20(1)
C(10)	5330(3)	5173(3)	6811(2)	21(1)
C(11)	6775(3)	5086(3)	6883(2)	22(1)
C(12)	7680(4)	4611(3)	6153(2)	25(1)
C(13)	6826(3)	4372(3)	5609(2)	24(1)
C(14)	5396(4)	4716(3)	6006(2)	23(1)
C(15)	5067(4)	2390(3)	7834(2)	34(1)
C(16)	5110(4)	2018(3)	7016(2)	33(1)
C(17)	6552(4)	1750(3)	6595(2)	29(1)
C(18)	7401(4)	1955(3)	7150(2)	30(1)
C(19)	6483(4)	2347(3)	7910(2)	32(1)
C(20)	2741(3)	6270(3)	6940(2)	20(1)
C(21)	2827(3)	7392(3)	6452(2)	22(1)
C(22)	1696(4)	7887(3)	6102(2)	25(1)
C(23)	472(3)	7309(3)	6214(2)	24(1)
C(24)	432(3)	6197(3)	6663(2)	23(1)
C(25)	1550(3)	5661(3)	7020(2)	21(1)
C(26)	4127(4)	8054(3)	6336(2)	27(1)
C(27)	3778(4)	9341(3)	6477(2)	34(1)
C(28)	5149(4)	7938(3)	5446(2)	34(1)

C(29)	-780(4)	7853(3)	5851(2)	28(1)
C(30)	-1235(4)	9100(3)	6045(2)	33(1)
C(31)	-485(4)	7753(3)	4880(2)	40(1)
C(32)	1438(3)	4429(3)	7496(2)	24(1)
C(33)	92(4)	4338(3)	8234(2)	32(1)
C(34)	1507(4)	3539(3)	6861(2)	31(1)
C(35)	2575(4)	2556(3)	506(2)	28(1)
C(36)	3084(4)	1432(3)	304(2)	34(1)
C(37)	3695(4)	639(3)	867(3)	37(1)
C(38)	3827(4)	961(3)	1634(3)	37(1)
C(39)	3360(4)	2078(3)	1836(2)	36(1)
C(40)	2724(4)	2862(3)	1284(2)	30(1)
C(41)	1813(4)	3391(3)	-64(2)	34(1)

Bond Lengths [Å] and Angles [deg] of QTBFT

Fe(1)-C(11)	2.039(3)	Fe(1)-C(10)	2.075(3)
Fe(1)-C(17)	2.041(3)	S(1)-C(2)	1.724(3)
Fe(1)-C(16)	2.044(3)	S(1)-C(5)	1.745(3)
Fe(1)-C(18)	2.049(3)	S(2)-C(9)	1.731(3)
Fe(1)-C(12)	2.052(3)	S(2)-C(6)	1.744(3)
Fe(1)-C(14)	2.054(3)	B(1)-C(10)	1.546(5)
Fe(1)-C(19)	2.056(3)	B(1)-C(7)	1.566(5)
Fe(1)-C(13)	2.058(3)	B(1)-C(20)	1.584(5)
Fe(1)-C(15)	2.059(3)	C(1)-C(2)	1.493(4)

C(2)-C(3)	1.356(5)	C(25)-C(32)	1.520(4)
C(3)-C(4)	1.423(4)	C(26)-C(27)	1.527(4)
C(4)-C(5)	1.364(4)	C(26)-C(28)	1.534(5)
C(5)-C(6)	1.461(4)	C(29)-C(30)	1.513(4)
C(6)-C(7)	1.389(4)	C(29)-C(31)	1.528(5)
C(7)-C(8)	1.436(4)	C(32)-C(33)	1.532(5)
C(8)-C(9)	1.361(4)	C(32)-C(34)	1.535(4)
C(9)-C(9)#1	1.445(6)	C(35)-C(40)	1.390(5)
C(10)-C(11)	1.438(4)	C(35)-C(36)	1.391(5)
C(10)-C(14)	1.448(4)	C(35)-C(41)	1.499(5)
C(11)-C(12)	1.416(4)	C(36)-C(37)	1.385(5)
C(12)-C(13)	1.423(4)	C(36)-H(36)	0.93
C(13)-C(14)	1.419(4)	C(37)-C(38)	1.376(5)
C(15)-C(19)	1.414(5)	C(38)-C(39)	1.377(5)
C(15)-C(16)	1.427(5)	C(39)-C(40)	1.381(5)
C(16)-C(17)	1.420(5)		
C(17)-C(18)	1.422(5)	C(11)-Fe(1)-C(17)	156.61(14)
C(18)-C(19)	1.416(5)	C(11)-Fe(1)-C(16)	162.26(14)
C(20)-C(25)	1.400(4)	C(17)-Fe(1)-C(16)	40.68(14)
C(20)-C(21)	1.415(4)	C(11)-Fe(1)-C(18)	122.80(14)
C(21)-C(22)	1.393(4)	C(17)-Fe(1)-C(18)	40.69(13)
C(21)-C(26)	1.518(4)	C(16)-Fe(1)-C(18)	68.26(14)
C(22)-C(23)	1.398(5)	C(11)-Fe(1)-C(12)	40.50(13)
C(23)-C(24)	1.380(4)	C(17)-Fe(1)-C(12)	119.28(14)
C(23)-C(29)	1.520(4)	C(16)-Fe(1)-C(12)	155.68(15)
C(24)-C(25)	1.401(4)	C(18)-Fe(1)-C(12)	105.41(14)
		C(11)-Fe(1)-C(14)	68.06(12)

C(17)-Fe(1)-C(14)	120.68(13)	C(17)-Fe(1)-C(10)	158.65(13)
C(16)-Fe(1)-C(14)	107.80(14)	C(16)-Fe(1)-C(10)	124.66(14)
C(18)-Fe(1)-C(14)	155.83(14)	C(18)-Fe(1)-C(10)	160.39(13)
C(12)-Fe(1)-C(14)	67.84(13)	C(12)-Fe(1)-C(10)	68.83(13)
C(11)-Fe(1)-C(19)	110.43(14)	C(14)-Fe(1)-C(10)	41.06(12)
C(17)-Fe(1)-C(19)	68.10(14)	C(19)-Fe(1)-C(10)	126.11(13)
C(16)-Fe(1)-C(19)	67.94(15)	C(13)-Fe(1)-C(10)	69.06(13)
C(18)-Fe(1)-C(19)	40.35(13)	C(15)-Fe(1)-C(10)	110.87(14)
C(12)-Fe(1)-C(19)	123.31(14)	C(2)-S(1)-C(5)	92.46(16)
C(14)-Fe(1)-C(19)	162.32(14)	C(9)-S(2)-C(6)	92.66(15)
C(11)-Fe(1)-C(13)	68.27(13)	C(10)-B(1)-C(7)	120.8(3)
C(17)-Fe(1)-C(13)	103.56(14)	C(10)-B(1)-C(20)	117.0(3)
C(16)-Fe(1)-C(13)	120.56(14)	C(7)-B(1)-C(20)	122.1(3)
C(18)-Fe(1)-C(13)	119.50(14)	C(3)-C(2)-C(1)	128.7(3)
C(12)-Fe(1)-C(13)	40.51(12)	C(3)-C(2)-S(1)	110.6(3)
C(14)-Fe(1)-C(13)	40.36(12)	C(1)-C(2)-S(1)	120.7(3)
C(19)-Fe(1)-C(13)	156.92(14)	C(2)-C(3)-C(4)	113.8(3)
C(11)-Fe(1)-C(15)	126.59(14)	C(5)-C(4)-C(3)	113.1(3)
C(17)-Fe(1)-C(15)	68.43(14)	C(4)-C(5)-C(6)	131.0(3)
C(16)-Fe(1)-C(15)	40.71(14)	C(4)-C(5)-S(1)	110.0(2)
C(18)-Fe(1)-C(15)	68.08(15)	C(6)-C(5)-S(1)	118.8(2)
C(12)-Fe(1)-C(15)	160.70(14)	C(7)-C(6)-C(5)	133.6(3)
C(14)-Fe(1)-C(15)	125.49(14)	C(7)-C(6)-S(2)	111.5(2)
C(19)-Fe(1)-C(15)	40.19(14)	C(5)-C(6)-S(2)	114.7(2)
C(13)-Fe(1)-C(15)	158.66(14)	C(6)-C(7)-C(8)	110.0(3)
C(11)-Fe(1)-C(10)	40.90(12)	C(6)-C(7)-B(1)	128.4(3)

C(8)-C(7)-B(1)	121.5(3)	C(17)-C(16)-C(15)	108.2(3)
C(9)-C(8)-C(7)	116.2(3)	C(17)-C(16)-Fe(1)	69.5(2)
C(8)-C(9)-C(9)#1	129.9(4)	C(15)-C(16)-Fe(1)	70.2(2)
C(8)-C(9)-S(2)	109.6(2)	C(16)-C(17)-C(18)	107.8(3)
C(9)#1-C(9)-S(2)	120.5(3)	C(16)-C(17)-Fe(1)	69.78(19)
C(11)-C(10)-C(14)	105.1(3)	C(18)-C(17)-Fe(1)	69.94(19)
C(11)-C(10)-B(1)	129.3(3)	C(19)-C(18)-C(17)	107.9(3)
C(14)-C(10)-B(1)	125.4(3)	C(19)-C(18)-Fe(1)	70.11(19)
C(11)-C(10)-Fe(1)	68.19(17)	C(17)-C(18)-Fe(1)	69.36(19)
C(14)-C(10)-Fe(1)	68.72(17)	C(15)-C(19)-C(18)	108.7(3)
B(1)-C(10)-Fe(1)	131.8(2)	C(15)-C(19)-Fe(1)	70.0(2)
C(12)-C(11)-C(10)	109.7(3)	C(18)-C(19)-Fe(1)	69.5(2)
C(12)-C(11)-Fe(1)	70.26(18)	C(25)-C(20)-C(21)	118.9(3)
C(10)-C(11)-Fe(1)	70.91(17)	C(25)-C(20)-B(1)	121.7(3)
C(11)-C(12)-C(13)	108.2(3)	C(21)-C(20)-B(1)	119.4(3)
C(11)-C(12)-Fe(1)	69.25(18)	C(22)-C(21)-C(20)	119.4(3)
C(13)-C(12)-Fe(1)	69.98(19)	C(22)-C(21)-C(26)	120.8(3)
C(14)-C(13)-C(12)	107.5(3)	C(20)-C(21)-C(26)	119.8(3)
C(14)-C(13)-Fe(1)	69.68(18)	C(21)-C(22)-C(23)	122.1(3)
C(12)-C(13)-Fe(1)	69.51(18)	C(24)-C(23)-C(22)	117.7(3)
C(13)-C(14)-C(10)	109.6(3)	C(24)-C(23)-C(29)	119.9(3)
C(13)-C(14)-Fe(1)	69.96(18)	C(22)-C(23)-C(29)	122.4(3)
C(10)-C(14)-Fe(1)	70.23(17)	C(23)-C(24)-C(25)	122.1(3)
C(19)-C(15)-C(16)	107.5(3)	C(20)-C(25)-C(24)	119.7(3)
C(19)-C(15)-Fe(1)	69.8(2)	C(20)-C(25)-C(32)	121.2(3)
C(16)-C(15)-Fe(1)	69.1(2)	C(24)-C(25)-C(32)	119.1(3)

C(21)-C(26)-C(27)	113.7(3)
C(21)-C(26)-C(28)	111.1(3)
C(27)-C(26)-C(28)	110.5(3)
C(30)-C(29)-C(23)	113.4(3)
C(30)-C(29)-C(31)	111.8(3)
C(23)-C(29)-C(31)	110.8(3)
C(25)-C(32)-C(33)	112.0(3)
C(25)-C(32)-C(34)	110.8(3)
C(33)-C(32)-C(34)	110.6(3)
C(40)-C(35)-C(36)	117.7(3)
C(40)-C(35)-C(41)	120.6(3)
C(36)-C(35)-C(41)	121.6(3)
C(37)-C(36)-C(35)	121.1(3)
C(38)-C(37)-C(36)	120.1(4)
C(37)-C(38)-C(39)	119.7(4)
C(38)-C(39)-C(40)	120.3(4)
C(39)-C(40)-C(35)	121.1(3)

Anisotropic Displacement Parameters (Å^{2}x 10^3) of QTBFT

	U11	U22	U33	U23	U13	U12
Fe(1)	27(1)	24(1)	18(1)	-5(1)	-8(1)	1(1)
S(1)	32(1)	25(1)	30(1)	-7(1)	-12(1)	1(1)
S(2)	29(1)	28(1)	16(1)	-6(1)	-9(1)	4(1)
B(1)	23(2)	18(2)	23(2)	0(2)	-5(2)	-6(2)
C(1)	48(3)	29(2)	35(2)	0(2)	-15(2)	4(2)
C(2)	29(2)	29(2)	20(2)	-3(2)	-3(2)	0(2)
C(3)	21(2)	38(2)	21(2)	2(2)	-6(2)	2(2)
C(4)	24(2)	27(2)	16(2)	-7(2)	-5(1)	1(1)
C(5)	26(2)	26(2)	15(2)	-2(1)	-3(1)	-2(1)
C(6)	23(2)	25(2)	15(2)	-2(1)	-7(1)	-5(1)
C(7)	23(2)	23(2)	16(2)	-1(1)	-7(1)	-7(1)
C(8)	25(2)	21(2)	16(2)	-4(1)	-7(1)	-2(1)
C(9)	26(2)	20(2)	16(2)	-4(1)	-6(1)	-3(1)
C(10)	28(2)	19(2)	16(2)	1(1)	-7(1)	-1(1)
C(11)	24(2)	24(2)	20(2)	-7(2)	-9(1)	-1(1)
C(12)	18(2)	28(2)	27(2)	-2(2)	-4(2)	-2(1)
C(13)	29(2)	27(2)	14(2)	-2(2)	-6(2)	0(2)
C(14)	29(2)	26(2)	14(2)	0(1)	-8(2)	-1(2)
C(15)	43(2)	25(2)	26(2)	2(2)	2(2)	-3(2)
C(16)	38(2)	19(2)	45(3)	-4(2)	-15(2)	-3(2)

C(17)	42(2)	22(2)	25(2)	-9(2)	-10(2)	3(2)
C(18)	34(2)	25(2)	31(2)	-4(2)	-12(2)	8(2)
C(19)	50(3)	24(2)	20(2)	-2(2)	-11(2)	4(2)
C(20)	23(2)	25(2)	11(2)	-7(1)	-3(1)	2(1)
C(21)	23(2)	27(2)	16(2)	-7(2)	-5(1)	0(1)
C(22)	37(2)	22(2)	16(2)	-3(1)	-7(2)	1(2)
C(23)	25(2)	28(2)	20(2)	-12(2)	-7(2)	5(2)
C(24)	22(2)	27(2)	23(2)	-10(2)	-6(1)	0(1)
C(25)	24(2)	23(2)	18(2)	-9(1)	-7(1)	2(1)
C(26)	32(2)	28(2)	23(2)	-1(2)	-12(2)	-4(2)
C(27)	44(2)	31(2)	31(2)	-3(2)	-10(2)	-13(2)
C(28)	29(2)	40(2)	33(2)	-6(2)	-3(2)	-8(2)
C(29)	25(2)	31(2)	31(2)	-5(2)	-13(2)	4(2)
C(30)	37(2)	33(2)	30(2)	-3(2)	-11(2)	4(2)
C(31)	42(2)	49(2)	33(2)	-13(2)	-18(2)	12(2)
C(32)	22(2)	27(2)	24(2)	-2(2)	-11(2)	-2(2)
C(33)	39(2)	26(2)	30(2)	0(2)	-9(2)	-1(2)
C(34)	37(2)	25(2)	32(2)	-2(2)	-13(2)	-2(2)
C(35)	21(2)	38(2)	25(2)	-2(2)	-2(2)	-4(2)
C(36)	35(2)	40(2)	25(2)	-5(2)	-2(2)	-5(2)
C(37)	30(2)	34(2)	40(3)	-1(2)	1(2)	2(2)
C(38)	26(2)	46(2)	33(2)	1(2)	-3(2)	0(2)
C(39)	33(2)	43(2)	31(2)	-8(2)	-5(2)	-9(2)
C(40)	30(2)	30(2)	32(2)	-7(2)	-6(2)	-3(2)
C(41)	35(2)	39(2)	26(2)	-1(2)	-6(2)	-6(2)
Fe(1)	27(1)	24(1)	18(1)	-5(1)	-8(1)	1(1)
S(1)	32(1)	25(1)	30(1)	-7(1)	-12(1)	1(1)

S(2)	29(1)	28(1)	16(1)	-6(1)	-9(1)	4(1)
B(1)	23(2)	18(2)	23(2)	0(2)	-5(2)	-6(2)
C(1)	48(3)	29(2)	35(2)	0(2)	-15(2)	4(2)
C(2)	29(2)	29(2)	20(2)	-3(2)	-3(2)	0(2)
C(3)	21(2)	38(2)	21(2)	2(2)	-6(2)	2(2)
C(4)	24(2)	27(2)	16(2)	-7(2)	-5(1)	1(1)
C(5)	26(2)	26(2)	15(2)	-2(1)	-3(1)	-2(1)
C(6)	23(2)	25(2)	15(2)	-2(1)	-7(1)	-5(1)
C(7)	23(2)	23(2)	16(2)	-1(1)	-7(1)	-7(1)
C(8)	25(2)	21(2)	16(2)	-4(1)	-7(1)	-2(1)
C(9)	26(2)	20(2)	16(2)	-4(1)	-6(1)	-3(1)
C(10)	28(2)	19(2)	16(2)	1(1)	-7(1)	-1(1)
C(11)	24(2)	24(2)	20(2)	-7(2)	-9(1)	-1(1)
C(12)	18(2)	28(2)	27(2)	-2(2)	-4(2)	-2(1)
C(13)	29(2)	27(2)	14(2)	-2(2)	-6(2)	0(2)
C(14)	29(2)	26(2)	14(2)	0(1)	-8(2)	-1(2)
C(15)	43(2)	25(2)	26(2)	2(2)	2(2)	-3(2)
C(16)	38(2)	19(2)	45(3)	-4(2)	-15(2)	-3(2)
C(17)	42(2)	22(2)	25(2)	-9(2)	-10(2)	3(2)
C(18)	34(2)	25(2)	31(2)	-4(2)	-12(2)	8(2)
C(19)	50(3)	24(2)	20(2)	-2(2)	-11(2)	4(2)
C(20)	23(2)	25(2)	11(2)	-7(1)	-3(1)	2(1)
C(21)	23(2)	27(2)	16(2)	-7(2)	-5(1)	0(1)
C(22)	37(2)	22(2)	16(2)	-3(1)	-7(2)	1(2)
C(23)	25(2)	28(2)	20(2)	-12(2)	-7(2)	5(2)
C(24)	22(2)	27(2)	23(2)	-10(2)	-6(1)	0(1)
C(25)	24(2)	23(2)	18(2)	-9(1)	-7(1)	2(1)

C(26)	32(2)	28(2)	23(2)	-1(2)	-12(2)	-4(2)
C(27)	44(2)	31(2)	31(2)	-3(2)	-10(2)	-13(2)
C(28)	29(2)	40(2)	33(2)	-6(2)	-3(2)	-8(2)
C(29)	25(2)	31(2)	31(2)	-5(2)	-13(2)	4(2)
C(30)	37(2)	33(2)	30(2)	-3(2)	-11(2)	4(2)
C(31)	42(2)	49(2)	33(2)	-13(2)	-18(2)	12(2)
C(32)	22(2)	27(2)	24(2)	-2(2)	-11(2)	-2(2)
C(33)	39(2)	26(2)	30(2)	0(2)	-9(2)	-1(2)
C(34)	37(2)	25(2)	32(2)	-2(2)	-13(2)	-2(2)
C(35)	21(2)	38(2)	25(2)	-2(2)	-2(2)	-4(2)
C(36)	35(2)	40(2)	25(2)	-5(2)	-2(2)	-5(2)
C(37)	30(2)	34(2)	40(3)	-1(2)	1(2)	2(2)
C(38)	26(2)	46(2)	33(2)	1(2)	-3(2)	0(2)
C(39)	33(2)	43(2)	31(2)	-8(2)	-5(2)	-9(2)
C(40)	30(2)	30(2)	32(2)	-7(2)	-6(2)	-3(2)
C(41)	35(2)	39(2)	26(2)	-1(2)	-6(2)	-6(2)

List of Publications

1) "Main Chain Donor-π-Acceptor Type Polymer Based on Fluorene and Triphenylamine Derivatives." **H. Li** and F. Jäkle. *Macromol. Rapid Commun.* (in press)

2) "Ferrocenylhydridoborates: Structural Characterization and Application to the Preparation of Ferrocenylborane Polymers." M. Scheibitz, **H. Li**, J. Schnorr, A. S. Perucha, J. B. Heilmann, M. Bolte, H.-W. Lerner, F. Jäkle, and M. Wagner, *J. Am. Chem. Soc.* **2009**, 131, 6319-16329.

3) ʺ9,10-Dihydro-9,10-diboraanthracene – a New Kind of Supramolecular Structure Formed by 3c-2e BHB Bonds and a Promising Building Block for Luminescent Conjugated Polymers.ʺ A. Lorbach, M. Bolte, **H. Li**, H.-W. Lerner, M. C. Holthausen, F. Jäkle, M. Wagner, *Angew. Chem. Int. Ed.* 2009, 48, 4584-4588**.**

4) "A Facile Route to Organoboron Quinolate Polymers through Boron-Induced Ether Cleavage." **H. Li** and F. Jäkle, *Macromolecules* 2009, 42, 3448-3453.

5) "A Universal Conjugated Organoborane Polymer Scaffold." **H. Li** and F. Jäkle, *Angew. Chem. Int. Ed.* 2009, 48, 2313-2316.

6) "A Donor-Acceptor Dyad with a Highly Lewis Acidic Boryl Group." A. Sundararaman, R. Varughese, **H. Li,** A. L. Rheingold, and F. Jäkle, *Organometallics* 2007**,** *26*, 6126-6131.

7) ʺOrganoborane Acceptor-Substituted Polythiophene via Side-Group Borylation." **H. Li**, A. Sundararaman, K. Venkatasubbaiah, F. Jäkle, *J. Am. Chem. Soc.* 2007**,** 129, 5792-5793.

VITA

Haiyan Li

Date of Birth:	Sep. 28th, 1978
Place of Birth	Fengning, Hebei, China
Name of the Father	Shuting Li
Name of the Mother	Fengqin Ao

Educational

background

1998-2002	Department of Chemistry
	Nankai University, Tianjin, China.
	Degree achieved: B. S. in Chemistry.
2002-2005	Institute of Polymer Chemistry
	Nankai University, Tianjin, China
	Degree achieved: M.S. in Polymer Chemistry
2005-present	Department of Chemistry
	Rutgers University-Newark, Newark, NJ.
	Degree sought: Ph.D. in Chemistry. Advisor: **Frieder Jäkle**.